

# University of Wollongong - Research Online

## Thesis Collection

Title: The influence of the mode of plasma generation on the plasma nitriding behaviour of a micor alloyed [i.e. microalloyed] steel

Author: Farzad Mahboubi

Year: 1998

Repository DOI:

### Copyright Warning

You may print or download ONE copy of this document for the purpose of your own research or study. The University does not authorise you to copy, communicate or otherwise make available electronically to any other person any copyright material contained on this site.

You are reminded of the following: This work is copyright. Apart from any use permitted under the Copyright Act 1968, no part of this work may be reproduced by any process, nor may any other exclusive right be exercised, without the permission of the author. Copyright owners are entitled to take legal action against persons who infringe their copyright. A reproduction of material that is protected by copyright may be a copyright infringement. A court may impose penalties and award damages in relation to offences and infringements relating to copyright material.

Higher penalties may apply, and higher damages may be awarded, for offences and infringements involving the conversion of material into digital or electronic form.

Unless otherwise indicated, the views expressed in this thesis are those of the author and do not necessarily represent the views of the University of Wollongong.

Research Online is the open access repository for the University of Wollongong. For further information contact the UOW Library: [research-pubs@uow.edu.au](mailto:research-pubs@uow.edu.au)



**RESEARCH ONLINE**

**University of Wollongong  
Research Online**

---

University of Wollongong Thesis Collection

University of Wollongong Thesis Collections

---

1998

# The influence of the mode of plasma generation on the plasma nitriding behaviour of a micor alloyed [i.e. microalloyed] steel

Farzad Mahboubi

*University of Wollongong*

---

## Recommended Citation

Mahboubi, Farzad, The influence of the mode of plasma generation on the plasma nitriding behaviour of a micor alloyed [i.e. microalloyed] steel, Doctor of Philosophy thesis, University of Wollongong. Department of Materials Engineering, University of Wollongong, 1998. <http://ro.uow.edu.au/theses/1529>

Research Online is the open access institutional repository for the University of Wollongong. For further information contact Manager Repository Services: [morgan@uow.edu.au](mailto:morgan@uow.edu.au).



**RESEARCH ONLINE**

## **NOTE**

This online version of the thesis may have different page formatting and pagination from the paper copy held in the University of Wollongong Library.

## **UNIVERSITY OF WOLLONGONG**

### **COPYRIGHT WARNING**

You may print or download ONE copy of this document for the purpose of your own research or study. The University does not authorise you to copy, communicate or otherwise make available electronically to any other person any copyright material contained on this site. You are reminded of the following:

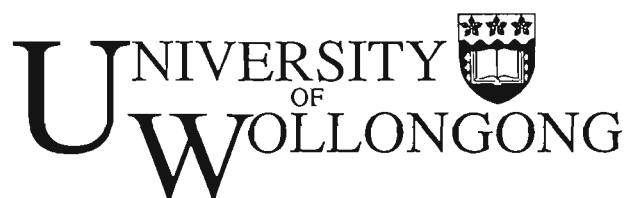
Copyright owners are entitled to take legal action against persons who infringe their copyright. A reproduction of material that is protected by copyright may be a copyright infringement. A court may impose penalties and award damages in relation to offences and infringements relating to copyright material. Higher penalties may apply, and higher damages may be awarded, for offences and infringements involving the conversion of material into digital or electronic form.

**THE INFLUENCE OF THE MODE OF PLASMA  
GENERATION ON THE PLASMA NITRIDING BEHAVIOUR  
OF A MICRALLOYED STEEL**

A thesis submitted in fulfilment of the requirements for the award of the  
degree of

**DOCTOR OF PHILOSOPHY**

from



by

**FARZAD MAHBOUBI, B. Sc., ME. (Hons.)**

**Surface Engineering Research Centre  
Department of Materials Engineering**

December, 1995

## **DECLARATION**

---

I, Farzad Mahboubi, hereby declare that the work presented in this thesis is my own work, except where acknowledged to others, and has not been submitted previously in whole or in part in respect of any other academic record.

.....  
Farzad Mahboubi

## **SYNOPSIS**

---

It is well understood that the introduction of nitrogen into metallic surfaces improves the mechanical properties of engineering components, such as hardness, wear and fatigue as well as the corrosion resistance. In addition to conventional techniques such as salt bath and gas nitriding there are currently several methods which utilise plasma environments for mass transfer, e.g. DC plasma nitriding, RF plasma nitriding and plasma immersion ion implantation (PI<sup>3</sup>).

It was the main aim of this investigation to study the plasma nitriding behaviour of a commercially available chromium bearing microalloyed steel, MAXIMA™, in the hot rolled and air cooled condition. The ultimate goal was to assess the possibility of using it as an alternative to conventional quenched and tempered nitriding steels, such as En19 (AISI 4140) which was used as a reference in this investigation. In order to identify the most suitable gas mixture for the nitriding of MAXIMA™, a comprehensive investigation of DC plasma nitriding at 450°C was performed by varying the hydrogen concentration in the nitriding atmosphere and examining the structure and the properties of the surface layers.

A detailed study of RF plasma nitriding and PI<sup>3</sup> was undertaken using MAXIMA™ steel. In order to gain an insight into the influence of different modes of plasma generation on the formation of the hardened layer and the mass transfer mechanisms involved, a comparison was also made with DC plasma nitriding. All the experiments were conducted on MAXIMA™ steel for five hours at the temperatures of 350, 400, 450, 500 and 550°C.

Optical, scanning electron and atomic force microscopy, in conjunction with microhardness and surface roughness measurements were employed to characterise the nitrided surfaces. X-ray diffraction, both in normal and glancing angle configurations and glow discharge optical emission spectroscopy were also utilised to identify the phases that formed on the surface of nitrided specimens and the concentration profiles of different elements.

It was found that DC plasma nitriding of MAXIMA™ at all temperatures developed cases with higher surface hardness and roughness, and a slightly thinner compound layer and diffusion zone than those obtained from En19 steel .

A comparative study between PI<sup>3</sup> and RF plasma nitriding revealed that the PI<sup>3</sup> process produced surface layers with more favourable properties, such as higher hardnesses and thicker cases, than RF plasma nitriding. Unlike DC plasma nitriding, for the conditions employed no compound layer was formed on the surface of the samples treated by either PI<sup>3</sup> or RF plasma nitriding.

The best case, in terms of hardness and depth, was produced by PI<sup>3</sup> at 350°C and by DC plasma nitriding at higher temperatures. At all temperatures, RF plasma nitriding produced the shallowest cases with the lowest hardnesses.

It has been argued that the mode of plasma generation plays a critical role in nitrogen mass transfer. More specifically, the operating pressure and ion energy have been found to be the key parameters in determining the total nitrogen adsorption on the surface. In DC plasma nitriding mass transfer is primarily controlled by sputtering and re-deposition. The moderate ion energy in DC plasma nitriding causes sputtering of the cathodic surfaces. Sputtered species undergo collision with the nitrogen in the vicinity of the surface because of low mean free path for collision (few millimetres) which is a direct result of the relatively high operating pressure of a DC plasma. In stark contrast, in PI<sup>3</sup> and RF plasma nitriding, the mean free path for collision of the ions and atoms is in the order of several centimetres because of low operating pressure, hence there will be no collisions near the sample and no re-deposition of sputtered material will take place. Owing to extremely high ion energies involved in PI<sup>3</sup>, ion implantation is the dominant mass transfer mechanism and sputtering of surface atoms is considerably lower than DC plasma nitriding. The lack of significantly energised ions in RF plasma nitriding eliminates the possibility of implantation and the main mass transfer mechanism is due to the adsorption of low energy neutral species which are incapable of inducing and sputtering.

## Key Words

Plasma nitriding, DC plasma nitriding, RF plasma nitriding, ion nitriding, glow discharge nitriding, plasma immersion ion implantation (PI<sup>3</sup>), high temperature ion implantation, nitrogen ion implantation, microalloyed steel, HSLA steel.

## **ACKNOWLEDGMENTS**

---

I would like to express my appreciation to my supervisor Dr. M. Samandi for his guidance and helpful supervision throughout the work particularly during the past six months. I would also like to sincerely thank Prof. D. Dunne, my co-supervisor for his help, continued support and encouragement.

Special thanks to the Ministry of Culture and Higher Education of Iran for award of a scholarship which allowed this work to be undertaken.

I am particularly grateful to Dr. G. A. Collins from ANSTO for his close cooperation, useful discussion and help. Grateful thanks to our other friends at ANSTO, Dr. J Tendys and Dr. K. Short, where the RF plasma nitriding and PI<sup>3</sup> treatments were performed with the support of the Australian Institute of Nuclear Science and Engineering. I would also like to thank Dr. M. Marychurch at BHP Research and Technology Centre for his kind cooperation in GDOES of the samples.

All my friends in the department deserve heartfelt thanks for their valuable friendship, especially Mr. A. Abdollahzadeh, M. Doroudian, S. Ghasemi, A. Razaghian, H. Zahiri J. Jones and Dr. C. Montross. I would also like to sincerely thank the secretary of the department, Mrs. R. Cambareri for her helpful and kind manner in dealing with the official matters. Special thanks go to the technical staff of the department, L. Brunckhorst, A. Scobe, G. Hamilton, G. Tillman, N. Mackie, R. Kinnell, R. De Jong, A. Bult and J. Gonzalez for their technical assistance.

Last but by far not least, I would like to express my sincere thanks to my wife and parents for their continuous support, encouragement and patience throughout my studies.

## PUBLICATIONS

---

Mahboubi F., Samandi M., Dunne D., Bloyce A., Bell T; "*Plasma nitriding of microalloyed steel*"; Surface and Coating Technology, 71 (1995) 135.

Mahboubi F., Samandi M., Dunne D.; "*Plasma Immersion Ion Implantation and RF Plasma Nitriding of a Microalloyed Steel*"; submitted to Surface and Coating Technology.

Mahboubi F., Samandi M., Dunne D.; "*Plasma Nitriding Behaviour of Low Alloy and Microalloyed Steels*"; 'The Heat Is On'; Proc. of the first int. conf. on the heat treatment, 24 & 25 May, 1995, Melbourne, Victoria, Institute of Metals & Materials, Australia.

Mahboubi F., Samandi M., Dunne D. and Collins G. A.; "*The Influence of the Mode of Plasma Generation on the Plasma Nitriding Behaviour of a Microalloyed Steel*"; Proc. of the 5th Word Seminar on Heat Treatment and Surface Engineering, 26-29 Sept. 1995, Isfahan, Iran.

# TABLE OF CONTENTS

---

<b>1. CHAPTER ONE: INTRODUCTION AND AIMS</b>	<b>23</b>
<b>1.1 Introduction</b>	<b>23</b>
<b>1.2 Aims of the Project</b>	<b>26</b>
<b>2. CHAPTER TWO: LITERATURE SURVEY</b>	<b>29</b>
<b>2.1 Iron-Nitrogen Phase Diagram</b>	<b>29</b>
<b>2.2 Nitrides of Iron</b>	<b>31</b>
<b>2.3 Structure of Nitrides</b>	<b>33</b>
2.3.1 $\gamma'$ - Fe <sub>4</sub> N	33
2.3.2 $\varepsilon$ - Fe <sub>2</sub> N <sub>(1-x)</sub>	34
2.3.3 $\zeta$ - Fe <sub>2</sub> N	36
2.3.4 $\alpha''$ - Fe <sub>16</sub> N <sub>2</sub>	37
<b>2.4 Nitriding</b>	<b>38</b>
<b>2.5 Kinetics of Nitriding</b>	<b>41</b>
<b>2.6 Nitriding Steels</b>	<b>46</b>
<b>2.7 HSLA Steels or Microalloyed Steels</b>	<b>50</b>
2.7.1 Brief Introduction to MAXIMA™ microalloyed steel	52

<b>2.8 Nitriding of Microalloyed Steels</b>	<b>53</b>
<b>2.9 Plasma Discharges</b>	<b>55</b>
2.9.1 Introduction	55
2.9.2 The DC Glow Discharge	56
2.9.3 Plasma Reaction Processes	62
2.9.4 Ion Interactions With Surface	63
2.9.5 The RF Glow Discharge	66
<b>2.10 Plasma Nitriding</b>	<b>69</b>
2.10.1 Introduction	69
2.10.2 Paschen's Law	71
2.10.3 Partial Pressure Operation	72
2.10.4 Nitrogen Activity	74
2.10.5 Equipment and Operation	75
2.10.6 Advantages and Disadvantages	78
2.10.7 Proposed Nitriding Models	81
<b>2.11 Ion Implantation</b>	<b>85</b>
2.11.1 Introduction	85
2.11.2 Basics of Ion Implantation	86
2.11.3 Strengthening Mechanisms of Ion Implantation	89
2.11.4 Plasma Source Ion Implantation (PSII)	91
2.11.5 Plasma Immersion Ion Implantation (PI <sup>3</sup> )	92
2.11.6 Advantages and Limitations of the Plasma Ion Implantation process	94

### **3. CHAPTER THREE: EXPERIMENTAL PROCEDURE \_\_\_\_\_ 97**

**3.1 Materials \_\_\_\_\_ 97**

**3.2 Specimen Preparation \_\_\_\_\_ 99**

**3.3 DC Plasma Nitriding \_\_\_\_\_ 100**

**3.3.1 Treatment Conditions \_\_\_\_\_ 102**

**3.4 PI<sup>3</sup> and RF Plasma Nitriding \_\_\_\_\_ 104**

**3.4.1 Treatment Conditions \_\_\_\_\_ 106**

**3.5 Characterisation Techniques \_\_\_\_\_ 107**

**3.5.1 Optical Microscopy \_\_\_\_\_ 107**

**3.5.2 Scanning Electron Microscopy \_\_\_\_\_ 107**

**3.5.3 X-ray Diffraction \_\_\_\_\_ 108**

**3.5.4 Glancing Angle X-ray Diffraction \_\_\_\_\_ 108**

**3.5.5 Glow Discharge Optical Emission Spectroscopy \_\_\_\_\_ 108**

**3.5.6 Hardness Measurements \_\_\_\_\_ 109**

**3.5.7 Surface Roughness Measurements \_\_\_\_\_ 110**

**3.5.8 Atomic Force Microscopy \_\_\_\_\_ 111**

### **4. CHAPTER FOUR: RESULTS \_\_\_\_\_ 113**

**4.1 Introduction \_\_\_\_\_ 113**

**4.2 Part I: Effect of Hydrogen Content on DC Plasma Nitriding of  
MAXIMA™ \_\_\_\_\_ 116**

4.2.1 Microstructural Examination	116
4.2.2 X-ray Diffraction	118
4.2.3 Glow Discharge Optical Emission Spectroscopy	120
4.2.4 Hardness Tests	120
4.2.5 Surface Topography	123
<b>4.3 Part II: DC Plasma Nitriding, RF Plasma Nitriding and PI<sup>3</sup></b>	<b>127</b>
4.3.1 Microstructural Examination	127
4.3.2 X-ray Diffraction	137
4.3.3 Glow Discharge Optical Emission Spectroscopy	141
4.3.4 Hardness Tests	147
4.3.5 Appearance of the Treated Samples	154
4.3.6 Surface Topography	155
<b>5. CHAPTER FIVE: DISCUSSION</b>	<b>171</b>
<b>5.1 Effect of Hydrogen on Layer Formation in DC Plasma Nitriding</b>	<b>171</b>
<b>5.2 Comparative Study of DC Plasma Nitriding Behaviour of MAXIMA™ and En19 Steels</b>	<b>176</b>
<b>5.3 Plasma Immersion Ion Implantation (PI<sup>3</sup>) and RF Plasma Nitriding of MAXIMA™</b>	<b>183</b>
<b>5.4 GENERAL DISCUSSION: The Influence of the Mode of Plasma Generation on the Plasma Nitriding Behaviour of MAXIMA™</b>	<b>188</b>
5.4.1 Introduction	188

5.4.2 Discussion	189
<b>6. CHAPTER SIX: CONCLUSIONS</b>	<b>204</b>
6.1 Effect of Hydrogen Content on DC Plasma Nitriding of MAXIMA™	204
6.2 Comparative Study of MAXIMA™ and En19 Steels	205
6.3 Plasma Immersion Ion Implantation and RF Plasma Nitriding of MAXIMA™	206
6.4 The Influence of the Mode of Plasma Generation on the Nitriding Behaviour of MAXIMA™	207
<b>7. APPENDICES</b>	<b>209</b>
7.1 Appendix A: Metallography of Nitrided Samples	209
7.1.1 Edge Retention	209
7.1.2 Grinding and Polishing	210
7.1.3 Etching	211
7.1.4 Nickel Electroplating in Watts Bath	212
7.2 Appendix B: Glow Discharge Optical Emission Spectroscopy	215
7.3 Appendix C Surface Roughness Measurement	218
7.4 Appendix D: Atomic Force Microscope	221
<b>8. REFERENCES</b>	<b>224</b>

# LIST OF FIGURES

---

<b>Figure 1.</b> Iron-Nitrogen phase diagram (Kubaschewski, 1982).	30
<b>Figure 2.</b> Octahedral of metal atoms in the three closed-packed metal arrangements (Jack and Jack, 1973).	33
<b>Figure 3.</b> The structure of nitrogen austenite and $\gamma'$ -Fe <sub>4</sub> N (Jack, 1948).	34
<b>Figure 4.</b> The crystal structure of epsilon nitride (Jack 1952).	35
<b>Figure 5.</b> The crystal structure of epsilon and zeta iron nitrides (Jack and Jack, 1973).	36
<b>Figure 6.</b> Crystal structure of $\alpha''$ -Fe <sub>16</sub> N <sub>2</sub> (Jack, 1989).	37
<b>Figure 7.</b> Crystal structure of $\alpha''$ -Fe <sub>16</sub> N <sub>2</sub> as a defect of fcc $\gamma'$ structure (Jack, 1975).	38
<b>Figure 8.</b> (a) Microhardness profiles of a "strong" interaction; (b) schematic drawing of the TiN, Ti, and N concentrations for a given nitriding time (Lightfoot and Jack, 1975).	42
<b>Figure 9.</b> (a) Microhardness profiles of a "weak" interaction or difficult nucleation; (b) schematic drawing of the concentrations of the nitride phase (in this case a metastable zone), Mo and N (Lightfoot and Jack, 1975).	45
<b>Figure 10.</b> (a) Microhardness profiles for an "intermediate" interaction; (b) schematic drawing of the concentrations of CrN, Cr, and N (Lightfoot and Jack, 1975).	46
<b>Figure 11.</b> Influence of alloying elements on hardness after nitriding. Base alloy 0.35% C, 0.30% Si, 0.70% Mn (Thelning, 1975).	47

**Figure 12.** Influence of alloying elements on depth of nitriding measured at 400 HV.

Nitriding for 8 h at 520 °C (Thelning, 1975). \_\_\_\_\_ 49

**Figure 13.** Current/voltage characteristic for a DC discharge. \_\_\_\_\_ 57

**Figure 14.** various regions between the cathode an the anode of a glow discharge and the accompanying changes in voltage, field strength, and net space charge across it (Howatson, 1965). \_\_\_\_\_ 60

**Figure 15.** (a) Inductively coupled plasma reactor. An alternating current power source creates a time varying current, the magnetic field from which generates a voltage that sustains the discharge. (b) Capacitively coupled plasma reactor. Similar to (a), except the two plates are used to create an electric field to sustain the discharge (Rossnagel et al, 1990). \_\_\_\_\_ 68

**Figure 16.** Electron energy vs. electron density in glow discharge plasmas compared to other well-known plasmas (Grube and Stephen; Kossoswsky (ed.), 1989). \_\_\_\_\_ 70

**Figure 17.** Paschen curves for a DC glow discharge between parallel-plate electrodes for various gases. The breakdown voltage,  $V_b$ , is plotted against  $P.d$  (the gas pressure times the distance,  $d$ , between the electrodes on log-log coordinates) (Grube and Stephen; Kossoswsky (ed.), 1989). \_\_\_\_\_ 71

**Figure 18.** Number of gas molecules versus probability of ionisation (Dressler; Sudarshan (ed.), 1989). \_\_\_\_\_ 73

**Figure 19.** Plasma nitriding unit. \_\_\_\_\_ 76

**Figure 20.** Relative glow distribution at (a) low pressure, and (b) increased pressure, for typical plasma nitriding gases (Kovacs and Russell, 1987). \_\_\_\_\_ 77

<b>Figure 21.</b> Surface reactions occurring during plasma nitriding (Edenhofer, 1974, part 1).	82
<b>Figure 22.</b> Processes occurring in a typical collision cascade (Solnick-Legg and Legg; Sudarshan (ed.), 1989).	88
<b>Figure 23.</b> Optical micrograph of as received (hot-rolled and air cooled) MAXIMA™ microalloyed steel, showing proeutectoid ferrite plus some bainitic products. Etched in 2.5% Nital.	98
<b>Figure 24.</b> Optical micrograph of En19 steel, showing some undissolved carbide in a matrix of tempered martensite. Etched in 2.5% nital.	98
<b>Figure 25.</b> 5 kW DC plasma nitriding unit designed and commissioned at the Surface Engineering Research Centre at the University of Wollongong.	102
<b>Figure 26.</b> Schematic of the DC plasma nitriding apparatus.	103
<b>Figure 27.</b> Schematic drawing of the table and samples used in the DC plasma nitriding unit.	103
<b>Figure 28.</b> Schematic of the PI <sup>3</sup> and RF plasma nitriding apparatus. Note that in PI <sup>3</sup> the sample is connected to the high voltage circuit while in RF plasma nitriding the sample is placed on a resistively heated stage.	106
<b>Figure 29.</b> SEM micrograph obtained from the surface of MAXIMA™ plasma nitrided for 5h at 450 °C in 75%N <sub>2</sub> -25% H <sub>2</sub> atmosphere.	111
<b>Figure 30.</b> The NanoScope® Atomic Force Microscope (AFM), from Digital Instruments, at the University of Wollongong.	112
<b>Figure 31.</b> Optical micrographs of cross-sections of MAXIMA™ ((a), (c)) and En19 ((b), (d)) specimens plasma nitrided for 5 h at nominal 550 °C using a 40 kW	

commercial scale unit. Samples were etched in 2.5% nital ((a), (b)), and 2.5% nital followed by Oberhoffer's, reagent ((c), (d)).

115

**Figure 32.** SEM micrograph showing the compound layer formed on the surface of MAXIMA™ plasma nitrided for 5h at 450 °C in atmospheres containing (a) 100% N<sub>2</sub>, (b) 75%N<sub>2</sub>-25% H<sub>2</sub>, (c) 50%N<sub>2</sub>-50% H<sub>2</sub>, and (d) 25%N<sub>2</sub>-75% H<sub>2</sub>. The samples were etched in 2.5% nital followed by Oberhoffer's reagent.

117

**Figure 33.** The effect of hydrogen concentration of the treatment atmosphere on the compound layer thickness formed on the surface of the treated MAXIMA™ samples.

118

**Figure 34.** X-ray diffraction patterns of the MAXIMA™ samples DC plasma nitrided at 450 °C for 5hrs at various N<sub>2</sub>+H<sub>2</sub> gas mixtures.

119

**Figure 35.** GDOES depth profiles for MAXIMA™ steel DC plasma nitrided at 450 °C in (a) 100% N<sub>2</sub>, (b) 75% N<sub>2</sub> - 25% H<sub>2</sub>, (c) 50% N<sub>2</sub> - 50% H<sub>2</sub>, and (d) 25% N<sub>2</sub> - 75% H<sub>2</sub>.

121

**Figure 36.** Surface hardness at different loads for samples DC plasma nitrided at 450 °C for 5 hours in atmospheres with different hydrogen concentrations.

122

**Figure 37.** The effect of hydrogen concentration in the treatment atmosphere on the hardness profile of the samples DC plasma nitrided at 450 °C for 5 hours.

122

**Figure 38.** The effect of hydrogen concentration in the nitriding atmosphere on the surface roughness of MAXIMA™ samples expressed as R<sub>a</sub>.

124

**Figure 39.** AFM image of plasma nitrided surfaces treated at 450 °C for 5 hours at atmospheres containing different H<sub>2</sub>-N<sub>2</sub> gas mixtures, (a) 100%N<sub>2</sub>, (b) 75%N<sub>2</sub>-25%H<sub>2</sub>.

125

**Figure 40.** AFM image of plasma nitrided surfaces treated at 450 °C for 5 hours at atmospheres containing different H<sub>2</sub>-N<sub>2</sub> gas mixtures, (a) 50%N<sub>2</sub>-50%H<sub>2</sub> and (b) 25%N<sub>2</sub>-75%H<sub>2</sub>. \_\_\_\_\_ 126

**Figure 41.** Optical micrographs of cross-sections of MAXIMA™ ((a), (c)) and En19 ((b), (d)) specimens plasma nitrided in 75%N<sub>2</sub> - 25%H<sub>2</sub> for 5 h at 450 °C and etched in 2.5% nital ((a), (b)), and 2.5% nital followed by Oberhoffer's reagent ((c), (d)). \_\_\_\_\_ 129

**Figure 42.** SEM micrographs of cross-sections of (a) MAXIMA™ and (b) En19 specimens plasma nitrided in 75%N<sub>2</sub> - 25%H<sub>2</sub> for 5 hours at 350 °C and etched in 2.5% nital followed by Oberhoffer's reagent. \_\_\_\_\_ 130

**Figure 43.** SEM micrographs of cross-sections of (a) MAXIMA™ and (b) En19 specimens plasma nitrided in 75%N<sub>2</sub> - 25%H<sub>2</sub> for 5 hours at 450 °C and etched in 2.5% nital followed by Oberhoffer's reagent. \_\_\_\_\_ 131

**Figure 44.** SEM micrographs of cross-sections of (a) MAXIMA™ and (b) En19 specimens plasma nitrided in 75%N<sub>2</sub> - 25%H<sub>2</sub> for 5 hours at 550 °C and etched in 2.5% nital followed by Oberhoffer's reagent. \_\_\_\_\_ 132

**Figure 45.** Comparison of the thickness of the compound layers formed on the surfaces of both steel DC plasma nitrided under similar conditions. \_\_\_\_\_ 133

**Figure 46.** Typical microstructures obtained from the transverse cross-section of MAXIMA™ steel (a) PI<sup>3</sup> and (b) RF plasma nitrided in 75%N<sub>2</sub> - 25%H<sub>2</sub> at 350 °C for 5 hours. Marbles etchant. \_\_\_\_\_ 134

**Figure 47.** SEM micrographs of cross-sections of MAXIMA™ steel PI<sup>3</sup> treated in 75%N<sub>2</sub> - 25%H<sub>2</sub> for 5 hours at (a) 350, (b) 450, and (c) 550 °C. The samples were etched in 2.5% nital followed by Oberhoffer's reagent. \_\_\_\_\_ 135

**Figure 48.** SEM micrographs of cross-sections of MAXIMA™ steel RF plasma nitrided in 75% $N_2$  - 25% $H_2$  for 5 hours at (a) 350, (b) 450, and (c) 550 °C. The samples were etched in 2.5% nital followed by Oberhoffer's reagent. \_\_\_\_\_ 136

**Figure 49.** X-ray diffraction patterns of the MAXIMA™ and En19 samples in the as polished condition. \_\_\_\_\_ 137

**Figure 50.** X-ray diffraction patterns of the MAXIMA™ samples DC plasma nitrided in 75% $N_2$  - 25% $H_2$  for 5 hours at various temperatures indicated. \_\_\_\_\_ 138

**Figure 51.** X-ray diffraction patterns of the En19 samples DC plasma nitrided in 75% $N_2$  - 25% $H_2$  for 5 hours at various temperatures indicated. \_\_\_\_\_ 139

**Figure 52.** Glancing angle X-ray diffraction pattern of (a) PI<sup>3</sup>, (b) RF plasma nitrided samples treated at 350 °C. Co K $\alpha$  radiation, 1° incident angle and 10 sec/step of 0.1°. \_\_\_\_\_ 141

**Figure 53.** GDOES depth profile for MAXIMA™ steel DC plasma nitrided at (a) 350, (b) 450, and (c) 550 °C. \_\_\_\_\_ 143

**Figure 54.** GDOES depth profile for En19 steel DC plasma nitrided at (a) 350, (b) 450, and (c) 550 °C. \_\_\_\_\_ 144

**Figure 55.** Nitrogen and carbon line profiles obtained by GDOES of the PI<sup>3</sup> treated samples at (a) 350, (b) 450, and (c) 550 °C. \_\_\_\_\_ 145

**Figure 56.** Nitrogen and carbon line profiles obtained by GDOES of the RF plasma nitrided samples at (a) 350, (b) 450, and (c) 550 °C. \_\_\_\_\_ 146

**Figure 57.** Hardness profiles of MAXIMA™ steel DC plasma nitrided at different temperatures. \_\_\_\_\_ 148

**Figure 58.** Hardness profiles of En19 steel DC plasma nitrided at different temperatures. \_\_\_\_\_ 148

**Figure 59.** Case depth of the samples DC plasma nitrided at different temperatures for 5 hours. \_\_\_\_\_ 149

**Figure 60.** The peak hardness and the core hardness of the samples after DC plasma nitriding at different temperatures. Note the hardness of the samples before treatment. \_\_\_\_\_ 150

**Figure 61.** Surface hardness at different loads for (a) PI<sup>3</sup> and (b) RF plasma nitrided samples. \_\_\_\_\_ 151

**Figure 62.** Hardness profiles of (a) PI<sup>3</sup> and (b) RF plasma nitrided samples at different temperatures for 5 hours. \_\_\_\_\_ 152

**Figure 63.** The peak surface hardness developed on the samples treated at temperatures ranging from 350 to 550C° by the PI<sup>3</sup> and RF plasma nitriding processes. \_\_\_\_\_ 153

**Figure 64.** Surface appearance of MAXIMA™ sample DC plasma nitrided at 550 °C. Note the dark ring parallel to the edge of the sample. \_\_\_\_\_ 154

**Figure 65.** Comparison of the surface roughness of both steels DC plasma nitrided under identical conditions for 5 hours at different temperatures. \_\_\_\_\_ 156

**Figure 66.** AFM images from the surface of (a) MAXIMA™ and (b) En19 samples DC plasma nitrided at 350 °C. \_\_\_\_\_ 158

**Figure 67.** AFM images from the surface of (a) MAXIMA™ and (b) En19 samples DC plasma nitrided at 450 °C. \_\_\_\_\_ 159

**Figure 68.** AFM images from the surface of (a) MAXIMA™ and (b) En19 samples DC plasma nitrided at 550 °C. \_\_\_\_\_ 160

**Figure 69.** AFM images from the surface of (a) MAXIMA™ and (b) En19 samples DC plasma nitrided at 550 °C at higher horizontal magnification. Note the nodular morphology of the deposited iron nitrides resembling the morphology of the CVD coatings. \_\_\_\_\_ 161

**Figure 70.** SEM of the surface of MAXIMA™ sample DC plasma nitrided at 550 °C at two magnifications. \_\_\_\_\_ 162

**Figure 71.** SEM of the surface of En19 sample DC plasma nitrided at 550 °C at two magnifications. \_\_\_\_\_ 163

**Figure 72.** Surface roughness ( $R_a$ ) for MAXIMA™ steel treated by PI<sup>3</sup> and RF plasma nitriding processes. \_\_\_\_\_ 165

**Figure 73.** Optical micrographs obtained from the surface of the MAXIMA™ samples treated by the PI<sup>3</sup> process at (a) 350 °C, (b) 450 °C and (c) 550 °C. \_\_\_\_\_ 166

**Figure 74.** Optical micrographs obtained from the surface of the MAXIMA™ samples RF plasma nitrided at (a) 350 °C, (b) 450 °C and (c) 550 °C. \_\_\_\_\_ 167

**Figure 75.** AFM images from the surface of the (a) PI<sup>3</sup> and (b) RF plasma nitrided samples at 350 °C. \_\_\_\_\_ 168

**Figure 76.** AFM images from the surface of the (a) PI<sup>3</sup> and (b) RF plasma nitrided samples at 450 °C. \_\_\_\_\_ 169

**Figure 77.** AFM images from the surface of the (a) PI<sup>3</sup> and (b) RF plasma nitrided samples at 550 °C. \_\_\_\_\_ 170

**Figure 78.** The changes in the applied voltage and current with changes in the hydrogen concentration of the treatment atmosphere. All the treatments were carried out at 450 °C for 5 hours. \_\_\_\_\_ 174

**Figure 79.** The voltage and current applied at different treatment temperatures for DC plasma nitriding. \_\_\_\_\_ 181

**Figure 80.** Hardness profiles of the MAXIMA™ samples treated with different processes at (a) 350, (b) 450 and (c) 550 °C for 5 hours. \_\_\_\_\_ 190

**Figure 81.** Comparison of the surface roughness,  $R_a$ , values obtained from the samples treated by different processes. \_\_\_\_\_ 191

**Figure 82.** Thickness of the compound layer formed on the surface of the DC plasma nitrided samples. \_\_\_\_\_ 191

**Figure 83.** X-ray diffraction patterns of the samples nitrided at 450 °C by (a) DC plasma, (b) PI<sup>3</sup>, and (c) RF plasma. \_\_\_\_\_ 192

**Figure 84.** Proposed models for nitrogen mass transfer in (a) DC plasma nitriding, (b) RF plasma nitriding, and (c) plasma immersion ion implantation (PI<sup>3</sup>). \_\_\_\_\_ 193

**Figure 85.** AFM images showing the surface topography of the samples treated by (a) DC plasma nitriding, (b) PI<sup>3</sup> and (c) RF plasma nitriding at 350 °C. \_\_\_\_\_ 196

**Figure 86.** AFM images showing the surface topography of the samples treated by (a) DC plasma nitriding, (b) PI<sup>3</sup> and (c) RF plasma nitriding at 450 °C. \_\_\_\_\_ 197

**Figure 87.** AFM images showing the surface topography of the samples treated by (a) DC plasma nitriding, (b) PI<sup>3</sup> and (c) RF plasma nitriding at 550 °C. \_\_\_\_\_ 198

**Figure 88.** SEM micrographs of samples (a) DC plasma nitrided (b) PI<sup>3</sup>, and (c) RF plasma nitrided at 350 °C. \_\_\_\_\_ 199

**Figure 89.** SEM micrographs of samples (a) DC plasma nitrided (b) PI<sup>3</sup>, and (c) RF plasma nitrided at 450 °C. \_\_\_\_\_ 200

**Figure 90.** SEM micrographs of samples (a) DC plasma nitrided (b) PI<sup>3</sup>, and (c) RF plasma nitrided at 550 °C. \_\_\_\_\_ 201

**Figure 91.** Schematic diagram of a Grimm lamp (Berneron et al, 1980). \_\_\_\_\_ 215

**Figure 92.** Graphical derivation of  $R_a$  (a) profile with centre line, (b) lower portions of the profile inverted and (c)  $R_a$  is the mean height of the profile. \_\_\_\_\_ 220

**Figure 93.** Schematic of a generalised scanning probe microscope (Howland et al, 1993). \_\_\_\_\_ 222

**Figure 94.** Beam deflection system for vertical motion detection. This system has the sensitivity to detect vertical motion of 0.01 nm as the tip scans the sample surface (Strausser and Heaton, 1994). \_\_\_\_\_ 223

## List of Tables

---

<b>Table 1.</b> Phases in the iron-nitrogen system; after Ruhl and Cohen (1969).	32
<b>Table 2.</b> Some nitride phases of the commonly occurring alloying elements in nitrided steels (Goldschmidt, 1967).	42
<b>Table 3.</b> Chemical composition of MAXIMA™ and En19 steels obtained by spark emission spectroscopy.	97
<b>Table 4.</b> Hardness ( $HV_{20}$ ) of the materials prior to surface treatment.	99
<b>Table 5.</b> $PI^3$ treatments parameters.	105
<b>Table 6.</b> Core hardness values obtained from the samples after DC plasma nitriding treatments.	149
<b>Table 7.</b> Surface roughness $R_a$ results after $PI^3$ and RF plasma nitriding at different temperatures for 5 hours in 75% $N_2$ -25% $H_2$ gas mixture.	165
<b>Table 8.</b> List of etching reagents and etching conditions (Mridha, 1982).	212
<b>Table 9.</b> The Watts bath compositions and it operational conditions (Samuels, 1967).	214

# **1. CHAPTER ONE:**

## **INTRODUCTION AND AIMS**

---

### **1.1 Introduction**

Modification of the surface or near surface region of engineering components such as bearings, dies, gears, shafts, and other parts for the purposes of improving appearance or performance is an important part of modern manufacturing practice. This is not surprising, since the interaction of materials with often hostile environments begins at the surface and it is from surface-initiated effects that most components fail. In many cases, tribological properties (friction and/or wear) are the limiting factor in performance and much more attention is now paid to understanding and optimising the tribological, as well as other properties, of the surfaces of engineering components.

The discipline of "Surface Engineering" emerged almost 15 years ago and has been greatly influenced and driven by the realisation that the surface is the most friable part of any engineering component. Surface Engineering encompasses many areas in engineering, physics, and materials science.

The fundamental principle of Surface Engineering was established when it was realised that it is inherently inefficient to utilise an expensive material in bulk simply to obtain the required surface properties. A more appropriate engineering solution is to use a cheaper,

more easily-formed, underlying material with adequate base properties and then to enhance the surface properties, either by deposition of suitable coatings or surface modification to provide an improved overall performance in service (Strafford *et al*, 1990). The engineering solution of forming essentially a composite material with enhanced properties in a case supported by a cheaper core material is almost always less expensive than the alternative, (where it is even possible), of using a bulk material with the desired combination of properties.

Surface engineering processes which are currently used to produce a hard surface on metal components fall into two broad categories. The first category includes those in which the hardened surface is produced by a heat treatment, usually accompanied or preceded by the diffusion of elements, such as carbon or nitrogen, into the surface. The second category is of those in which a layer of hard material is formed or deposited on the surface (Spalvins, 1987).

The introduction of nitrogen into metallic surfaces has been practised for a long time in order to improve mechanical properties, such as hardness, wear and fatigue as well as the corrosion resistance of industrial parts. To achieve this goal, several methods have been developed using gaseous, salt-bath or plasma environments.

Plasma nitriding is now widely used to impart surface hardening to metals, particularly steels, for a wide variety of applications. As the name implies, the process is carried out in a plasma medium containing ionised/excited nitrogen, alone or in combination with other gases, to react with the work surface. The process was independently patented by Egan (1931) and Berghaus (1932, 1939) and following advances in the field of power electronics, has been commercially available since the early 1970s. It is widely used in

the machinery, car and oil industries and for measuring instruments, parts of aircraft engines, diesel engines, turbines, cutting tools and dies.

Plasma immersion ion implantation (PI<sup>3</sup>), on the other hand, is a relatively new innovation developed by the Australian Nuclear Science and Technology Organisation (ANSTO). Details of the technique were first published in 1988 (Tendys *et al*, 1988) and development of it has continued (Collins *et al*, 1991; Hutchings *et al*, 1992, Collins *et al*, 1993). PI<sup>3</sup> is a hybrid technique, combining plasma nitriding and nitrogen ion implantation. In this technique the workpiece is immersed in an inductively coupled radiofrequency (RF) nitrogen plasma and implanted by the application of a pulsed negative bias of 45 kV.

In the PI<sup>3</sup> technique, the sample is heated by the high voltage ion bombardment but an RF plasma nitriding treatment without any ion implantation is also possible in which the specimen is heated to the nitriding temperatures, using auxiliary heating through a resistively heated stage.

By combining HV ion bombardment with low pressure RF plasma nitriding, PI<sup>3</sup> offers the possibility of lowering the treatment temperature. This is particularly interesting for the treatment of steels such as some HSLA steels which soften at normal nitriding temperatures.

## 1.2 Aims of the Project

In the plasma nitriding process, the part to be nitrided is usually in the quenched and tempered (Q&T) condition in order to obtain the desired physical properties of the core, to ensure proper grain refinement, and to have a stable microstructure at the plasma nitriding temperature.

Microalloyed or high strength low alloy (HSLA) steels are carbon-manganese steels containing small amounts of Nb, V or Ti. The excellent mechanical properties of these alloys, particularly high yield strength, usually obviate the need for expensive quench and tempering operations. Microalloying principles have been applied to some higher alloy steels for use in the quench and tempered condition, but such steels also have the potential for direct use after hot forming which is the processing route used for microalloyed low carbon structural steels. Furthermore, the presence of a significant amount of nitride forming elements in these higher alloy steels has generated interest in their applicability as a new generation of nitriding steels. Thus, substituting a traditional nitriding steel with a microalloyed steel would allow elimination of an expensive quench and tempering operation and simplify the manufacturing steps, leading to a significant cost reduction and time saving.

One of the objectives of this project was to study the response to plasma nitriding of a commercially available hot rolled chromium-bearing microalloyed steel, "MAXIMA<sup>TM</sup>", and the possibility of using it as an alternative to conventional nitriding steels. Since En19 (AISI 4140) steel is the most widely used nitriding alloy in industry and much work has been carried out on its nitriding behaviour (Bell *et al*, 1975; Jones *et al*, 1975;

Edenhofer, 1980; Robino and Inal, 1983), it was selected as a reference for comparison with MAXIMA™.

Over the past 35 years a number of theories have been proposed to model what occurs at the plasma-surface interface and in the bulk material during plasma nitriding. However, it is difficult to develop a unique picture of the mechanisms involved due to the complexity of the process and since the experimental results obtained under different process conditions employed different materials. Consequently, there is no universally accepted model which conclusively explains the mass transfer of nitrogen to the workpiece surface and the layer formation mechanisms. Therefore, the other objective of this project was to make a laboratory scale investigation to compare the effects of different modes of plasma generation on the formation of nitrided surface layers by studying the compound layer and diffusion zones formed on MAXIMA™ steel during DC plasma nitriding, RF plasma nitriding, and plasma immersion ion implantation, PI<sup>3</sup>. Furthermore, in an effort to separate the influence of high voltage implantation and thermochemical treatment, a comparison was made between the RF plasma nitriding process and PI<sup>3</sup>.

Throughout this work, unlike the traditionally employed pure nitrogen atmosphere in PI<sup>3</sup> treatments, a 75%N<sub>2</sub>-25%H<sub>2</sub> atmosphere has been used. This was done for two main reasons; to compare the PI<sup>3</sup> treatment with the DC and RF plasma nitriding processes which were also carried out in atmospheres with the same N<sub>2</sub>-H<sub>2</sub> percentages, and to study PI<sup>3</sup> in the atmospheres with lower N<sub>2</sub> concentrations.

In Chapter Two, some fundamental principles of glow discharges and plasmas, plasma nitriding processes and nitrides in steels are reviewed. Particular emphasis has been

placed on plasma nitriding and the physics of plasmas, interaction of plasmas with surfaces and proposed models of plasma nitriding. Experimental procedure, the details of different plasma processing apparatus and characterisation techniques are presented in Chapter Three. Experimental results and discussion are given in Chapter Four and Chapter Five, respectively. Chapter Six contains the conclusions obtained from this work.

## **2. CHAPTER TWO: LITERATURE SURVEY**

---

The nitriding process has been known since the beginning of this century, when Braune in 1905 found that heating steel to 800°C in a flowing stream of ammonia could change its mechanical properties and microstructure (Shoemaker, 1975). Chizhevskii in 1907-1914 carried out the first systematic investigations of nitriding and of the reaction of nitrogen with iron, steel and other metals. He also studied the properties of many nitrides, determined the optimum temperature for the reactions between nitrogen and iron in ammonia and laid down the principles of the Fe-N phase diagram (Karpenko, *et al*, 1979). Since then, variants of the nitriding process have continuously been developed and it can now be applied to a much larger number of steels than was originally thought possible. Nitriding can in practice be performed in powder, liquid, gas or plasma transfer media. However, the emphasis of this literature review is placed on plasma nitriding.

### **2.1 Iron-Nitrogen Phase Diagram**

Figure 1 shows an iron-nitrogen phase diagram constructed by Kubaschewski (1982). The maximum solubility of nitrogen in  $\alpha$  (Fe) in equilibrium with  $\gamma'$ -Fe<sub>4</sub>N is 0.1 wt.% (0.4 at.%) at 590 °C, the eutectoid temperature. The lattice parameter is practically identical to that of  $\alpha$ -Fe. The solubility at room temperature is only  $10^{-4}$  wt.%, therefore on quench aging either pure nitrogen-ferrite or any ferritic alloy nitrided under

the usual commercial conditions,  $\gamma$  might be expected to precipitate (Jack, 1975). The  $\gamma$  phase is isomorphous with the  $\gamma$ -austenite phase in the Fe-C system and has a fcc structure (Kubaschewski, 1982). When the nitrogen content exceeds 0.1 wt.% (0.4 at. %),  $\gamma$ -nitride with the chemical formula  $\text{Fe}_4\text{N}$  is formed.

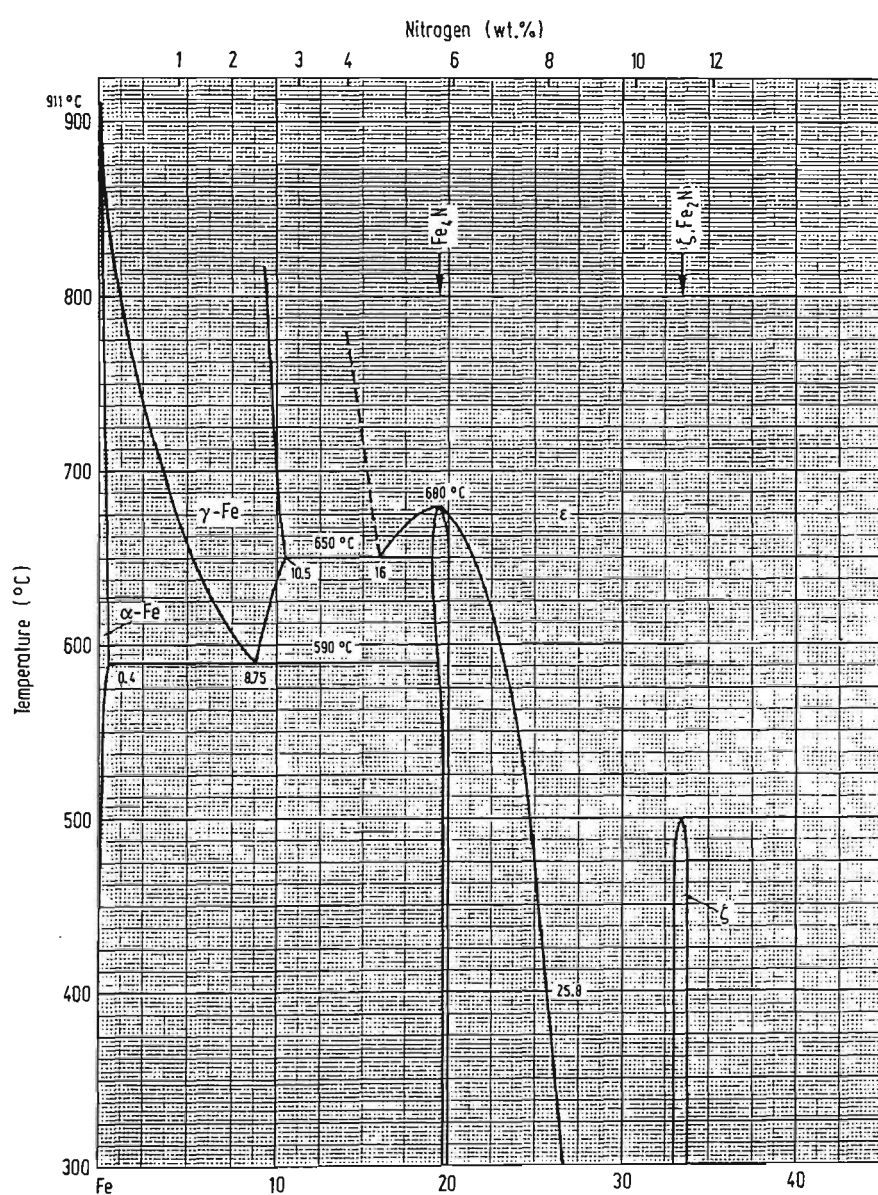


**Figure 1.** Iron-Nitrogen phase diagram (Kubaschewski, 1982).

If the nitrogen concentration exceeds about 6 wt.% (26.4 at.%), the  $\gamma'$ -nitride starts to change into  $\epsilon$ -nitride, the chemical formula of which is  $\text{Fe}_2\text{N}$ . Below 500 °C  $\zeta$ -nitride begins to form. The nitrogen content of this phase is about 11wt.% (49 at.%) and its chemical formula is  $\text{Fe}_2\text{N}$ . In the  $\zeta$ - $\text{Fe}_2\text{N}$  structure the Fe atoms retain the same relative position as in  $\epsilon$ - $\text{Fe}_2\text{N}$ , however, because of a rearrangement of the nitrogen atoms, which in  $\zeta$  are more closely packed in one direction, the iron-atom lattice is anisotropically distorted, (Jack 1952).

## 2.2 Nitrides of Iron

Table 1 lists the phases of the iron-nitrogen system. All the nitrides displayed in this table are metastable with respect to one atmosphere of molecular nitrogen. However, they are usually found during the nitriding of steels or during the aging of nitrogen-ferrite (Jack and Jack, 1973). Molecular nitrogen is the phase in equilibrium with solid solutions of nitrogen in iron. Nevertheless there is a great deviation from thermodynamic equilibrium and the phases produced are highly metastable with respect to nitrogen. For example, the maximum solubility of nitrogen in austenite is 0.26 wt% in equilibrium with one atmosphere nitrogen gas, but is 2.8 wt% with respect to  $\gamma'$ - $\text{Fe}_4\text{N}$ , for which the corresponding equilibrium pressure of gaseous nitrogen is  $10^4$  atm (Jack and Jack, 1973).

There are two types of interstices in the metal-atom arrangements of iron, surrounded respectively by a tetrahedron of four metal atoms and by an octahedron of six metal atoms. Carbon and nitrogen always occupy the octahedral holes in fcc  $\gamma$ -austenite and bcc  $\alpha$ -ferrite and never the tetrahedral ones. The octahedron in the bcc structure is

distorted compared with the regular octahedron of metal atoms in the fcc and cph structures, Figure 2. The regular metal-atom environment is rebuilt by the insertion of interstitial carbon or nitrogen but a large anisotropic strain in the surrounding matrix is produced. Therefore the solubility of nitrogen in  $\alpha$ -iron is very small, see Table 1. There is an isotropic expansion as interstitial atoms fill the octahedral holes in fcc iron. At equal interstitial atom: metal-atom ratios, the unit-cell dimensions of Fe-C and Fe-N austenites are approximately equal.

**Table 1.** Phases in the iron-nitrogen system; after Ruhl and Cohen (1969).

Phase	Composition	Wt.%N	At.%N	Interstitial atoms per 100 iron atoms	Bravais lattice	Unit-cell dimensions, Å
Ferrite ( $\alpha$ )	Fe	0.10	0.40	—	bcc	a, 2.8664
Austenite ( $\gamma$ )	Fe	2.8	11	12.4	fcc	a, 3.572+0.0078 (at %N)
Martensite ( $\alpha'$ )	Fe	2.6	10	11.1	bct	a, 2.8664-0.0018 (at ratio %N)
						c/a, 1.000+0.0091 (at ratio %N)
$\alpha''$	$Fe_{16}N_2$	3.0	11.1	12.5	bc tertag.	a, 5.72
						c/a, 1.10
$\gamma'$	$Fe_4N$	5.9	20	25	cubic	a, 3.795
$\epsilon$	$Fe_2N_{(1-x)}$	4.5-11.0	18-32	22-49.3	hex.	a, 2.764*(at 35 at.%N)
						c/a, 1.599
$\xi$	$Fe_2N$	11.14	33.3	50	ortho.	a, 5.530
						b, 4.480
						c, 4.425

\* Unit cell for cph metal atom arrangement at composition limit  $Fe_2N$ .

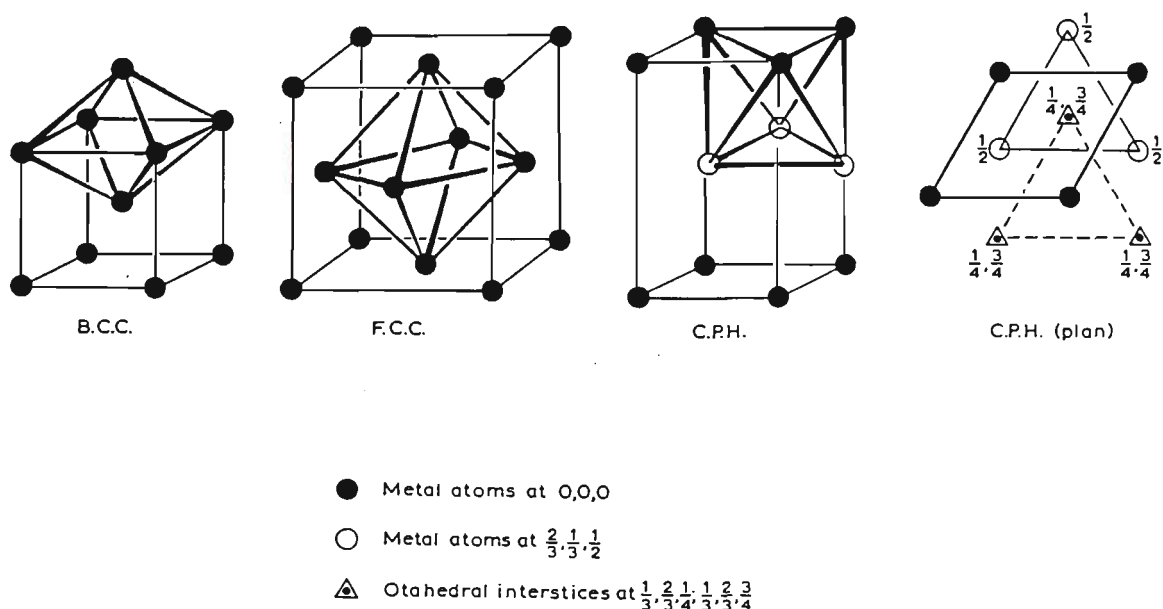


**Figure 2.** Octahedral of metal atoms in the three closed-packed metal arrangements (Jack and Jack, 1973).

## 2.3 Structure of Nitrides

### 2.3.1 $\gamma'$ - $\text{Fe}_4\text{N}$

Gamma prime nitride exists over a narrow range of composition corresponding approximately to the stoichiometric composition  $\text{Fe}_4\text{N}$  and is stable only below 680°C.

Figure 1. Perfect stoichiometry gives a nitrogen content of 5.9 wt.%. The metal-atom arrangement is fcc like that of nitrogen austenite, Figure 3. However, unlike austenite, the nitrogen atoms are not situated at random, but occupy one-quarter of the number of octahedral interstices in a completely ordered manner (Jack, 1948). This is to minimise the strain energy and the mutual repulsion between neighbouring nitrogen atoms.

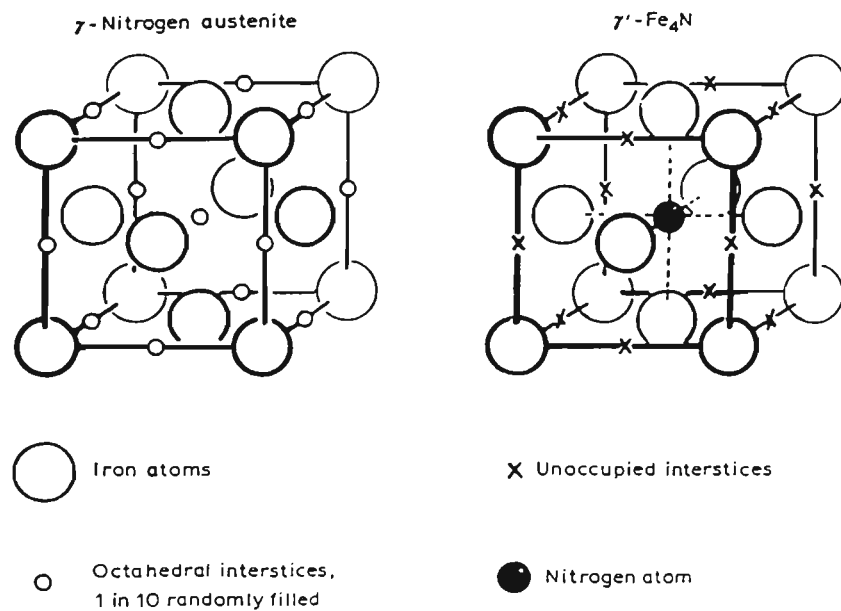


**Figure 3.** The structure of nitrogen austenite and  $\gamma'\text{-Fe}_4\text{N}$  (Jack, 1948).

Gamma prime -  $\text{Fe}_4\text{N}$  is the only iron-nitride which occurs by decomposition of nitrogen-austenite above the martensite start temperature  $M_s$ . Although  $\gamma'\text{-Fe}_4\text{N}$  is metastable with respect to nitrogen gas, it persists for prolonged periods at temperatures below 650°C. The decomposition of  $\gamma'\text{-Fe}_4\text{N}$  to form molecular nitrogen is inhibited by the sluggishness of the surface reaction:  $2\text{N} \rightleftharpoons \text{N}_2$ . The phase has a Curie temperature of 490°C (Jack and Jack, 1973).

### 2.3.2 $\epsilon$ - $\text{Fe}_{2-\text{x}}\text{N}_{(\text{1}-\text{x})}$

The epsilon phase exists over a wide range of compositions. The lower limit of nitrogen concentration varies greatly with temperature, whilst at the upper limit, the nitrogen content is just insufficient to form the stoichiometric composition  $\text{Fe}_2\text{N}$ . The empirical formula of the phase is  $\text{Fe}_{2-\text{x}}\text{N}$  however  $\text{Fe}_{2-\text{x}}\text{N}_{(\text{1}-\text{x})}$  gives a more accurate description of

the phase. The metal atom arrangement in the phase is closed-packed hexagonal and the unit cell contains six Fe atoms. The octahedral interstices within the structure are arranged in layers perpendicular to the c-axis with an inter-planer distance of  $C/2$  and with two-dimensional close packing in each layer, see Figure 4.

For descriptive purposes the two planes of interstices within the unit cell can be labelled A and B. One third of the interstices in each layer are occupied at the composition  $\text{Fe}_3\text{N}$  so that each nitrogen atom has six vacant sites surrounding it and a vacant site above and below it (Jack, 1952). The homogeneity range of epsilon phase extends almost to the composition  $\text{Fe}_2\text{N}$  in which the nitrogen atoms are arranged in such a manner that alternate layers of octahedral interstices are one-third and two-thirds filled respectively, Figure 5.

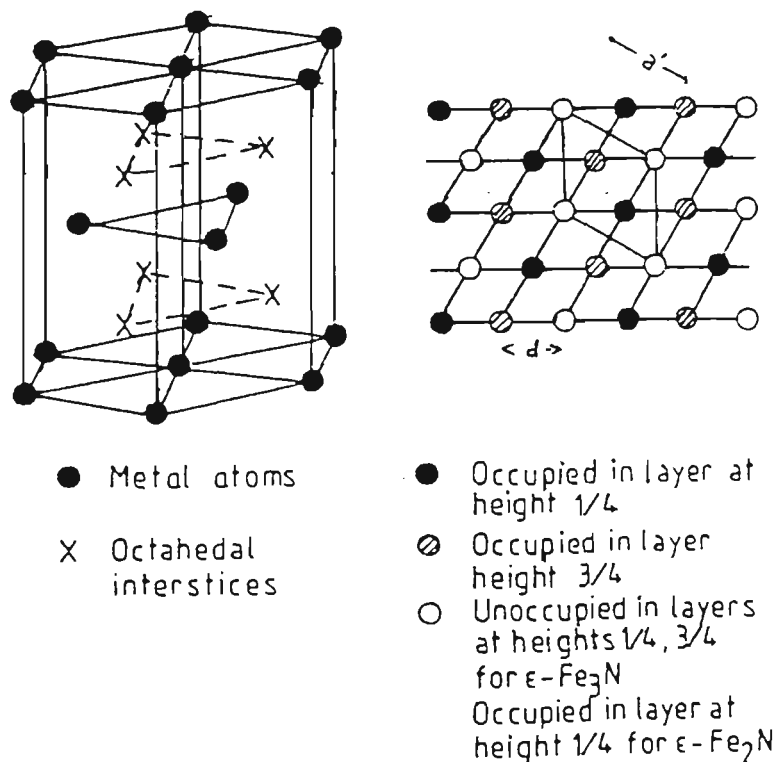


**Figure 4.** The crystal structure of epsilon nitride (Jack 1952).

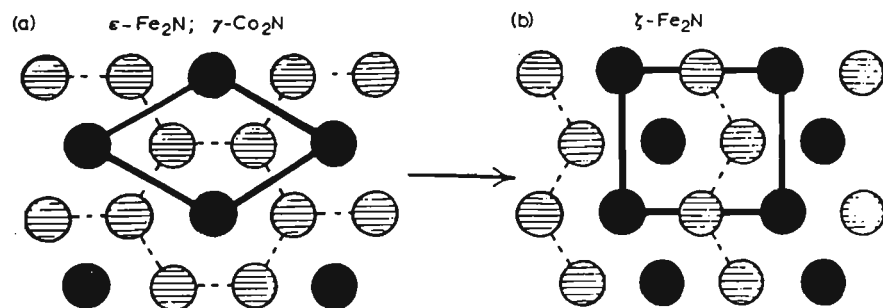


**Figure 5.** The crystal structure of epsilon and zeta iron nitrides (Jack and Jack, 1973).

The structure of epsilon nitride with compositions between  $\text{Fe}_2\text{N}$  and  $\text{Fe}_3\text{N}$  is based on the  $\text{Fe}_2\text{N}$  structure, whereby the nitrogen atoms have been removed from the B layer interstices in a strictly ordered manner.

### 2.3.3 $\zeta$ - $\text{Fe}_2\text{N}$

Just before the ideal  $\epsilon\text{-Fe}_2\text{N}$  composition is reached there is a phase change to  $\zeta$ -iron nitride. This new phase has a stoichiometric composition  $\text{Fe}_2\text{N}$ . The iron atoms retain their same relative positions and are still in an approximately hexagonal closed-packed array. However, one-half of the octahedral interstices in each layer plane are occupied such that each nitrogen atom again has unoccupied holes above and below it in adjacent planes, Figure 5. The nitrogen atom arrangement symmetry is orthorhombic. In each layer the nitrogen atoms are distributed in zig-zag chains parallel to the orthohexagonal b axis (Jack and Jack, 1973). This new phase is highly metastable and decomposes at temperatures above 450°C.

### 2.3.4 $\alpha''$ - $\text{Fe}_{16}\text{N}_2$

This phase has a fully ordered nitrogen-atom arrangement in a slightly distorted bcc iron-atom array, Figure 6.  $\alpha''\text{-Fe}_{16}\text{N}_2$  is merely ferrite with a nitrogen superlattice, thus it fits perfectly with the ferrite matrix in the  $a$ -direction, but there is a misfit in the  $c$ -direction (Jack, 1975). In formation of  $\alpha''$  there is no considerable movement of iron atoms. The precipitates grow coherently as very thin platelets in the ferrite merely by localised clustering of nitrogen atoms followed by their ordering. It has been observed by Dahmen and co-workers (1987) that  $\alpha''$  plate is made up of different segments with slightly different orientations.

As shown in Figure 7,  $\alpha''\text{-Fe}_{16}\text{N}_2$  phase can also be regarded as fcc  $\gamma'\text{-Fe}_4\text{N}$  in which alternate nitrogen atoms are missing and which fits with the  $\alpha$ -matrix in a Bain orientation relationship (Jack, 1975):

$$(001)\alpha \parallel (001)\text{Fe}_4\text{N}_{0.5}; \{110\}\alpha \parallel \{100\}\text{Fe}_4\text{N}_{0.5}$$

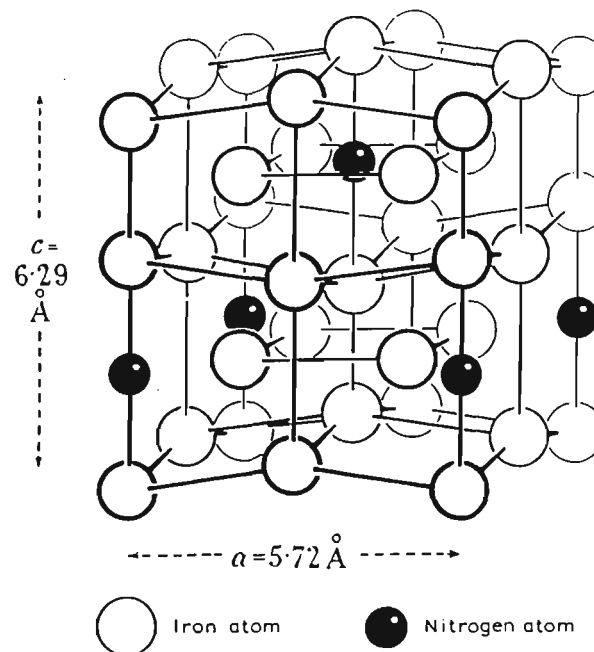


**Figure 6.** Crystal structure of  $\alpha''\text{-Fe}_{16}\text{N}_2$  (Jack, 1989).

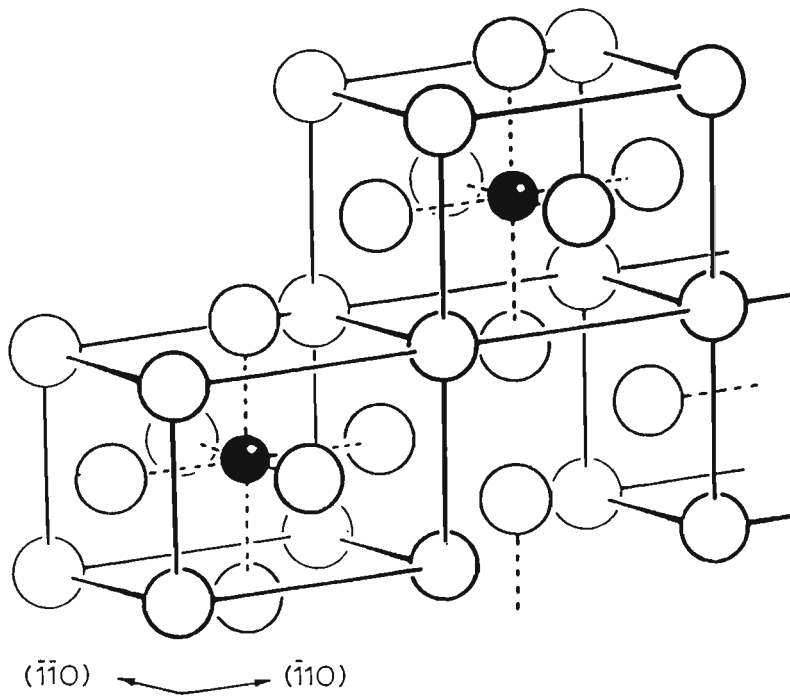


**Figure 7.** Crystal structure of  $\alpha''\text{-Fe}_{16}\text{N}_2$  as a defect of fcc  $\gamma'$  structure (Jack, 1975).

## 2.4 Nitriding

Nitriding is a thermochemical treatment in which nitrogen is diffused into the surface of metals, usually steels. The process is carried out at a temperature below the eutectoid temperature of Fe-N system usually within the range 490-530°C. At higher temperatures there is a reduction in hardness due to precipitate coarsening and also tempering of the core with a reduction in its strength as well as the possibility of distortion due to phase transformation. At lower temperatures, rates of nitriding are impractically slow (because the rate of dissociation of ammonia is low). During the process atomic or nascent nitrogen is adsorbed from either a gaseous, liquid (salt), or plasma carrier and subsequently diffused into the base metal with a layer of iron nitrides forming on the

surface of the component being treated. This layer is often referred to as 'white layer' due to its optical metallographic appearance (Edenhofer, 1974, part 2) and it consists of a mixture of a face centred cubic  $\gamma'$ -Fe<sub>4</sub>N phase, and a close packed hexagonal  $\epsilon$ - Fe<sub>2</sub>N<sub>(1-x)</sub> phase of higher nitrogen content (refer to Fe-N phase diagram, Figure 1). This layer is of metallic appearance and is normally indistinguishable from the steel unless examined microscopically (Child, 1980). From this layer, nitrogen diffuses into the underlying steel. Most air-melted steels contain a small amount of nitrogen, generally less than 0.1wt%. The maximum solubility of nitrogen in pure iron at 590°C is only 0.1 wt%, see Figure 1. As nitrogen diffuses into the steel the solubility limit is soon reached and, in the presence of alloying elements, nitrides are formed and precipitated in a very dispersed form.

Since diffusion of the alloying elements at these low temperatures is very limited, nitrides are produced in the immediate locality of the alloy atoms and little growth occurs. The hardness is increased partly by distortion of the ferrite lattice by the high-volume fraction of alloy nitrides and partly by the inherent hardness of the nitrides. The expansion of the surface layers due to precipitation of alloy nitrides results in the development of high surface compressive stresses of up to 750 N/mm<sup>2</sup> (Child, 1980).

The white layer, which can be up to 50  $\mu\text{m}$  thick (Bell, *et al*, 1975), is thin but brittle and often must be removed by grinding or by chemical treatment before use, both of which are relatively expensive (Bell, 1973). The necessity to remove the white layer arises primarily from the possibility of spalling in service. The thickness of the underlying case, the diffusion zone, is usually 0.2 -0.7 mm and has a peak hardness of 900 -1100 HV (International Research & Development Co. Ltd., 1986), excellent abrasion resistance, and gives rise to a marked improvement in fatigue performance. It usually contains a

fine dispersion of alloying-element nitrides. The enhancement of the fatigue resistance is ascribed to macro- and microstresses provided by these nitrides in the diffusion zone. The case is temper-resistant up to  $\sim 500^{\circ}\text{C}$ . No phase transformation is involved to room temperature, and quenching is not required to develop surface hardness, consequently, there is less distortion than in carburising or carbonitriding, although some growth does occur due to the increase in volume of the case. However, this growth is constant and predictable for a given part and cycle, so that in most cases parts may be machined very close to final dimensions before nitriding (Avner, 1974). Nevertheless, the surface compressive stresses developed in the case on nitriding, which improve fatigue resistance, can also lead to distortion in hollow thin-walled components. Consequently, nitriding is best carried out on substantially rigid, preferably axi-symmetrical components such as shafts, thick walled cylinders, gears and die blocks, crankshafts, valve stems, injectors and many other engineering components.

The properties imparted to steel by nitriding can be summarised as follows (Thelning, 1975):

1. The high-hardness surface layer has high resistance to galling, seizing, and scuffing, even when poorly lubricated.
2. Wear resistance is increased.
3. Because of the compressive residual stress, low notch sensitivity is achieved; notched fatigue strength is much higher than that of unnitrided steels, and approaches the value of that of unnotched steel.
4. Fatigue strength is increased mainly by development of surface compressive stresses.
5. Hot hardness and resistance to tempering are improved.
6. Corrosion resistance for non-stainless steels is moderately improved.

7. High dimensional stability.

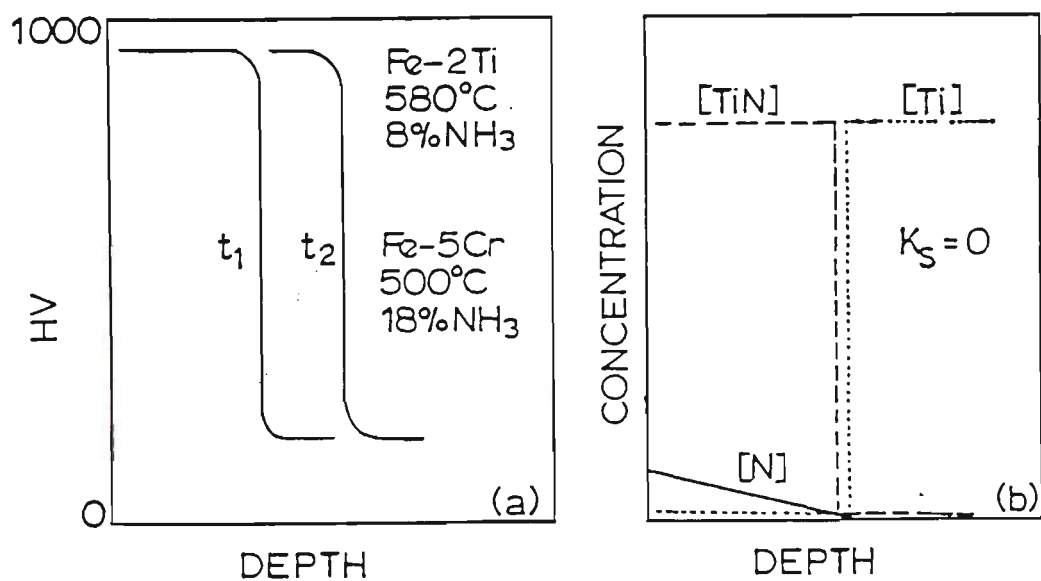
## 2.5 Kinetics of Nitriding

The nitrides of the common alloying elements in nitrided steels are listed in the Table 2. The strength of the interaction between nitrogen and the alloying element is indicated by the heat of formation. The crystal structure of the nitride gives an indication of the ease of nucleation of nitride precipitates in a ferrite matrix. Formation of fcc phases with  $a \sim 4.05 \text{ \AA}$  on the cube planes of ferrite is possible with a Bain orientation as coherent or semi-coherent plates. Except for AlN, which is known to nucleate heterogeneously on dislocations, such precipitates, or in some cases metastable zones, can nucleate homogeneously (Lightfoot and Jack, 1975). The strength of the interaction between the alloying element and nitrogen as well as the ease of nucleation of the nitride phase dictate the form of the hardness profile developed during nitriding of alloyed iron.

When there is a strong interaction between nitrogen and substitutional solute atoms, nitriding proceeds by the formation of a uniformly hard subscale, which advances progressively into the core. The microstructure is characterised by a relatively sharp case/core boundary, see Figure 8. All the alloying element (M) in the nitrided case has precipitated and nitrogen is substantially absent in the core. Nitrogen diffusion in ferrite predominantly controls the nitriding kinetics.

**Table 2.** Some nitride phases of the commonly occurring alloying elements in nitrided steels (Goldschmidt, 1967).

Phase	Bravais lattice	Unit-cell dimensions, Å	Heat of formation, kcal/mol nitride
TiN	fcc	a, 4.244	- 80
AlN	hex.0.	a, 3.110	- 72
		c, 4.975	
VN	fcc	a, 4.139	- 52
CrN	fcc	a, 4.149	- 30
Mo <sub>2</sub> N	fcc	a, 4.169	-19.5
W <sub>2</sub> N	fcc	a, 4.126	- 17



$K_s = [wt-\% Ti] [wt-\% N]$  for homogeneous precipitation is assumed to be zero

**Figure 8.** (a) Microhardness profiles of a "strong" interaction: (b) schematic drawing of the TiN, Ti, and N concentrations for a given nitriding time (Lightfoot and Jack, 1975).

The plate-like nitrides formed have a fcc sublattice of M atoms and the interface between the broad faces of the platelets and the matrix is coherent. This has been observed with Fe-Ti alloys, with Fe-5.6wt.%Cr, and with Fe-V (Jack, 1975). A model for the reaction has been derived from theories of diffusion accompanied by a phase change which have been applied to internal oxidation (Lightfoot and Jack, 1975). This model assumes that :

1. Diffusion of the substitutional alloying element can be neglected.
2. Before moving of the nitriding front, all the alloying element at the interface between nitrided and non-nitrided regions is reacted.
3. For homogeneous precipitation of the alloy nitride, the solubility product,  $K_s = (\text{nitrogen concentration}) \times (\text{alloy element concentration})$ , is negligibly small.
4. The surface nitrogen concentration is constant.

The analysis predicts that, in the absence of iron nitride formation, the subscale thickness ( $\xi$ ) varies with time (t) according to:

$$\xi^2 = \frac{2[N]}{r[M]} Dt \quad (1)$$

[N] is the atomic concentration of nitrogen in solution at the metal surface, [M] is the original alloy element atomic concentration, r is the atomic ratio of nitrogen to alloy element, N/M, in the phase formed by nitriding, and D is the diffusivity of nitrogen.

The square of the case depth is inversely proportional to alloy concentration and is directly proportional to the surface nitrogen concentration, the bulk diffusivity of nitrogen in ferrite, and time of nitriding. In this case, the precipitation reaction is so rapid that the nitriding reaction is controlled by bulk diffusion of nitrogen from the surface to the reaction front.

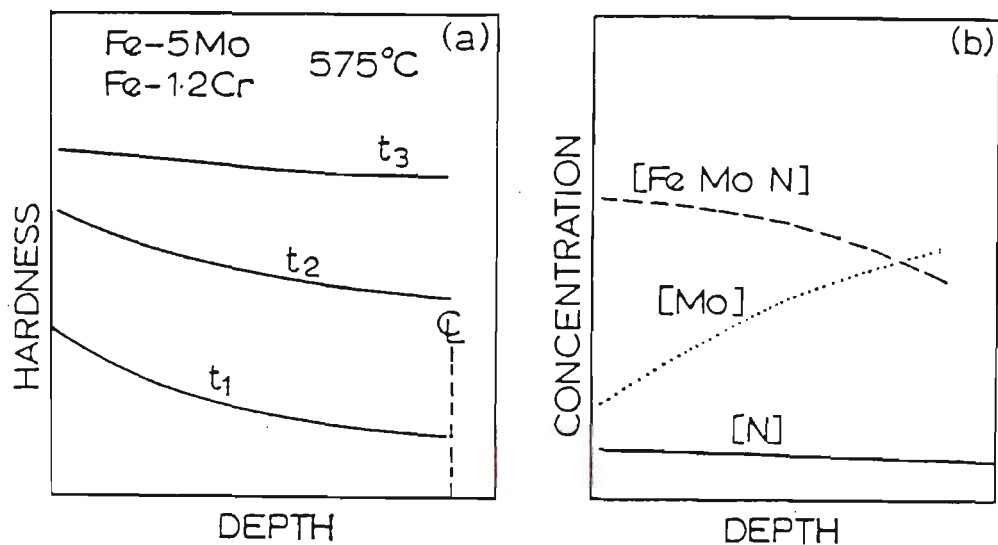
If the interaction between the alloying element and nitrogen is less strong, nucleation of stable precipitates will not occur until a relatively large supersaturation of nitrogen is achieved. In thin sections, the rate of hardening will be controlled by the rate of reaction to form the nitride phase. After nitriding, the interface between the nitrided case and the core is more diffuse and the microstructure is characterised by a very faint (or no) case/core boundary in conjunction with a virtually constant nitrogen concentration.

Figure 9 schematically shows the development of nitrided hardness for a “weak” interaction or difficult nucleation. Diffusion of alloying elements in the ferrite predominantly controls the nitriding kinetics. The nucleation is difficult and the nitride/matrix interface is incoherent because of the large crystallographic difference between the nitrides (usually hexagonal) and the ferrite lattice. The presence of dislocations facilitates heterogeneous precipitation of this kind of nitride. In addition, nitriding kinetics on prolonged nitriding is accelerated due to the production of dislocations for accommodation of the volume misfit between matrix and nitride particles during precipitation of nitrides (Somers, 1989). The rate of homogeneous precipitation is expected to be a sensitive function of supersaturation.

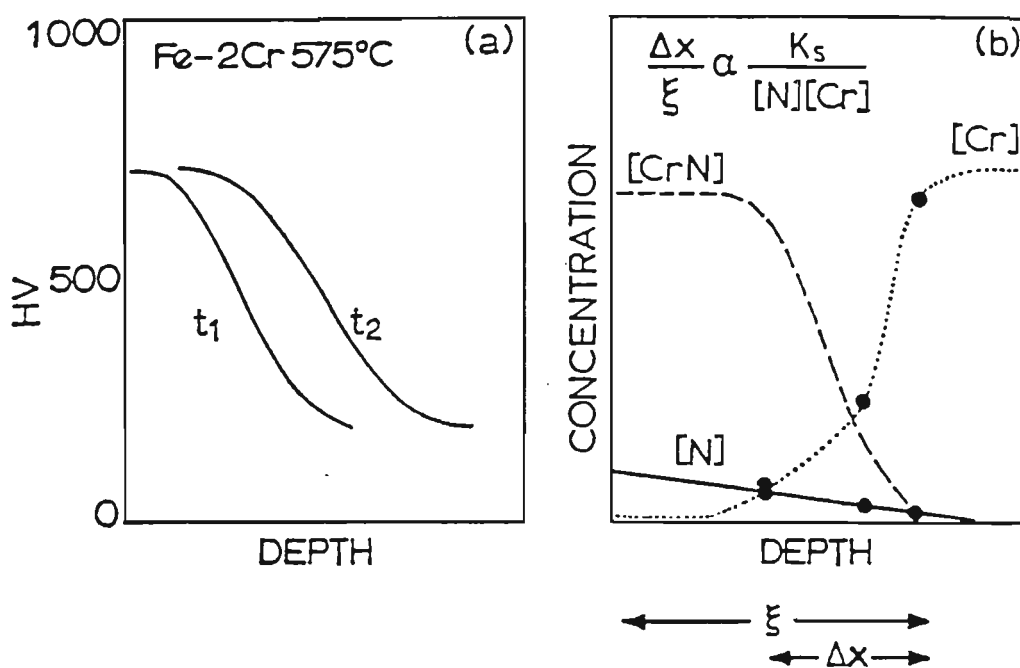
This indicates that the nitriding response of alloys with relatively unstable nitrides is determined by the rate of precipitation. The supply of nitrogen to the interior of the specimen in thicker sections will also exercise control. Iron-chromium alloys can show nitriding response characteristic of “strong” or “weak” interactions, depending on the chromium concentration. The case/core interface is less abrupt than that for a typical “strong” interaction. Figure 10 illustrates an intermediate type of behaviour.

Since the critical solubility product for the nucleation of homogeneous precipitation for CrN is higher than that for TiN but not so high as that for the nitride phase in Fe-Mo

alloys, such intermediate behaviour is seen in iron-chromium alloys. Meijring (1971) has shown that the diffuseness of the interface,  $\Delta x/\xi$ , is proportional to solubility product,  $K_s/[\%N][\%Cr]$ , Figure 9-b. Since,  $K_s$  will increase by increasing the nitriding temperature so will the diffuseness of the interface. The case/core boundary becomes more abrupt by increasing the surface nitrogen concentration and increasing alloy content.



**Figure 9.** (a) Microhardness profiles of a "weak" interaction or difficult nucleation; (b) schematic drawing of the concentrations of the nitride phase (in this case a metastable zone), Mo and N (Lightfoot and Jack, 1975).



*at all points on the curves the product  $K_s = [\text{wt-\%Cr}] [\text{wt-\%N}]$  is constant and non-zero*

**Figure 10.** (a) Microhardness profiles for an "intermediate" interaction; (b) schematic drawing of the concentrations of  $\text{CrN}$ ,  $\text{Cr}$ , and  $\text{N}$  (Lightfoot and Jack, 1975).

## 2.6 Nitriding Steels

The presence of strong nitride forming elements in a steel is the main selection criterion for the composition of a nitriding steel for which high surface hardness is required. It is possible to investigate the tendency of the different alloying elements to form hard nitrides or to increase the hardness of the steel by precipitation hardening mechanism, by measuring the hardness of nitrided different alloy steels. Figure 11 shows the results obtained by such investigations (Thelning, 1975).

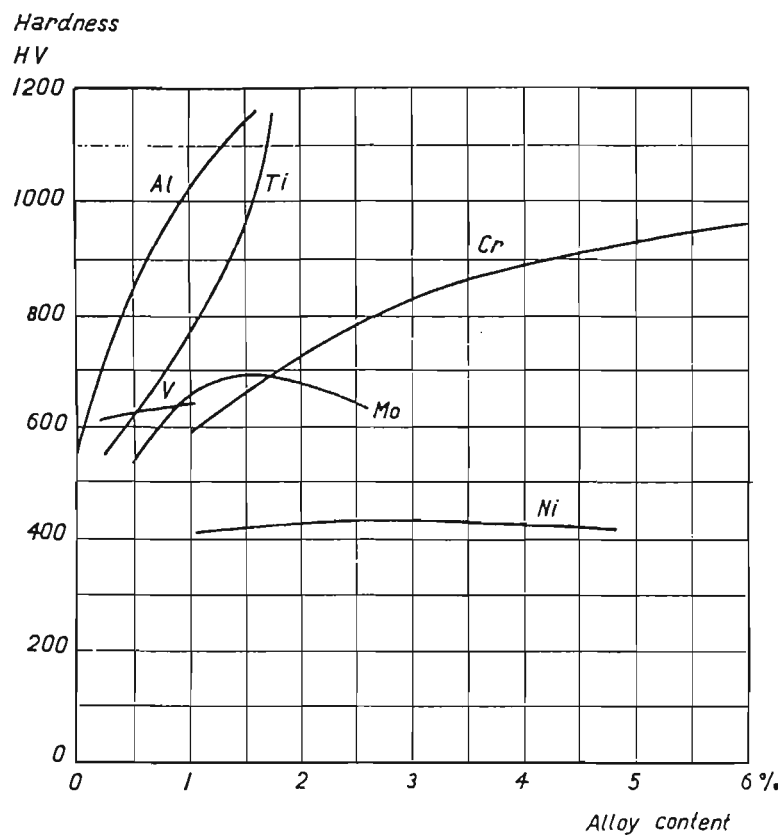


**Figure 11.** Influence of alloying elements on hardness after nitriding. Base alloy 0.35% C, 0.30% Si, 0.70% Mn (Thelning, 1975).

The diagram illustrates how different alloying elements affect the surface hardness after nitriding. Aluminium and titanium have the greatest effect on hardness, even at small concentration (~1%) followed by chromium, molybdenum, and vanadium. The hardening capacity of chromium increases as its concentration increases. In addition to the contribution of molybdenum as a nitride former, it also decreases the possibility of embrittlement at nitriding temperature (Knerr *et al*, 1991). The effect of other alloying elements such as nickel, copper, silicon, and manganese on nitriding characteristics is not considerable. Higher hardness values are obtainable in steels containing several alloying elements, than if the alloying elements are used separately. Increasing the concentration, especially of the strong nitride-formers, decreases the effective case depth, as shown in

especially of the strong nitride-formers, decreases the effective case depth, as shown in Figure 12 (Thelning, 1975).

Strong nitride forming elements such as Al and Ti, which have a pronounced effect on hardness, also delay the diffusion of nitrogen into the steel as their contents increase. At roughly 1% Al content, an optimum value for hardness and depth of nitriding is obtained. This amount of Al is normally used in Al-alloyed nitriding steels. Another element which has a strong inhibiting effect on the diffusion of nitrogen is carbon (Thelning, 1975).

Aluminium containing steels (0.85 to 1.50% Al) yield the hardest nitrided case since aluminium is the strongest nitride forming element. Nevertheless, the low ductility of the nitrided case is a limitation that should be considered for the selection of these steels. On the other hand, low alloy chromium-bearing steels produce a more ductile nitrided case but with lower hardness (Knerr *et al*, 1991). Unalloyed carbon steels are not suitable for nitriding because they form an extremely brittle case that spalls readily and also the diffusion case is not significantly harder than the core.

Nitralloy series are the premier nitriding steels and contain approximately 1 wt % Al with 1.0 to 1.5 wt % Cr. Medium-carbon, chromium-containing low-alloy steels such as the 4100, 4300, 5100, 6100, 8600, 9300, and 9800 series form excellent diffusion cases. Other suitable nitriding steels include hot-work die steels containing 5% chromium such as H11, H12, and H13., low-carbon, chromium-containing low-alloy steels of the 3300, 8600, and 9300 series, air-hardening tool steels such as A-2, A-6, D-2, D-3, and S-7, high-speed tool steels such as M-2 and M-4, ferritic and martensitic stainless steels of the 400 and 500 series, austenitic stainless steels of the 200 and 300 series, Nitronic stainless steels such as 30, 40, 50 and 60, and precipitation-hardening stainless steels such as 13-8

PH, 15-5 PH, 17-4 PH, 17-7 PH, A-286, AM350, and AM355 (Knerr *et al*, 1991).

Powder metallurgy (P/M) parts can also be nitrided but due to the characteristic porosity of these parts, precleaning is more critical than with wrought alloys.

In cast iron or carbon steels, significant hardening in the diffusion zone cannot be developed. Nevertheless, a compound zone which is often excellent for wear resistance in lightly loaded parts, can be formed. These materials are not suitable for applications involving high localised stresses because the compound zone is supported by a relatively soft diffusion zone (Knerr *et al*, 1991).

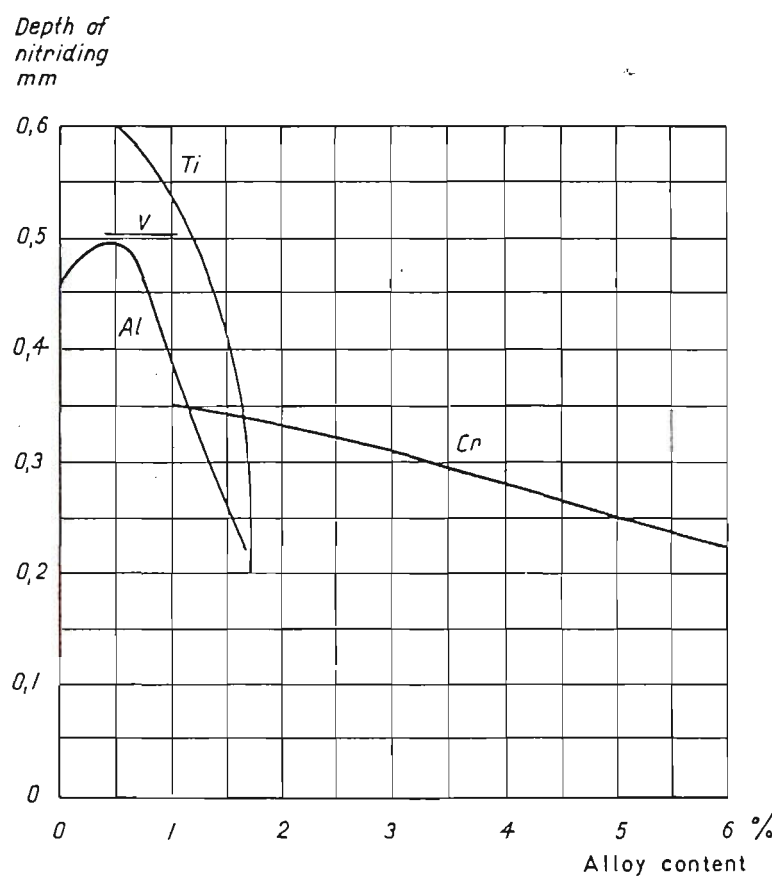


**Figure 12.** Influence of alloying elements on depth of nitriding measured at 400 HV. Nitriding for 8 h at 520 °C (Thelning, 1975).

## 2.7 HSLA Steels or Microalloyed Steels

To date, HSLA steels have mainly been used in pipe lines, heavy industrial machinery, pressure vessels, ship building, and more recently for off shore platforms and in the automotive industry. HSLA steels have characteristics and properties that result in economies to the user when the steels are properly applied. They are considerably stronger and in many instances tougher than structural carbon steel, yet have sufficient ductility, formability, weldability and fatigue resistance to be fabricated successfully by customary forming methods.

The earliest microalloyed steels were developed over 25 years ago, and the metallurgical principles on which they are based are well-documented in many excellent technical publications (Paules, 1991). The motivation for the application of HSLA steels is cost reduction. High strength steels can bear service loads with thinner sections, providing weight savings. Lower costs can be realised if a microalloyed steel replaces an alloy steel containing significant amounts of expensive elements such as nickel, chromium and molybdenum. However, the most significant cost reduction provided by microalloyed steels is the elimination of expensive heat treatment steps. As-rolled microalloyed steels exhibit properties comparable to normalised or quenched and tempered steels. The costs associated with heat treatment, inventory, handling, energy, decarburisation and scale (oxidation) loss are avoided with the microalloying approach.

Microalloying elements are added to steel for two purposes: to produce grain refinement and/or precipitation strengthening. Both of these phenomena result from the precipitation of small microalloy carbides (NbC, VC, TiC), nitrides (NbN, VN, TiN), or complex carbonitrides [Nb(C,N), V(C,N), Ti(C,N)] (Paules, 1991). Microalloyed steels

are usually furnished in the hot rolled condition. The most important method used to increase the strength of the HSLA steels involves a refinement of the grain size. A major factor in reducing the ferritic grain size is the addition of a small amount of a strong carbide-forming element or elements to HSLA steels. The most important of these elements is niobium, which can have a significant effect on the properties of the steel even in amounts less than 0.05 percent. Because these grain-size controlling additions are introduced in such small proportions, it is a common practice to call the steels containing them "microalloyed", even though they may contain more conventional alloying elements in relatively large concentrations.

The principal effect of these grain-size controlling elements is to markedly increase the time required to recrystallise the austenite during hot rolling. The ability of these microalloying elements to slow down recrystallisation is due to the fact that they tend to precipitate as particles (carbides, nitrides, and carbonitrides) that can interact with the austenite grain boundaries. These precipitate particles can restrict both the recrystallisation and the grain growth of the austenite. There is a temperature, however, above which each type of precipitate dissolves and the microalloying element goes back into solution. Just above this solution temperature, the austenite grains become subject to coarsening. Improvement in strength is also obtained by precipitation hardening.

The microalloying elements can also produce other precipitates in the ferrite. These are finer than those that appear in the austenite and form largely as a result of interphase precipitation at ferrite-austenite boundaries during the transformation of austenite to ferrite. However, these hardening precipitates may also nucleate inside the ferrite grains. This type of precipitation has to be the result of the lower solubility of the microalloying elements in the ferrite than in the austenite. Adding alloying elements such as manganese

that increase the strength of the ferrite matrix by solid solution strengthening is another method to increase the strength and other desirable properties of a HSLA steel (Hill and Abbaschian, 1992). Strain aging and processing that increases the dislocation density of the substructure of the steel are also strengthening mechanisms used with HSLA steels.

### **2.7.1 Brief Introduction to MAXIMA™ microalloyed steel**

MAXIMA™ is a commercial high strength microalloyed steel which is designed so that upon quenching it develops predominantly lath martensite to the exclusion of twinned martensite, which has a high hardness but quite poor toughness and ductility. The chemical composition of this steel is shown in Table 3, page 97. MAXIMA™ is also designed to have markedly improved toughness due to the presence of a small but significant amount of retained austenite, less than 5 Vol % (Bangaro *et al*, unpublished paper).

The primary functions of microalloying in MAXIMA™ are:

1. To induce a very fine grained microstructure in the cast or wrought conditions.
2. To achieve very favourable mechanical properties.

Unlike many (HSLA) steels, microalloying in MAXIMA™ is not intended to provide any appreciable precipitation strengthening. Titanium-niobium additions in conjunction with appropriate levels of Al and N, develop and maintain austenite grain sizes less than about 50 $\mu\text{m}$ . Controlled addition of Ti-Nb also enables relatively small grain sizes to be produced in the weld HAZ.

Copper induces atmospheric/sour environment-corrosion resistance which decreases the generation and absorption of H (atomic hydrogen) and reduces the susceptibility of MAXIMA™ to hydrogen induced cracking in sour service and makes it more resistant to weld cold cracking. Copper also enhances the stability of retained austenite and enables the austenite to act as an effective sink for H, thus decreasing the stress corrosion cracking susceptibility (Bangaro *et al*, unpublished paper).

It has also been claimed that the low Si content of MAXIMA™ along with the reduced carbon level, eliminates the formation of undesirable twinned martensite in the weld HAZ.

## **2.8 Nitriding of Microalloyed Steels**

The attractive properties of microalloyed steels and the presence of nitride forming elements such as chromium in some of these steels, have generated interest in the applicability of these alloys as a new generation of nitriding steels. In recent years there have been some efforts to study the nitriding behaviour of some of these steels. Mongis *et al* (1984) carried out an investigation to assess the nitriding kinetics of microalloyed steel grades S800, S1000, U1000, F1200 and Z1300 in the as-rolled condition in comparison with the conventional steels 120M19 and 150M36 in the quenched and tempered condition. They found that the nitriding kinetics of S800 and S1000 microalloyed steels were about 50% higher than those of 120M19 and 150M36 conventional steels. They ascribed the higher nitriding kinetics to greater hardening at the base of the diffusion zone caused by the presence of niobium and vanadium. They

also proposed the substitution of low alloy nitriding steels with microalloyed steels in order to simplify the processing procedure by eliminating quenching and tempering operations.

In an effort to compare the properties obtained from plasma nitriding of two low carbon thermochemically processed microalloyed steels and a quenched and tempered medium carbon steel, Palmiere *et al* (1988) conducted several experiments. They also made a comparison between the plasma nitrided properties of the two microalloyed steels and an induction hardened medium carbon quenched and tempered steel. They found that the increase in surface hardness obtained by plasma nitriding of both low carbon microalloyed steels was better than that achieved for the medium carbon quenched and tempered steel by either plasma nitriding or induction hardening. They also found that after plasma nitriding, the microalloyed steels had superior fatigue resistance over the heat treatable steel. The improved properties of one microalloyed steel were attributed to the presence of  $(\text{FeMo})_2\text{N}$  and "ultra-fine"  $\text{Mo}_x\text{N}$  precipitates in the diffusion zone.

A series of experiments were conducted by Kuppusami and co-workers (1993) to compare the plasma nitriding behaviour of type 316 stainless steel and a microalloyed steel. They examined the effects of treatment temperature and ion current on the maximum surface hardnesses obtainable for these steels. Cyclic plasma nitriding developed a uniform surface morphology on the stainless steel while this process was found not to be necessary for the microalloyed steel. Maximum surface hardness was obtained at 575°C for the stainless steel and at 500°C for the microalloyed steel under similar conditions of time and ion current.

Hanada and co-workers (1995) have studied the nitriding response of a newly developed high strength low alloy bainitic steel in comparison with that of En40B steel. They found that the peak hardness of the bainitic steel was maintained over a much greater nitriding temperature range and that its wear and fatigue behaviour was acceptable.

## **2.9 Plasma Discharges**

### **2.9.1 Introduction**

Plasma is nature's "unnatural" fourth state of matter, an electronic jelly, or foam, consisting of positively and negatively charged particles as well as neutral species. On average a plasma is electrically neutral, because any charge imbalance would result in electric fields that would tend to move the charges in such a way as to eliminate the imbalance. As a result, the density of electrons plus the density of negative ions will be equal to the density of positive charged ions. Some energy is required for forming and sustaining a plasma. In steady state, the rate of ionisation must balance the losses of ions and electrons from the plasma volume by recombination and diffusion or convection to the boundary.

The plasmas which will be considered here are initiated and sustained by electric fields which are produced by either direct current DC or alternating current AC power supplies. A typical AC frequency of excitation is 13.56 MHz in the radio frequency RF portion of the spectrum which will be discussed later. These plasmas are also referred to as *electric discharges*, *gaseous discharges*, or *glow discharges*.

## 2.9.2 The DC Glow Discharge

The flow of electric current through a gaseous medium is described by the term 'gas discharge'. The basic requirements for such a passage of current are that some of the gas particles should be ionised, by whatever means are available, and that there should exist an electric field to drive the charged particles so produced to form a current. The steady state gas discharges may be conveniently be classified in three types according to the current which they carry (Howatson, 1965). These are:

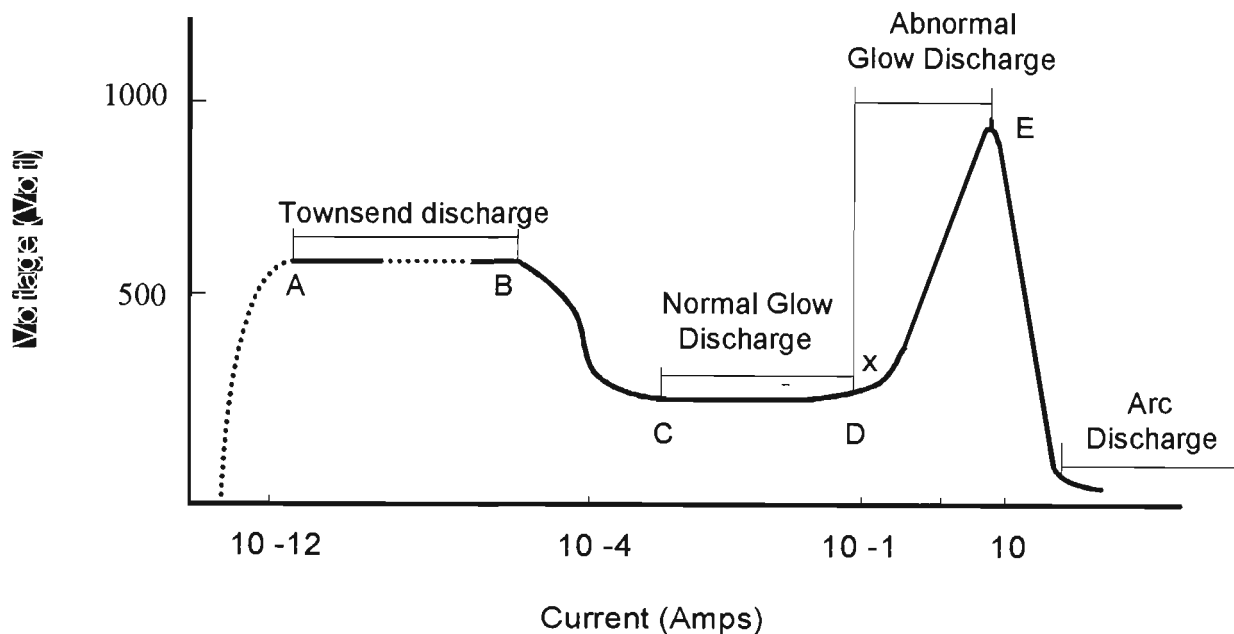
- 1- The Townsend or dark discharge, which carries currents up to  $\sim 10^{-6}$  A.
- 2- The glow discharge, which carries currents from  $\sim 10^{-6}$  to  $\sim 10^{-1}$  A.
- 3- The arc discharge, which carries currents of  $\sim 10^{-1}$  A upwards.

Figure 13 illustrates the current/voltage characteristics of different types of discharges. In this Figure a rough order of magnitude of the voltage drop across the discharge is plotted as a function of the total discharge current.

The Townsend discharge, region A-B, is characterised by its extremely low current. It is not a self sustaining discharge and can only be sustained by an additional external source of electrons. The discharge appears dark because the currents involved are very small and so the density of excited atoms which emit light is correspondingly small. This type of discharges are of no interest in plasma processing (Staines, 1985).

The region C-D is the regime of the self sustaining *normal glow discharge*. In this region, the voltage across the discharge is totally independent of the current which it is carrying. The colour and intensity of the glow depends upon the current and also the nature and pressure of the gas which constitutes the discharge medium. Normal glow

discharges are used in industry for lamps, fluorescent tubes, etc., and can be maintained with relatively low energies and weak currents (Edenhofer, 1974, part 1).



**Figure 13.** Current/voltage characteristic for a DC discharge.

The main reason that the normal glow is not used in plasma surface treatments is that the surface coverage of the component is not complete. However, as the current increases the surface coverage is increased and the current reaches a critical value where there is a sudden transition, complete surface coverage occurs and the voltage is more sensitive to changes in the applied current, region D-E. This region is called the *abnormal glow discharge* and the plasma behaves as an ohmic load, i.e. increasing the voltage increases the current. Most plasma processes are carried out using the high current and power densities that occur in the region of the abnormal and unstable glow discharge. The cathode glow is due to excitation of gas atoms by the positive ions which possess greater

velocities in the abnormal discharge. The abnormal discharge hence operates using ionisation by positive ions as well as by secondary electrons.

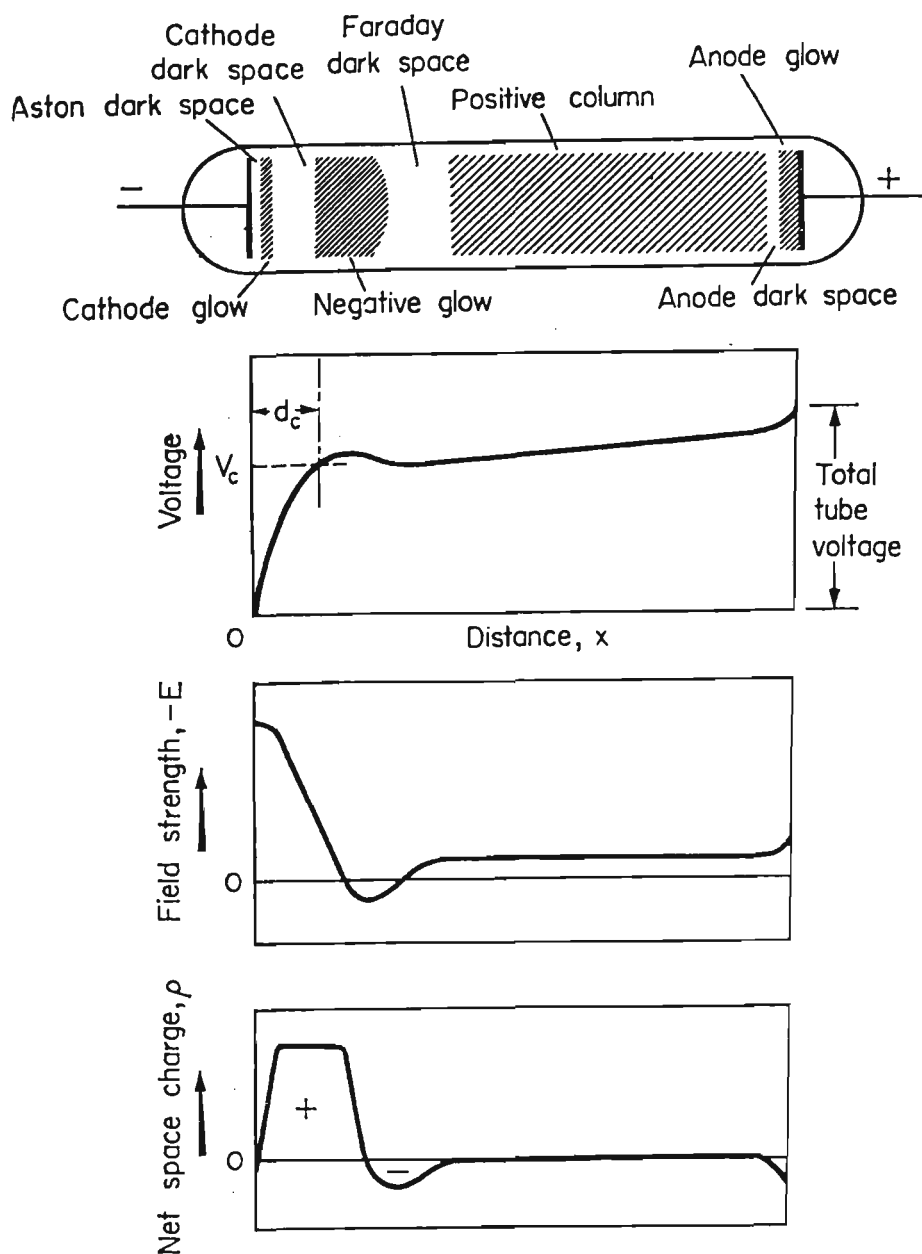
When operating an abnormal discharge, heating of the cathode occurs as the colliding particles give up their energy to the metallic surface. The amount of heating is proportional to the current density. If the current density is increased beyond a critical maximum value, point E, the voltage across the electrodes drops rapidly away to several tens of volts and it would quickly result in a concentration of the discharge at that particular point and formation of an *arc discharge* (Edenhofer, 1974, part 1). Severe damage to both components and equipment can be expected if such a condition is maintained. Therefore, plasma heat treatment units incorporate advanced circuit breaker systems which are capable of interrupting and extinguishing any arc discharges which may occur.

Figure 14 illustrates schematically the various regions between the cathode and the anode of a glow discharge and the accompanying changes in voltage, field strength, and net space charge across it. Pressure, voltage, current and type of gas, dictate the slopes and inflection points of the curve. Each region is characterised by its relative luminosity which gives an indication of the collision and reaction processes occurring within it

The electrons required for maintaining the discharge are produced at the cathode by secondary electron emission resulting mainly from positive-ion bombardment and are then accelerated towards the anode. During their journey these electrons are subjected to collisions with gas atoms and molecules within the discharge space, ionising gas molecules, and forming fall of positive charge towards the cathode. The electric field magnitude and the density of the gas are such that a self sustaining state is effected. The

electron-gas collisions and the secondary electron emission processes produce sufficient electrons to maintain a stable discharge. Starting at the cathode, there is a very thin dark area known as the Aston dark space. It lies directly in front of the cathode surface, and represents a region in which the electrons have not yet moved sufficiently far in the cathode electric field to acquire threshold excitation energies. As one moves away from the cathode, a layer of neutral atom radiations called the cathode glow appears. The luminosity in this region is produced by the recombination of incoming positive ions with slow electrons, for which the recombination coefficient is high (Howatson, 1965). Next outward is a region of far less luminosity called the Crookes or Hittorf's or cathode dark space. In this region, gas atoms and molecules are ionised by electrons which have passed through the cathode glow without interaction. The region appears dark since the electrons liberated by these collisions do not have sufficient energy themselves to excite the gas molecules around them.

The three regions, Aston dark space, cathode glow and cathode dark space, make up the cathode fall. Near to the cathode surface, the electrons before gaining appreciable velocity, form a negative space charge. But the space charge becomes positive a short distance from the cathode and remains positive throughout the cathode dark space producing a large voltage gradient.



**Figure 14.** various regions between the cathode an the anode of a glow discharge and the accompanying changes in voltage, field strength, and net space charge across it (Howatson, 1965).

Therefore, most of the voltage is taken up in this region and the electrons are accelerated sufficiently to produce intense ionisation and hence multiplication. The electrons carry nearly all the current by the end of the cathode dark space. The large number of electrons emitted from the cathode fall is enough to considerably reduce the net positive

space charge and to produce a reversal in the sign of the space charge from positive to negative in the region neighbouring the cathode dark space. Just prior to this, the voltage gradient becomes slightly negative. Therefore there is a small, local reversal in the direction of the electric field. Consequently, the fast electrons emerging from the cathode fall are no longer accelerated and their energy is absorbed mainly by intense ionisation and excitation, producing the bright negative glow.

As the electrons are slowed down, the negative space charge reaches a maximum. The electrons have little energy left for further excitation and ionisation. They do not regain energy rapidly due to the very weak electric field in this region of the discharge and this leads to the formation of the Faraday dark space.

The positive column is the ionised region that extends from the Faraday dark space almost to the anode. It is not an essential part of the discharge, and for very short tubes it is absent. It serves merely to maintain the conduction of current by electrons which is established in the cathode region and has little or no net space-charge. The field strength in this region is weak and is just sufficient to produce ionisations to counteract losses by recombination and diffusion, and hence carry the current to the anode. In the region near the anode, the net space charge becomes negative again and this is accompanied by an increase in the electric field strength. The presence of this positive anode fall is often accompanied by an anode dark space and an anode glow.

## 2.9.3 Plasma Reaction Processes

In the glow discharge, various chemical and physical reactions occur between the highly active and energetic particles mainly by collisions, of which we may distinguish different types.

### 2.9.3.1 Collisions

An *elastic collision* is one in which the energy exchanged is translational kinetic energy only. The atomic or molecular structure is unchanged and no excitation or ionisation occurs. In such a collision, the particles behave like elastic spheres and their interaction can be predicted by classical mechanics using conservation of momentum and energy. The nature of the collision between two particles depends upon the angle between their velocity vectors, the line joining their centres of impact and the ratio of their masses.

In an *inelastic collision*, the gas atom or molecule becomes excited or ionised by acquired energy from the incident particle (Nasser, 1971). This means that a portion of the kinetic energy of the system prior to impact has been converted to potential energy of one of the particles in the system. Generally speaking, whenever conversion from kinetic to potential energy, or vice-versa, occurs, the collision is inelastic.

There are two kinds of inelastic collision, (a) *collision of the first kind* in which one of the colliding species releases some of its kinetic energy and increases the potential energy of the other particle and (b) *collision of the second kind* which is an inverse of the above process. One particle strikes another and absorbs some of its potential energy, moving off with greater kinetic energy (Howatson, 1965).

Potential energy transfer between atoms and ions is an important class of second kind inelastic collision. An ion and neutral atom may collide and exchange positive charge, the ion capturing an electron from the atom. Excitation energy can be exchanged between atoms in a similar way. In some cases the excitation energy of one neutral atom is enough to ionise another atom. Such a process is made more probable if the excited atom is in a metastable state. This phenomenon is called the *Penning Effect* and can be an important ionising agent for discharges in mixtures containing atoms which have metastable states of high energy.

*Attachment and recombination* are other important inelastic collision processes. The process in which an electron, colliding with a neutral particle, forms a negative ion is called attachment. It can be an important process in the removal of free electrons from an ionised gas. Of similar nature to attachment is recombination which can happen when a positive ion collides with either an electron or a negative ion and is neutralised.

#### **2.9.4 Ion Interactions With Surface**

When a fast incident particle strikes the surface of the target, its momentum is transferred to the atoms in the target material. The interactions between the incident particle and the target material may be split into two broad categories:

- i) Elastic effects where striking particles, ions and electrons, may set up a series of collisions between atoms of the target resulting in ejection of one of these atoms, a process referred to as sputtering.
- ii) Inelastic effects where colliding cations interact with lattice electrons to yield optical and x-radiation together with secondary electron emission.

### 2.9.4.1 Sputtering

The removal or ejection of atoms or molecules of a surface by impacting particles is called sputtering. Edenhofer (1974, part 1) considered the process as a vaporisation of the surface by very "hot" ions which strike the surface and intensely heat a localised surface area of the workplace leading to vaporisation of the atoms in that particular region. Sputtering is now considered as a cascade of atomic collisions by the lattice recoil from incident particles due to momentum transfer (Wehner, 1965). The series of collisions in the target, generated by the primary collision at the surface, is known as a collision cascade. It will be a matter of luck whether this cascade leads to the sputter ejection of an atom from the surface or whether the cascade heads off into the interior of the target, progressively dissipating the energy of the primary impact, finally to lattice vibrations, i.e. heat.

Sigmund (1969) suggested that sputtering was based on random collision processes. When the energy transferred from the incident particles is greater than the displacement energy of a lattice atom, collision cascades are initiated. Sputtering occurs if and when the cascade intersects the surface with atoms of energy greater than the surface binding energy.

The incident particle has to be of atomic dimensions, in order for the sputtering process to be efficient. A very small particle, such as an electron, does not carry enough momentum to be effective, whereas a large particle, such as an atomic cluster or macroparticles, is so massive that it cannot interact with individual atoms or molecules in the surface.

A useful measure of the strength of the momentum transfer process for each material is the sputtering yield  $S$ , defined as the number of target atoms (or molecules) ejected per incident ion (Sigmund, 1969). For ion bombardment the sputtering yield  $S$  is given by the following equation (2):

$$S = \frac{3\alpha}{4\pi} \frac{4M_i M_t}{(M_i + M_t)} \frac{E}{U_0} \quad (2)$$

Here  $M_i$  is the mass of colliding atom,  $M_t$  is the mass of target atom,  $E$  is the energy of incident atom,  $U_0$  is the surface binding energy of the material being sputtered, and  $\alpha$  is a monotonic increasing function of  $M_i / M_t$ .

The incident ions should have an energy exceeding a threshold value which is necessary for sputtering process to occur. This threshold value for iron and its alloying elements is between 20 and 30 eV (Keller, 1969). Above the threshold, the sputtering rate increases to a maximum as the ion energy increases. At very high energies, the sputtering rate decreases due to ion penetration into the sub-surface region and ion implantation becomes dominant. The sputtering rate is seen to be dependent upon several parameters such as the mass of the impinging ion, the kinetic energy of the colliding ion, the cathode fall voltage, the discharge gas pressure, and the discharge current.

#### 2.9.4.2 Secondary Electron Emission

The impact of the ion may cause the target to eject an electron, usually referred to as a secondary electron. The number of electrons ejected per incident particle is called the secondary electron coefficient or yield. This value is dependent upon the particle velocity, the discharge gas, and the electrode material (Howatson, 1965). Electron emission yield, as with sputtering, is also dependent upon colliding ion energies-

increasing with higher energies up to the point where ion penetration predominates. Lighter ions produce larger numbers of high energy electrons.

If the ionisation potential of the ion is less than twice the cathode material work function (4.77 eV for iron), no electron will be released. However, if the total energy of the colliding ion exceeds twice the cathode metal work function, then one electron may be ejected whilst a second electron neutralises the ion.

At low ion energy levels, less than 1keV, there are two forms of electron emission, potential and kinetic emission. At higher ion energy levels, kinetic emission prevails. The ionisation potential for  $H_2^+$  and  $N_2^+$  from their gases are 15.43 and 15.55 eV (Field and Franklin, 1957) respectively, hence potential emission is the dominate process and is the means by which secondary electron emission sustains the glow in plasma nitriding.

### 2.9.5 The RF Glow Discharge

Most of the input power in a DC glow discharge is used to accelerate the ions through the cathode sheath and appears as heat when the ions strike the cathode. If the secondary electron coefficient, the number of electrons ejected per incident particle, were 0.1, then, to a good approximation, only 10% of the power will end up in the negative glow from the secondary electrons which are accelerated in the sheath (Rossnagel *et al*, 1990). In this sense, the DC glow discharge is a rather inefficient plasma generator.

The necessity of conducting net current to sustain the discharge is an even more serious limitation of a DC glow discharge. This requirement generally prevents the use of insulating materials in sputtering targets, substrates, or deposited films, because the

insulators would hinder DC current conduction. These shortcomings of the DC glow discharge can be assuaged by using an AC power source.

An RF discharge may be maintained either by inductive or capacitive coupling with the power source, Figure 15. In the case of capacitive coupling the high frequency electric field is responsible for maintaining the discharge. In contrast, an inductively coupled discharge is maintained by the time varying magnetic field.

RF discharge is in some ways quite similar to, and in other ways very different from, the DC discharge that was discussed previously. Unlike the DC discharge, in such system there is no real cathode or anode since the net flow of charge to either electrode is zero. There is also no uniquely defined floating potential (Chapman, 1980). The potential reached by an electrically isolated surface is called floating potential (Thornton, 1987). Such surfaces are bombarded by equal fluxes of electrons and ions.

In RF discharges, elastic collisions of charged particles with the background gas is the major mechanism by which the power is coupled into the discharge. RF discharges have been utilised to achieve higher degrees of ionisation and dissociation and to obtain better control over ion energies than is conceivable for DC discharges (Lisper, 1994).

The RF glow discharge manifests many of the same qualitative features of the DC glow discharge, with the formation of sheaths in which strong electric fields will accelerate ions and electrons.

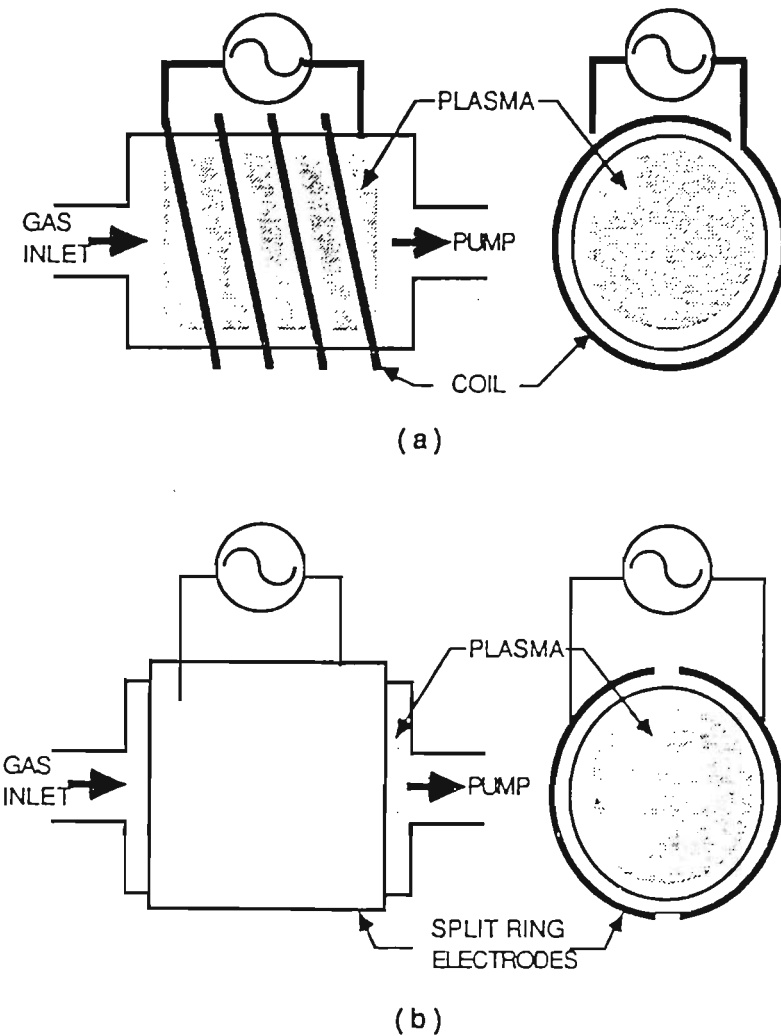


**Figure 15.** (a) Inductively coupled plasma reactor. An alternating current power source creates a time varying current, the magnetic field from which generates a voltage that sustains the discharge. (b) Capacitively coupled plasma reactor. Similar to (a), except the two plates are used to create an electric field to sustain the discharge (Rossnagel et al, 1990).

At low frequency (up to 50 kHz), with a period which is long compared to the time it takes for the plasma particles to come to equilibrium with electric field, the AC discharge is very similar to the DC discharge. As the frequency increases, the massive ions have too much inertia to respond to the instantaneous electric field in the sheath region, while the lighter electrons will. Here, for discharge configurations with unequal electrode

areas and where the electrons are the dominant negative charge carriers, a self-bias will arise which will produce a time-average negative voltage on the smaller electrode. Ions will be accelerated by the difference between the time-average plasma potential and the time-average bias (Rossnagel *et al*, 1990). Generally, the energy of the bombarding ions in an RF discharge will increase as the driving frequency is decreased and/or the neutral pressure is decreased.

There are three mechanisms through which the energy input to the RF discharge occurs. Firstly, striking the electrode by energetic ions will cause the formation of secondary electrons. The acceleration of these electrons through the sheath will cause ionisation as in the sheath and negative glow regions of the DC discharge. Secondly, the oscillating electric fields in the glow can input energy directly into the electrons, much in the same way as the positive column of the DC discharge. Finally, the electrons in the glow will be accelerated by the oscillating sheath electric field, a “surf-riding” mechanism which has no direct analogue in the DC discharge.

## 2.10 Plasma Nitriding

### 2.10.1 Introduction

Plasma nitriding or ion nitriding is a modern process used to impart surface hardening to metals for a wide variety of applications. As the name implies, the process is carried out in a plasma media containing ionised nitrogen alone, or in combination with other gasses to react with the work surface. The process was independently patented by Egan

(1931), and Berghaus (1932, 1939), and advances in the field of power electronics have caused the process to gain world wide popularity in a variety of applications.

Glow discharges which are typically utilised for introducing interstitial elements into the surface of metals possess electron densities and electron energies as shown in Figure 16. From this Figure it can be seen that the glow discharge plasma contains a very high density of electrons ( $1 \times 10^{12}/\text{cm}^3$ ) with an average energy in the range of 1 to 10 eV. Diatomic molecules are ionised or dissociated by electrons of this energy range and produce chemically active atoms that are needed for the process.

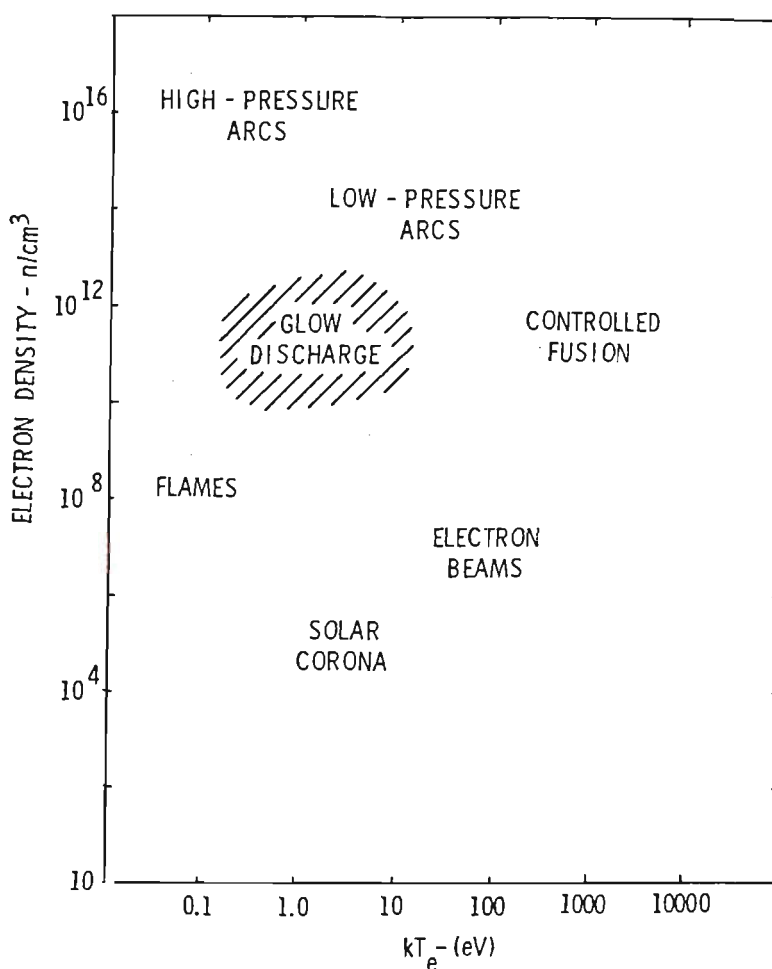


**Figure 16.** Electron energy vs. electron density in glow discharge plasmas compared to other well-known plasmas (Grube and Stephen; Kossowsky (ed.), 1989).

## 2.10.2 Paschen's Law

Under the constant pressure and the voltage, by decreasing the distance between anode and cathode,  $d$ , the positive column simply shrinks in length until it disappears entirely as the anode enters the Faraday dark space. None of the discharge parameters change appreciably until the anode approaches the negative glow. Up to this point little change occurs in the glow regions near the electrodes. When the anode is very near the negative glow, the discharge is still stable, but at a slightly higher voltage. The voltage necessary to maintain stable operation will increase, as  $d$  is further decreased, unless the pressure is increased in order to maintain approximately the same total amount of gas between the electrodes as when  $d$  was large.

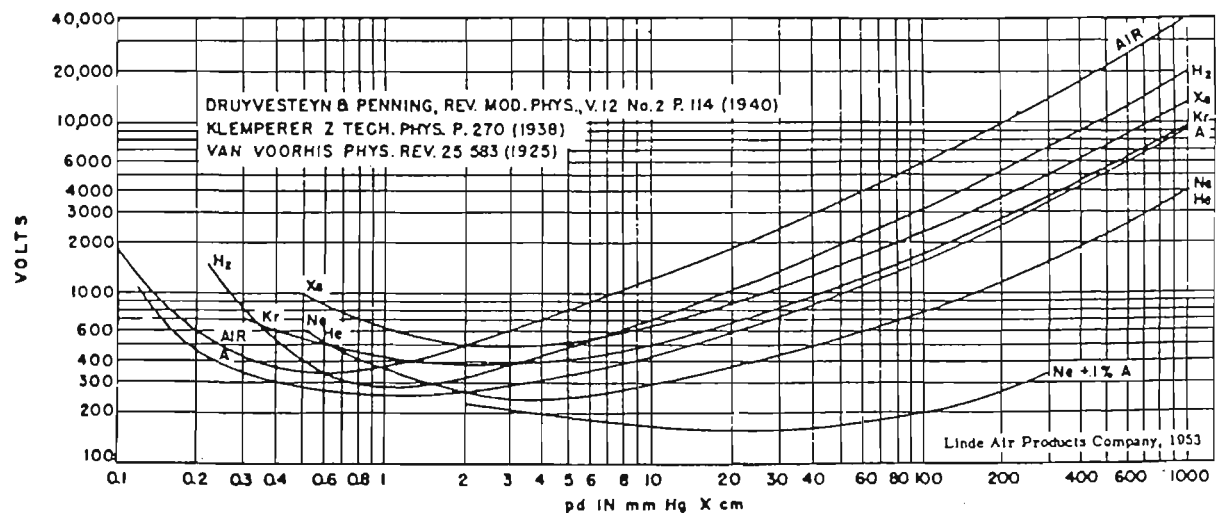


**Figure 17.** Paschen curves for a DC glow discharge between parallel-plate electrodes for various gases. The breakdown voltage,  $V_b$ , is plotted against  $P.d$  (the gas pressure times the distance,  $d$ , between the electrodes on log-log coordinates) (Grube and Stephen; Kossoswsky (ed.), 1989).

As can be seen from the Paschen curves, Figure 17, the voltage required to maintain a stable discharge in a gas at low pressure is a function of the product of the pressure  $p$  and the distance  $d$  between the electrodes. Hence, the pressure must be increased, as  $d$  is further decreased, in order to permit operation at the minimum voltage of the Paschen curve. Operating near the minimum voltage of the Paschen curve is an advantage because it eases the requirements on the power supply and also it minimises the voltage required to obtain complete coverage of the cathode (workpiece) by the plasma which is essential in order to ensure a case of uniform depth over the entire surface of the part. This minimum voltage is indicated by  $x$  in Figure 13.

### **2.10.3 Partial Pressure Operation**

The pressure of the gas mixture for the glow discharge is an important factor that bears directly on the probability that molecular elements in the gas mixture will be ionised by a collision with an electron travelling from the cathode to the anode. Mean free path is the distance that an electron will travel before colliding with a gas molecule. This mean free path is inversely proportional to the gas pressure and proportional to the absolute temperature of the gas. If the pressure of the processing chamber is below  $10^{-2}$  mbar (1 Pa), good vacuum (Figure 18), the mean free path will be large and few gas molecules will be in the electron path between electrodes (Dressler; Sudarshan (ed.), 1989). Thus there will be too few collisions between electrons and the gas molecules to sustain an electrical current. The applied voltage governs partly the number of electrons leaving the cathode. A high voltage can be applied, if necessary, to produce a large number of electrons to increase the probability of ionisation. Nevertheless, in a good vacuum,

where there is considerable distance between gas molecules, the probability of an electron-gas molecule collision will still be low.

If the partial pressure of the gas mixture is increased to between  $10^{-2}$  and 10 mbar (1 and 1000 Pa), there will be a reduction in mean free path and there will be an adequate number of gas molecules to ensure gas ionisation levels that can sustain a glow discharge with a current value suitable for plasma treatment. By further increasing the gas pressure, there will be more than enough gas molecules to ensure collisions with electrons. But, the electrons will now have such a short mean free path between collisions that they will probably not acquire enough energy to cause ionisation of any of the gas molecules encountered unless the voltage is made higher than values considered practical for plasma treating.

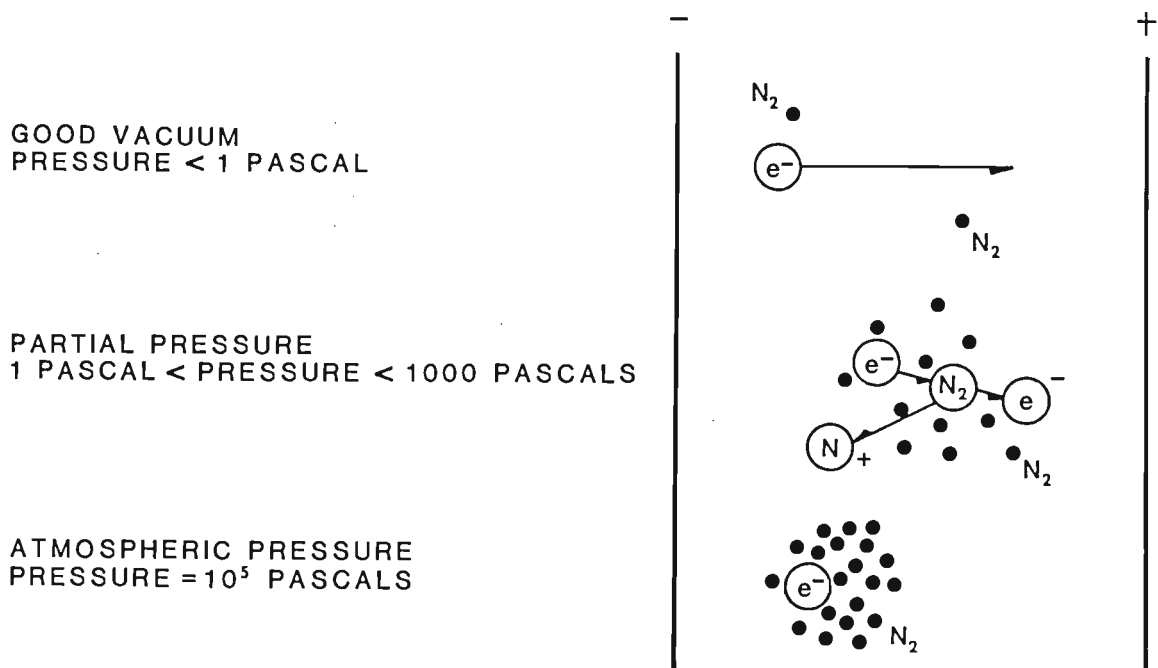


**Figure 18.** Number of gas molecules versus probability of ionisation (Dressler; Sudarshan (ed.), 1989).

## 2.10.4 Nitrogen Activity

In an abnormal glow discharge the density of each molecular species in the gas mixture is important due to its individual contribution to electrical conductance and to the final metallurgy of the surface. The nitrogen activity which is a measure of the nitrogen that is actually available for the nitriding reaction, is a function of many parameters that cannot always be accurately calculated. However, at present time, a good assumption is that this activity is proportional to the nitrogen partial pressure and to the current density at the work surface (Dressler; Sudarshan (ed.), 1989). Current density at the surface of the workpiece is responsible for most of the metallurgical and thermal effects at the surface. The surface area of the workpiece can be calculated and the power supply current is also measured easily, hence the surface current density can be calculated easily. The current density in a plasma process is a function of the gas density or the number of molecules per unit of volume. Increasing the gas pressure increases the current density by increasing the number of available charge carriers if other plasma parameters are fixed.

The gas composition has also an important effect on current density. For most plasma nitriding processes a mixture of nitrogen and hydrogen gases is generally used. If the other parameters remain fixed, the gases that are ionised more easily will produce higher current densities. Increasing the concentration of nitrogen at any fixed gas pressure lowers the resistivity of the plasma and allows an increase in the current density (Dressler; Sudarshan (ed.), 1989). Although the percentage of N<sub>2</sub> in the gas mixture is an easily measured quantity, it should be remembered that the more important physical parameter is the partial pressure of the gas, not the percentage of the gas. The current density is also an important function of plasma voltage.

To calculate similar plasma conditions where current densities can be expected to be nearly the same, the equation of state can be used in the following form, provided the gas composition remains constant:

$$J_1 P_1 / T_1 = J_2 P_2 / T_2$$

J = current density

P = gas pressure

T = surface temperature in degree Kelvin

For example the current density in a plasma discharge at 100Pa and at 100°C will be approximately equal to the current density in a discharge at 200Pa at 473°C. The current density decreases with increasing temperature since the gas density decreases with decreasing gas pressure and increasing temperature.

## **2.10.5 Equipment and Operation**

Figure 19 shows schematically the arrangement of the apparatus needed for plasma nitriding. The main elements are the vacuum furnace, the power supply, and the gas distribution system with a gas-mixing panel or other mass flow controls. An isolated heartplate or work support fixturing is also required to ensure electrical isolation between the workpiece and vacuum vessel. An auxiliary heating system and a rapid cooling system can also be included. The vacuum pump together with the gas distribution system, evacuate the furnace from any possible contaminating gasses such as air, and provide proper mix ratios and flow rate to maintain the required pressure, usually between 10Pa (0.1 torr) to 1000Pa (10 torr) (Edenhofer, 1974, part 1). In the system, a DC potential which can have a value from about 300 volts up to 1500 volts, is placed

across the heartplate and the vessel wall. The heartplate is at the negative potential (cathode) and the vessel wall is at the positive potential (anode).

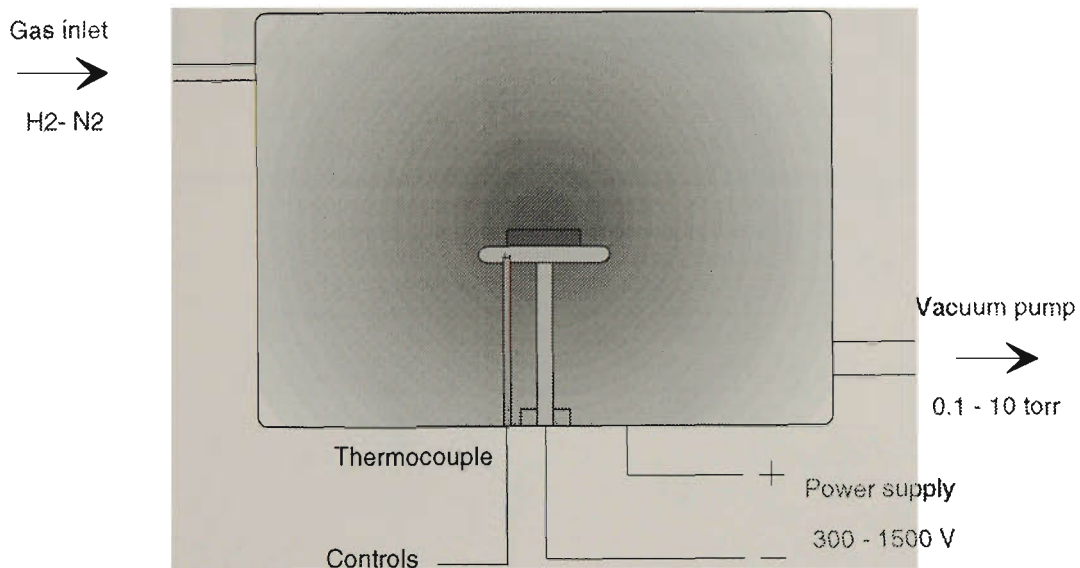
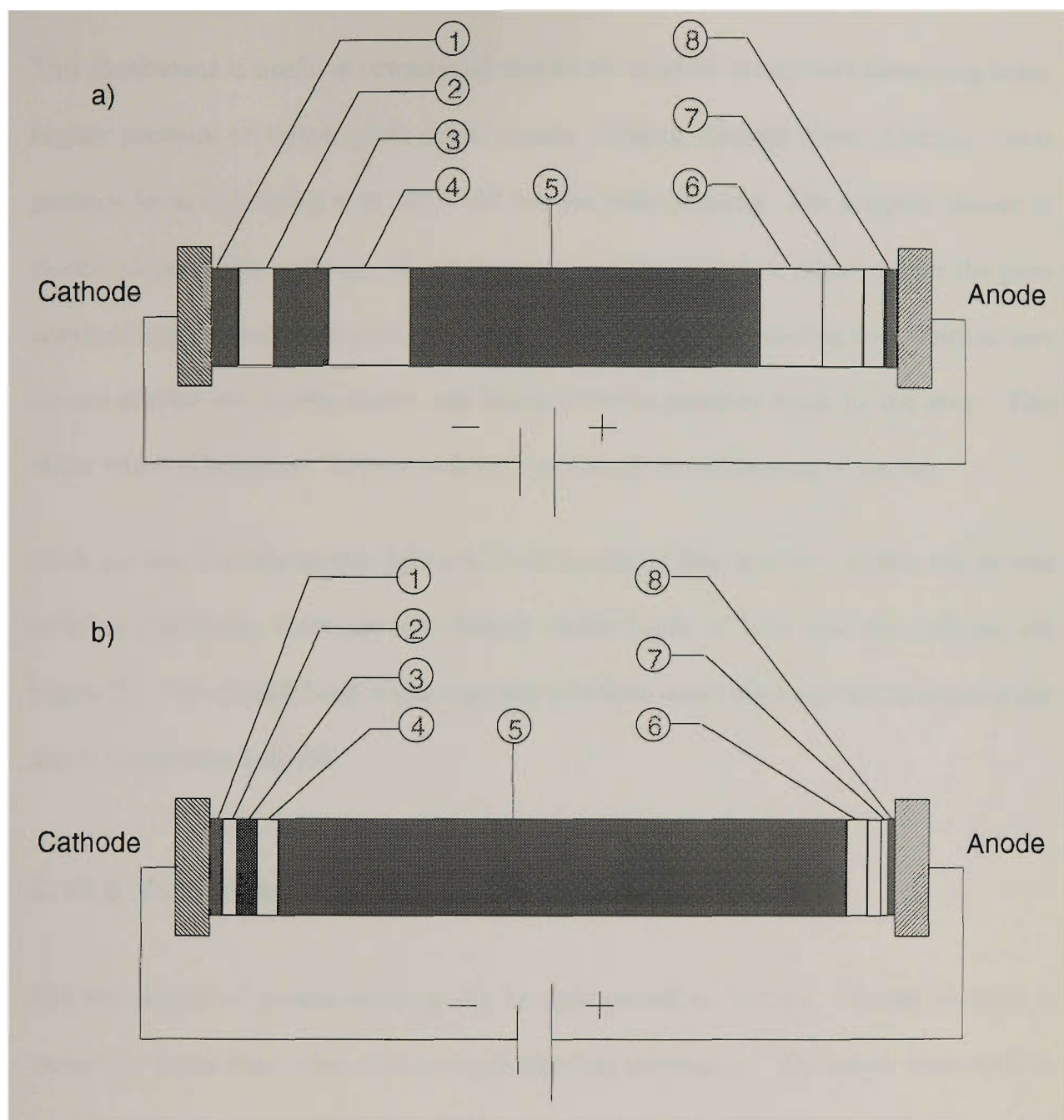


**Figure 19.** Plasma nitriding unit.

When the voltage is applied under process conditions, the potential difference excites and ionises the molecules and atoms of the treatment gas and produces the typical luminous phenomenon known as glow discharge.

Plasma nitriding is carried out at current densities typically from  $0.5 \times 10^{-3}$  A/cm<sup>2</sup> to  $3.0 \times 10^{-3}$  A/cm<sup>2</sup>. Figure 20-a,b (Kovacs and Russell, 1987) show the effect of pressure on the visible glow distribution between the anode and the cathode. The cathodic luminous phenomena, which will be referred to as "glow seam" is limited to a narrow space around the workpiece. It can be seen that the "glow seam" surrounding the cathode, conforms more tightly to the cathode by increasing pressure in the range of 0.5 torr (Figure 20-a) to 3 torr (Figure 20-b) (Kovacs and Russell, 1987).



- |                        |                        |
|------------------------|------------------------|
| (1) Aston dark space   | (5) Faraday dark space |
| (2) Cathode glow       | (6) Positive column    |
| (3) Cathode dark space | (7) Anode glow         |
| (4) Negative glow      | (8) Anode dark space   |

**Figure 20.** Relative glow distribution at (a) low pressure, and (b) increased pressure, for typical plasma nitriding gases (Kovacs and Russell, 1987).

This phenomena is useful in commercial plasma nitriding of workpieces containing holes. Higher pressure or tighter glow seam, causes nitriding through holes, whereas, lower pressure leads to jumping over holes and prevent their nitriding. For irregular shaped or closely placed parts, variation of pressure may put the glow in a region where the glow seams of opposite surfaces meet or overlap. This will lead to trapping ions which in turn causes heavier ion bombardment and higher current densities local to the area. This effect which is known as "hollow cathode", will result in overheating of part(s).

Each gas has its own unique light and dark spaces or line spectra. Under the normal nitriding conditions, there are two distinct visible bands of light near the cathode, see Figure 20. The closest band is thin and pink in colour while the next band is much wider and is purple-blue colored.

### **2.10.6 Advantages and Disadvantages**

The advantages of plasma nitriding can be summarised as follows. Plasma nitriding is essentially faster than other conventional nitriding techniques. *Treatment times* half as long for the same case depth have been quoted (Loh, 1980). This accelerated rate of nitriding may be attributed to the presence of a strong electric field in the plasma nitriding process which creates a net flux of ions and energetic neutral molecules (which arise from charge exchange collisions) towards the workpiece surface. Hence, for a given pressure, the workpiece surface receives a far greater number of 'active' species per unit time in a glow discharge environment than the number of molecules available for an equivalent gaseous system. An increase in reaction rate may therefore be expected at the early stages of the treatment. Nevertheless, as treatment proceeds, diffusion of nitrogen within the material becomes rate controlling. Hence when hardness profiles obtained

from materials treated at similar temperatures for identical times by gas nitriding and plasma nitriding processes are compared, there are only small differences in case depth (Staines, 1985). In materials with passive oxide films, eg austenitic stainless steels, it is possible to achieve reductions in processing time. This is due to *depassivation* of the surfaces and removal of passive oxide films and contaminants present on workpiece surfaces by the sputtering effect of the glow discharge, whereas conventional nitriding processes cannot de-passivate surfaces in the same way. Furthermore, post treatments may be eliminated in most cases due to the inherently high quality of *surface finish* obtained.

The use of vacuum environment allows savings as high as 95% to be made in treatment *gas consumption*, compared to gaseous treatment. An extensive investigation on *energy utilisation* have been carried out by Marciniak and Karpinski (1980). They suggested that for fully loaded units there is no significant savings, but when the loading is light plasma nitriding units are more economic with regard to electrical energy consumption. This reduction in energy consumption is achieved not only because treatment times are reduced but because it is only the cathodically charged workpieces that are heated and there is no need to heat up the whole furnace chamber.

Proper control of the temperature, atmosphere composition, and discharge parameters can lead to production of *superior microstructure* and permit better control over the composition of the final product surface, its structure, and its properties. Loh (1980) has claimed that single-phase compound layers may be formed, which is not possible with conventional nitriding treatments.

Operating conditions ensure a uniform glow seam independent of their distance to the anode and thus uniform treatment of all exposed surfaces leading to an improvement in the *uniformity* of the hardness profile on complex shapes.

Unlike conventional nitriding treatments the process can operate at a temperature as low as 350 °C. *Low temperature* nitriding allows high surface hardness to be achieved along with the maintenance of high core strength in low temperature tempering steels. Furthermore, treating at these low temperatures keeps distortion to a minimum.

Unlike conventional nitriding in which tin plating, copper plating, and liquid glass are used as a protective coating, *easy masking* is possible by use of mechanical masks to prevent full coverage of the surface by the treatment plasma. Areas can be protected by sheet-materials or by special sleeves slit a few hundredth of a mm, because a glow discharge cannot form in such gaps.

Plasma nitriding is environmentally *non polluting*. The gas discharge from a plasma nitriding furnace is non-toxic and can be vented directly to an outdoor location.

There are few disadvantages of the plasma nitriding process. These can be summarised as follows:

*Cleanliness* of surface of the components is essential to hinder unstable arc discharges forming during the heating cycle. The need to *fixture* parts to avoid overheating is another disadvantage of plasma treatment. Because of power/surface area relationships, components with *similar size* may not be plasma nitrided in one batch. The last and perhaps the most disadvantageous of plasma processes is the high initial plant cost.

## 2.10.7 Proposed Nitriding Models

One of the most widely used model for plasma nitriding is based on the work done by Kölbel between 1965 and 1968. The model is based on the sputtering by ion bombardment. Figure 21 illustrates the layer formation mechanism suggested by Kölbel. Initially, incoming nitrogen ions and highly energised neutral particles sputter elemental iron from the cathode workpiece surface. These ion atoms reacts with nitrogen neutrals in the cathode fall region and form FeN which is deposited on the workpiece surface. Since FeN is not thermally stable compound, it degrades to iron nitrides with a lower nitrogen content, producing nitrogen atoms that are capable of diffusion.

A significant limitation imposed by Kölbel is that repurified nitrogen must be used. This model cannot be considered valid if small quantities of hydrogen are present (Kölbel, 1965). The findings of Keller (1971) and Edenhofer (1974, part 1) further support this model. Their investigations on the plasma nitriding of spheroidal graphite iron showed that a uniform compound layer of iron nitrides was produced even on the graphite nodules cut by the specimen's surface. They interpreted this result as confirmation of Kölbel's layer formation model. Nevertheless, in investigations into the industrial plasma nitriding of cast iron, no compound layer was detected on the surface at the sites of graphite lamella penetration (Lampe, 1993). This would indicate that Kölbel's layer formation mechanism plays a minor role in industrial plasma nitriding using nitrogen-hydrogen mixtures.

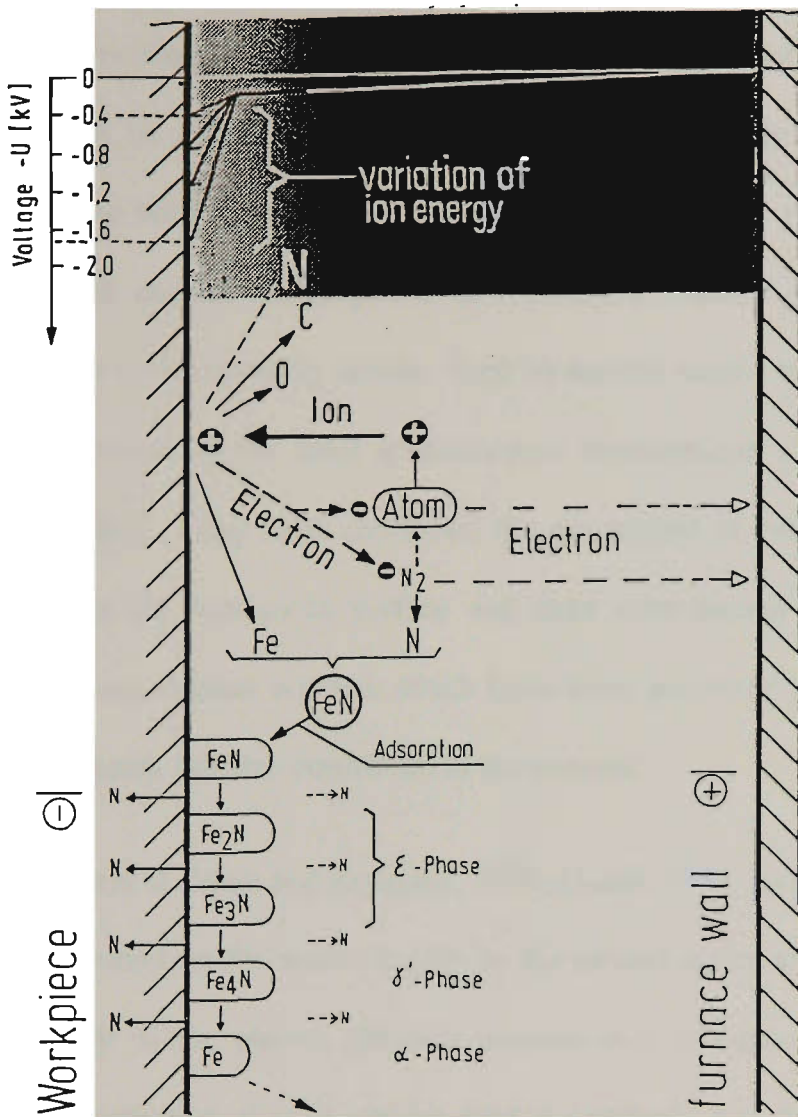


**Figure 21.** Surface reactions occurring during plasma nitriding (Edenhofer, 1974, part 1).

Another model proposed by Tibbets (1974) is based on the mass transfer of neutral atoms to the workpiece surface. According to Tibbets the mass transfer occurs mainly by the adsorption of neutral atoms, not of ions on the metal surface. A positively biased grid was placed 1.5 mm from the cathode within a N<sub>2</sub>/H<sub>2</sub> glow discharge plasma. Tibbets found that the cathode continued to nitride even when the grid potential was such as to repel almost all positive ions from the specimen surface. It was shown that the nitriding rates for materials with or without the grid were almost the same. From his

calculations Tibbets concluded that there were no neutral or excited N/H molecules with sufficient lifetimes to effect any nitriding once passed through the grid. He also supported his view with the fact that the level of ionisation of particles in the glow discharge used for plasma nitriding is low, typically a fraction of  $\sim 10^{-7}$ . Tibbets concluded that the active nitriding species must be neutral atomic nitrogen. This model was partially supported by the mass spectroscopic investigations carried out by Szabo and Wilhelm (1984). They have confirmed the adsorption of neutral particles of the form  $\text{FeNH}_2\cdot 3$  on the workpiece surface and their contribution to layer formation. Neutral particles and excited neutrals which have been generated by sputtering and/or reactions in the plasma can also contribute to the process.

A number of authors (Lakhtin and Krymskii, 1970; Hudis, 1973; Jones *et al*, 1975), have claimed that the mass transfer occurs mainly by the ionised atoms and molecules. Hudis performed a study of the plasma nitriding process in a nitrogen-hydrogen-argon gas mixture. The distribution of ionic species near the cathode was determined utilising a mass and energy analyser. He concluded that  $\text{NH}_3^+$  molecular ion species were mainly responsible for nitriding. Nevertheless, he claimed that the ionised environment alone is not sufficient to nitride the work piece. Employing RF plasma, he observed that the nitriding occurred only if a potential difference across the electrode was applied. He also verified that the process operates via particle bombardment and not via simple gas absorption. By introducing hydrogen to a nitrogen/argon atmosphere, Hudis noticed a great improvement in the nitriding rate. The optimum nitriding condition were observed when all the argon had been replaced with hydrogen.

Ricard *et al* (1989) have investigated nitriding of steels in post discharge and obtained results which were comparable to the nitriding in glow discharge. They have

demonstrated using emission and absorption spectroscopy, that the long lived active species, the  $\text{N}_2^+$  ions, the vibrational  $\text{N}_2$  and N neutral species are responsible for nitriding in post discharges. From their experiments it can be concluded that the sputtering is not an essential prerequisite for plasma nitriding.

By superimposing a crossed magnetic field onto a glow discharge plasma, Brockman and Tuler (1981) have been able to perform nitriding at low pressures. They showed that the ratio of electric field/pressure (E/P) dictated the surface atomic concentration and found that the nitrided case depth varied only with current density for a fixed time and fixed E/P ratio. Consequently, they concluded that the nitriding process is controlled by ionic flux and not by atomic nitrogen concentration as proposed by Tibbets.

Xu and Zhang (1987) have suggested a collision dissociation model. They claim that in plasma nitriding the process of nitrogen atom migration from gas phase to solid phase is achieved basically by penetration of active nitrogen atoms produced by collision dissociation. Positive ions of high energy dissociate  $\text{N}_2$  or  $\text{NH}_3$  to produce active N atoms by inelastic collisions. They have also claimed that hydrogen has a significant role in plasma nitriding. The strong deoxidation and sputtering capability of hydrogen atoms helps eliminate the passivated film and activate the metal surface. It also significantly reduces the energy required for collision dissociation to produce active N atoms.

A detailed study of the species present within a glow discharge plasma have been made by Ricard *et al* (1982). Based on the evidence achieved they claimed that, both ionic and neutral atom bombardment of the surface occurs and that it is high energy neutrals that are the main species responsible for the heating and nitriding action. They also found that the addition of hydrogen to the plasma produces an increase in the secondary

electron coefficient of the ferrous surface which in turn influences the ratios of the plasma constituents and enhances the nitrogen potential of the medium.

A study of plasma nitriding by Petitjean and Ricard (1984) has been conducted in a nitrogen-hydrogen gas mixture using optical emission spectroscopy. They found that the addition of a few percent of hydrogen leads to a significant increase of discharge current and sample temperature.

Although many plasma diagnostic investigation have been carried out and some models have been suggested, further critical experimentation is required to reconcile the various points of views. It would appear that all of the mechanisms suggested by different authors so far play some role in the process but which is the main factor is not obvious and depends greatly on operating conditions.

## **2.11 Ion Implantation**

### **2.11.1 Introduction**

Ion implantation is a modern surface modification technique that causes hardening by entirely different mechanisms compared to nitriding. It was first used in the 1960s to dope semiconductor materials for the electronics industry. Due to its accuracy, speed, cleanliness and controllability it has become the standard method for this type of work. In the early 1970s the idea of using ion beams to enhance the surface properties of metals

became a reality. Ion implantation of metal surfaces was found to produce surprising results in reducing wear, friction and corrosion (Hartley *et al*, 1972).

Ion implantation is the process of introducing atoms of alloying elements into the surface of materials by accelerating the atoms to very high energies of 50-200 keV and allowing them to strike the metal surface (Kossowsky, 1989). It requires the formation of an ion beam which is rastered in a predetermined pattern across the surface of the material to be implanted. For treating complex parts, they may also need to be manipulated remotely to allow a complete surface treatment (Elder *et al*, 1989). Implanted layers are typically in the order of 0.01-1 $\mu$ m thick, depending on the energy of the ions. The need for high temperatures to produce a thermal diffusion of the incident atoms into the surface is eliminated due to the mechanical injection of the atoms into the surface. Hence, heating of the workpiece by ion bombardment is usually undesirable and is avoided by using a cooled platform. The temperature of the implanted part is typically kept below 100°C.

## 2.11.2 Basics of Ion Implantation

Ion Implantation processes are generally carried out in a high vacuum, 1 mPa, in order to minimise scattering or neutralisation of the beam (Dearnaley *et al*, 1986). In its simplest form the implanter contains an ion source , in which the ions are created from a plasma, and a chamber containing the items to be treated. The material to be ionised is introduced into a chamber as a gas. It may already be in the form of a gas (e.g. nitrogen), or the gas may be produced by vaporisation from a source, or it can be produced by other means. Biasing the source at 50-200 keV (and in some cases up to 4 MeV) accelerates the ions to high speeds and directs them into the chamber. The process is line-of-sight, since the ions enter the chamber as a beam. Because many ions

are produced from compounds, if a single ion species is needed the beam must be filtered. The ions can be separated according to charge and mass by passing through a suitably controlled magnetic or electrostatic field. A magnetic field is commonly used. The ions are forced into an arc path, and the field adjusted to only allow those of the desired mass or charge to pass through the opening at the entrance to the accelerator. The selected ions then enter an accelerator which is basically a series of plates that are progressively charged to a high potential. For proper implantation, the final energy must be in the range of kilo-electron volts which is much higher than that required for ionisation or dissociation.

When the highly energetic ions strike the surface, a number of near surface phenomena take place. Collision cascades and sputtering are the two major occurrences which are illustrated in Figure 22 and have been already discussed previously.

As the incident ion impinges the surface, its kinetic energy will be dissipated in elastic collisions with substrate atoms and by excitation of bound electrons. The energetic ion collides with the atoms of the solid and continue its way to a depth of many hundred Angstroms. Along this path, it displaces many atoms by primary and secondary encounters, and for a time of about  $10^{-11}$  s creates a region of the material containing hundreds of interstitials and vacancies, Figure 22, (Solnick-Legg and Legg; Sudarshan (ed.), 1989). This is known as a collision cascade and is often visualised as a very localised spike of thermal energy, although it cannot truly be thought of as a thermal process. As the ion continues to penetrate, it will collide with more atoms, continually dissipating energy and will finally come to a rest.

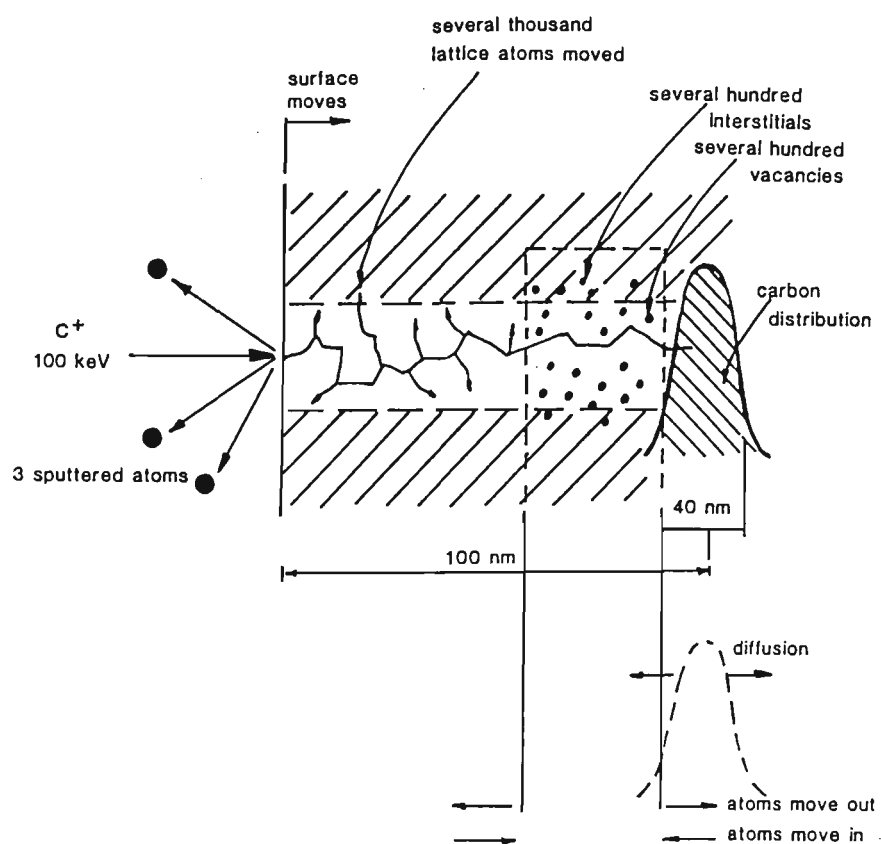


**Figure 22.** Processes occurring in a typical collision cascade (Solnick-Legg and Legg; Sudarshan (ed.), 1989).

The maximum penetration of the ions is a function of atomic number and mass of incident species and substrate elements, and energy and angle of incidence of the ion beam (Fenske, 1992). As the energy of the ion beam is increased or the atomic number, density of the substrate and mass of the incident decreased, deeper penetration is achieved. The depth profile is, generally, Gaussian with a slightly pronounced tail, and can be calculated using Monte Carlo simulation programs.

When the high energy ions strike the surface, they may have sufficient energy to cause some of the atoms of the material to be sputtered from the surface. This can occur by single or double collision events and cascades, accumulation in the gradual erosion of the surface. The same factors which control the depth of penetration also control the

sputtering rate. Generally, if the depth of penetration is increased, sputtering is diminished.

Dose or fluence is the common term used to describe the amount of ions implanted into a material. It is defined as the total number of ions which have impinged the surface during implantation per  $\text{cm}^2$  (Elder *et al*, 1989). It is important to differentiate between dose (fluence) and retained dose, the number of ions embedded in the material per  $\text{cm}^2$ . Due to ablation at the surface, the retained dose is always less than the dose.

Nitrogen ion implantation was developed in mid 70s to increase the useful life of production tooling. It is now being used commercially for improving the wear and corrosion resistance of a wide variety of tools. The implantation processes for nitrogen ions use energies of 50-150 keV and doses of  $1\text{-}10 \times 10^{17}$  ion  $\text{cm}^{-2}$  (Legg and Solnick-Legg, 1988). Nitrogen ion implantation is usually carried out in a simple ion implanter not equipped for mass separation of different ion species, so all the ions produced in the ion source are fired into the sample. Sample or beam scanning, while sometimes used, can often be discarded in favour of simply using a broad ion beam of reasonable uniformity.

### 2.11.3 Strengthening Mechanisms of Ion Implantation

Elder *et al* (1989) suggested three mechanisms which are responsible for the increase in the surface hardness of an ion implanted material and a brief summary of the proposed mechanisms is given here. The first mechanism is a *damage and defect induced effect* caused by the slowing implanted ions, producing results similar to those obtained through shot peening and cold working. Ion implantation results in compressive surface

residual stresses. These stresses are due to the expansion of the lattice in an ion implanted layer, from the accommodation of large numbers of impurity atoms, which results in the constraint of the substrate putting the surface in compression. Strain hardening in the implanted layer arises from a dense network of tangled dislocations and dislocation loops, generated as a result of the collapse of vacancy clusters during implantation. These strain fields create a large energy barrier, which prevents plastic flow.

*Solid solution strengthening* is the second mechanism. Strengthening is achieved by blocking the movement of dislocations. This is done by creating obstacles, i.e., points at which energy is absorbed in the movement of a dislocation. Foreign atoms, either interstitial or substitutional, are the simplest obstacles. The strain field associated with substitutional impurities hinders dislocations movement. Interstitial atoms are able to segregate at dislocation, if they are mobile, and form Cottrell atmospheres which resist deformation.

The third proposed mechanism is *second-phase strengthening*, where the dislocations are pinned at the sites of the second phase particles. A dispersion of second phase particles will resist deformation, particularly if they are hard. However, if they are too large the interface can crack. Since ion implantation is carried out at low temperatures, it is ideal for introducing a very fine dispersion of second-phase precipitates.

The dose governs the contribution from each of these mechanisms to the total hardness of the implanted layer (Leutenecher, 1989). Damage induced hardening effects dominate for very low doses,  $10^{15}$ - $10^{16}$  ions  $\text{cm}^{-2}$ . The contribution from solid solution strengthening becomes more dominant for intermediate doses,  $10^{16}$ - $10^{17}$  ions  $\text{cm}^{-2}$ . For

high doses,  $> 10^{17}$  ions  $\text{cm}^{-2}$ , the contribution from precipitation strengthening tends to dominate.

#### **2.11.4 Plasma Source Ion Implantation (PSII)**

The main problem with conventional ion implantation is that the ion beam must be directed to the surface of the part and the best implantation is obtained when the beam is normal to the surface. This is a line-of-sight process, and the parts being implanted, as mentioned earlier, generally require manipulation in fixtures to implant the desired surfaces. Manipulation adds complexity to the process and limits the size of component that can be implanted.

In a new method, plasma source ion implantation (PSII) developed by Conrad and co-workers (1987) in Wisconsin, USA, the part is placed directly in the plasma source and is pulse-biased to a negative potential of -10 to -100kV relative to the chamber walls. A thick ion matrix sheath forms around the target. On each pulse, ions are sucked out of the plasma directly into the sample surface from all directions simultaneously. This gives relatively uniform implantation and overcomes the line-of-sight restriction. In order to prevent the plasma losing all of its ions, the pulse is turned off after a few microseconds. In this way the implant dose is built up by a series of very short pulses. The beam current in each pulse can be very high (many amperes), but the dose rate is determined by the average current. This is limited by sample heating considerations and by the capability of the power supply. Unlike other ion-assisted surface modification techniques such as ion plating, ion coating, or plasma nitriding, PSII produces a deposition profile characteristic of high-energy ion implantation.

## 2.11.5 Plasma Immersion Ion Implantation (PI<sup>3</sup>)

Plasma immersion ion implantation (PI<sup>3</sup>) was developed by ANSTO (Australian Nuclear Science and Technology Organisation) at Lucas Heights, Australia, and the details of the process were first published in 1988 (Tendys *et al*, 1988). Depending on treatment temperature, it has been demonstrated to impart properties to the treated material typical of ion implantation, plasma nitriding or a combination of both. The process has been able to overcome some of the problems associated with ion implantation, utilising a gas plasma in combination with high voltage pulses to form an evenly treated layer. Although PI<sup>3</sup> was developed independently, it is closely related to PSII.

The difference between the two techniques lies in the method of plasma generation. In PSII, the plasma is generated by high energy electrons emitted from a biased multidipole filament and confined by an array of permanent magnets situated around the chamber (Conrad *et al*, 1987). In contrast, the PI<sup>3</sup> plasma is an inductively-coupled radio frequency (RF) glow discharge and there is no magnetic confinement. The PI<sup>3</sup> apparatus has been discussed in detail in the literature (Tendys *et al*, 1988; Collins *et al*, 1991; Hutchings *et al*, 1992), and only a brief summary is given below.

In a cylindrical vacuum vessel, a suitable gas (or gas mixture) is used at a filling pressure between  $1\text{--}2 \times 10^{-3}$  mbar. The workpiece is supported in the centre of the vessel by an isolated conducting stage which supplies the bias voltage for implantation. Approximately 300W of RF power at 13.56 MHz is used to produce a plasma with an ion density of  $2 \times 10^9 \text{ cm}^{-3}$ . The target forms the cathode of the bias circuit which supplies -45 kV pulses of 100  $\mu\text{s}$  duration. The high voltage is pulsed because of the large

current density drawn from the plasma. The body of the vessel is grounded and forms the anode of the implantation circuit.

An ion rich sheath is formed which effectively insulates the target from the surrounding neutral plasma and ions are accelerated across the sheath and strike the surface at angles close to normal. This will result in a high retained dose and minimal ion sputtering. The high ionisation rate of the RF glow discharge is believed to form a sheath of equilibrium width several microseconds after the initiation of each high voltage pulse. This is in contrast to the continuously expanding sheath observed in PSII (Collins, 1990). In other words, in PSII the sheath is quickly depleted and has to expand to acquire nitrogen, while in PI<sup>3</sup>, the RF plasma supplies an abundant amount of nitrogen ions which enter the sheath and are accelerated towards the target.

The current density in the pulse ranges from 1 to 2 mA cm<sup>-2</sup>, which is two order of magnitude higher than for conventional implantation. The heating contribution of ion bombardment is significantly increased and the frequency of pulse repetition or the duty cycle are regulated to control the surface temperature of the sample which is measured using an infra-red pyrometer installed at the top of the chamber. Elevated temperature treatment enables diffusion of nitrogen to significantly greater depths than those achieved in conventional ion implantation. Thermal equilibrium of the target is usually reached after 20-30 minutes of treatment time and radiation provides the dominant cooling mechanism. Treatment temperatures range from 150°C up to approximately 600°C (Hutchings R., 1994).

It is beyond the scope of this section to discuss the results obtained by other workers in order to evaluate the capabilities of the PI<sup>3</sup> technique. Hutchings (1994) and Collins and

co-workers (1994) have thoroughly reviewed the relevant literatures. Nevertheless, it is worth mentioning some of the materials employed during these investigations, such as mild steel and stainless steel (Collins *et al*, 1991), tool steels including AISI H13 (Hutchings *et al*, 1991; Hutchings *et al*, 1992), AISI S1 and Viking™ (Samandi *et al*, 1992; Collins *et al*, 1993), austenitic stainless steels AISI 304 (Collins *et al*, 1991) and AISI 316 (Samandi *et al*, 1993). All the experiments have been conducted in a pure nitrogen atmosphere.

In PI<sup>3</sup> treatment at low temperature (below 200°C in steels), although nitrogen is confined to the top 100nm of the material, significant improvements in wear performance have been obtained. At higher temperatures, nitrogen diffuses to depths well beyond the implantation range and structures are formed that are more like those obtained in plasma nitriding with significant increase in hardness and load-bearing capacity. At these temperatures, nitrogen can also be thermochemically absorbed from the RF plasma so the process can be considered as a hybrid treatment combining low-pressure plasma nitriding with high energy ion bombardment (Samandi *et al*, 1992).

## **2.11.6 Advantages and Limitations of the Plasma Ion Implantation process**

There are several advantages of plasma-base ion implantation over traditional methods of plasma nitriding such as (Collins *et al*, 1994):

- 1) The possibility of production of a nitrided layer at temperatures as low as 250°C.

- 2) Nitriding can be carried out at atmosphere containing nitrogen with no hydrogen at pressures typically  $10^{-3}$  mbar.
- 3) Target bias is separated from the plasma generation circuit which in turn reduces the possibility of arcing and offers better control of the process.
- 4) Production of surface "metastable" phases with superior wear and corrosion resistance compared to the equilibrium phases obtained by thermochemical processes.
- 5) Remarkable dimensional stability and good surface dignity of the treated samples.

Several advantages have been attributed to the plasma-based ion implantation process over the conventional methods of ion implantation, including uniform coverage, low unit cost, the easing of line-of-sight restriction and the ability to treat complex shapes. Additionally, it is easier to scale to large targets, offering the prospect of a technologically simple implanter design (Collins *et al*, 1991). However, the limitations of the plasma-based ion implantation compared with traditional methods of ion implantation are as follows (Collins *et al*, 1994).

- 1) Contrary to the earlier claims, plasma ion implantation dose not completely overcome the line-of-sight restrictions of traditional ion implantation.
- 2) There are limitations on the packing density for multiple components of complex shape. The distance between the components needs to be in excess of 10cm due to the relatively large sheaths (Conrad *et al*, 1989).
- 3) The ion energy achievable by plasma ion implantation is restricted not only by the technical problems but also by safety hazards associated with electric shock and x-ray production. Furthermore, practical considerations such as field emission from the target,

larger cathodic sheaths, reduced efficiency from secondary-electron emission, heat dissipation in the surface and the increased current requirements of the modulator, put the maximum operating high voltage in the range 50-100kV.

- 4) For the development of particular applications, conventional ion beam techniques offer better species and dose control which may be advantageous in certain situations.

# **3. CHAPTER THREE:**

## **EXPERIMENTAL PROCEDURE**

---

### **3.1 Materials**

Two materials were used in this investigation, a commercially available chromium bearing microalloyed steel, MAXIMA™ and a conventional nitriding steel, En19, which was used as a reference. The chemical composition of these steels which obtained by spark emission spectroscopy is shown in Table 3. The structure of MAXIMA™ and En19 steels prior to nitriding were examined by optical microscope. The photomicrograph in Figure 23 shows the microstructure of as received MAXIMA™, consisting of proeutectoid ferrite plus bainite. The grain boundaries are clearly visible indicating a grain size of ~ 40-70 $\mu\text{m}$ . The microstructure of En19 steel consists mainly of tempered martensite plus some undissolved carbides, Figure 24.

**Table 3.** *Chemical composition of MAXIMA™ and En19 steels obtained by spark emission spectroscopy.*

Steel	Element, wt. %										
	C	Mn	Cr	Mo	Si	Ni	Cu	Al	Nb	Ti	V
<b>MAXIMA™</b>	0.21	1.57	1.9	0.03	0.05	0.255	0.41	0.029	0.01	0.012	0.005
<b>En19</b>	0.4	0.79	1.05	0.17	0.26	0.042	0.056	0.037	<0.003	<0.003	0.003



25  $\mu\text{m}$

**Figure 23.** Optical micrograph of as received (hot-rolled and air cooled) MAXIMA™ microalloyed steel, showing proeutectoid ferrite plus some bainitic products. Etched in 2.5% Nital.



25  $\mu\text{m}$

**Figure 24.** Optical micrograph of En19 steel, showing some undissolved carbide in a matrix of tempered martensite. Etched in 2.5% nital.

The majority of inclusions in both steels were found to be MnS, judging by their distinct grey colour under the optical microscope, and also confirmed by energy dispersive spectroscopy.

The hardness of the specimens before the surface treatments was determined by a Vickers hardness tester using 20 kg load. The results are presented in Table 4.

**Table 4.** Hardness ( $HV_{20}$ ) of the materials prior to surface treatment.

Steel	Hardness, $HV_{20}$
<b>MAXIMA™</b>	366
<b>En19</b>	340

## 3.2 Specimen Preparation

Samples in the form of discs 25 mm in diameter and 5 mm thick were sectioned from the steels. MAXIMA™ samples were cut from a 20 cm diameter bar in the as-received condition, hot rolled and air cooled (details of the heat treatment were not provided by the manufacturer of MAXIMA™ steel). The En19 samples were made from a 30 mm diameter quenched and tempered (at 580°C for one hour) bar.

The surfaces to be treated were polished to a 1 $\mu\text{m}$  diamond finish, using standard metallographic techniques. The samples were degreased in acetone prior to treatment.

### **3.3 DC Plasma Nitriding**

DC plasma nitriding was carried out using two different plasma nitriding units. At the inception of this work no plasma nitriding facility was available at the University of Wollongong, therefore, the preliminary DC plasma nitriding treatments were performed in a 40 kW Klöckner Ionnon industrial scale unit at the University of Birmingham, England.

Further experiments were later carried out using a unit designed and commissioned at the Surface Engineering Research Centre at the University of Wollongong, see Figure 25. It uses a 5 kW switch mode power supply equipped with arc suppression circuitry. A schematic of the unit is displayed in Figure 26. All treatments were carried out with power regulation to maintain the desired temperature. During treatment, the temperature was monitored by an inconel sheathed chromel-alumel thermocouple embedded in the specimen and electrically isolated by a ceramic sleeve. The temperature was controlled by a Eurotherm temperature controller within  $\pm 1^{\circ}\text{C}$ . The voltage and current parameters were automatically varied to maintain the temperature at the pressure setting.

The processing gases were provided using pre-mixed gas bottles. Since the pumping speed as well as the conductance of the throttle valve are different for nitrogen and hydrogen, the actual gas composition inside the chamber during the process is expected to be different from the feeding gas. In an effort to monitor the nitrogen and hydrogen partial pressures (actual gas composition) of the nitriding atmosphere, a HIDEN HAL-100 residual gas analyser was utilised. Since the operating pressure of the gas analyser was several orders of magnitude lower than the nitriding pressure, an orifice was

installed between the chamber and the gas analyser instrument. However, the requirement for using orifice precluded the utilisation of the instrument at chamber pressures higher than 1.5 mbar which was lower than the processing pressure (4mbar). It should be mentioned, if it were possible to monitor the partial pressures of the gases in the processing atmosphere using an orifice, the readings still would not be the real gas composition of the treatment atmosphere. This is again due to the difference in the gas conductance of the orifice for nitrogen and hydrogen. Nitrogen and hydrogen molecules (ions) pass through the orifice and reach the gas analyser detector with different speeds.

Bearing in mind the above mentioned points, the gas compositions stated in DC plasma nitriding hereafter, is the feeding gas composition which might be different from the actual processing composition.

The treatment pressure was monitored by both mechanical and pirani gauges and regulated by up-stream control of process gas through a needle valve.

The specimens were symmetrically positioned on a steel table (Figure 27), 15 cm in diameter, in order to eliminate any risk of temperature non-uniformity.

The chamber was evacuated twice to  $10^{-2}$ mbar and purged with nitrogen prior to the treatment. Heating of the specimens was performed in a hydrogen plasma, which involved gradually increasing the pressure from  $5 \times 10^{-1}$  mbar to the treatment pressure of 4 mbar. All heating was supplied by the glow discharge, and once the treatment temperature was achieved, (usually within 1 hour), the hydrogen was replaced by the treatment gas. After treatment, the specimens were slowly cooled to room temperature in a nitrogen environment.

### 3.3.1 Treatment Conditions

DC plasma nitriding of the samples, using a 40 kW industrial scale unit, were carried out at different temperatures, namely 350, 400, 450, 500, and 550°C in a 75%N<sub>2</sub>-25%H<sub>2</sub> atmosphere. The treatment duration was 5 and 10 hours and the pressure was 4 mbar.

Two series of experiments were performed using the 5kW prototype unit. In order to gain a rough idea about the optimum N<sub>2</sub>-H<sub>2</sub> gas mixture for nitriding of MAXIMA™, preliminary experiments were carried out at 450°C in atmospheres containing different concentrations of N<sub>2</sub>-H<sub>2</sub>, i.e., 100%N<sub>2</sub>, 75%N<sub>2</sub>-25%H<sub>2</sub>, 50%N<sub>2</sub>-50%H<sub>2</sub>, and 25%N<sub>2</sub>-75%H<sub>2</sub>. The other series of experiments was conducted using both MAXIMA™ and En19 samples, at 350, 400, 450, 500, and 550°C in a 75%N<sub>2</sub>-25%H<sub>2</sub> atmosphere. In all cases, the treatment time was 5 hours and the pressure during the treatments was 4mbar.

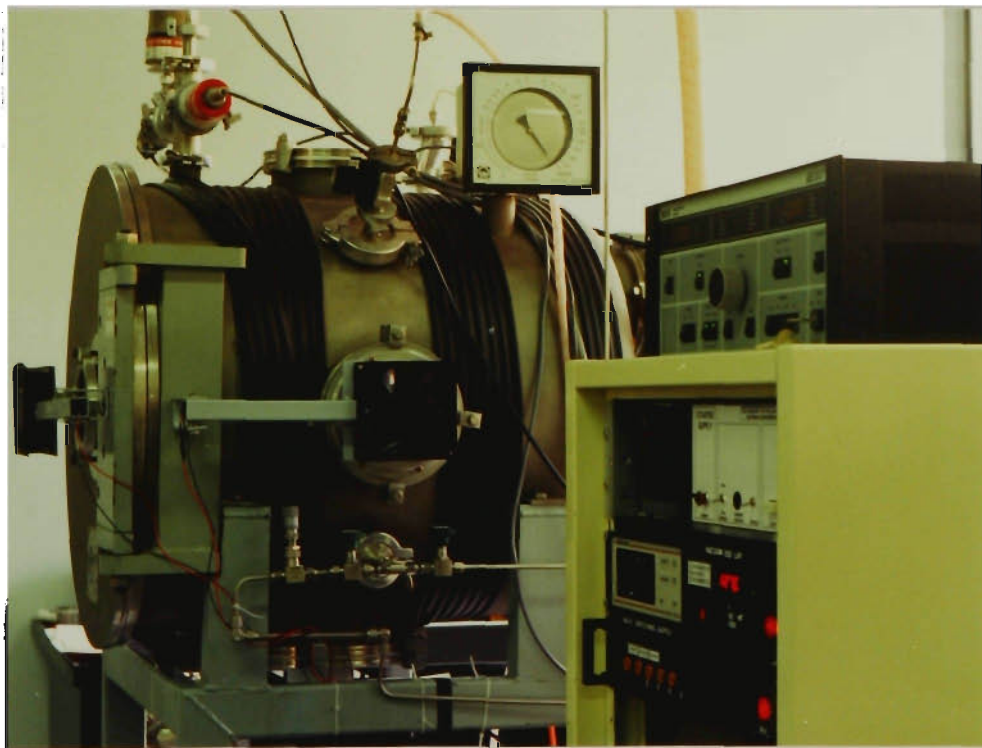


**Figure 25.** 5 kW DC plasma nitriding unit designed and commissioned at the Surface Engineering Research Centre at the University of Wollongong.

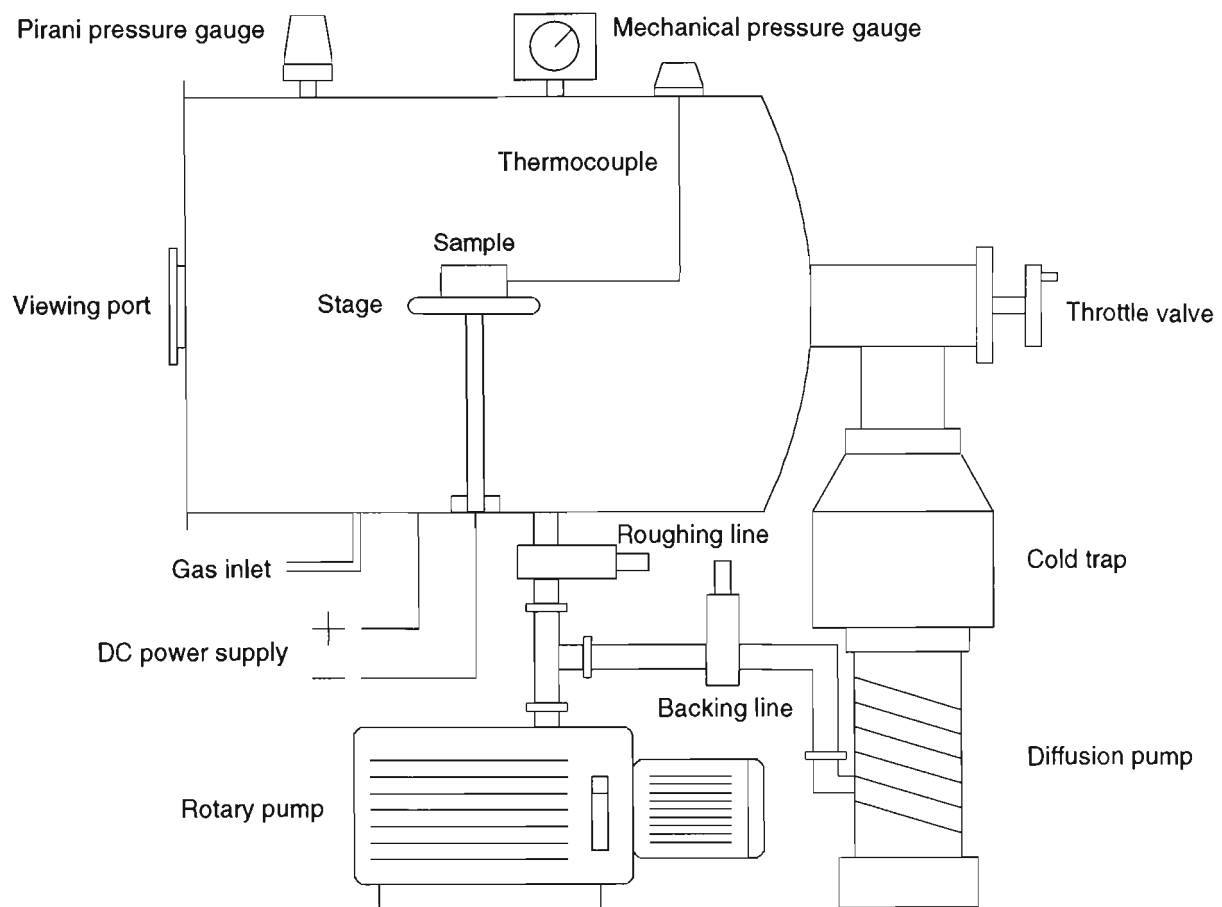


**Figure 26.** Schematic of the DC plasma nitriding apparatus.

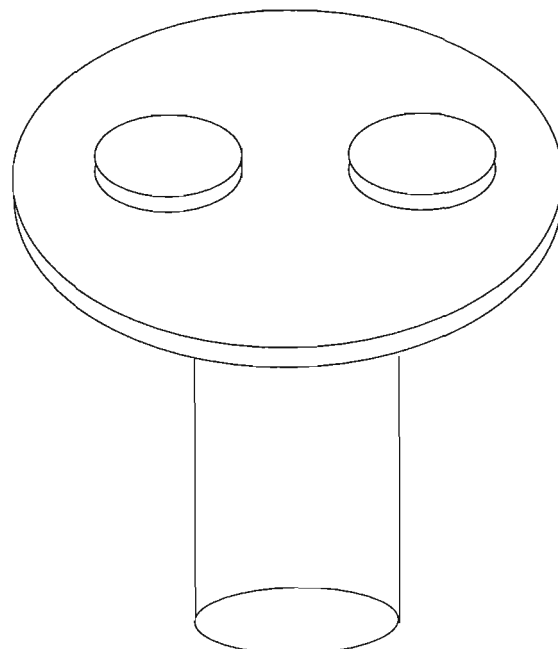


**Figure 27.** Schematic drawing of the table and samples used in the DC plasma nitriding unit.

### 3.4 PI<sup>3</sup> and RF Plasma Nitriding

PI<sup>3</sup> and RF plasma nitriding were carried out using only MAXIMA™ samples in a unit developed at ANSTO. A schematic drawing of the unit is illustrated in Figure 28. For both PI<sup>3</sup> and RF plasma nitriding, the unit was operated at a filling pressure of  $1.6 \times 10^{-3}$  mbar, with 300W of RF power at 13.56 MHz. Nitrogen and hydrogen gasses were provided in separate bottle and were fed to the chamber by means of mass flow controllers, with flows of 9 and 10 sccm, respectively. A HIDEN HAL-100 residual gas analyser was used to monitor the nitrogen and hydrogen partial pressures during the processes. A separately pumped chamber was used for the residual gas analyser, connected to the main chamber through a small orifice. The residual gas analyser readings were calibrated in terms of the partial pressures of hydrogen and nitrogen in the process chamber. To obtain the 75%N<sub>2</sub>-25%H<sub>2</sub> ratio inside the chamber a 53%N<sub>2</sub>-47%H<sub>2</sub> gas mixture had to be used. The reason for this is that the hydrogen was pumped out faster than the nitrogen due to the conductance of the throttling valve used which was nearly 4 times greater for hydrogen than nitrogen. After the processes were completed, the samples were allowed to cool to room temperature in the chamber.

The details and functioning of the PI<sup>3</sup> process were covered in the previous chapter. All the PI<sup>3</sup> treatments were carried out using high voltage pulses of - 43kV amplitude, 100μsec duration and 0.95A current. Secondary electron coefficient,  $\gamma$ , was 3 (secondary electron/ion) and current density during HV pulses was 1.2 mA/cm<sup>2</sup>. The PI<sup>3</sup> treatment parameters are given in Table 5.

**Table 5.** *PI<sup>3</sup> treatments parameters.*

Temp., °C	Time to temp., min.	Freq. to temp., Hz	Freq. at temp., Hz	Total dose, atom/cm <sup>2</sup>
350	20	200	72	25.35 x 10 <sup>17</sup>
400	24	200	105	32.49 x 10 <sup>17</sup>
450	39	200	146	46.55 x 10 <sup>17</sup>
500	47	250	180	57.85 x 10 <sup>17</sup>
550	68	260	200	68.67 x 10 <sup>17</sup>

Since no high voltage pulses were involved in RF plasma nitriding, the samples were heated to the nitriding temperatures in vacuum, using auxiliary heating through a resistively heated stage. After reaching the temperature the RF plasma was turned on for 5 hours. The temperature was monitored by means of two thermocouples, one inserted in the stage, near the surface region, and the other in a sample placed on the stage. After PI<sup>3</sup> and RF plasma nitriding treatments, the samples were allowed to cool in the vacuum chamber.

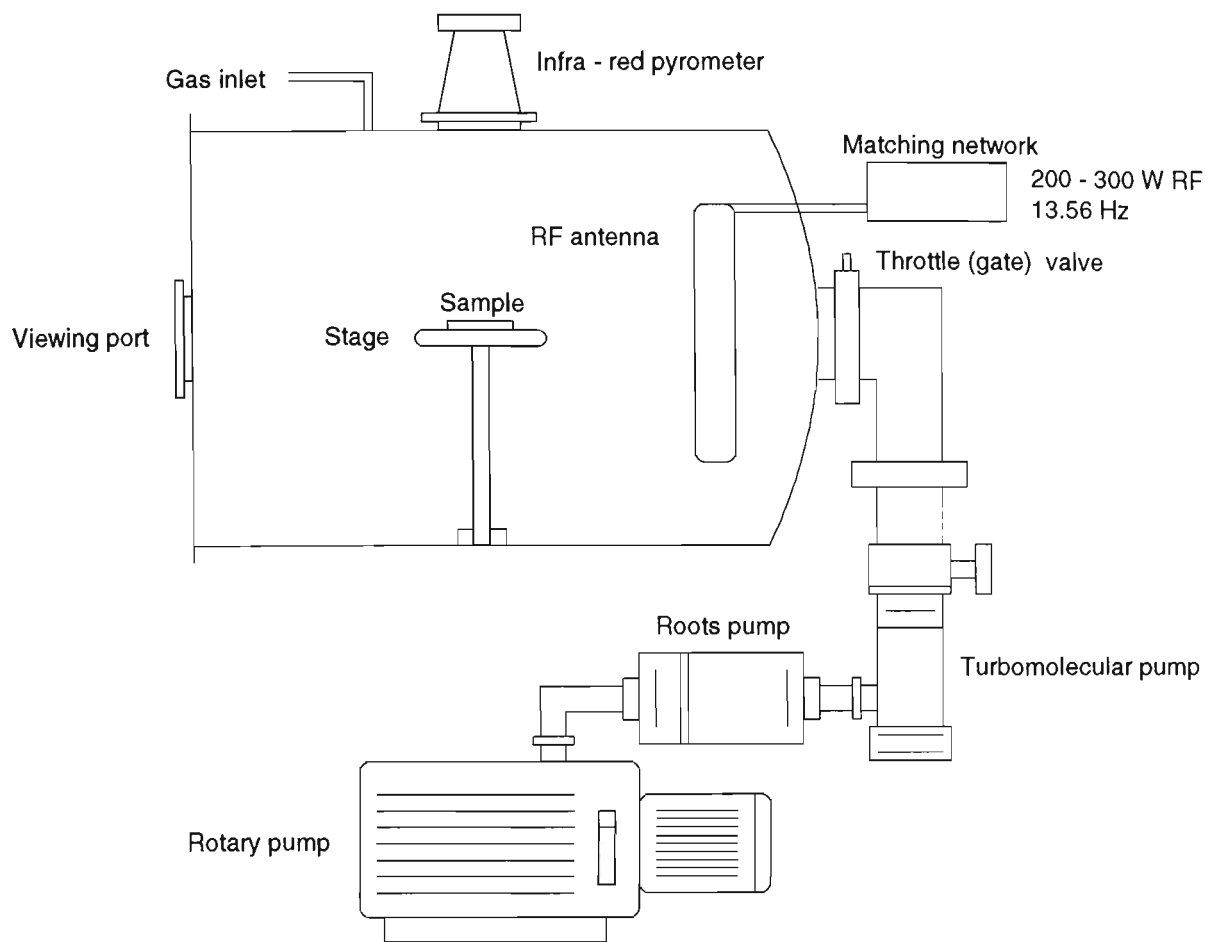


**Figure 28.** Schematic of the  $\text{PI}^3$  and RF plasma nitriding apparatus. Note that in  $\text{PI}^3$  the sample is connected to the high voltage circuit while in RF plasma nitriding the sample is placed on a resistively heated stage.

### 3.4.1 Treatment Conditions

Apart from the mode of heating, other nitriding parameters, such as time, temperature and atmosphere were kept constant for both RF plasma nitriding and  $\text{PI}^3$  treatments. For both processes, the MAXIMA<sup>TM</sup> specimens were treated in a 75%N<sub>2</sub>-25%H<sub>2</sub> atmosphere for 5 hours at different temperatures, namely 350, 400, 450, 500 and 550°C.

## 3.5 Characterisation Techniques

### 3.5.1 Optical Microscopy

The treated samples were sectioned normal to the surface. An electroplated nickel layer was deposited on the nitrided specimens using a Watt's bath (see Appendix A) in order to protect the edges and to preserve the white layer. The thickness of the nickel layer was about  $60\mu\text{m}$ . After surface grinding, the specimens were polished on 6 and  $1\mu\text{m}$  diamond lapping wheels.

Several etchants such as 2.5% nital, Oberhoffer's, and Marbel's reagent, were used in this investigation to reveal different constituents of the microstructure of the nitrided cases. The composition of these etchants is given in Appendix A. Optical microscopy was carried out on both etched and unetched (as polished) surfaces using a Nikon optical microscope. The thickness of the compound layers produced by nitriding was also measured by optical microscopy using an eyepiece graticule. The samples were etched in 2.5% nital prior to the measurements. The thickness values quoted are the average of at least 25 readings.

### 3.5.2 Scanning Electron Microscopy

A Leica Stereoscan 440 scanning electron microscope was employed to study in more detail the layers formed on the surface of the treated samples. The samples were prepared in a similar manner to those used in optical microscopy, except for the fact that they were slightly over etched. Furthermore, the samples were coated with a thin layer of gold sputtered on the surface to improve electrical conduction and to avoid charging

which causes drifting of the image. SEM was also used to examine the morphological features of the surface of the treated samples.

### **3.5.3 X-ray Diffraction**

X-ray diffraction was employed as the major analysis technique for identification of the phases formed on the surface of the treated samples. A Philips X-ray diffractometer was used to perform the analyses utilising an iron filtered, Co K<sub>α</sub> radiation. The scanning angle ( $2\theta$ ) ranged from  $30^\circ$  to  $100^\circ$  and the scanning speed was  $1^\circ/\text{min}$ . The measurement conditions of the tube voltage and current were 40 kV and 25 mA respectively. A detailed study of the surface of the samples was made in both the as-received and treated conditions.

### **3.5.4 Glancing Angle X-ray Diffraction**

Glancing angle X-ray diffraction using a Siemens D500  $\theta$ -2 $\theta$  diffractometer was also utilised to identify the phases formed on the surface of RF plasma nitrided and PI<sup>3</sup> treated samples. The incident radiation was Co K<sub>α</sub>, with a range of incident angles ( $\alpha$ ) between  $1^\circ$  and  $5^\circ$  used to evaluate the distribution of phases with depth. Bragg angles ( $2\theta$ ) between  $40^\circ$  and  $90^\circ$  were examined with a scan step of  $0.1^\circ$  and dwell time of 10 seconds between each step.

### **3.5.5 Glow Discharge Optical Emission Spectroscopy**

Nitrogen and carbon concentration profiles at the surface of treated samples were determined by Glow Discharge Optical Emission Spectroscopy (GDOES) using a Jobin-

Yvon GDS-JY50S instrument. Briefly, the GDOES technique involves cathodic sputtering of the specimen surface by applying a controlled voltage across the specimen being analysed at a controlled argon pressure. The sputtered surface atoms diffuse into the argon plasma where excitation provides optical emission spectra with a linear relationship between element concentration and spectral intensity. More details of the process are explained in Appendix B.

The instrument comprises a Grimm-style glow discharge lamp, using ultrahigh purity argon as the plasma gas. To ensure that the sample is effectively the sole cathode, a ceramic support was used. A 4mm diameter anode was utilised and the sample-to-anode distance was set to  $140\pm20\text{ }\mu\text{m}$ . GDOES enables the determination of elemental depth profiles to a maximum depth close to  $50\mu\text{m}$ . The depth of the crater created by sputter erosion was measured using a Taylor-Hobson Form Talysurf-120 profilometer, thus allowing a quantitative assessment of the sputter rate to be made.

### **3.5.6 Hardness Measurements**

A Leco M-400-H1 Vickers microhardness tester was used to obtain indentations on treated surfaces at 25, 50, 100, 300 and 1000 gram load. At least 10 indentations were made on each sample at each load, and a set loading pattern was maintained.

The hardness profiles of the samples across the treated case were measured on metallographically prepared cross sections with a load of 50g. The hardness values quoted are the average of at least 5 readings. All precautions were taken to ensure consistent and reliable results. The nitrided case depth was measured from the hardness profiles using the Japanese Industrial Standard (JIS) G0562 (1995) in which the case

depth is defined as the distance from the surface of the specimen to the point at which the microhardness profile reaches a value 50 Vickers point (or Knoop) above the core hardness.

To check for softening of the material during treatment, several 20 kg hardness indentations were also made in the core of each sample after treatment.

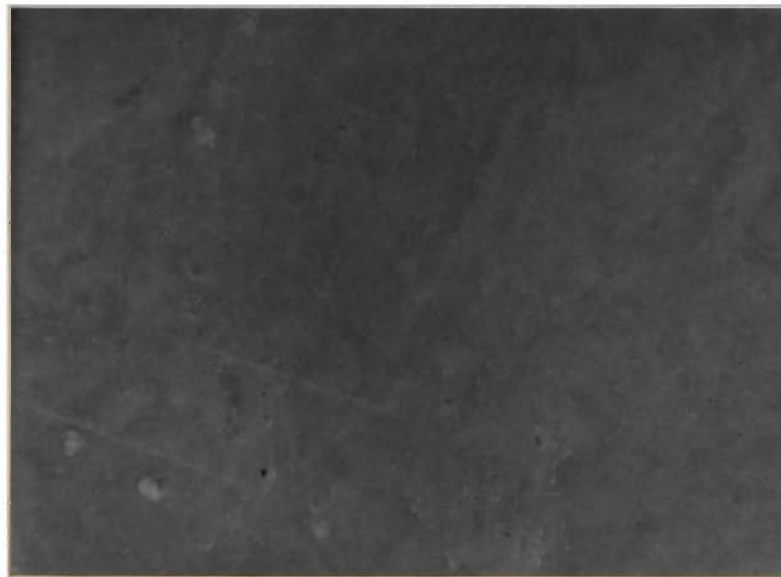
### **3.5.7 Surface Roughness Measurements**

Surface roughness was characterised with a Talysurf stylus instrument. The diamond tipped stylus has a chisel edge, with the flat, contacting face of the stylus having dimensions of 0.2 by 1  $\mu\text{m}$  (Dagnall, 1980). The instrument converts the vertical height as a function of horizontal displacement to a voltage as a function of time leading to a graphical representation of the surface by a line profile. Once the trace has been produced, filters are applied numerically to the recorded raw profile, enabling the removal of either short or long wavelength components (Maddrell, 1991).

Comparison of surface roughness was based on Roughness Average,  $R_a$ , measurement.  $R_a$  is universally recognised and the most common statistical description of surface roughness. It is the arithmetic mean of the departures of the profile from the mean line. The principles of surface roughness measurements are discussed in more detail in Appendix C. An evaluation length of 9.6mm was used throughout this investigation. A Gaussian high pass filter with a cut-off wavelength of 0.8mm in conjunction with a bandwidth of 300:1 were used in the calculation of  $R_a$ .

### 3.5.8 Atomic Force Microscopy

Except for the samples DC plasma nitrided at high temperatures such as 500 and 550°C, SEM examination of the surface of the other samples did not provide any clear or informative images due to the low topographical features, see Figure 29. In order to study the surface topography of the treated samples in more detail, a NanoScope® Atomic Force Microscope (AFM), from Digital Instruments, was utilised in the contact mode, see Figure 30. Briefly, in AFM a sharp tip mounted on the end of a cantilever with a low spring constant, is brought close to the sample surface. Interactions between the tip and sample deflect the cantilever. As the tip is scanned over the sample by a piezoelectric scanner, a detector measures the cantilever deflection.



25  $\mu\text{m}$

**Figure 29.** SEM micrograph obtained from the surface of MAXIMA™ plasma nitrided for 5h at 450 °C in 75%N<sub>2</sub>-25% H<sub>2</sub> atmosphere.

The measured cantilever deflections allow a computer to generate a map of the surface topography and converts the data into an image (Howland R. S. *et al*, 1993). More details of the technique and the instrument are presented in Appendix D.



**Figure 30.** The NanoScope® Atomic Force Microscope (AFM), from Digital Instruments, at the University of Wollongong.

# **4. CHAPTER FOUR:**

## **RESULTS**

---

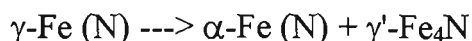
### **4.1 Introduction**

After characterising the samples plasma nitrided in the 40 kW Klöckner Ionnon industrial scale unit at the University of Birmingham, it was realised that the samples were treated at higher temperatures than those intended, especially at nominal 550°C.

The hardness of MAXIMA™ steel is strongly dependent on treatment temperature. At 550°C, the core hardness should be approximately 290 HV<sub>20</sub>, whereas the hardness of the MAXIMA™ sample after treatment was about 248 HV<sub>20</sub>, indicating a much higher treatment temperature than the nominal 550°C.

The other observation which supports the fact that the treatment temperature was actually higher than the intended temperature of 550°C, is the dark etching band in the interface between the compound layer and the diffusion zone of both steels treated at nominal 550°C, see Figure 31. This is believed to be the product of eutectoid decomposition of  $\gamma$  (nitrogen austenite) upon cooling from temperatures above the eutectoid temperature (590°C) in the iron-nitrogen phase diagram, see Figure 1. It should be stated that most alloying elements raise the eutectoid temperature in Fe-N system. Nitriding at temperatures above the eutectoid initially results in nitrogen

saturation of ferrite and, when the limit of solid solubility is exceeded,  $\gamma$  phase will form. When  $\gamma$ -phase is saturated,  $\gamma'$  phase is formed at the surface, and finally, the  $\varepsilon$ -phase precipitates at higher nitrogen content. Thus the nitrided layer from the surface toward the core consists of  $\varepsilon + \gamma' + \gamma + \alpha$  at the treatment temperature (Gulyaev, 1980). Slow cooling in the chamber results in the decomposition of the  $\varepsilon$  and  $\alpha$  phases according to the equilibrium diagram (Figure 1) and precipitation of surplus  $\gamma'$  phase. Furthermore, according to the following reaction, the  $\gamma$ -phase undergoes a eutectoid decomposition into  $\alpha + \gamma'$ , manifested as the dark etching band shown in the micrographs of Figure 31.



Unfortunately, the exact cause of this over-heating could not be ascertained. Dirtiness, or lack of calibration or misplacement of the thermocouple cannot be over-ruled. The other factor which can be considered as the source of the overheating, is the overshooting of the power supply due to a fault in the temperature controller or mis-programming of it.

In order to make a reliable comparison between different nitriding processes and to gain a better understanding of the nitrided layer formation and nitrogen mass transfer mechanism in DC plasma nitriding, RF plasma nitriding and PI<sup>3</sup>, it was decided to repeat the DC plasma nitriding treatments under more controlled conditions with a 5 kW prototype unit.

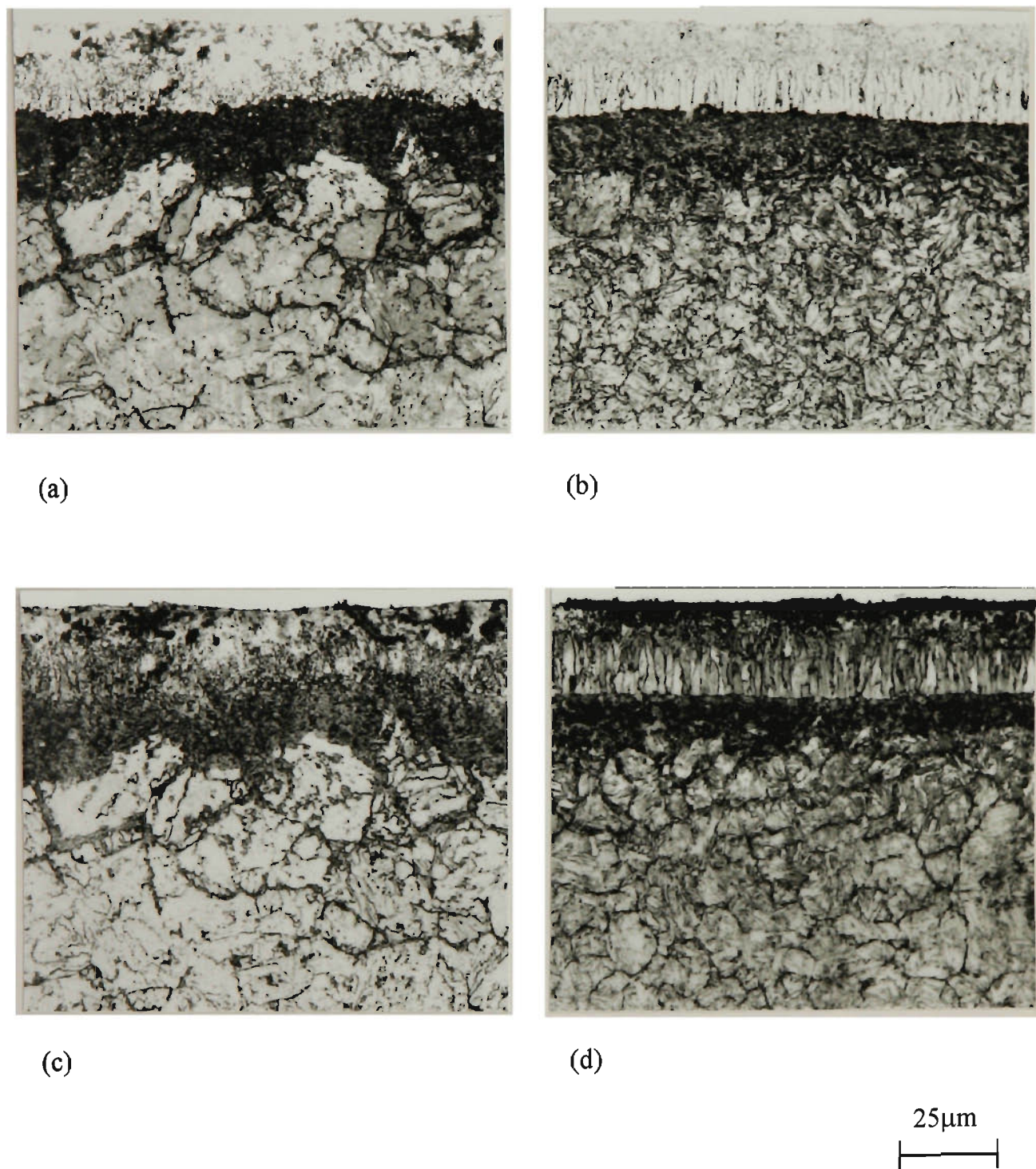


**Figure 31.** Optical micrographs of cross-sections of MAXIMA™ ((a), (c)) and En19 ((b), (d)) specimens plasma nitrided for 5 h at nominal 550 °C using a 40 kW commercial scale unit. Samples were etched in 2.5% nital ((a), (b)), and 2.5% nital followed by Oberhoffer's, reagent ((c), (d)).

The following section comprises two parts. Part I presents the results of a series of DC plasma nitriding treatments carried out using the prototype unit to find the optimum gas composition for nitriding of MAXIMA™. In part II, the results of DC plasma nitriding of MAXIMA™ and En19 steels in conjunction with those obtained from PI<sup>3</sup> and RF plasma nitriding of MAXIMA™ are reported.

## **4.2 Part I: Effect of Hydrogen Content on DC Plasma Nitriding of MAXIMA™**

### **4.2.1 Microstructural Examination**

Typical images obtained by SEM from the cross section of the nitrided samples are shown in Figure 32. The morphology of the compound layers developed on the surface of the samples treated under the various conditions were almost similar to each other, except for the thickness of the layers. The differences in the thickness of the compound layers are clearly seen in these micrographs. Samples treated in 75%N<sub>2</sub>-25%H<sub>2</sub> developed the thickest compound layer whereas treatment in 25%N<sub>2</sub>-75%H<sub>2</sub> atmosphere produced the thinnest compound layer. The actual values for the thickness of layers are shown in Figure 33. In all samples, the iron nitride at the interface of the compound layer with the diffusion zone has grown in an acicular morphology towards the core.

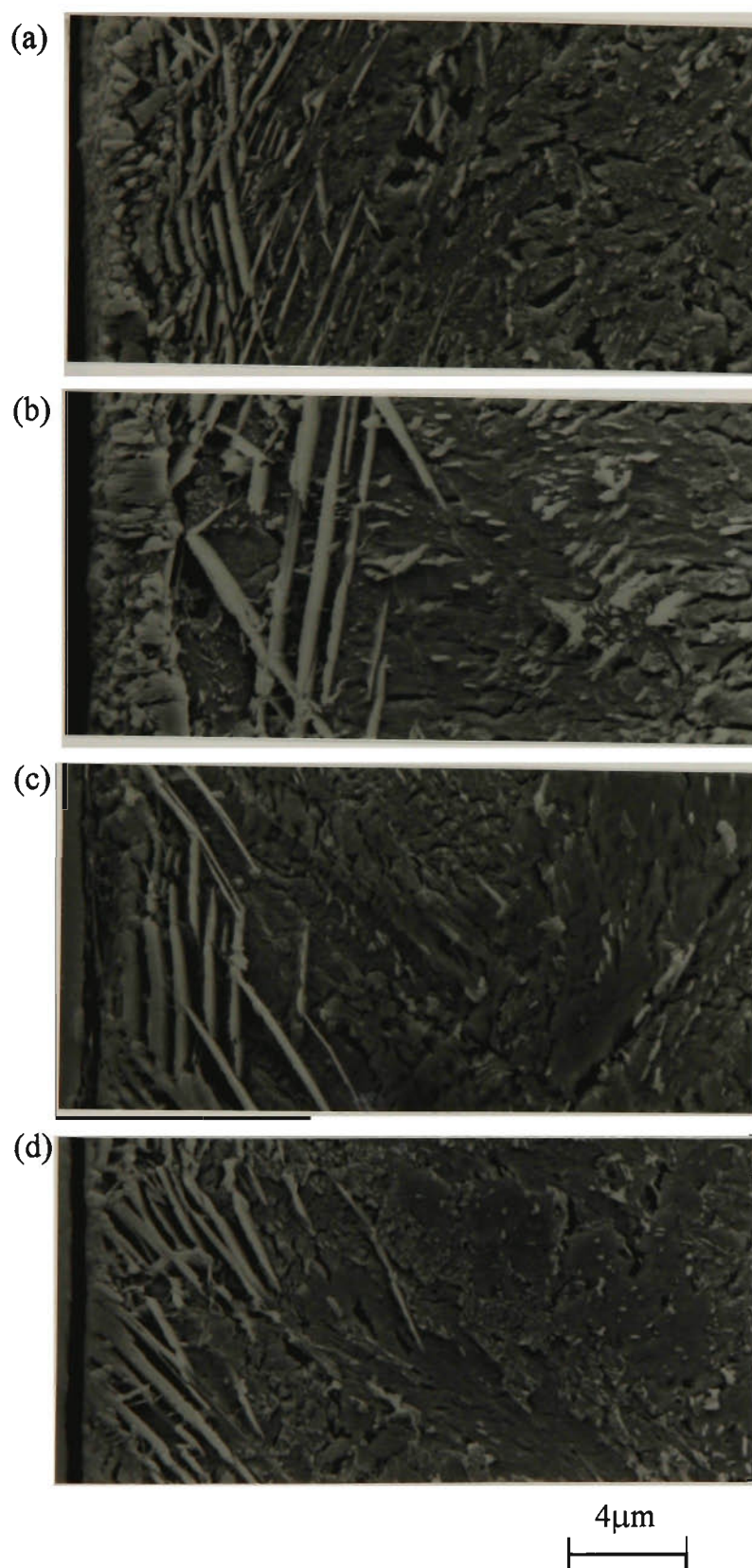


**Figure 32.** SEM micrograph showing the compound layer formed on the surface of MAXIMA™ plasma nitrided for 5 h at 450 °C in atmospheres containing (a) 100%  $N_2$ , (b) 75%  $N_2$ -25%  $H_2$ , (c) 50%  $N_2$ -50%  $H_2$ , and (d) 25%  $N_2$ -75%  $H_2$ . The samples were etched in 2.5% nital followed by Oberhoffer's reagent.

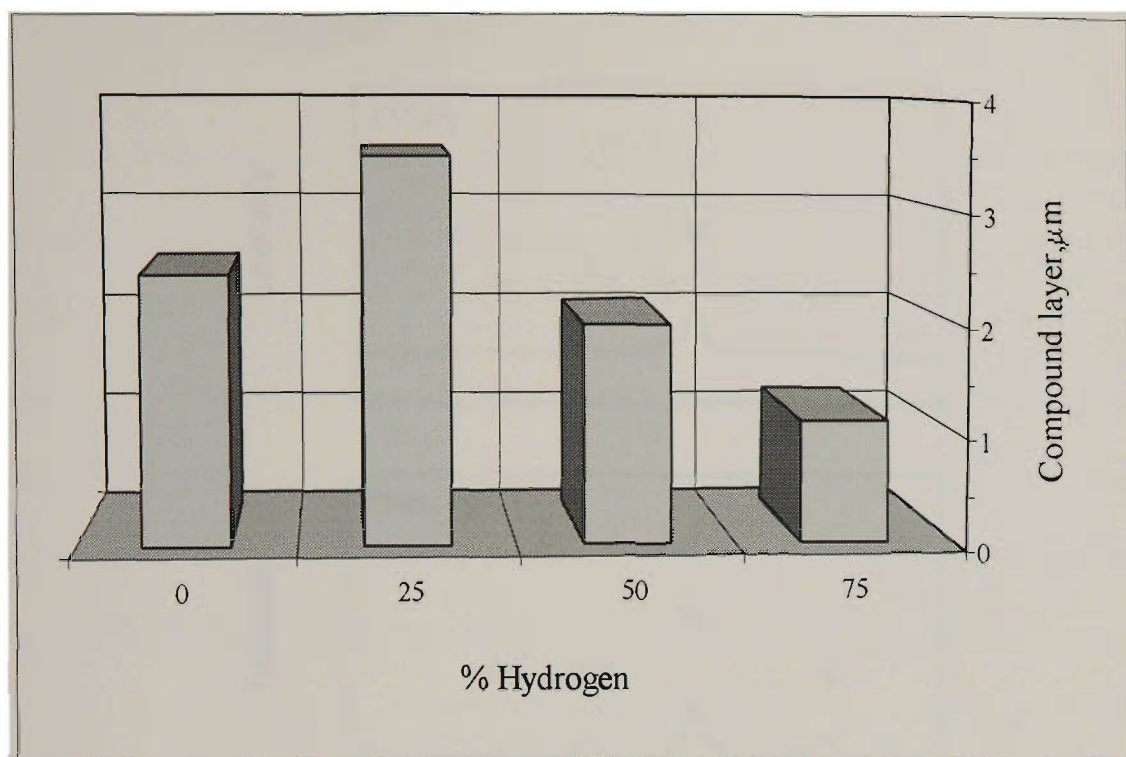


**Figure 33.** The effect of hydrogen concentration of the treatment atmosphere on the compound layer thickness formed on the surface of the treated MAXIMA™ samples.

#### 4.2.2 X-ray Diffraction

X-ray diffraction patterns of the samples are displayed in Figure 34. Treatment in 100% nitrogen atmosphere (0% H<sub>2</sub>) resulted in the formation of a dual phase ( $\epsilon+\gamma'$ ) compound layer composed mainly of  $\epsilon$  iron nitride. Increasing the hydrogen concentration of the treatment atmosphere resulted in a decrease in the  $\epsilon$  phase and corresponding increase in  $\gamma'$  phase. Treatment in 25%N<sub>2</sub>-75%H<sub>2</sub> produced a predominantly  $\gamma'$  compound layer. Furthermore, for this sample the intensity of the  $\alpha$ -iron peak was increased, indicating a reduction in the thickness of compound layer.

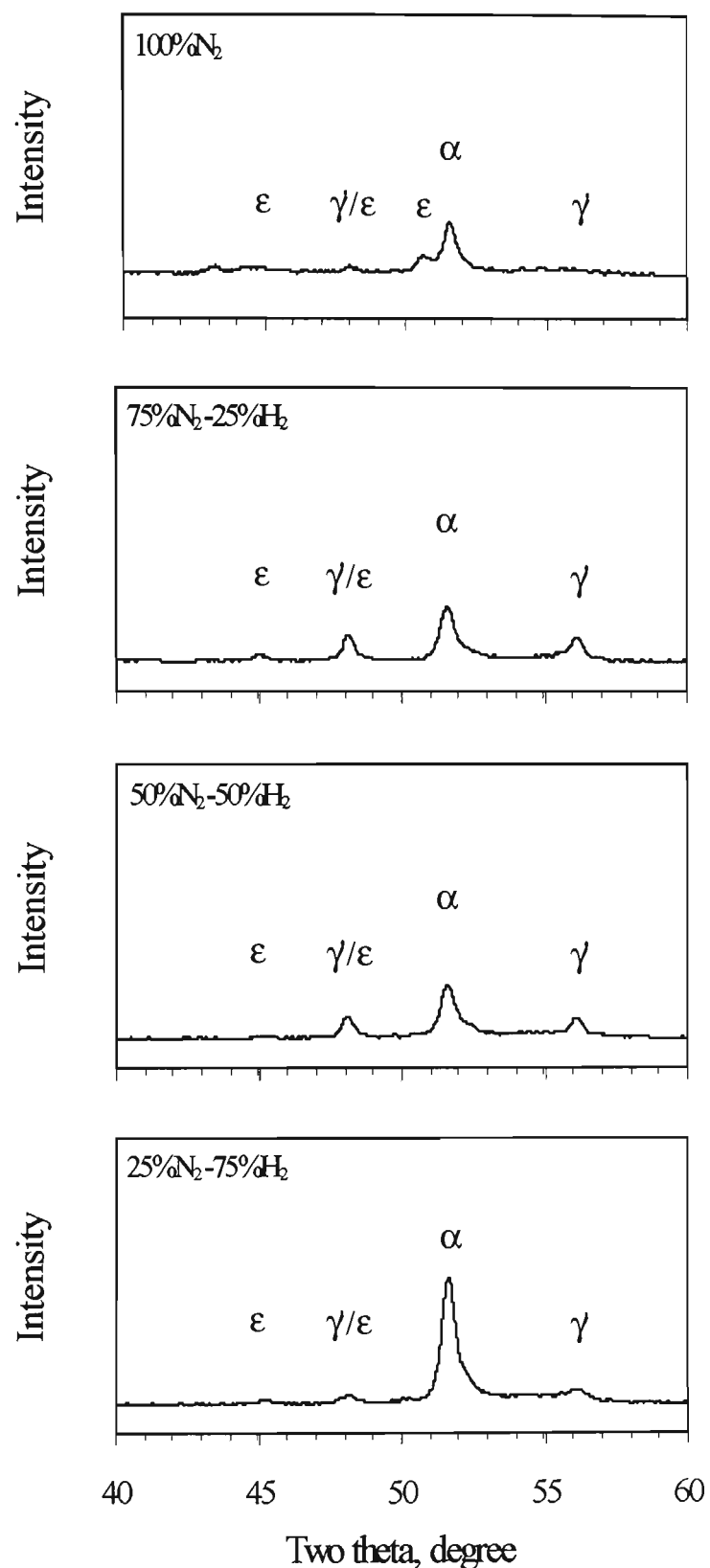


**Figure 34.** X-ray diffraction patterns of the MAXIMA™ samples DC plasma nitrided at 450 °C for 5 hrs at various N<sub>2</sub>+H<sub>2</sub> gas mixtures.

### 4.2.3 Glow Discharge Optical Emission Spectroscopy

Figure 35 illustrate the nitrogen and carbon depth profiles obtained by GDOES. Samples treated in a 100% nitrogen atmosphere showed the highest nitrogen content in the compound layer whereas treatment in 25%N<sub>2</sub>-75%H<sub>2</sub> atmosphere resulted in the formation of a compound layer with the least nitrogen content. The GDOES depth profiles of the sample treated in 75%N<sub>2</sub>-25%H<sub>2</sub> was similar to that of the sample treated in 50%N<sub>2</sub>-50%H<sub>2</sub>, except for the extend of the nitrogen profile which was deeper for the former, indicating a thicker compound layer. A trend was observed between the nitrogen and carbon concentration in the compound layer. Generally, higher nitrogen level in the layer was accompanied by a decrease in the carbon concentration and vice versa. There is also evidence of carbon being pushed out of the compound layer, appearing as a hump in carbon profile at the interface with the diffusion zone.

### 4.2.4 Hardness Tests

Surface hardnesses at different loads for the samples treated in different atmospheres are shown in Figure 36. The core hardness of the samples is also indicated in this Figure. The sample treated in 75%N<sub>2</sub>-25%H<sub>2</sub> atmosphere showed the highest surface hardness at all loads whereas samples treated in 100%N<sub>2</sub> gas developed the least hard surface. Treatment in 50%N<sub>2</sub>-50%H<sub>2</sub> and 25%N<sub>2</sub>-75%H<sub>2</sub> gave fairly similar surface hardnesses which lie between the results obtained from treatments in the atmospheres of 75% N<sub>2</sub>-25% H<sub>2</sub> and 100%N<sub>2</sub>. Hardness profiles were also obtained from the cross-section of the samples to evaluate the microhardness distribution across the treated cases, see Figure 37. The results are consistent with the hardness profiles obtained from the surface hardness at different loads described above.

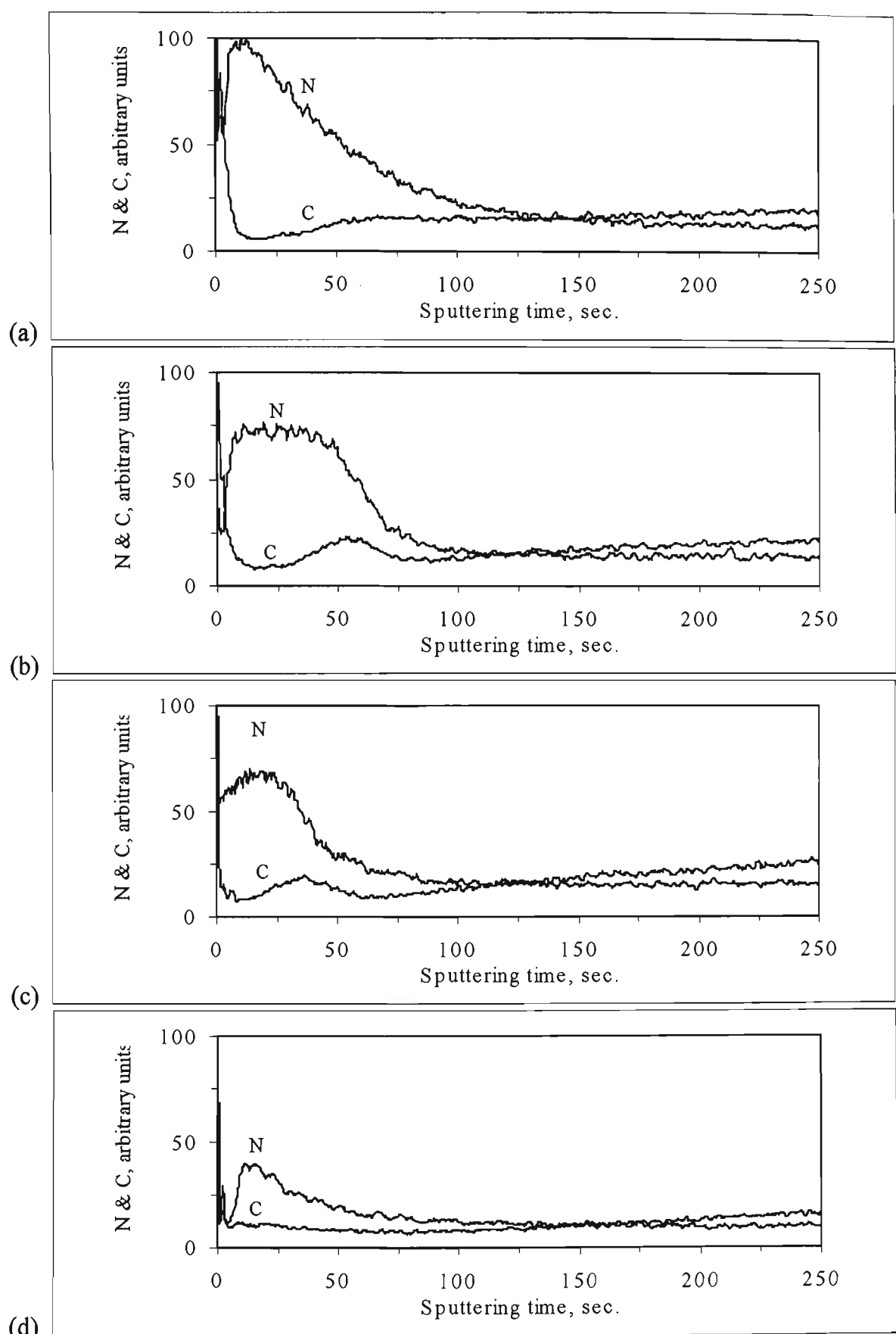


**Figure 35.** GDOES depth profiles for MAXIMA™ steel DC plasma nitrided at 450 °C in (a) 100% N<sub>2</sub>, (b) 75% N<sub>2</sub> - 25% H<sub>2</sub>, (c) 50% N<sub>2</sub> - 50% H<sub>2</sub>, and (d) 25% N<sub>2</sub> - 75% H<sub>2</sub>.

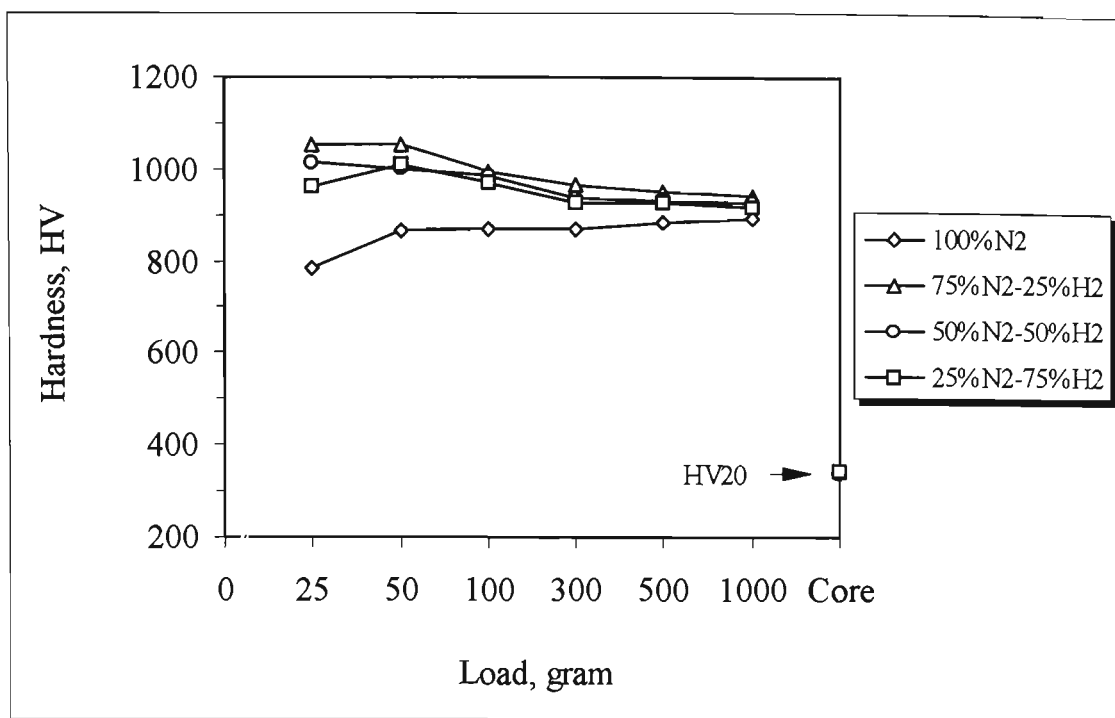


**Figure 36.** Surface hardness at different loads for samples DC plasma nitrided at 450 °C for 5 hours in atmospheres with different hydrogen concentrations.

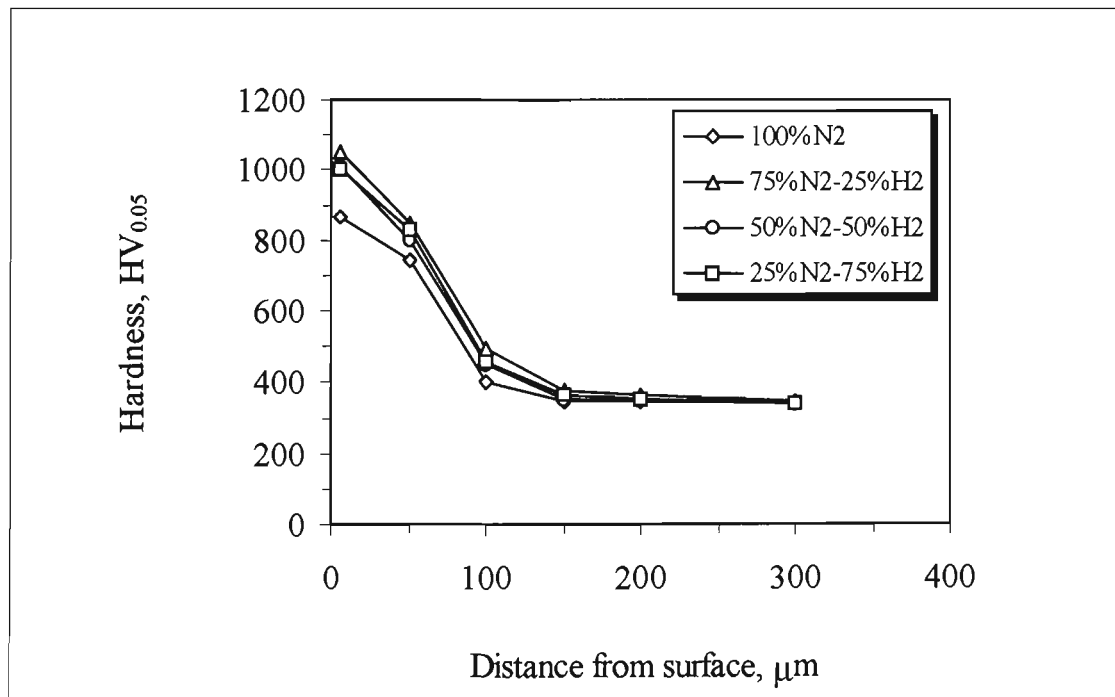


**Figure 37.** The effect of hydrogen concentration in the treatment atmosphere on the hardness profile of the samples DC plasma nitrided at 450 °C for 5 hours.

#### **4.2.5 Surface Topography**

The surface roughness of the samples is illustrated in Figure 38. Samples treated in a 100% N<sub>2</sub> atmosphere showed the highest level of surface roughening whereas other gas compositions developed surfaces with lower surface roughness values.

This trend of surface roughness was also confirmed by Atomic Force Microscopy (AFM) examination of the treated samples, Figures 39 and 40. Nitriding in a 100% nitrogen atmosphere resulted in a surface with an irregular morphology with maximum sputtering effect. Small needle-shaped features superimposed on larger undulations, Figure 39-a, are also visible. The surface roughness of the sample treated in 75%N<sub>2</sub>-25%H<sub>2</sub> (Figure 39-b) was decreased substantially and its morphology was completely different from that treated in 100%N<sub>2</sub>. The grain boundaries were highlighted and the sample was covered with very fine and uniform nodular particles, superimposed on larger wavelength undulations. The morphology of the sample treated in 50%N<sub>2</sub>-50%H<sub>2</sub> (Figure 39-c) was a combination of those treated in 75% N<sub>2</sub> and 25% N<sub>2</sub> (rest H<sub>2</sub>), fine nodular particles superimposed on irregularities. The surface of the sample treated in 25%N<sub>2</sub>-75%H<sub>2</sub> showed large irregularities again, see Figure 39-d.

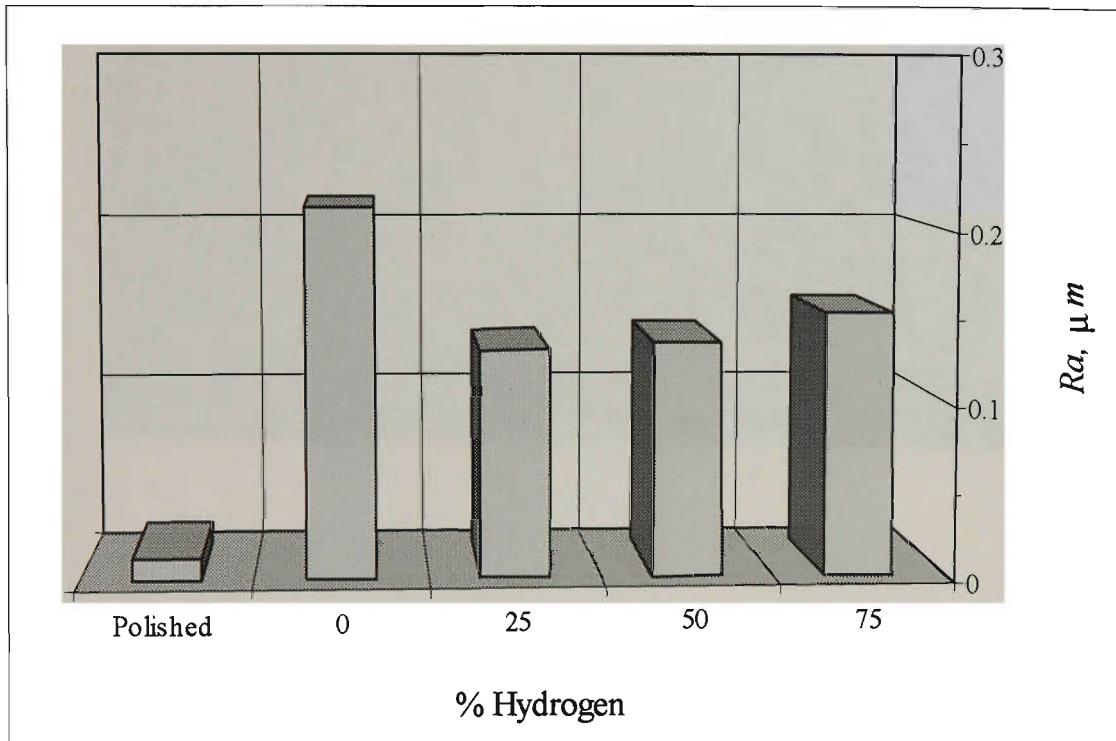
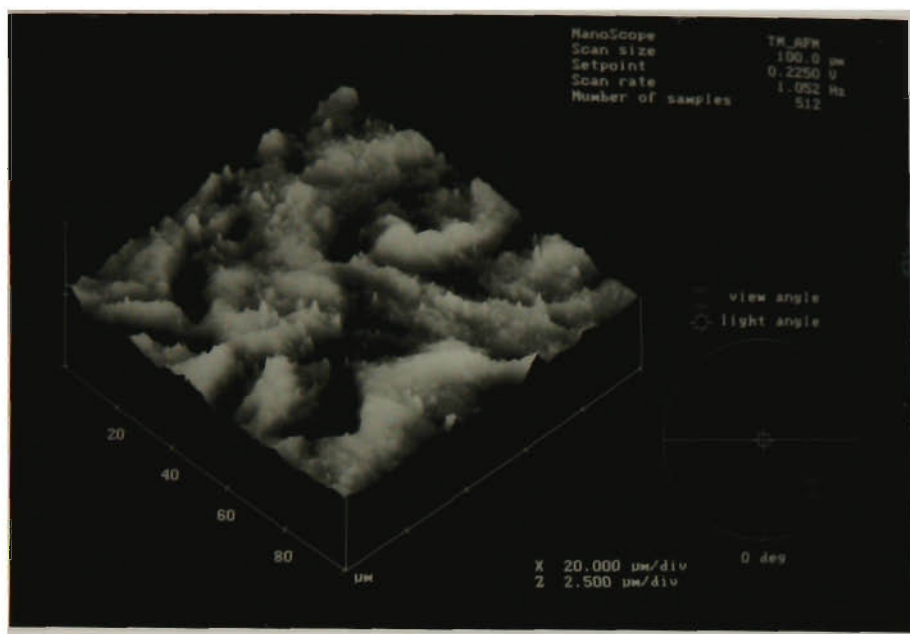
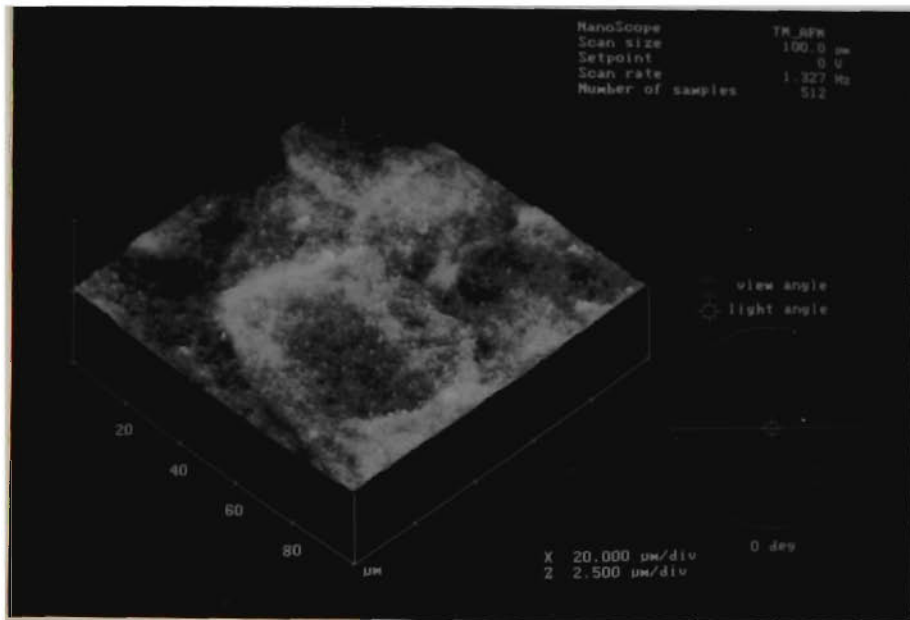


**Figure 38.** The effect of hydrogen concentration in the nitriding atmosphere on the surface roughness of MAXIMA™ samples expressed as  $R_a$ .

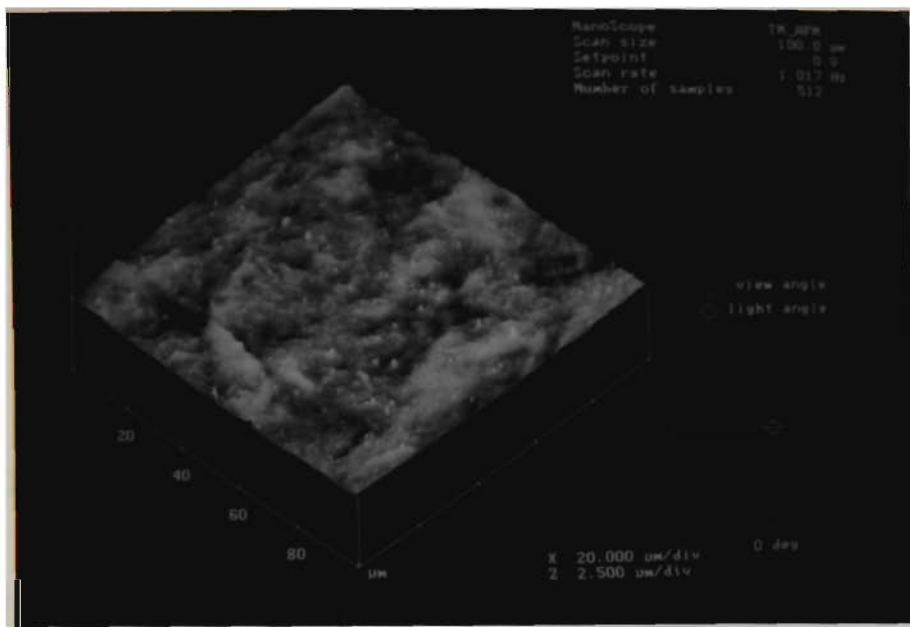


(a)

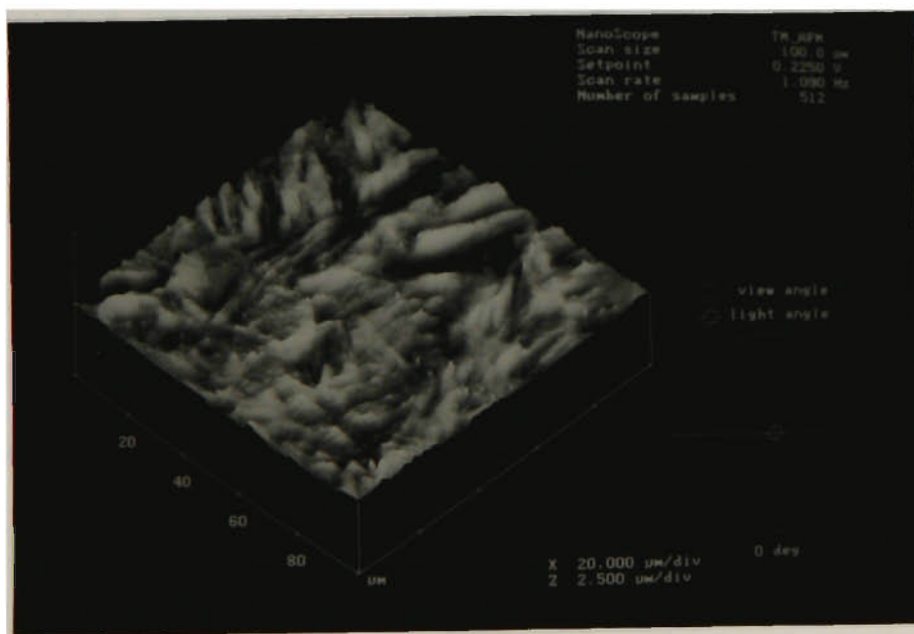


(b)

**Figure 39.** AFM image of plasma nitrided surfaces treated at 450 °C for 5 hours at atmospheres containing different H<sub>2</sub>-N<sub>2</sub> gas mixtures, (a) 100%N<sub>2</sub>, (b) 75%N<sub>2</sub>-25%H<sub>2</sub>.



(a)



(b)

**Figure 40.** AFM image of plasma nitrided surfaces treated at 450 °C for 5 hours at atmospheres containing different H<sub>2</sub>-N<sub>2</sub> gas mixtures, (a) 50%N<sub>2</sub>-50%H<sub>2</sub> and (b) 25%N<sub>2</sub>-75%H<sub>2</sub>.

## 4.3 Part II: DC Plasma Nitriding, RF Plasma Nitriding and PI3

### 4.3.1 Microstructural Examination

#### 4.3.1.1 DC Plasma Nitriding

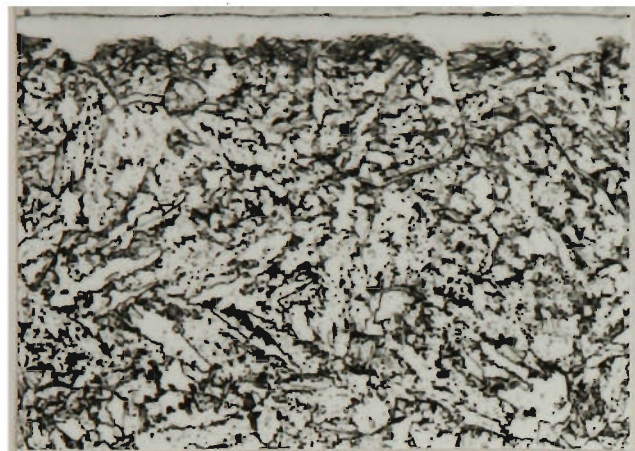
Typical microstructures obtained from the MAXIMA™ and En19 samples treated at 450°C in a 75%N<sub>2</sub>-25%H<sub>2</sub> atmosphere are displayed in Figure 41. The compound layers or so called white layers, are clearly highlighted after etching with nital (Figure 41-a,b). Oberhoffer's reagent attacks different constituents of the compound layer differently and distinguishes them, see Figure 41-c,d, showing duo-phase compound layer.

SEM micrographs obtained from the MAXIMA™ and En19 samples DC plasma nitrided in a 75%N<sub>2</sub>-25%H<sub>2</sub> atmosphere at 350, 450 and 550°C are displayed in Figures 42-44, respectively. The increase in thickness of these layers as a function of treatment temperature is illustrated. A distinct difference is observable between the morphology of the compound layer formed on the MAXIMA™ and En19 specimens plasma nitrided under identical conditions. The compound layer on MAXIMA™ is uneven and in some areas in the interface of compound layer and the diffusion zone has grown with an acicular morphology towards the core. In the case of En19 a more uniform layer with a sharp interface with the diffusion zone was formed.

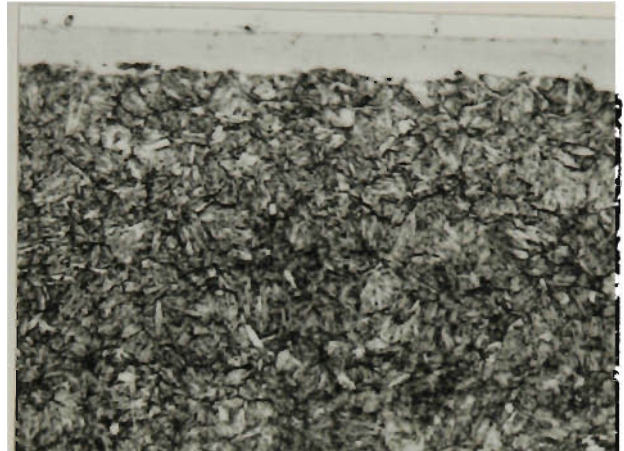
At some points along the interface, the compound layer is extended into the grain boundaries for both steels. Iron (carbo)nitrides are preferentially precipitated at the grain

boundaries parallel to the outer surface, since the material is free to expand perpendicular to the surface, Figure 43. For both steels some pores and cracks were also evident in the compound layer of the samples treated at high nitriding temperature of 550°C.

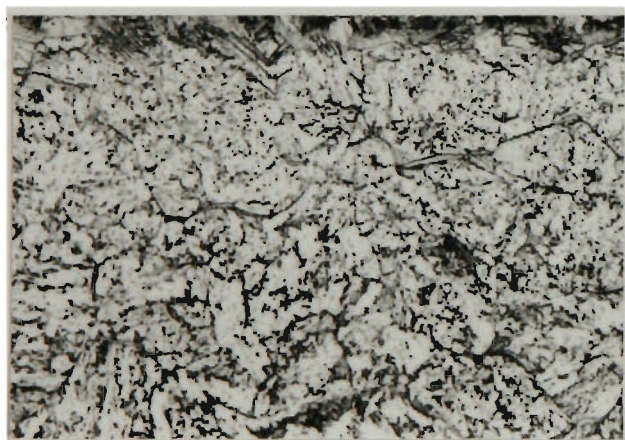
Increasing the nitriding temperature gives rise to an increase in compound layer thickness for both MAXIMA™ and En19 steels, Figure 45. At all temperatures, the compound layer formed on the surface of the En19 samples were thicker than those formed on the MAXIMA™.



(a)



(b)



(c)



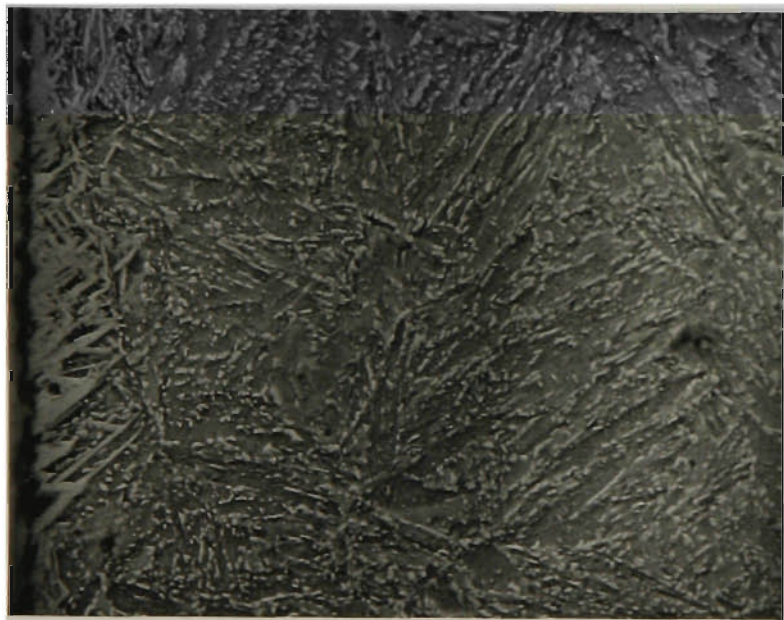
(d)

A scale bar consisting of a horizontal line with a vertical tick mark at each end, labeled "20μm".

**Figure 41.** Optical micrographs of cross-sections of MAXIMA™ ((a), (c)) and En19 ((b), (d)) specimens plasma nitrided in 75% $N_2$  - 25% $H_2$  for 5 h at 450 °C and etched in 2.5% nital ((a), (b)), and 2.5% nital followed by Oberhoffer's reagent ((c), (d)).



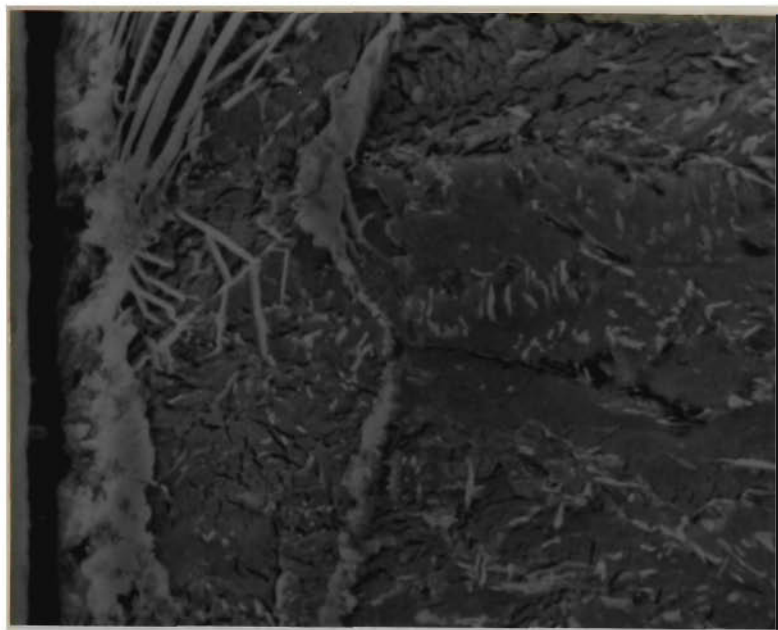
(a)



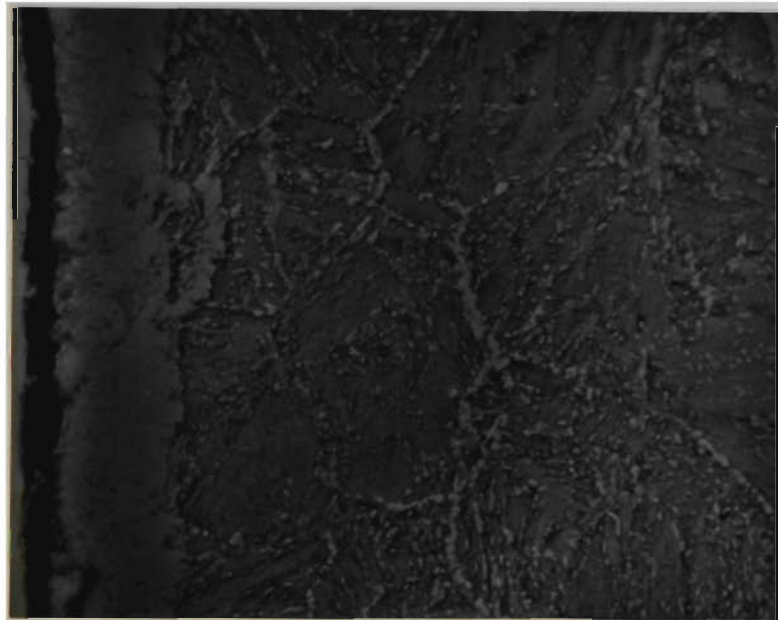
(b)

A scale bar consisting of a horizontal line with a vertical tick mark at each end, labeled "4μm" above it.

**Figure 42.** SEM micrographs of cross-sections of (a) MAXIMA™ and (b) En19 specimens plasma nitrided in 75%N<sub>2</sub> - 25%H<sub>2</sub> for 5 hours at 350°C and etched in 2.5% nital followed by Oberhoffer's reagent.



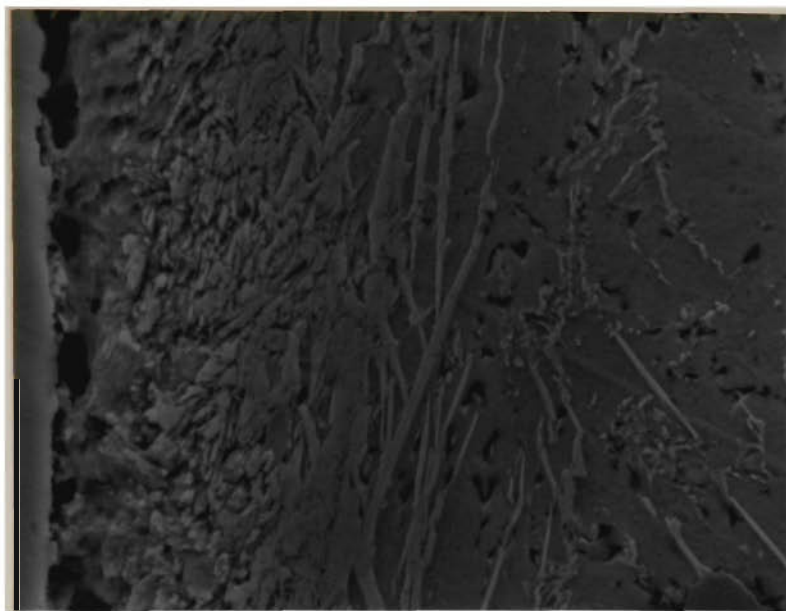
(a)



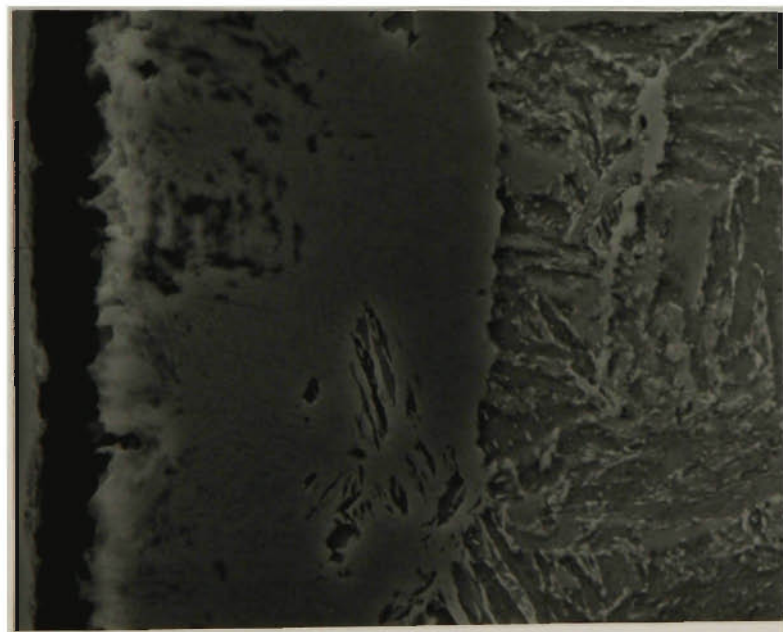
(b)

4 $\mu$ m

**Figure 43.** SEM micrographs of cross-sections of (a) MAXIMA™ and (b) En19 specimens plasma nitrided in 75%N<sub>2</sub> - 25%H<sub>2</sub> for 5 hours at 450°C and etched in 2.5% nital followed by Oberhoffer's reagent.



(a)



(b)

A horizontal scale bar with the text "4μm" above it, indicating the scale of the SEM micrographs.

**Figure 44.** SEM micrographs of cross-sections of (a) MAXIMA™ and (b) En19 specimens plasma nitrided in 75%N<sub>2</sub> - 25%H<sub>2</sub> for 5 hours at 550 °C and etched in 2.5% nital followed by Oberhoffer's reagent.

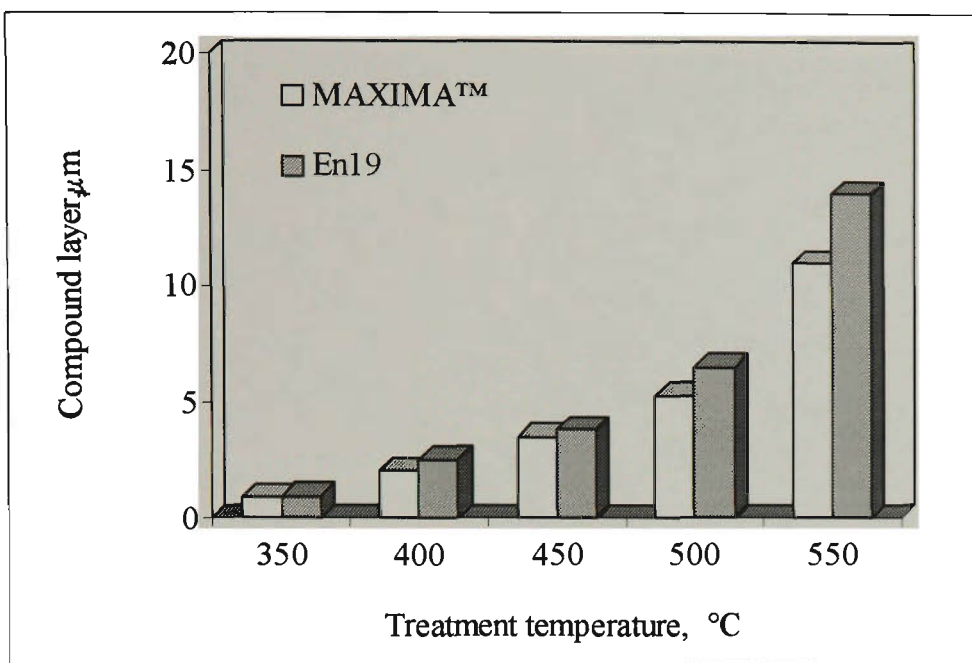
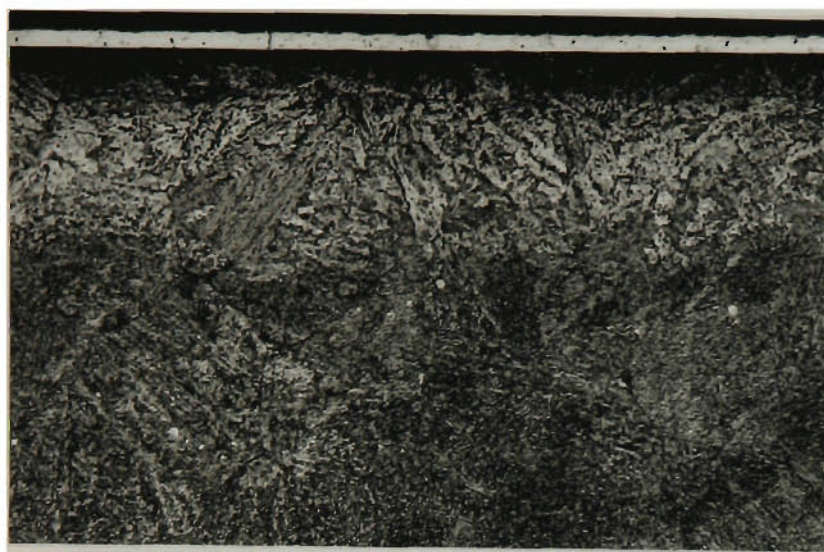


**Figure 45.** Comparison of the thickness of the compound layers formed on the surfaces of both steel DC plasma nitrided under similar conditions.

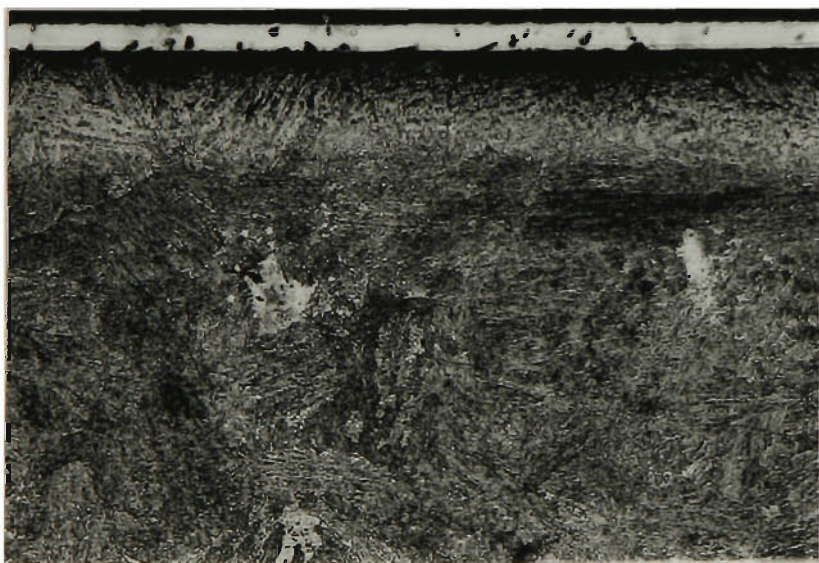
#### 4.3.1.2 RF Plasma Nitriding and PI<sup>3</sup>

No compound layer was observed on MAXIMA™ after PI<sup>3</sup> and RF plasma nitriding in a 75%N<sub>2</sub>-25%H<sub>2</sub> atmosphere at 350 °C, see Figure 46-a,b. The extent of nitrogen diffusion as revealed by etching with Marbles reagent was found to be deeper for the sample treated by PI<sup>3</sup> process.

SEM micrographs presented in Figures 47 and 48, show that for both processes, treatments at 350°C developed some iron nitride ( $\gamma'$ ) platelets in some surface areas which are extended towards the core of the samples, see Figures 47-a and 48-a. Nevertheless, RF plasma nitriding produced more surface iron nitride platelets than the PI<sup>3</sup> process. It should be noted that the nitrides are not continuous and do not form compound layer. Samples treated at higher temperatures by both treatments did not show any evidence of surface iron nitride formation, see Figures 47-b,c and 48-b,c.



(a)



(b)

50μm

**Figure 46.** Typical microstructures obtained from the transverse cross-section of MAXIMA™ steel (a) PI<sup>3</sup> and (b) RF plasma nitrided in 75%N<sub>2</sub> - 25%H<sub>2</sub> at 350 °C for 5 hours. Marbles etchant.

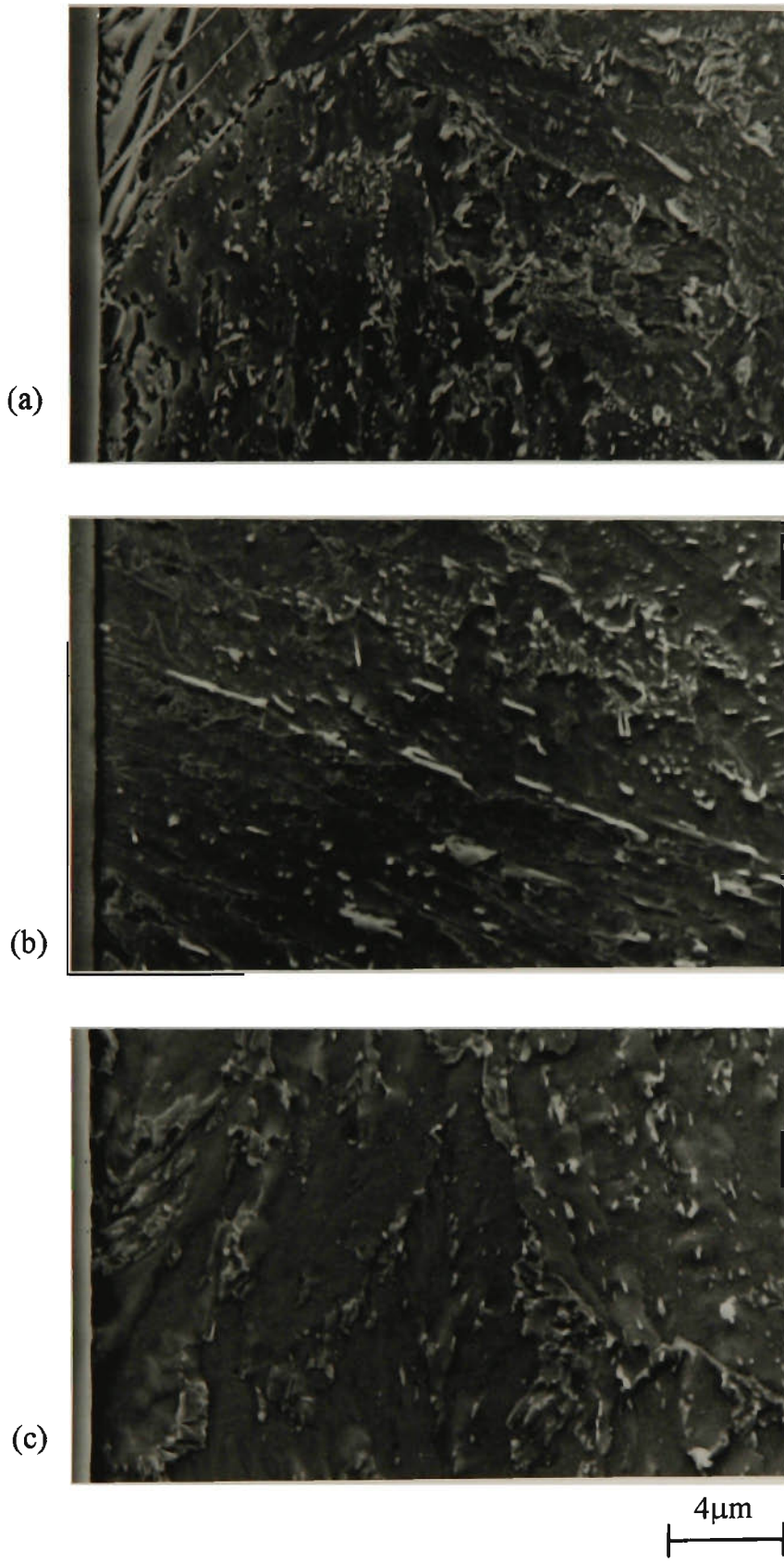


**Figure 47.** SEM micrographs of cross-sections of MAXIMA™ steel PI<sup>3</sup> treated in 75%N<sub>2</sub> - 25%H<sub>2</sub> for 5 hours at (a) 350, (b) 450, and (c) 550°C. The samples were etched in 2.5% nital followed by Oberhoffer's reagent.

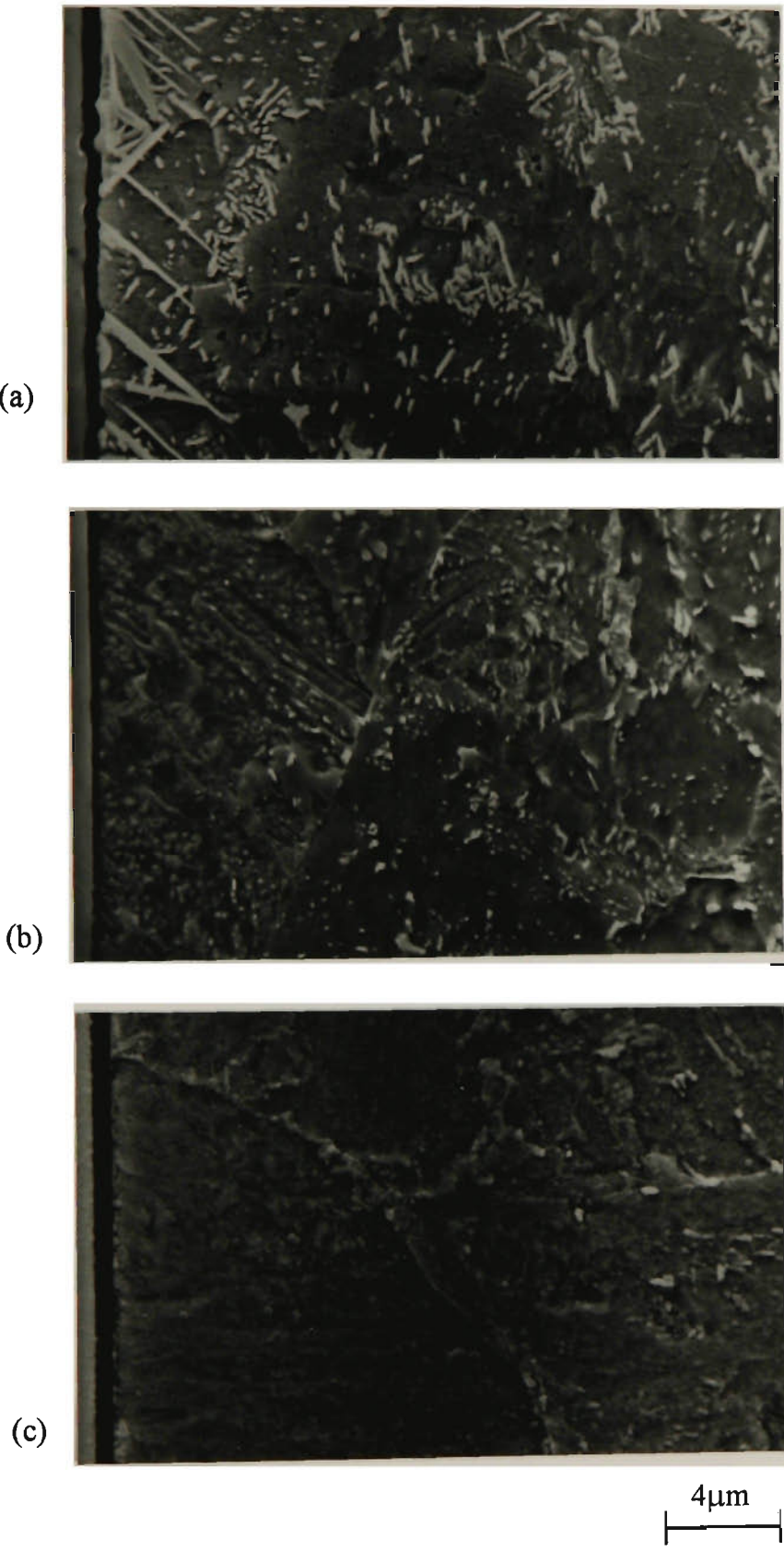


**Figure 48.** SEM micrographs of cross-sections of MAXIMA™ steel RF plasma nitrided in 75% $N_2$  - 25% $H_2$  for 5 hours at (a) 350, (b) 450, and (c) 550 °C. The samples were etched in 2.5% nital followed by Oberhoffer's reagent.

## 4.3.2 X-ray Diffraction

### 4.3.2.1 DC Plasma Nitriding

The x-ray diffraction patterns obtained from the as polished MAXIMA™ and En19 samples before plasma nitriding are shown in Figure 49. A small peak attributable to (austenite)  $\gamma_{200}$  phase was found in the MAXIMA™ sample which could not be detected in the En19 sample.

Figure 50 shows typical x-ray diffraction patterns of the MAXIMA™ samples after DC plasma nitriding treatment at 350, 450 and 550°C. The austenite phase ( $\gamma$ ), described above, has disappeared, indicating the decomposition of the austenite to ferrite and cementite at these treatment temperatures. Reflections from  $\epsilon$  and  $\gamma'$  nitrides in the compound layer can be observed as well as reflections from underlaying  $\alpha$  iron matrix.

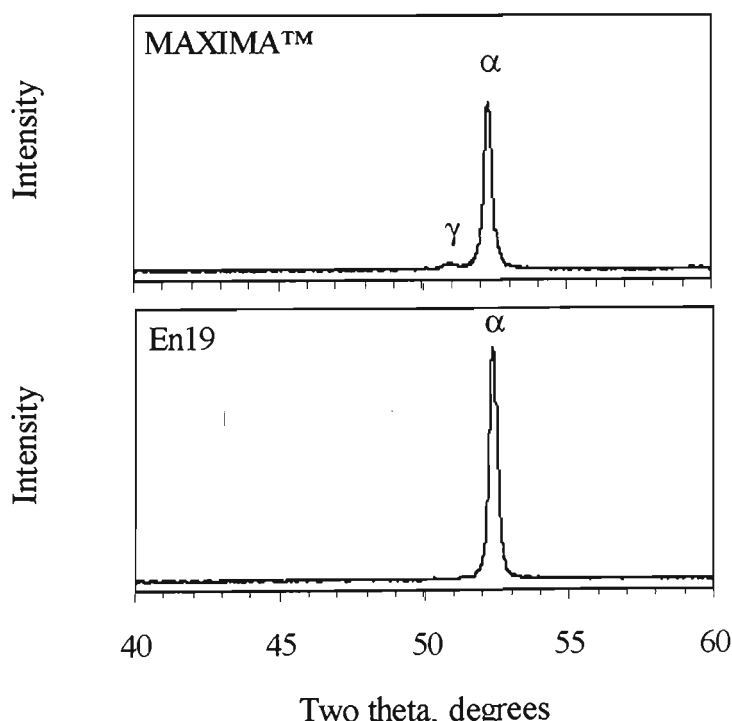


**Figure 49.** X-ray diffraction patterns of the MAXIMA™ and En19 samples in the as polished condition.

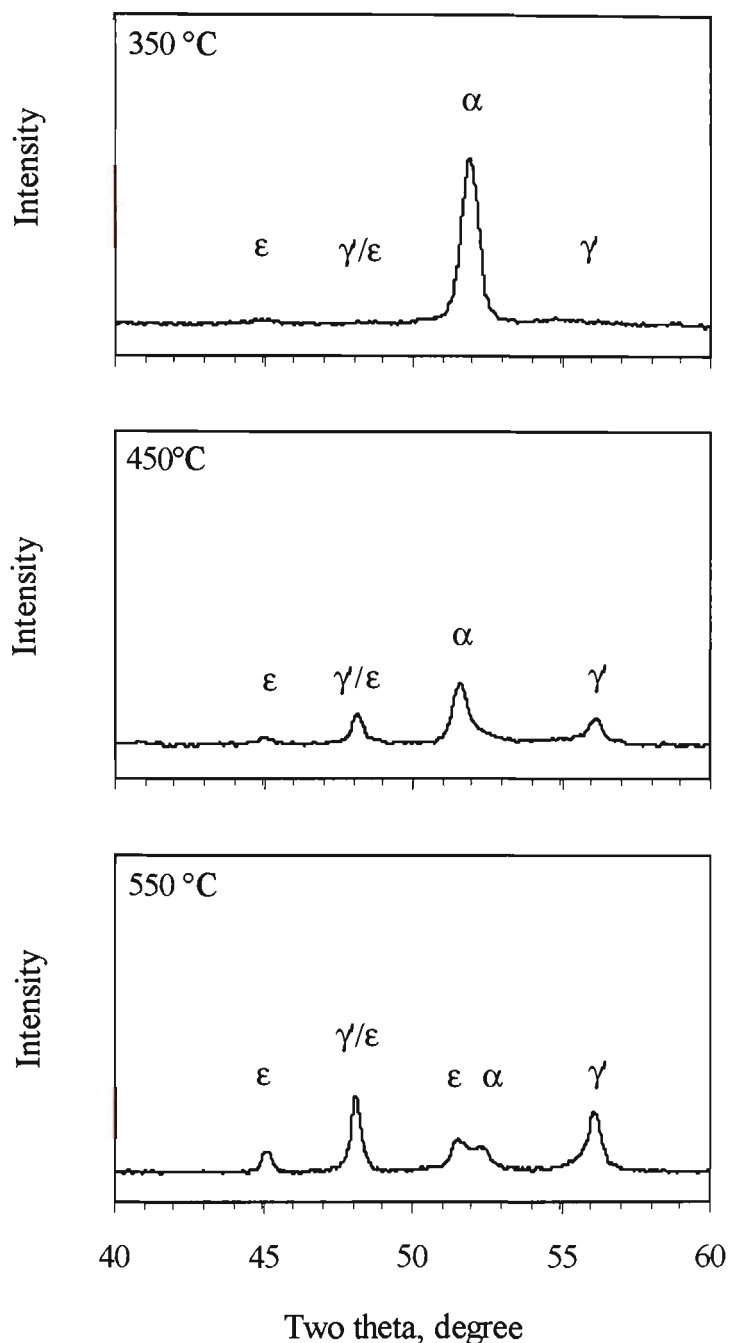


**Figure 50.** X-ray diffraction patterns of the MAXIMA™ samples DC plasma nitrided in 75% $N_2$  - 25% $H_2$  for 5 hours at various temperatures indicated.

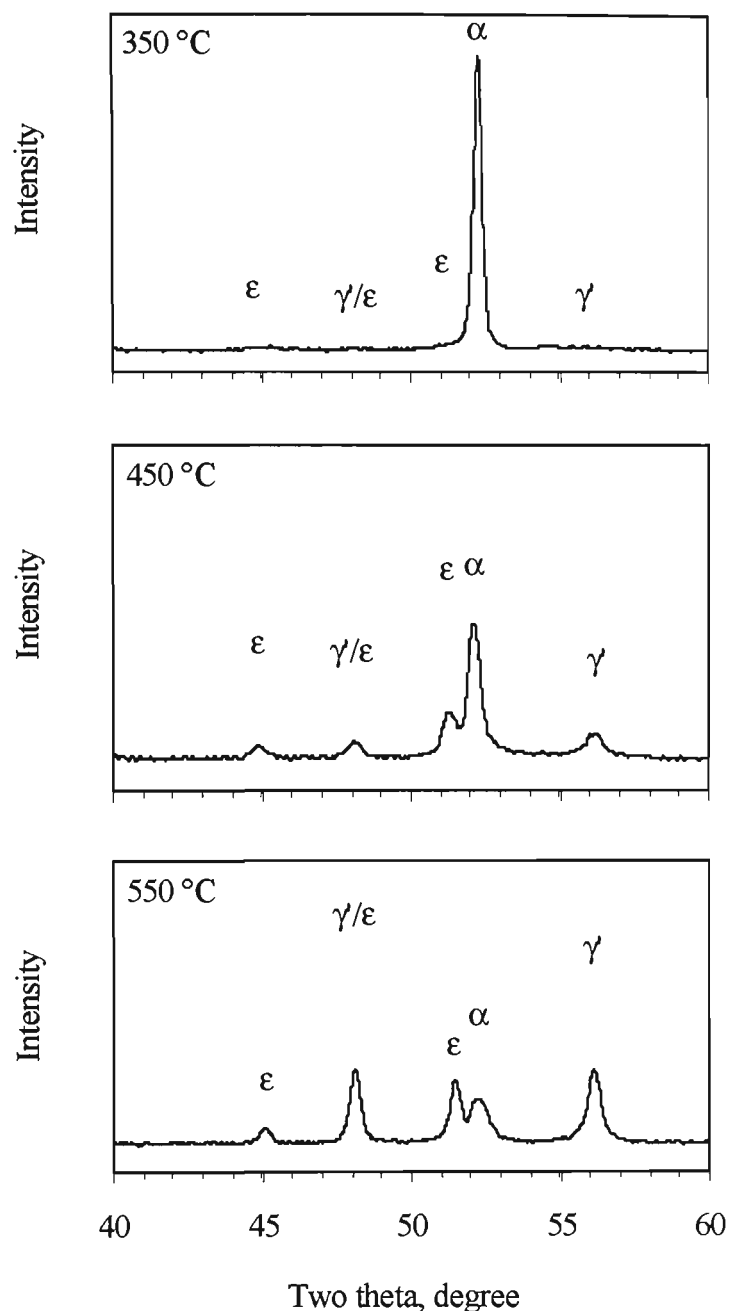


**Figure 51.** X-ray diffraction patterns of the En19 samples DC plasma nitrided in 75% $N_2$  - 25% $H_2$  for 5 hours at various temperatures indicated.

The sample treated at 350°C shows traces of  $\epsilon$  and  $\gamma'$  iron nitride peaks and a reduction in  $\alpha$ -Fe peak intensity. With increasing the nitriding temperature the intensity of the diffraction peaks of  $\epsilon$  and  $\gamma'$  phases increased and the intensity of the  $\alpha$ -Fe phase decreased while its width increased and shifted to lower angles. This apparent shift may simply be due to overlapping with  $\epsilon$  peak. Diffraction patterns obtained from the En19 samples nitrided at 350, 450 and 550°C are illustrated in Figure 51. As in MAXIMA™ samples, the  $\epsilon$  phase was detected with  $\gamma'$  nitride in all samples, with their peaks intensity increasing with increasing treatment temperature indicating the formation of a thicker compound layer. The intensity of the  $\alpha$ -iron peak is again reduced, widened and shifted to lower  $2\theta$  angles with increasing treatment temperature.

#### 4.3.2.2 RF Plasma Nitriding and PI<sup>3</sup>

X-ray diffraction failed to show any evidence of compound layer formation on PI<sup>3</sup> or RF plasma nitrided samples. A more detailed analysis of the surfaces of the RF plasma nitrided and PI<sup>3</sup> treated samples was undertaken using the glancing angle X-ray diffraction technique. Except for the RF plasma nitrided sample treated at 350°C, shown in Figure 52, no iron nitride peaks were detected on the remainder of the samples. Although peaks of  $\gamma'$  iron nitride were identified in the RF plasma nitrided sample treated at 350°C, the SEM micrograph (Figure 48-a) show that the  $\gamma'$  phase was not continuous and was in the form of isolated plates which formed on the surface and grew towards the core of the sample in preferential orientations.

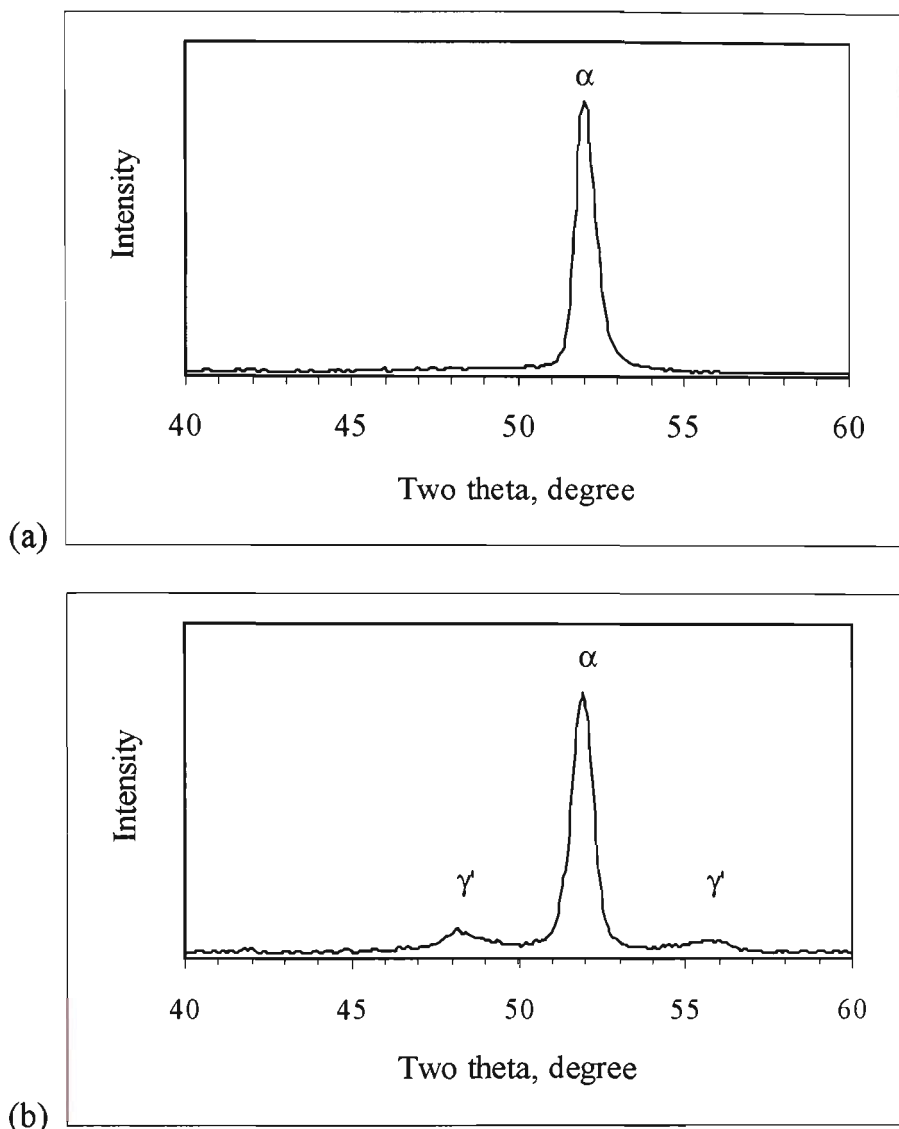


**Figure 52.** Glancing angle X-ray diffraction pattern of (a) PI<sup>3</sup>, (b) RF plasma nitrided samples treated at 350 °C. Co K $\alpha$  radiation, 1° incident angle and 10 sec/step of 0.1°.

### 4.3.3 Glow Discharge Optical Emission Spectroscopy

#### 4.3.3.1 DC Plasma Nitriding

The qualitative GDOES profiles for carbon and nitrogen are illustrated in Figure 53 for MAXIMA™ steel and Figure 54 for En19 steel. The sputtering rate was measured to be approximately 0.04 $\mu$ m/sec for MAXIMA™ and En19 samples. The trend of the profiles

is almost the same for both steels treated at similar temperature. Samples treated at lower nitriding temperatures show higher nitrogen concentration. This decreases with increasing treatment temperature. However, the depth of nitrogen penetration into the substrate increases with increasing nitriding temperature. Furthermore, the nitrogen concentration decreases with distance from the surface. In the sample treated at 450°C, the trend is similar to that of the sample treated at 350°C, but with the overall nitrogen concentration being higher. In the case of the sample treated at 550°C, the nitrogen concentration profile is almost uniform before it drops considerably in the lower region of the compound layer. At all treatment temperatures, the nitrogen profile intensity of the MAXIMA™ steel was higher than that of En19 steel.

Depletion of carbon in the compound layer and its build up ahead of the compound layer where the nitrogen concentration decreases was observed at all treatment temperatures for both steels.

#### **4.3.3.2 RF Plasma Nitriding and PI<sup>3</sup>**

GDOES profiles for nitrogen and carbon obtained from the surface of the samples treated by the PI<sup>3</sup> and RF plasma nitriding processes are presented in Figures 55 and 56, respectively. For both processes the maximum nitrogen concentration was obtained from the sample treated at 350°C and the minimum at 550°C. The samples treated at 450°C showed an intermediate nitrogen concentration. The GDOES profiles for RF plasma nitriding, however, showed unexpectedly higher nitrogen levels than that for PI<sup>3</sup> at 350°C. Although unexpected, this could be due to the very low sputtering of RF nitriding compared to PI<sup>3</sup> treatment.

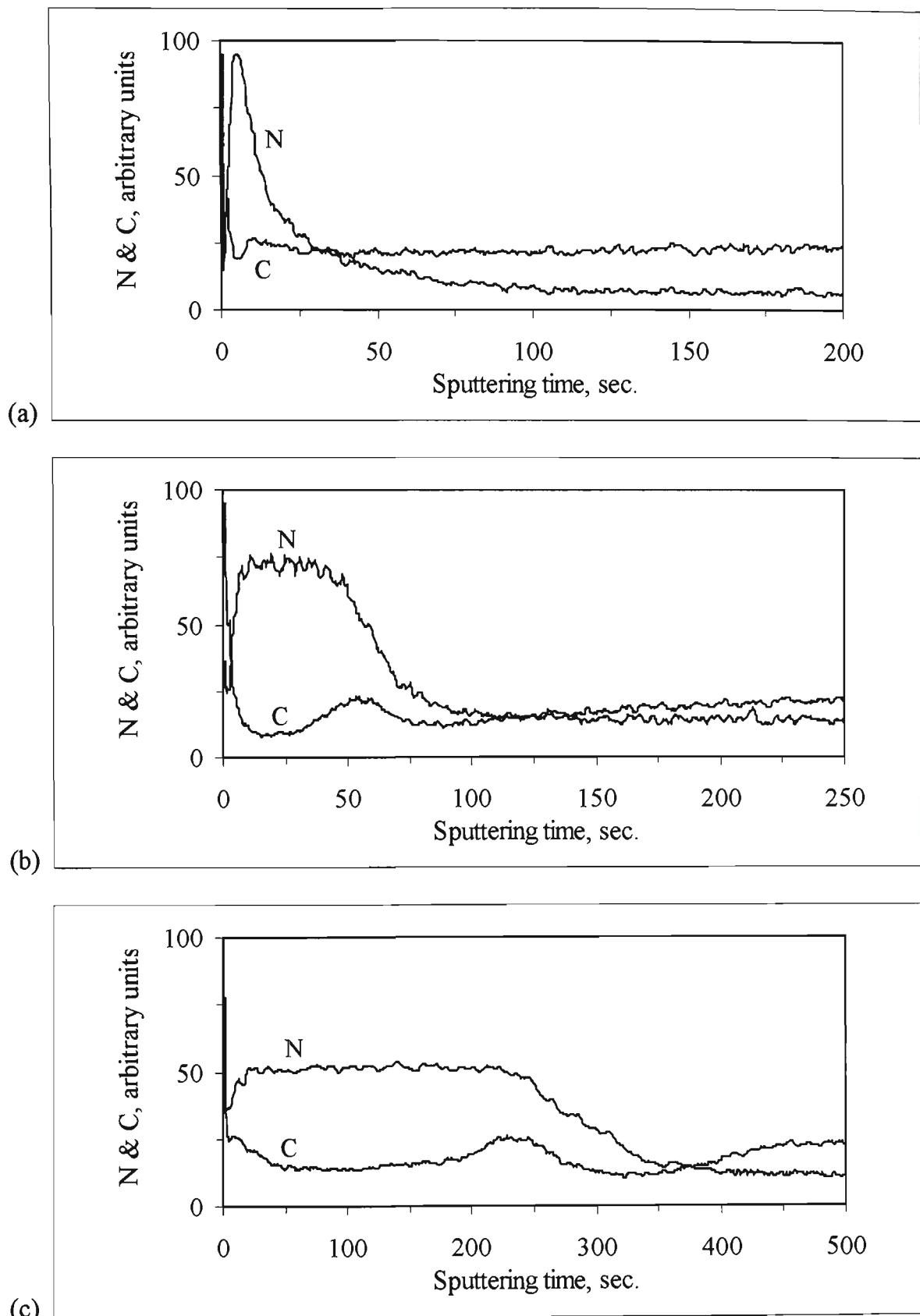


**Figure 53.** GDOES depth profile for MAXIMA™ steel DC plasma nitrided at (a) 350, (b) 450, and (c) 550°C.

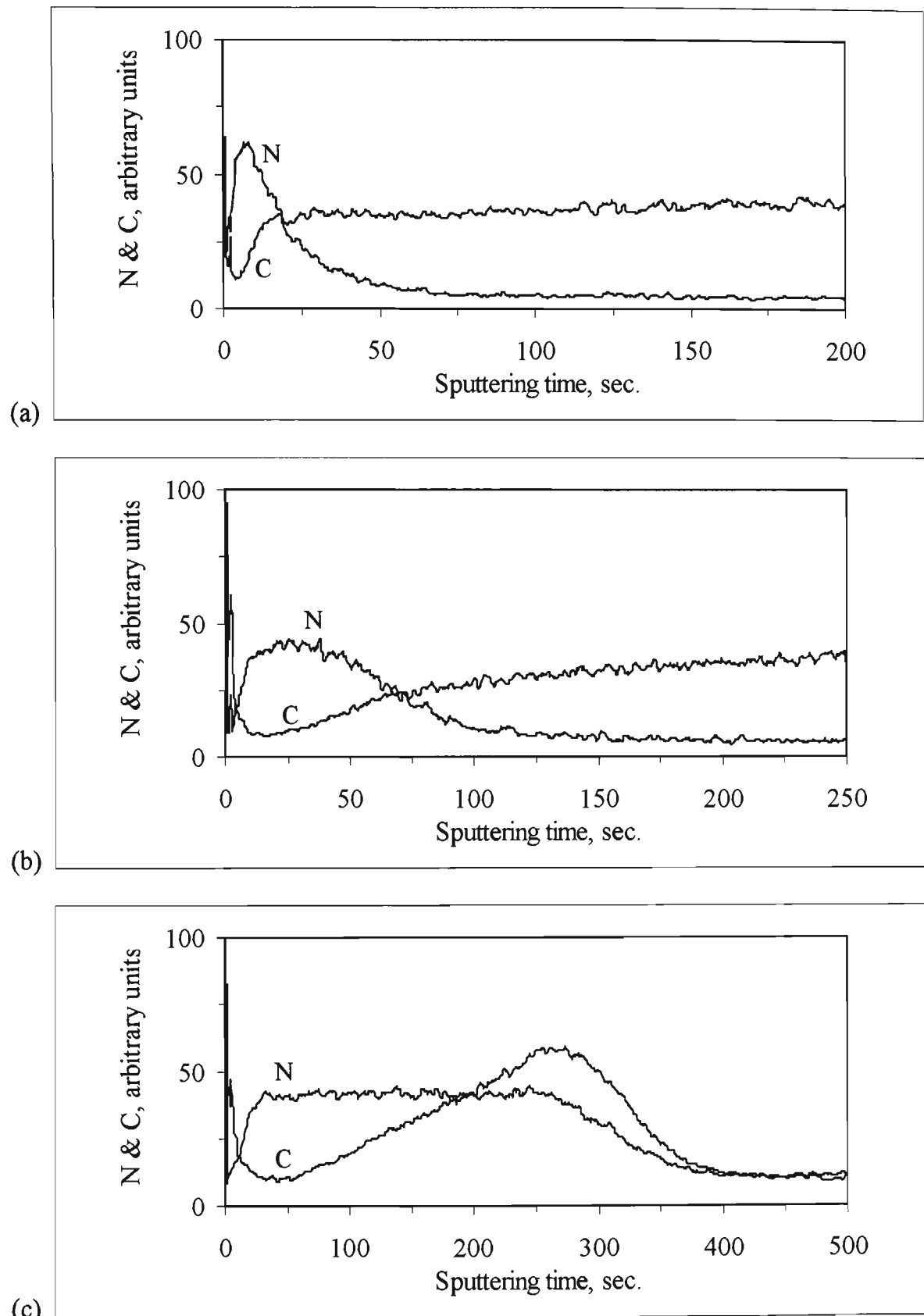


**Figure 54.** GDOES depth profile for En19 steel DC plasma nitrided at (a) 350, (b) 450, and (c) 550°C.

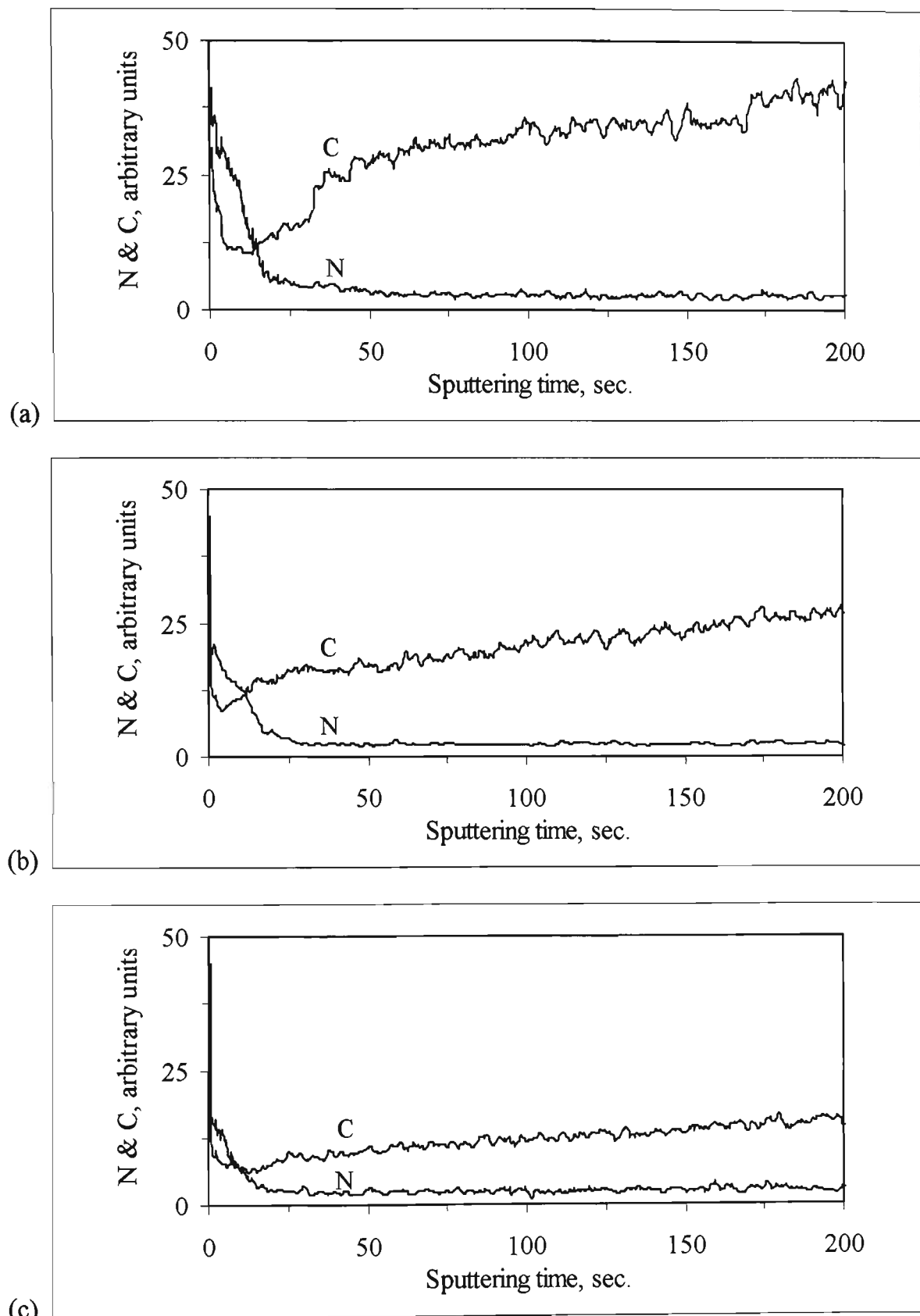


**Figure 55.** Nitrogen and carbon line profiles obtained by GDOES of the  $\text{PI}^3$  treated samples at (a) 350, (b) 450, and (c) 550 °C.

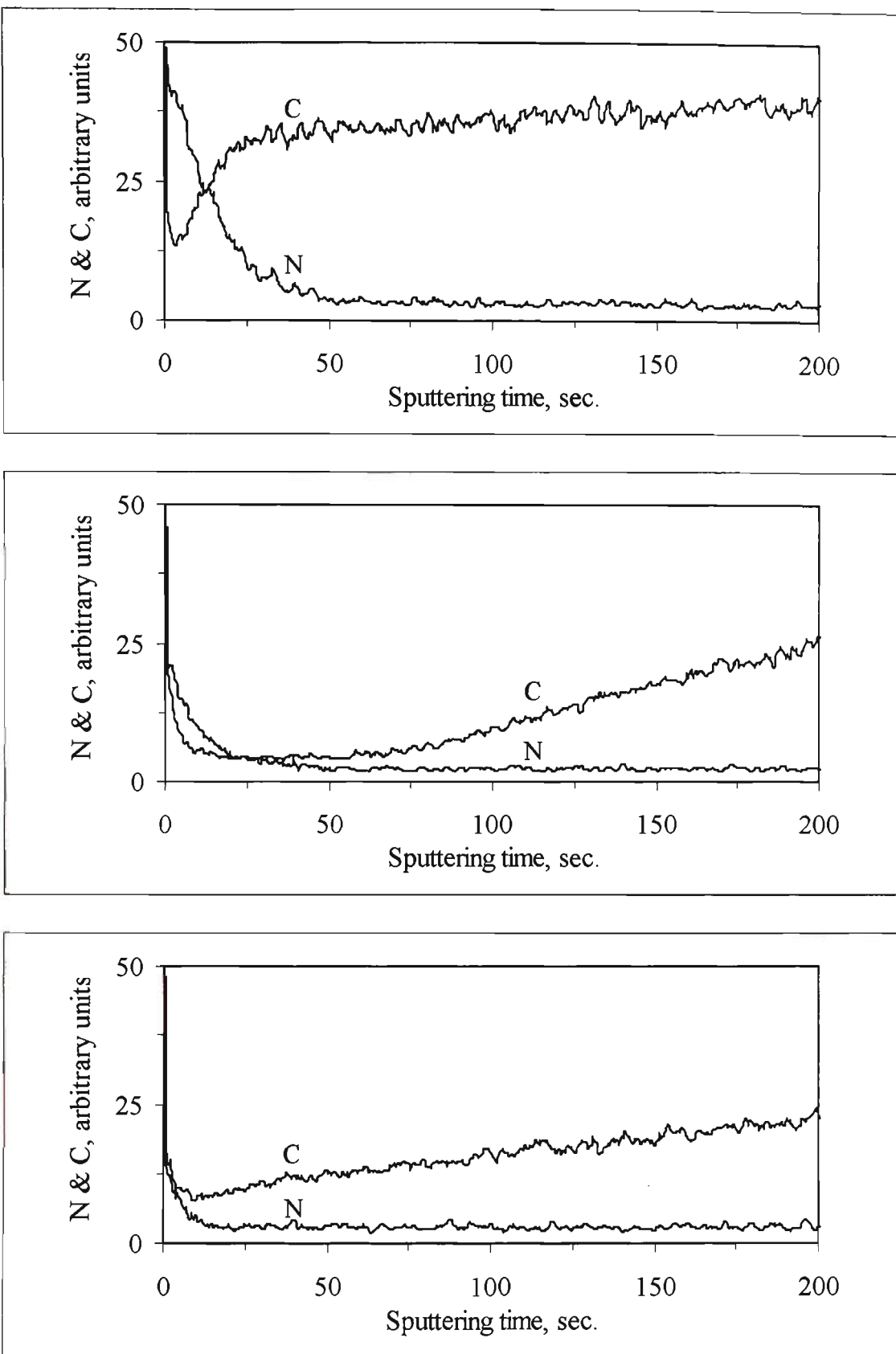


**Figure 56.** Nitrogen and carbon line profiles obtained by GDOES of the RF plasma nitrided samples at (a) 350, (b) 450, and (c) 550 °C.

## 4.3.4 Hardness Tests

### 4.3.4.1 DC Plasma Nitriding

Figures 57 and 58 display the hardness profiles of the samples nitrided at different temperatures ranging from 350 to 550°C for MAXIMA™ and En19 steels, respectively. Samples treated at lower temperatures developed steep hardness profiles, while at higher nitriding temperatures a more gradual hardness profile was developed.

The peak hardness achieved by MAXIMA™ at all treatment temperatures was higher than that of En19. MAXIMA™ exhibited a sharper case/core interface while En19 showed a smoother transition from the nitrided case to the core. The transition from case to core for MAXIMA™ after 550°C treatment was not smooth and a hump in the profile was observed. The hardness levels at any depth within the case were generally lower for En19.

The case depths have been determined from the graphs of micro-hardness vs depth (Figures 57 and 58). Figure 59 shows the general trend in case depth variation measured against plasma nitriding temperature for both steels. It can clearly be seen that the nitrided case depth increases with increasing nitriding temperatures.

The core hardness values of the samples after plasma nitriding at different temperatures are presented in Table 6.

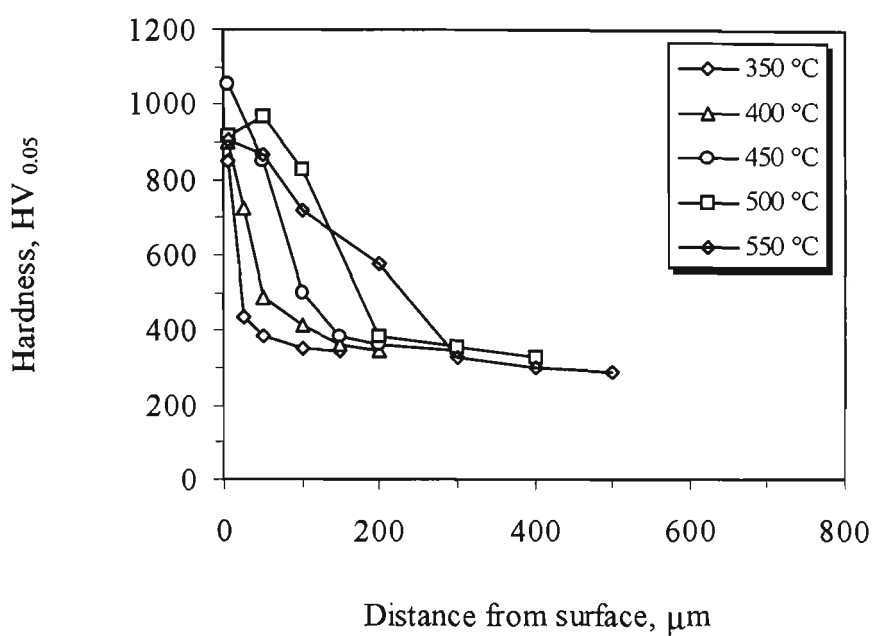


**Figure 57.** Hardness profiles of MAXIMA™ steel DC plasma nitrided at different temperatures.

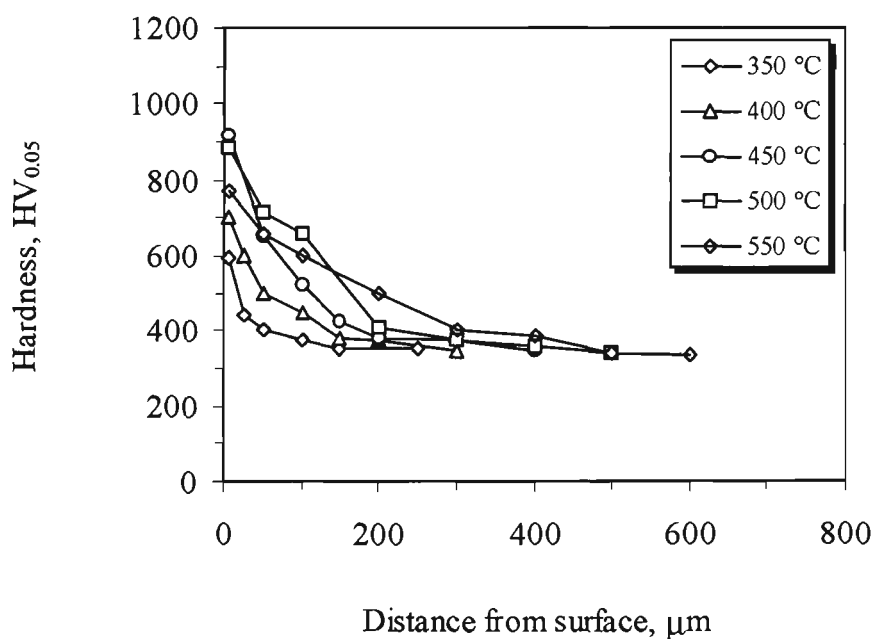


**Figure 58.** Hardness profiles of En19 steel DC plasma nitrided at different temperatures.

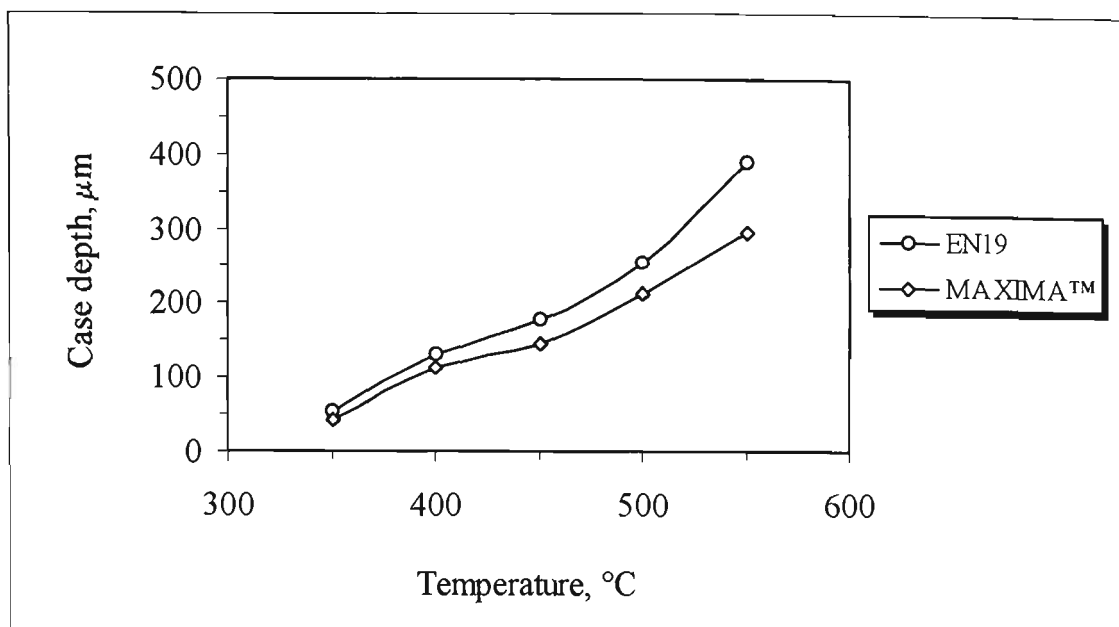


**Figure 59.** Case depth of the samples DC plasma nitrided at different temperatures for 5 hours.

**Table 6.** Core hardness values obtained from the samples after DC plasma nitriding treatments.

Steel	Hardness, HV <sub>20</sub>				
	After treatment				
	Temperature, °C				
MAXIMA™	350	400	450	500	550
MAXIMA™	348	345	343	328	293
En19	349	346	345	340	319
					366
					340

Figure 60 shows the variation in core hardness values as well as the peak hardness, of the samples plasma nitrided at different temperatures. In the case of MAXIMA™ steel, samples plasma nitrided at lower temperatures, ranging from 350 to 450°C, show a slight reduction in core hardness, while those treated at higher temperatures, indicate a higher degree of softening which was more pronounced for the sample treated at 550°C. There was not any discernible softening for En19 samples plasma nitrided at 350-500°C.

temperatures. A slight reduction in core hardness was observed for the 550°C treatment temperature.

Comparison of peak hardness curves of MAXIMA™ and En19 steels reveals that the trend is the same for both steels, see Figure 60. The highest peak hardness with no significant reduction to the core strength was achieved at 450°C for both steels.

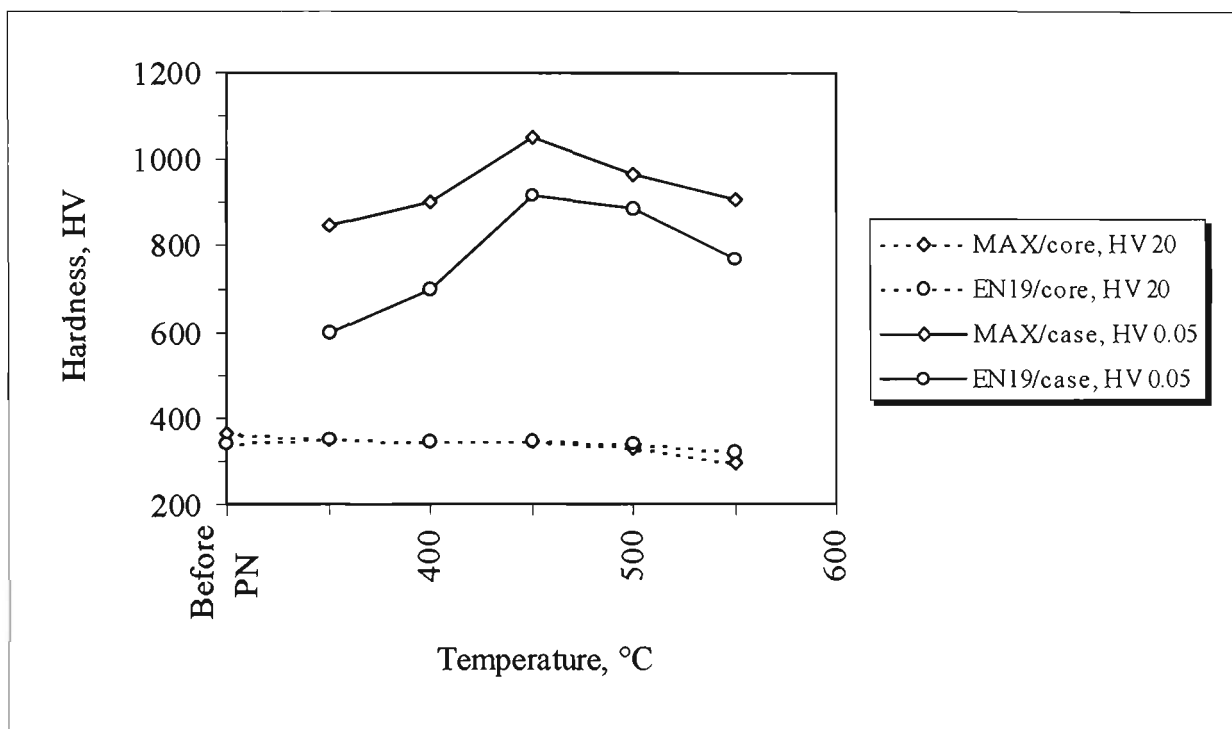


**Figure 60.** The peak hardness and the core hardness of the samples after DC plasma nitriding at different temperatures. Note the hardness of the samples before treatment.

#### 4.3.4.2 RF Plasma Nitriding and PI<sup>3</sup>

Surface hardness at different loads for PI<sup>3</sup> and RF plasma nitriding treatments at 350, 450 and 550°C are presented in Figure 61. The core hardnesses (HV<sub>20</sub>) after each treatment are also included.

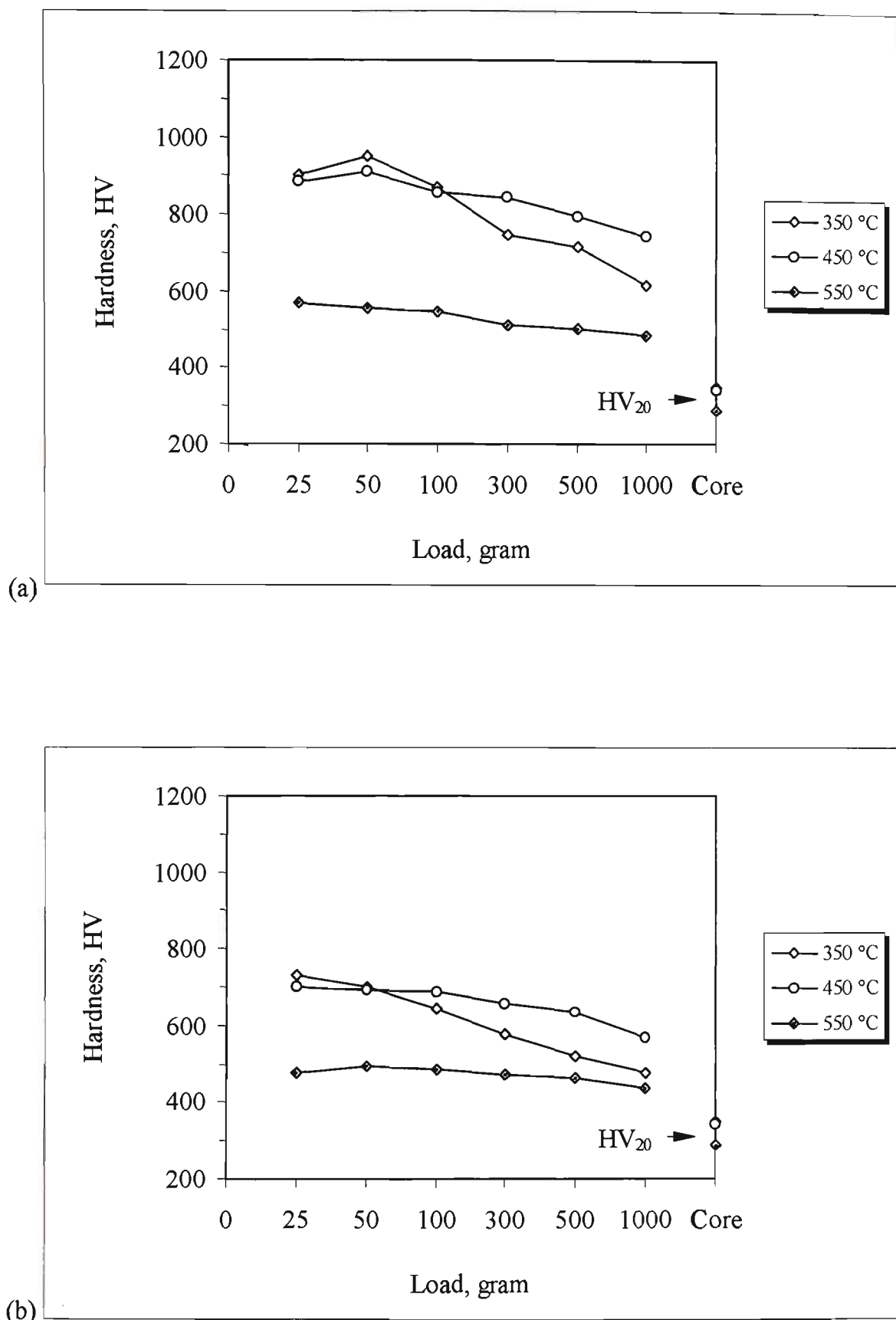
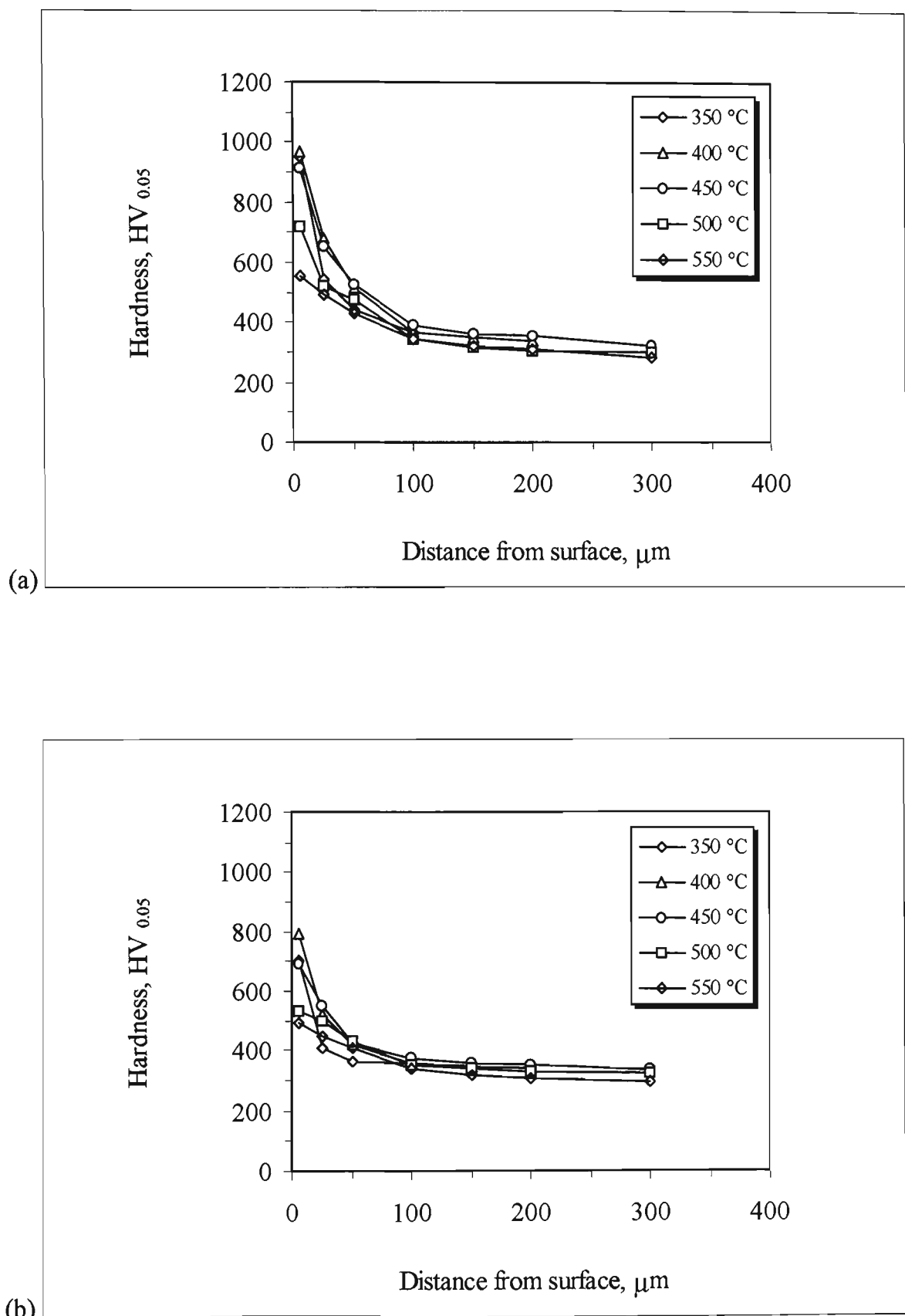


Figure 61. Surface hardness at different loads for (a)  $\text{PI}^3$  and (b) RF plasma nitrided samples.



**Figure 62.** Hardness profiles of (a) PI<sup>3</sup> and (b) RF plasma nitrided samples at different temperatures for 5 hours.

Since the depth of penetration increases by increasing the indentation load, and the measured hardness is affected by material up to 10 times the indent depth, a judgement as to the case depth should be possible from the trend of hardness with increasing load.

Figure 62 illustrates the hardness profiles after PI<sup>3</sup> and RF plasma nitriding which are consistent with the surface hardness measurements seen in Figure 61. The samples treated at 400°C developed cases with maximum hardness, whereas samples treated at 550°C showed the minimum surface hardness, see Figure 63. From the hardness profiles, increasing treatment temperature increased case depth and decreased surface hardness.

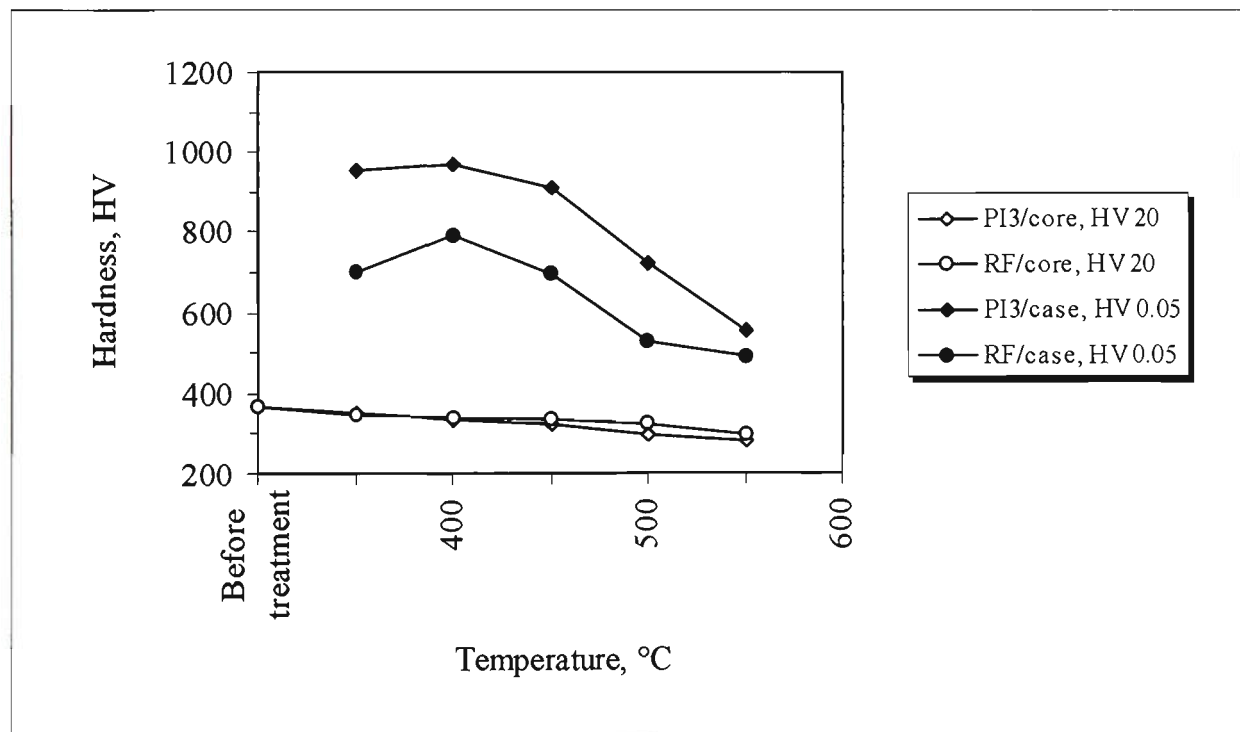


**Figure 63.** The peak surface hardness developed on the samples treated at temperatures ranging from 350 to 550°C by the PI<sup>3</sup> and RF plasma nitriding processes.

### 4.3.5 Appearance of the Treated Samples

#### 4.3.5.1 DC Plasma Nitriding

After DC plasma nitriding all the samples treated at different temperatures displayed a greyish (dark) ring parallel to their edge, see Figure 64. The degree of the darkening was dependent upon the treatment temperature; the higher the temperature the darker the ring.



*Figure 64. Surface appearance of MAXIMA™ sample DC plasma nitrided at 550°C. Note the dark ring parallel to the edge of the sample.*

#### 4.3.5.2 RF Plasma Nitriding and PI<sup>3</sup>

After RF plasma nitriding, except for the sample treated at 350°C, no noticeable change in the appearance of samples was observed and the samples were still shiny (similar to

their as polished condition). The sample treated at 350°C, however, had lost its reflectivity and was slightly grey in colour.

Samples treated by the PI<sup>3</sup> displayed some changes in reflectivity, especially the sample treated at 350°C which showed the most darkening compared to those treated at higher temperatures.

Unlike the DC plasma nitrided sample, no dark ring was formed on the surface of the samples treated by RF plasma nitriding and PI<sup>3</sup> processes.

### **4.3.6 Surface Topography**

#### **4.3.6.1 DC Plasma Nitriding**

Definite trends in the surface roughness as a function of the treatment temperatures were evident for both steels, see Figure 65. Minimum roughening occurred at 350°C treatment temperature, while 550°C temperature resulted in the roughest surface.

Generally speaking, increasing the treatment temperature increased the roughness of the surface. Comparison of the two steels treated under identical conditions revealed that the surface roughness of MAXIMA™ samples was greater than that of the En19 samples.

AFM images of MAXIMA™ and En19 samples nitrided at 350, 450 and 550°C are displayed in Figures 66-68. As the treatment temperature increased, the surface morphology changed and the nodular particles deposited on the surface of the steels became larger in size.

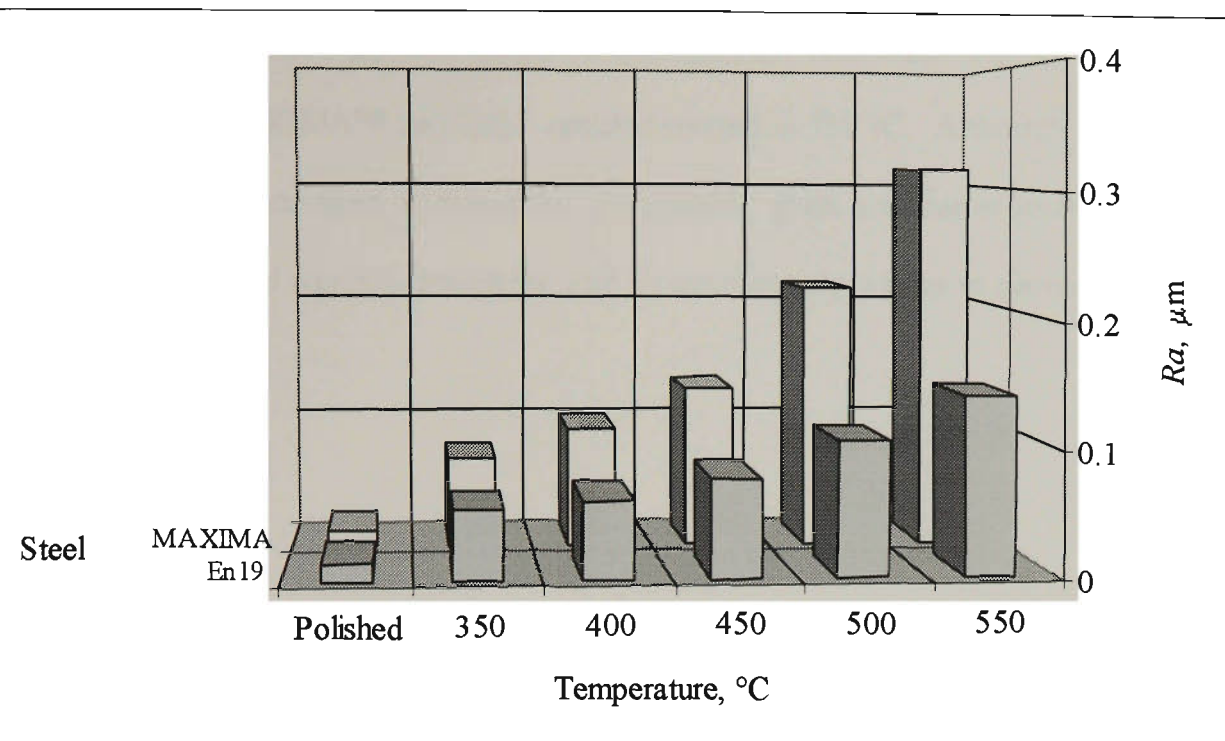
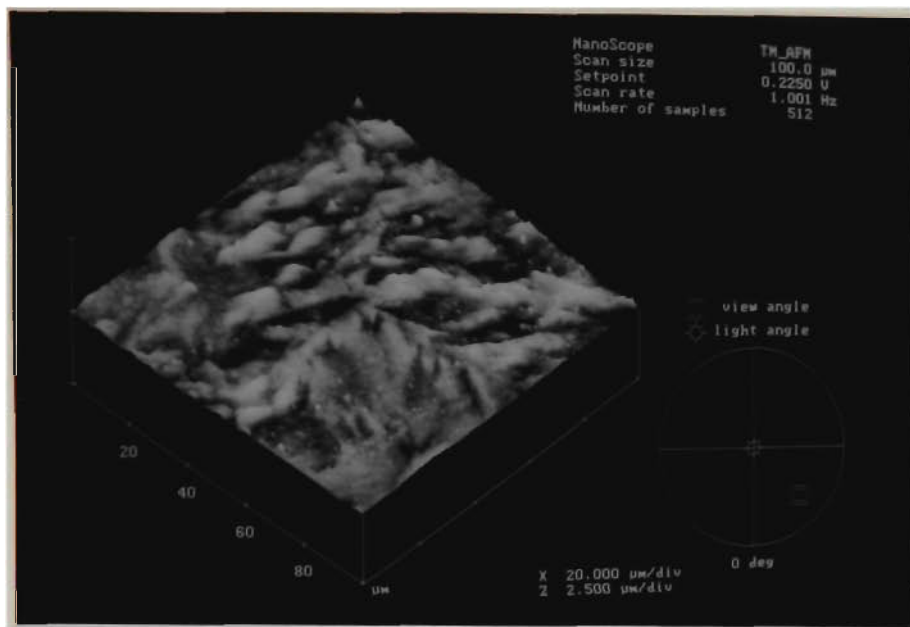


**Figure 65.** Comparison of the surface roughness of both steels DC plasma nitrided under identical conditions for 5 hours at different temperatures.

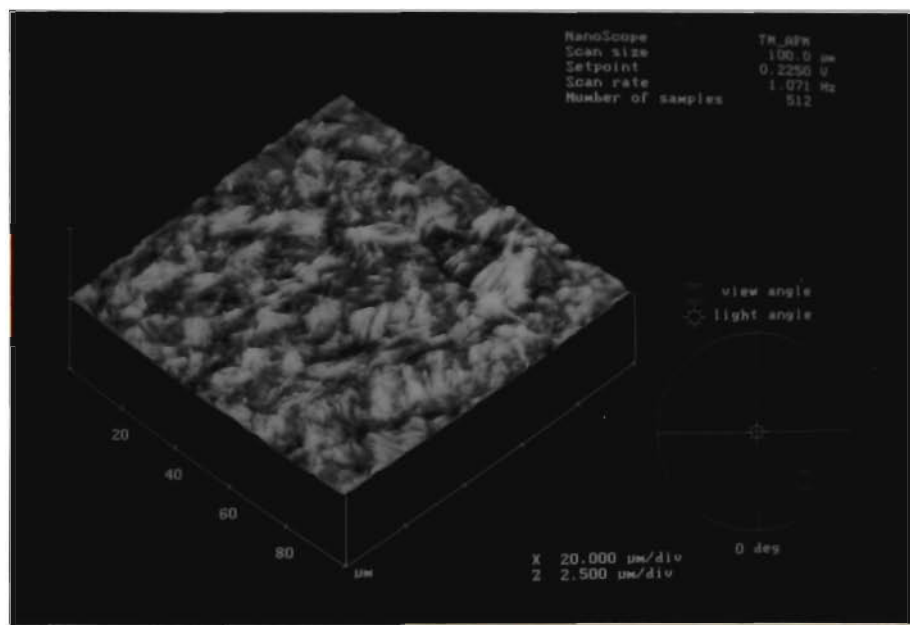
The surface topography at lower treatment temperature ( $350^{\circ}\text{C}$ ) was substantially different from that of higher treatment temperature, i.e. 450 and  $550^{\circ}\text{C}$ . At  $350^{\circ}\text{C}$ , the surface appeared to have a morphology typical of surface relief, perhaps slightly modified by some sputtering and re-deposition, see Figure 66-a,b. Nevertheless, the morphology of En19 steel is similar to its pre-nitriding fine tempered martensitic microstructure while MAXIMA™ exhibits coarser irregularities.

At higher treatment temperatures the surface morphology is significantly changed, particularly at  $550^{\circ}\text{C}$ . Samples developed morphologies similar to the nodular morphology usually observed in CVD coatings. Needle-shape features are seen at higher magnifications in Figure 69.

SEM micrographs in Figures 70 and 71 clearly show the difference in the surface topography of MAXIMA™ and En19 samples treated at 550 °C. Although, the surface of both steels was covered with nodular precipitates, grain boundaries in MAXIMA™ were also delineated which is consistent with its microstructure prior to nitriding.

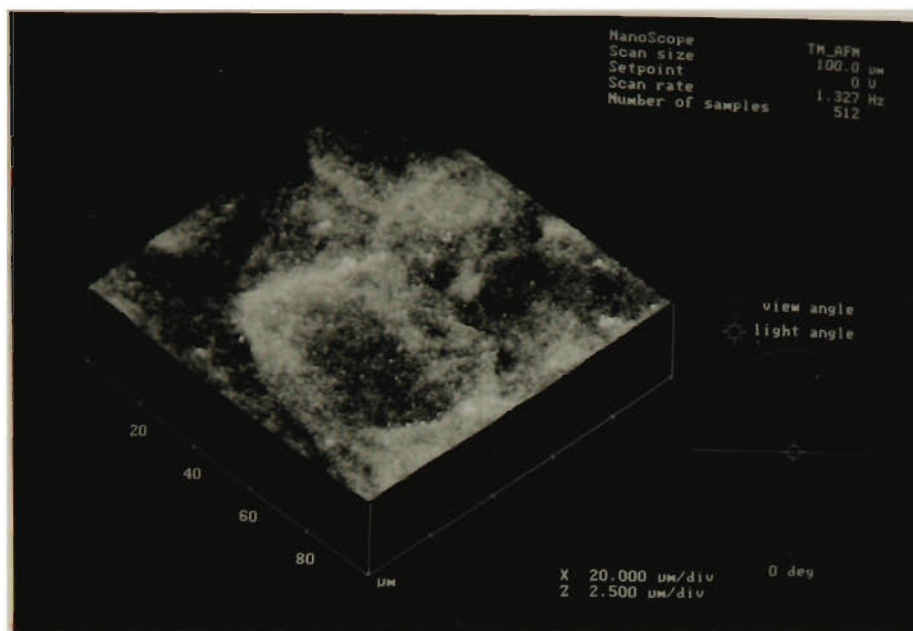


(a)

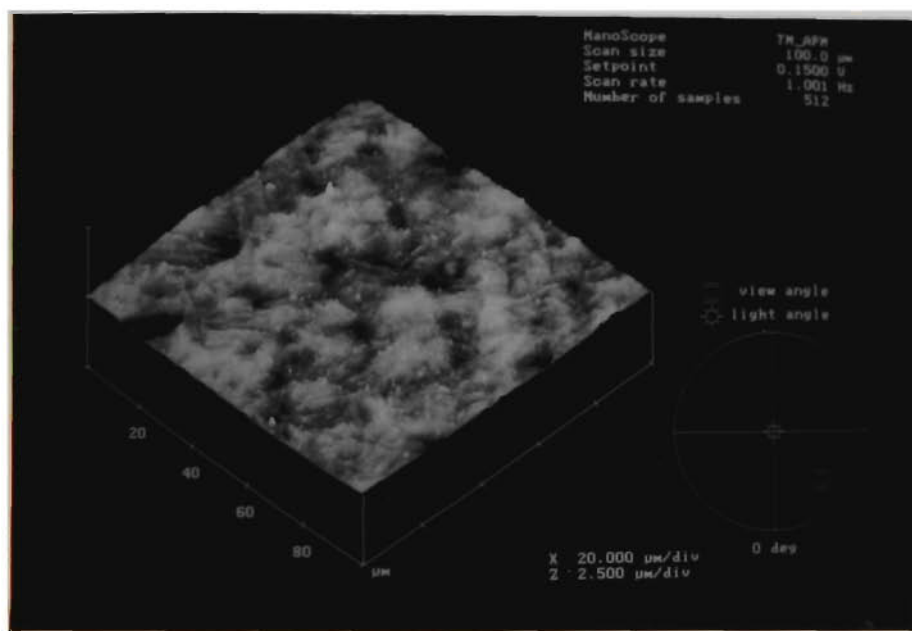


(b)

**Figure 66.** AFM images from the surface of (a) MAXIMA™ and (b) En19 samples DC plasma nitrided at 350 °C.

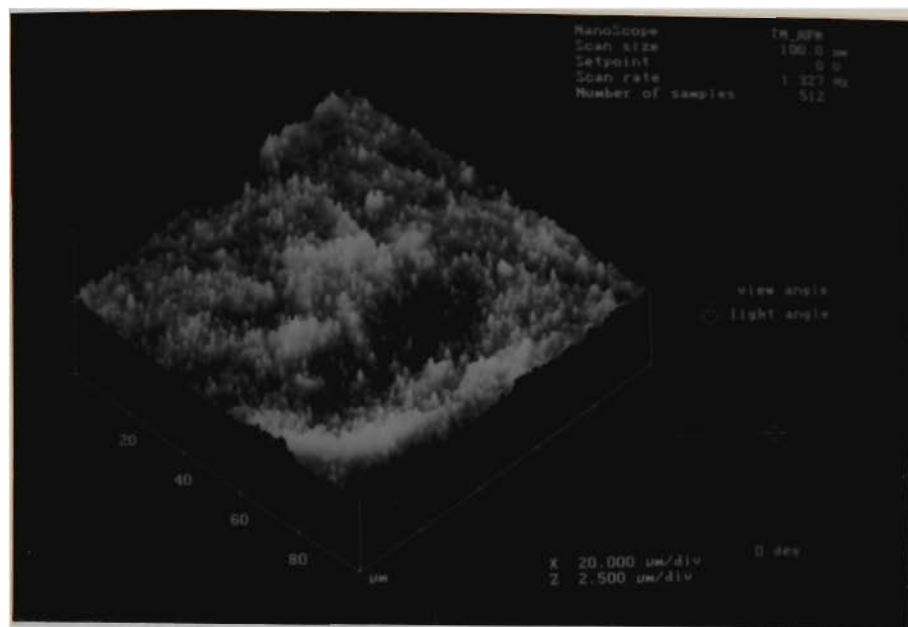


(a)

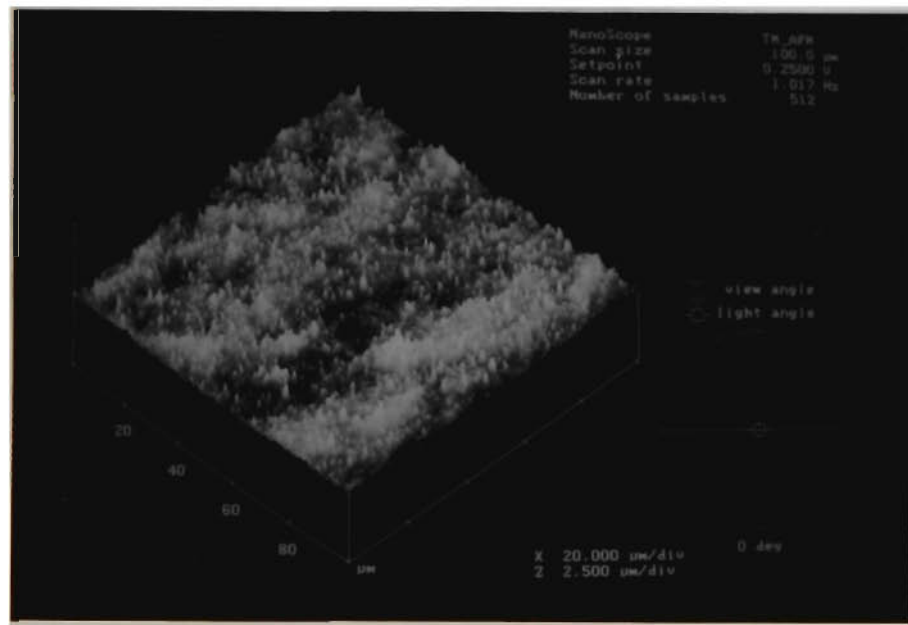


(b)

**Figure 67.** AFM images from the surface of (a) MAXIMA™ and (b) En19 samples DC plasma nitrided at 450 °C.

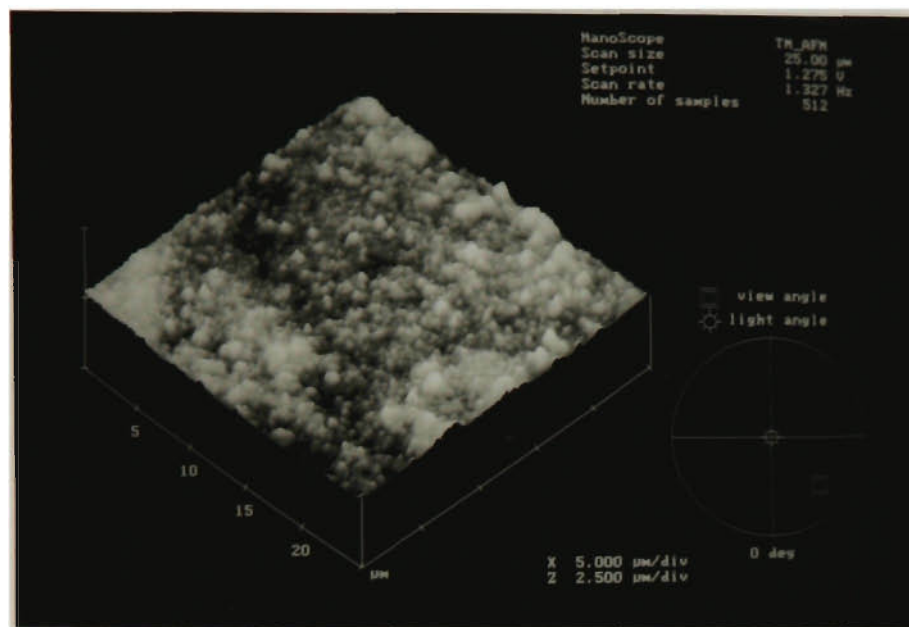


(a)

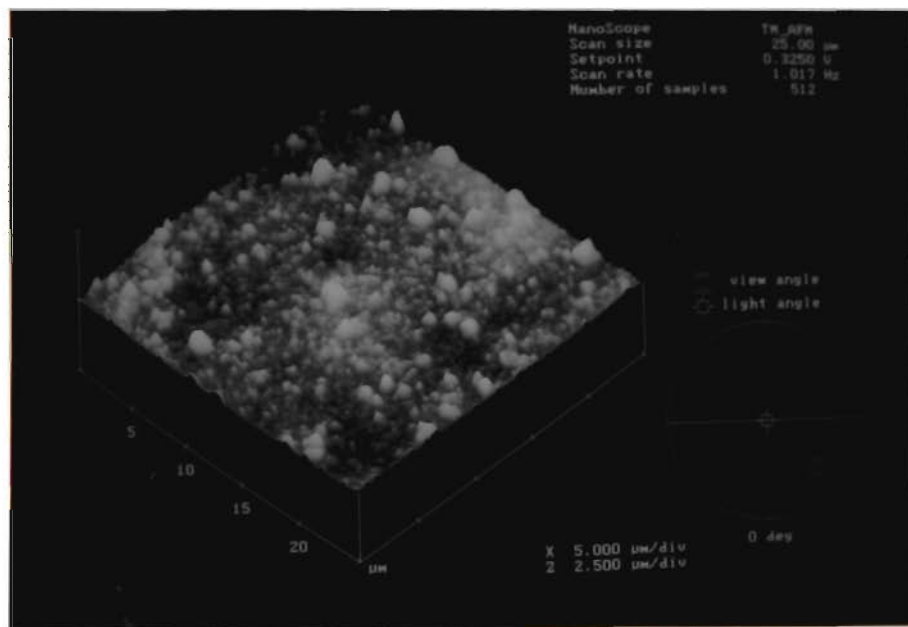


(b)

**Figure 68.** AFM images from the surface of (a) MAXIMA™ and (b) En19 samples DC plasma nitrided at 550 °C.



(a)

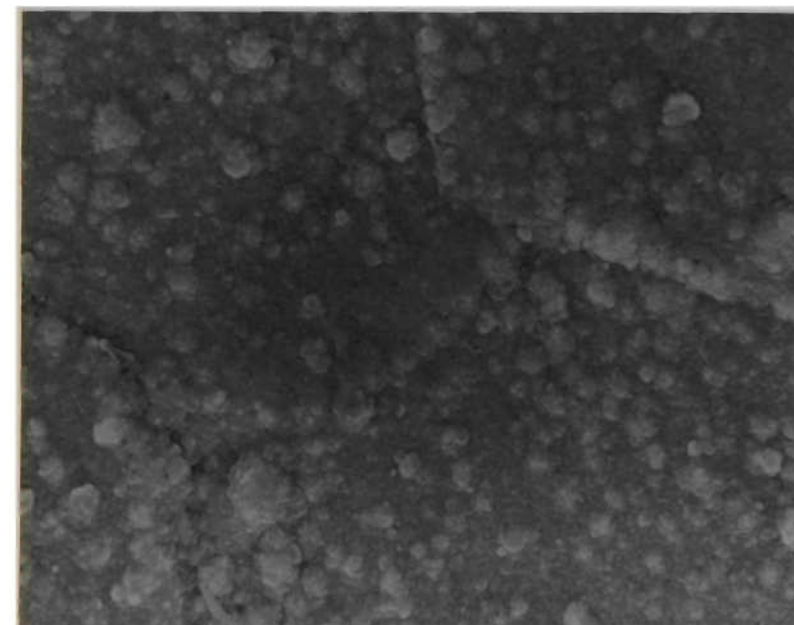


(b)

**Figure 69.** AFM images from the surface of (a) MAXIMA™ and (b) En19 samples DC plasma nitrided at 550 °C at higher horizontal magnification. Note the nodular morphology of the deposited iron nitrides resembling the morphology of the CVD coatings.



(a)

20 $\mu\text{m}$ 

(b)

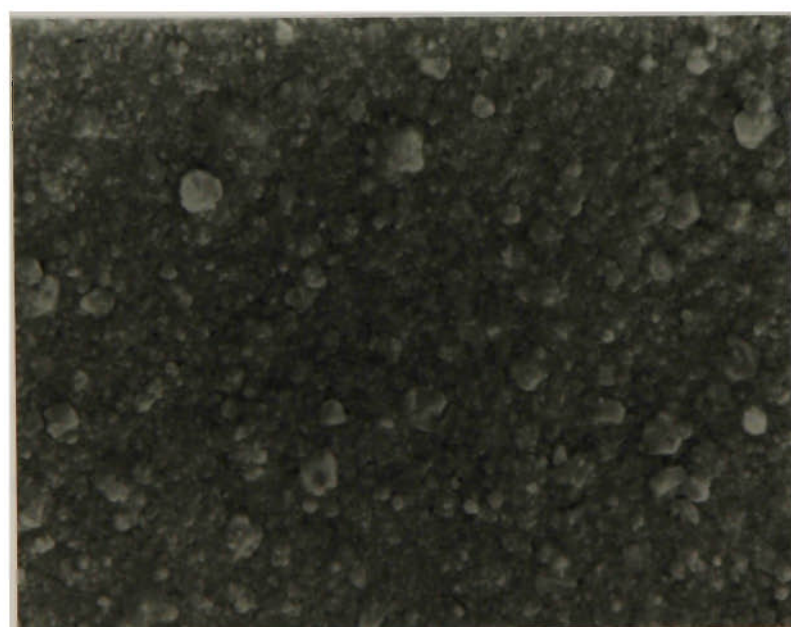
4 $\mu\text{m}$ 

**Figure 70.** SEM of the surface of MAXIMA™ sample DC plasma nitrided at 550 °C at two magnifications.



(a)

A scale bar consisting of a horizontal line with a vertical tick at each end, labeled "20μm".



(b)

A scale bar consisting of a horizontal line with a vertical tick at each end, labeled "4μm".

**Figure 71.** SEM of the surface of En19 sample DC plasma nitrided at 550°C at two magnifications.

#### **4.3.6.2 RF Plasma Nitriding and PI<sup>3</sup>**

The results of the surface roughness measurements, of the PI<sup>3</sup> and RF plasma nitrided samples are presented in Table 7 and Figure 72. Similar trends in the surface roughness occurred with treatment temperature for both treatments. Maximum roughening took place at 350°C, minimum roughening at 450°C and intermediate roughening at 550°C. At all temperatures the surface roughness of the samples treated by PI<sup>3</sup> were greater than those of RF plasma nitrided samples.

Optical micrographs from the surface of the samples treated by the PI<sup>3</sup> process and RF plasma nitriding are shown in Figures 73 and 74, respectively. Both processes at 350°C developed surfaces with morphologies resembling surface relief, see Figures 73-a and 74-a. Higher treatment temperatures for both processes, however, resulted in surfaces with morphologies typical of sputter etching, the severity of which increases with increasing temperature, see Figures 73-b,c and 74-b,c. Note that grains as well as grain boundaries were sputter etched in PI<sup>3</sup> treated samples, while only grain boundaries were highlighted in RF plasma nitrided samples.

The AFM images in Figures 75, 76 and 77 reveal the above mentioned observations in more detail. Generally speaking, the severity of sputter etching was greater for PI<sup>3</sup> than RF plasma nitriding.

**Table 7.** Surface roughness  $R_a$  results after PI<sup>3</sup> and RF plasma nitriding at different temperatures for 5 hours in 75%  $N_2$ -25%  $H_2$  gas mixture.

Treatment	$R_a$ , $\mu\text{m}$					
	Temperature, $^{\circ}\text{C}$					As polished
	350	400	450	500	550	
PI3	0.086	0.048	0.045	0.051	0.053	0.012
RF	0.065	0.028	0.026	0.029	0.032	0.012

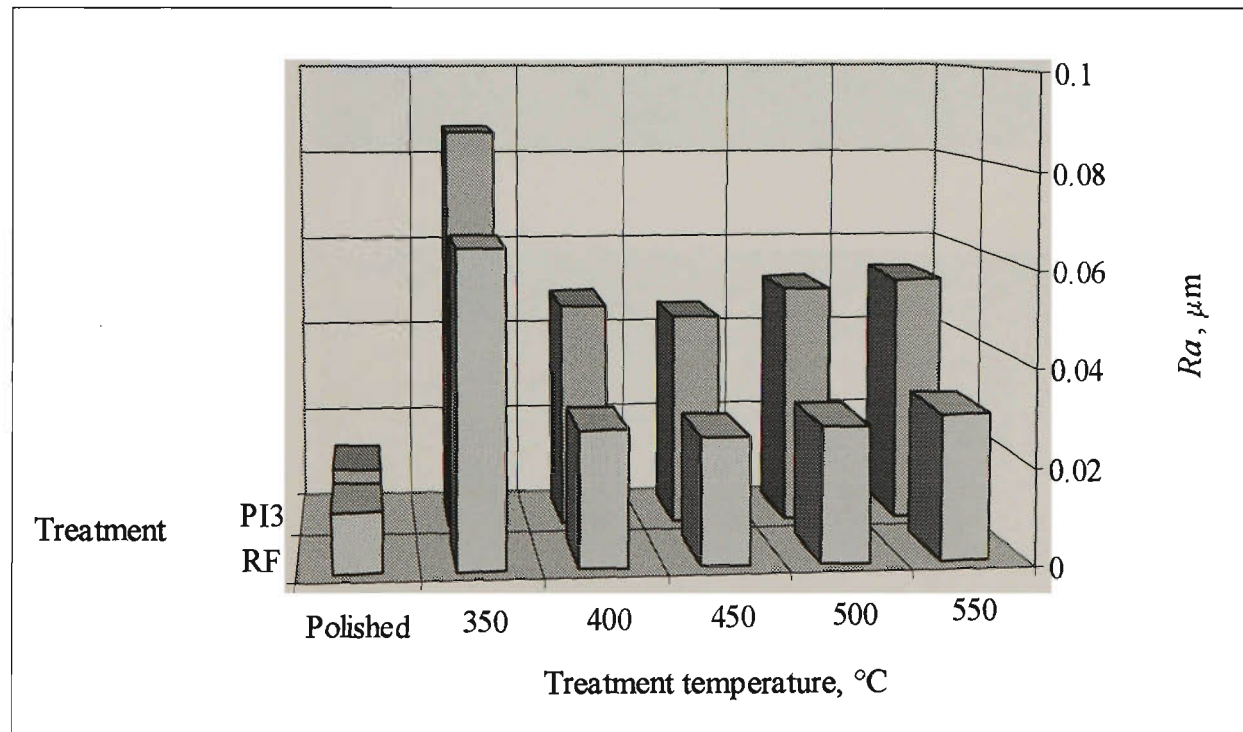


**Figure 72.** Surface roughness ( $R_a$ ) for MAXIMA™ steel treated by PI<sup>3</sup> and RF plasma nitriding processes.

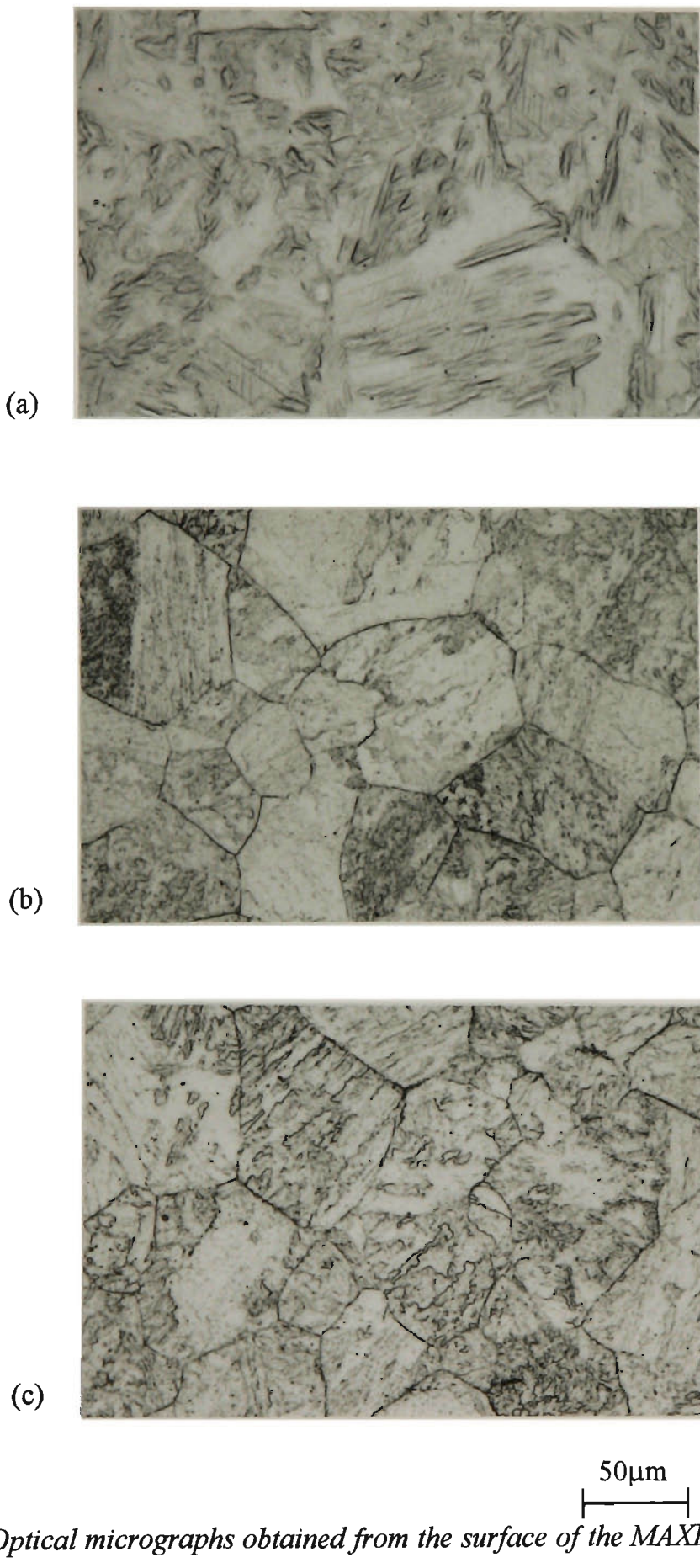


**Figure 73.** Optical micrographs obtained from the surface of the MAXIMA™ samples treated by the PI<sup>3</sup> process at (a) 350 °C, (b) 450 °C and (c) 550 °C.

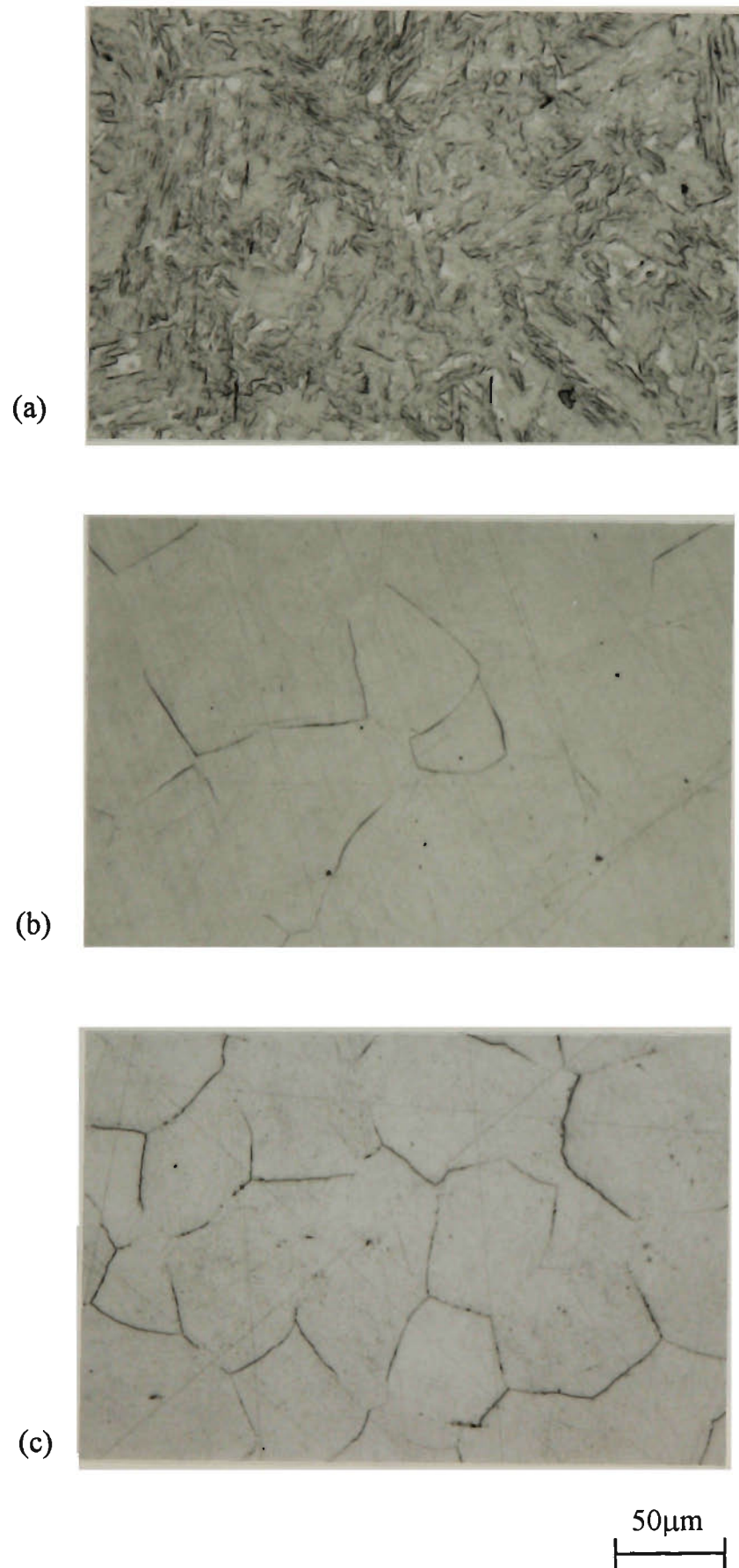
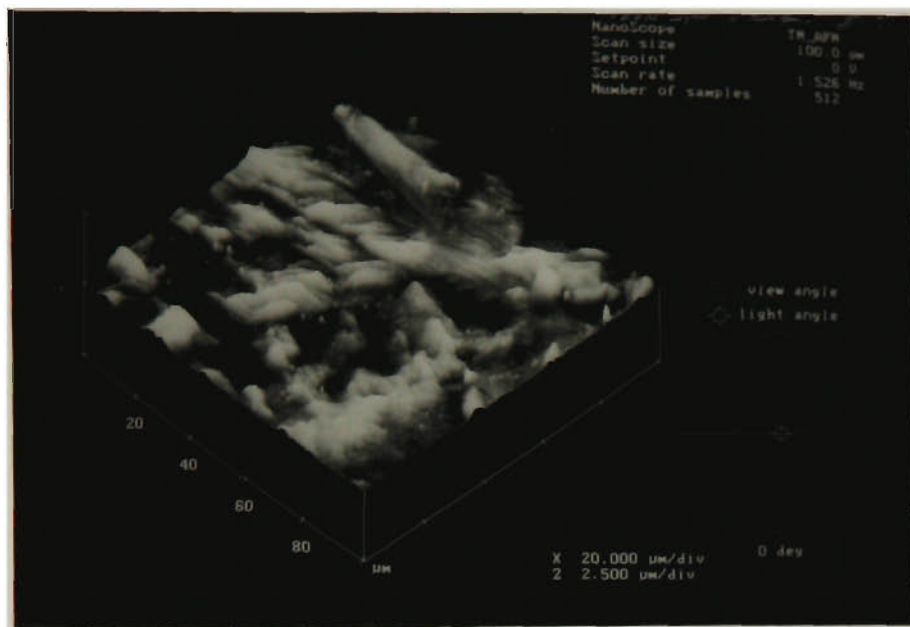
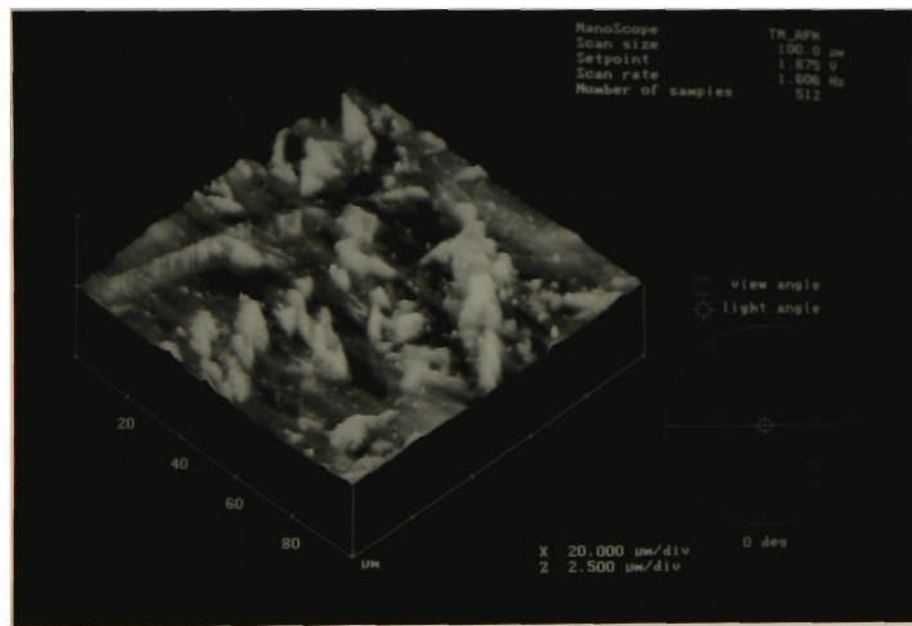


**Figure 74.** Optical micrographs obtained from the surface of the MAXIMA™ samples RF plasma nitrided at (a) 350 °C, (b) 450 °C and (c) 550 °C.

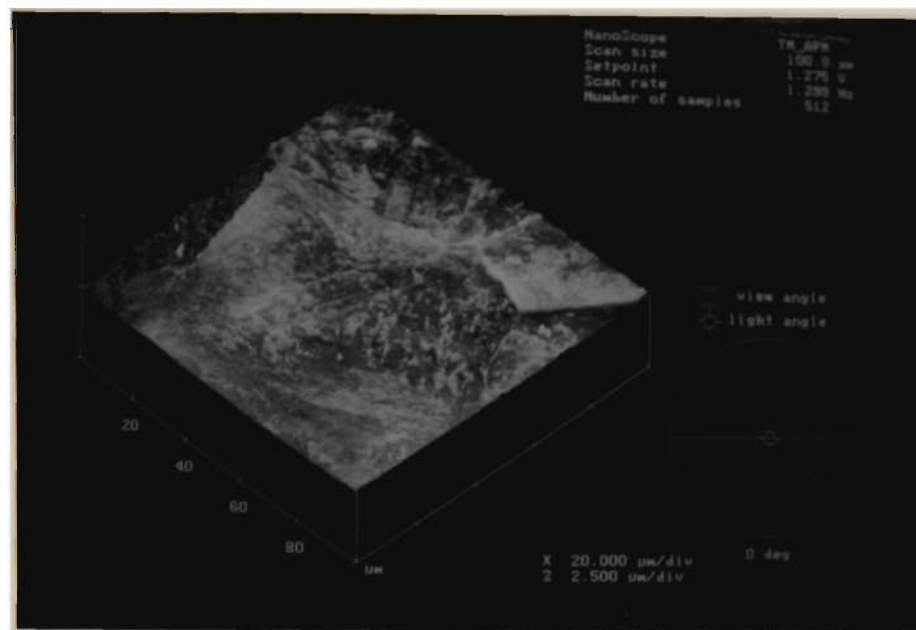


(a)

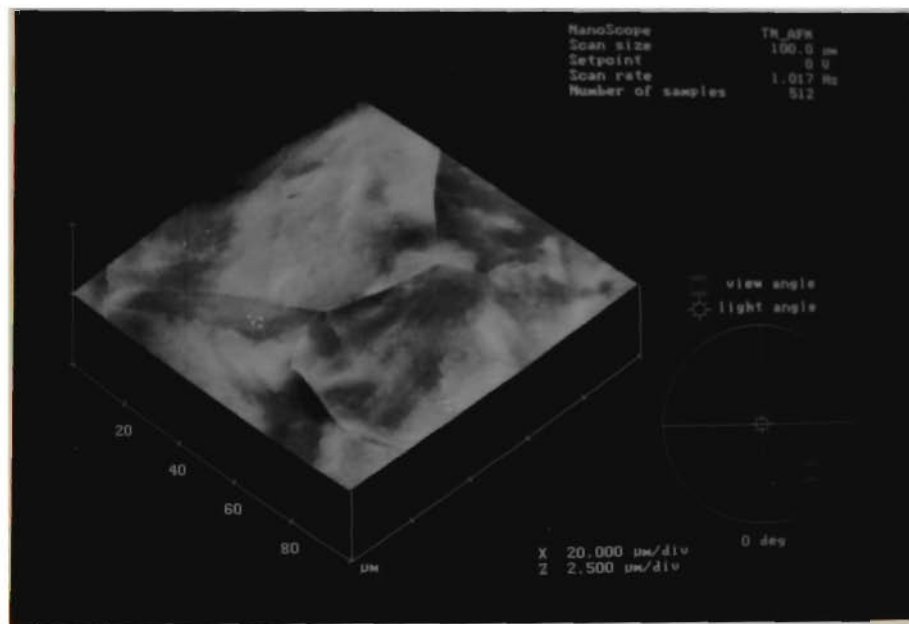


(b)

**Figure 75.** AFM images from the surface of the (a)  $\text{PI}^3$  and (b) RF plasma nitrided samples at 350 °C.

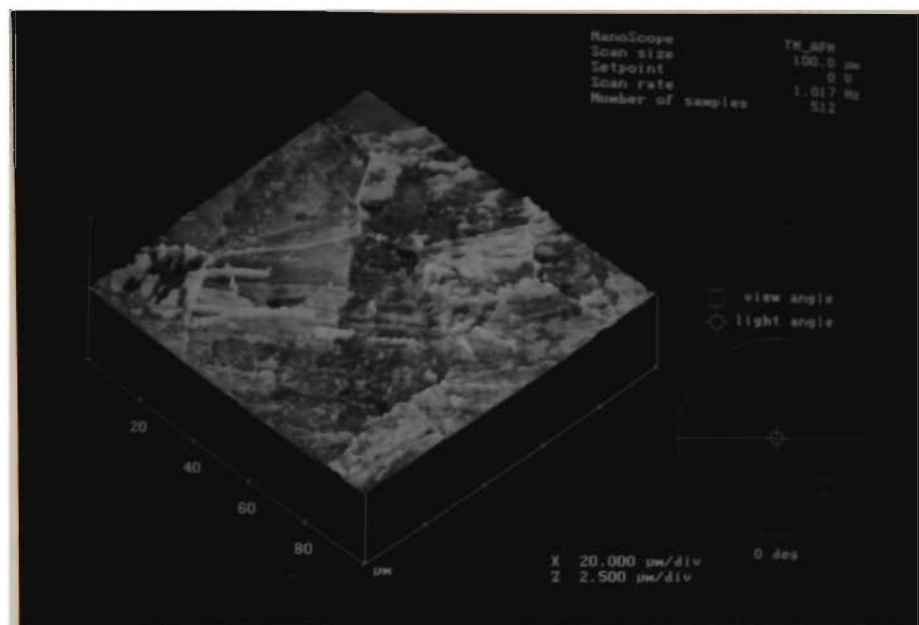


(a)

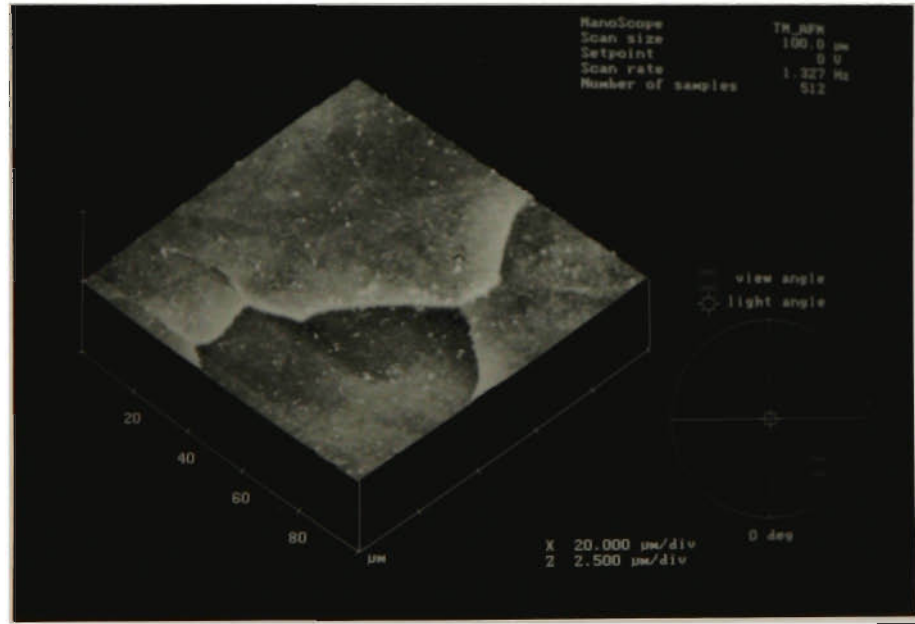


(b)

**Figure 76.** AFM images from the surface of the (a) PI<sup>3</sup> and (b) RF plasma nitrided samples at 450 °C.



(a)



(b)

**Figure 77.** AFM images from the surface of the (a) PI<sup>3</sup> and (b) RF plasma nitrided samples at 550°C.

## **5. CHAPTER FIVE: DISCUSSION**

---

### **5.1 Effect of Hydrogen on Layer Formation in DC Plasma Nitriding**

Considerable differences have been observed in the properties of the sample nitrided in pure nitrogen and those nitrided in atmospheres containing various percentages of hydrogen. Nitriding in pure nitrogen developed the least hard and the roughest surface while treatment in 75%N<sub>2</sub>-25%H<sub>2</sub> resulted in the formation of the hardest and smoothest surface with the thickest compound layer.

Although nitriding in atmospheres containing hydrogen resulted in higher hardness and a deeper case, pure nitrogen atmospheres also produced a hardened case. This cannot be explained by the model suggested by Hudis (1973) in which the hydrogen-nitrogen molecular ions are regarded as a decisive factor in plasma nitriding. The results, however, may partly be explained by the collision dissociation model proposed by Xu and Zhang (1987). They have claimed that the nitrogen atom migration from gas phase to solid phase in plasma nitriding is achieved essentially by the penetration of active nitrogen atoms produced by collisional dissociation. Nevertheless, in a pure nitrogen atmosphere the nitrogen ions need to have high energy to obtain good nitriding effects.

This high ion energy is obtained if the pressure is low and the applied voltage is high. On the other hand, the ion energy in plasma nitriding in an atmosphere containing hydrogen, appears to have no obvious relationship to nitriding results within the energy ranges tested (Fangli, 1981).

In pure nitrogen, the dissociation of N<sub>2</sub> molecules through inelastic collision is only possible by N<sup>+</sup> ions whose energies exceed 15 eV, whereas H<sup>+</sup> ions with less mass can dissociate N<sub>2</sub> molecules with only 10eV energy (Xu and Zhang, 1987). Therefore, the role of hydrogen in nitriding is very important due to its contribution in lowering the energy required for collision dissociation to produce active nitrogen atoms. Furthermore, the strong deoxidation properties of hydrogen, which chemically remove the oxide film and activate the surface of the metal makes it an important constituent of the nitriding atmosphere. In addition, hydrogen in the nitriding atmosphere has been observed to be the main source of both the secondary electron emission and the sputtering of ferrous surfaces. For a positive nitriding capacity, a minimum level of ~10%H<sub>2</sub> has been suggested by Petijean and co-workers (1982).

Increasing the hydrogen concentration of the treatment atmosphere led to a decrease in both the nitrogen concentration profile as well as the amount of ε-iron nitride phase in the compound layer, see Figures 34 and 35. This effect seems likely to be due to the significant reduction of the amount of nitrogen ions (molecules, atoms) in the nitrogen-hydrogen plasmas due to the formation of N-H ions (molecules).

The ions N<sup>+</sup> and N<sub>2</sub><sup>+</sup> are the dominant charged species in nitrogen plasmas (Hudis, 1973). Nevertheless, in a nitrogen-hydrogen plasma the number of nitrogen ions decreases in favour of H<sup>+</sup> and N-H ions i.e., NH<sup>+</sup>, NH<sub>2</sub><sup>+</sup>, NH<sub>3</sub><sup>+</sup>, NH<sub>4</sub><sup>+</sup>, which suppresses sputtering by

$\text{N}_2^+$  (Motsumoto *et al*, 1982). Furthermore, Bougdira and co-workers (1991) have shown that the introduction of a small amount of  $\text{H}_2$  in the nitriding atmosphere decreases the sputtering of the substrate. This may explain why the sample treated in pure nitrogen developed a surface with the highest level of roughness due to the high sputtering, see Figures 38-40. It is worth mentioning that the AFM examination of the nitrided surfaces which has not been reported by previous workers, is a powerful technique to study the topography and morphology of the modified surfaces. AFM is very useful, particularly for the surfaces with miniature topographical features which other instruments such as SEM cannot reveal them.

Although the nitrogen concentration in the compound layer of the sample treated in pure nitrogen was higher than that treated in 75% $\text{N}_2$ -25% $\text{H}_2$ , the thickness of the compound layer of the latter was greater, see Figure 32. Again the higher sputtering rate in the pure nitrogen atmosphere, is believed to be responsible for the lower thickness of the compound layer formed in the pure nitrogen atmosphere. Another possibility is that the higher applied voltage (Figure 78) which is required to sustain the ion current density necessary to maintain the sample at the treatment temperature in a pure nitrogen atmosphere is responsible for the higher sputtering leading to a reduction in the compound layer thickness.

Further increases of the hydrogen concentration in the nitriding atmosphere resulted in a further decrease in the compound layer thickness, Figures 32 and 33. This may be explained by the results of an investigation carried out by Bougdira *et al* (1991). By optical spectroscopic analysis of plasmas having different nitrogen-hydrogen percentages, they found a decrease in  $\text{N}_2$  and  $\text{N}_2^+$  emission line intensities with increasing

$\text{H}_2$  content. The reduction in the  $\text{N}_2$  and  $\text{N}_2^+$  species which are vital for the compound layer formation and growth, will cause a reduction in the thickness of compound layer.

With 25% $\text{N}_2$  content of treatment gas, the thinnest compound layer consisting predominantly of  $\gamma'$  phase was formed. The small thickness of this layer may be attributed to the limited composition range of  $\gamma'$  phase, leading to a very low concentration gradient which is not enough to induce any further growth of the layer, as also pointed out by Edenhofer (1974, part 2). Nevertheless, nitriding in atmospheres with higher nitrogen concentrations, such as 50%, 75%, and even 100%, did not result in production of an  $\epsilon$  monophase layer but a dual phase ( $\epsilon+\gamma'$ ) compound layer. Low proportions of nitrogen and carbon in these layers is believed to be the main reason for the tendency for  $\gamma'$  phase formation (Lampe *et al*, 1993).

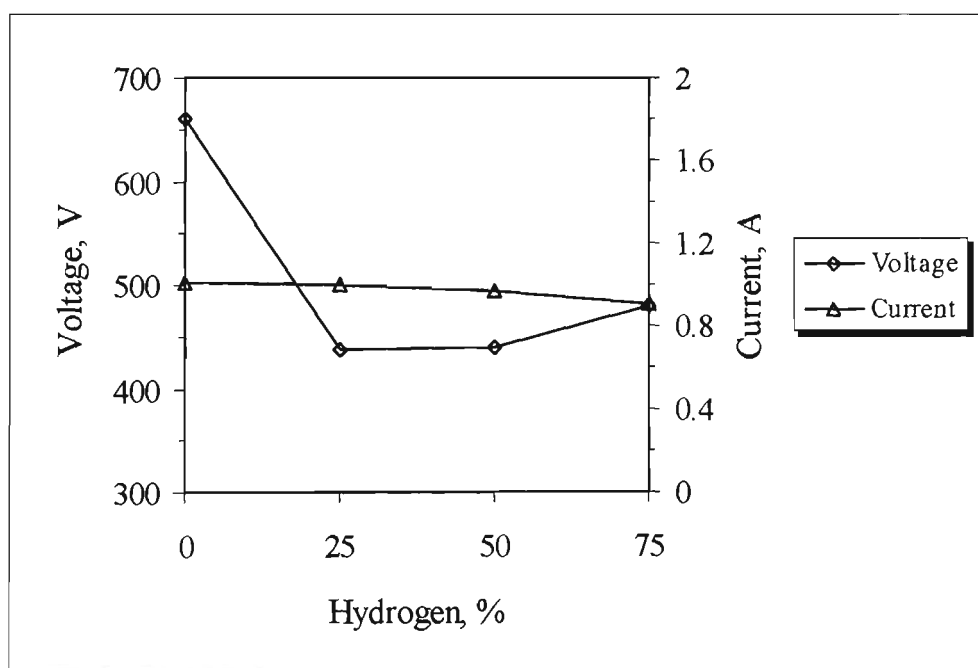


**Figure 78.** The changes in the applied voltage and current with changes in the hydrogen concentration of the treatment atmosphere. All the treatments were carried out at 450 °C for 5 hours.

The distribution of carbon determined by the GDOES analysis of the treated samples (Figure 35), particularly those treated in 75%N<sub>2</sub>-25%H<sub>2</sub> and 50%N<sub>2</sub>-50%H<sub>2</sub>, shows a higher carbon concentration at the top and bottom part of the compound layer. In the centre of the compound layer, however, there is a carbon depleted zone. It is difficult to explain the exact reason for this phenomena. However, the higher affinity of chromium for nitrogen than for carbon may be responsible. Upon diffusion of nitrogen into the specimen and formation of the compound layer, chromium carbides normally present in the compound layer tend to convert to chromium nitrides or carbo-nitrides. Consequently, (some) carbon will be liberated which can diffuse to either side of the compound layer and enrich those regions with carbon.

The case depth and hardness achieved in a pure nitrogen atmosphere are lower than those obtained from treatment in atmospheres containing nitrogen-hydrogen mixtures, see Figures 36 and 37. Although many authors have observed similar results, no convincing explanation has yet been suggested. According to Szasz *et al* (1989), in a pure nitrogen atmosphere, the sticking coefficient is much less, leading to a smaller nitriding depth and hardness (Hudis, 1973). Addition of hydrogen to the nitriding atmosphere, however, results in a reduction of stoichiometric iron nitride formation which in turn leads to an increased hardness (Grill and Itzhak, 1983). The formation of randomly distributed chromium nitride particles and the introduction of large internal stresses are responsible for high hardness (Rozendaal *et al*, 1985). This implies that the formation of a homogeneously nitrided matrix is mainly responsible for the surface hardening, rather than simply a precipitated iron nitride phase.

## 5.2 Comparative Study of DC Plasma Nitriding

### Behaviour of MAXIMA™ and En19 Steels

Comparison of the hardness profiles of the MAXIMA™ and En19 DC plasma nitrided samples, (Figures 57 and 58), reveals that at all treatment temperatures the surface hardnesses achieved by MAXIMA™ were higher than those of En19. MAXIMA™ exhibited a sharper case/core interface, while En19 showed smoother transition from the nitrided case to the core. Both the ease of nucleation of a nitride phase and the strength of the interaction between the alloying elements and nitrogen govern the form of the hardness profiles that develop during the nitriding process (Lightfoot and Jack, 1975). Strong nitrogen-alloy interaction leads to a sharp interface between the case/core region, whereas a weak interaction results in a more diffuse interface. Furthermore, increasing the concentration of a nitride-forming alloying element tends to sharpen the case/core interface. The results obtained are readily explained according to established theory of nitriding and internal oxidation. The higher Cr content of MAXIMA™ (1.9 %), compared to that of En19 (1.05 %), Table 3, is believed to be the major factor responsible for the higher hardness, sharper hardness profile and shallower case depth obtained from plasma nitriding of MAXIMA™ microalloyed steel. The results are in accordance with findings of Robino and Inal, (1983), and Inal and Kazim (1987). It can also be seen in Figure 59 that the case depth increases for both steels for increasing treatment temperature due to the increased nitrogen diffusivity.

As with age hardening alloys, where at a particular temperature and time the maximum hardness is achieved, in plasma nitriding the maximum hardness achieved by the process is governed by the precipitate size and density (number). Higher treatment temperatures

and longer times results in precipitate coarsening and further tempering of the matrix. Both steels exhibit similar behaviour and show a maximum surface hardness at 450°C, Figure 60, which is consistent with the findings of Edenhofer and Bewley (1976). This can be explained by the temperature dependence of the dispersion hardening of the (chromium) nitride precipitates within the matrix. Precipitates of a certain size and number will be the most effective in preventing the movement of dislocations and in producing the maximum strengthening and hardness. The 450°C treatment produced an optimum nitride precipitate size and density. At a low nitriding temperature of 350°C, the nitrogen uptake and precipitate density were low leading to a low hardening effect. On the other hand, as the nitriding temperature was increased (550°C) the precipitates became larger in size, leading to a reduction in precipitate density and hence lower hardness. Moreover, at the higher temperature, the chromium available in solid solution will combine with the carbides present in the matrix therefore reducing the strength of the steel. As a consequence, there is less chromium left in solid solution for nitride formation.

The En19 steel treated at different temperatures showed no significant reduction in core hardness, while MAXIMA™ samples exhibited some softening which was more noticeable for the sample treated at 550°C, as shown in Table 6. Softening of the MAXIMA™ substrate at the higher nitriding temperature may be attributed to the coarsening of carbides, recovery of dislocation structure, and the growth of ferrite grains present in the as-rolled condition.

X-ray diffraction patterns of the nitrided surfaces, shown in Figures 50 and 51, indicate that the compound layer developed on both steels was dual phase consisting of  $\gamma'$  and  $\varepsilon$  iron nitrides. In general, increasing the treatment temperature resulted in an increase in

the intensity of the iron nitride peaks and a reduction of the iron peaks. This may be explained by the increase in the compound layer thickness for an increase in the treatment temperature, see Figure 45. Since plasma nitriding is a diffusion-controlled process, the thickness of the compound layer also increases as the treatment temperature increases (Inal and Robino, 1982). The thicker compound layers prevent the incident x-rays from reaching the ferritic substrates. Moreover, the iron peaks were broadened and shifted to lower angles. The line broadening is brought about by small crystallite size, microstrains while the line shift is due to the presence of macrostrains in the ferrite lattice (Kool *et al*, 1981).

The intensity of the iron nitride peaks in En19 steel were slightly higher than those in MAXIMA™ steel. The most probable reason for this is the thicker compound layer produced on the En19, see Figure 45.

There is an important difference in the diffraction patterns of MAXIMA™ and En19 steels. The  $\alpha$ -iron and  $\epsilon$ -nitride peaks which appear at diffraction angles around 51-52° in the MAXIMA™ steel are merged, and the linewidth was increased, while for En19 steel no peak overlap was observed and two distinctive  $\alpha$  and  $\epsilon$  peaks were resolved. This phenomenon is most likely due to the higher carbon content of En19 steel, which is twice that of MAXIMA™ steel. The presence of carbon stabilises the  $\epsilon$  phase due to the very wide solubility range for both nitrogen and carbon (Slycke and Sproge, 1989). Therefore, the En19 steel, containing more carbon, develops more  $\epsilon$  phase during nitriding and consequently the  $\epsilon$  phase peak in the diffraction pattern is more intense.

Although the x-ray analysis results indicated that the compound layer developed at different nitriding temperatures consisted of  $\gamma'$  and  $\epsilon$  for both steels, the morphologies of

the layers were distinctly different, as seen in Figures 42-44. The difference in the morphologies of the compound layers formed in MAXIMA™ and En19 is likely to be due to the difference in their pre-nitriding microstructure. The acicular morphology of the compound layer in MAXIMA™ is similar in appearance to the Widmanstatten side-plate growth of ferrite into austenite in carbon steels. In the present case, iron nitride plates have extended into the ferrite matrix of the MAXIMA™ (Mahboubi *et al*, 1995). Such growth is favoured by lower transformation temperatures and is characterised by the development of parallel plates along a low energy crystallographic interface plane within a given ferrite grain. The apparent absence of this acicular morphology in En19 can be associated with the different substrate microstructure of tempered lath/plate martensite. The small plate widths present orientation changes over a scale which may be fine enough to prevent the development of an observable acicular morphology.

In both steels, some pores and cracks were evident in the compound layer adjacent to the surface region of the samples treated at higher temperature, particularly 550°C. The development of porosity in the compound layer is a well-known phenomenon which is observed in most nitriding processes. Pore formation may be explained in a similar way to that suggested by Somers and Mittemeijer (1992). Nitrogen atoms diffusing through the compound layer can coalesce to form molecular nitrogen, particularly at energetically favourable sites, such as grain boundaries.

Growth of the compound layer is controlled by diffusion of nitrogen through this layer (Edenhofer and Bewley, 1976). As with the diffusion layer thickness, the general trend is an increasing thickness with increasing treatment temperature for both steels, although the compound layer formed on En19 was thicker than that of MAXIMA™, as seen in Figure 45.

The thickness of the compound layer depends on the carbon content and other alloying elements of the steel. The higher thickness of the compound layer of En19 may be attributed to the higher carbon content (Cho and Lee, 1980) of this steel (0.4% C) which is twice that of MAXIMA™ steel (0.21% C). The higher carbon content in En19 steel stabilises the  $\epsilon$  phase so that it will form at much lower nitrogen activities. This leads to a faster growth of the compound layer due to the much wider solubility range of carbon and nitrogen in the  $\epsilon$  phase. The difference in the compound layer thicknesses is more evident for higher treatment temperatures.

Increasing the nitride forming alloying elements, such as chromium, decreases the growth rates of the compound layer and the diffusion zone due to the higher demand for nitrogen (Slycke and Sproge, 1989). The higher nitrogen content of the MAXIMA™ compound layer in comparison to that of the En19 steel was confirmed by the GDOES of the treated samples, see Figures 53 and 54. Therefore, the thinner compound layer of MAXIMA™ can also be associated with the higher chromium content of this steel (1.9% Cr) in comparison to that of En19 (1.05% Cr).

The diffusion zone in the case of En19 is reminiscent of a tempered martensite structure whereas MAXIMA™ displays a predominantly ferritic structure, consistent with the pre-nitriding microstructures.

Surface roughness of both steels increased with increasing the treatment temperature, see Figure 65. At 350°C, the surface roughness was mainly due to the surface relief caused by the volumetric expansion associated with the formation of nitrides. Iron nitrides formed on the surface and grew towards the core. The nucleation and growth of the nitrides is accompanied by surface roughening. Nevertheless, sputtering and re-

deposition of the sputtered material on the surface may have also played some minor role in the surface roughening, Figure 66. Slight differential sputtering of grain boundaries also occurred which was due to the higher free energies of the grain boundaries, making them more susceptible to sputtering.

Surface roughening at higher treatment temperatures was due to a similar expansion effect as well as preferential sputtering combined with the re-deposition of iron nitrides on the surface, Figure 67. More importantly, increasing the treatment temperature involves an increase in the applied voltage (Figure 79) which in turn increases the kinetic energy of the incident ion (or atom). Therefore the sputtering yield ( $S$ ) which is dependent upon the kinetic energy of the colliding ions, increases with increasing temperature, leading to an increase in the surface roughness. Thus, the samples treated at 550°C show the highest value of surface roughness, see Figure 68.

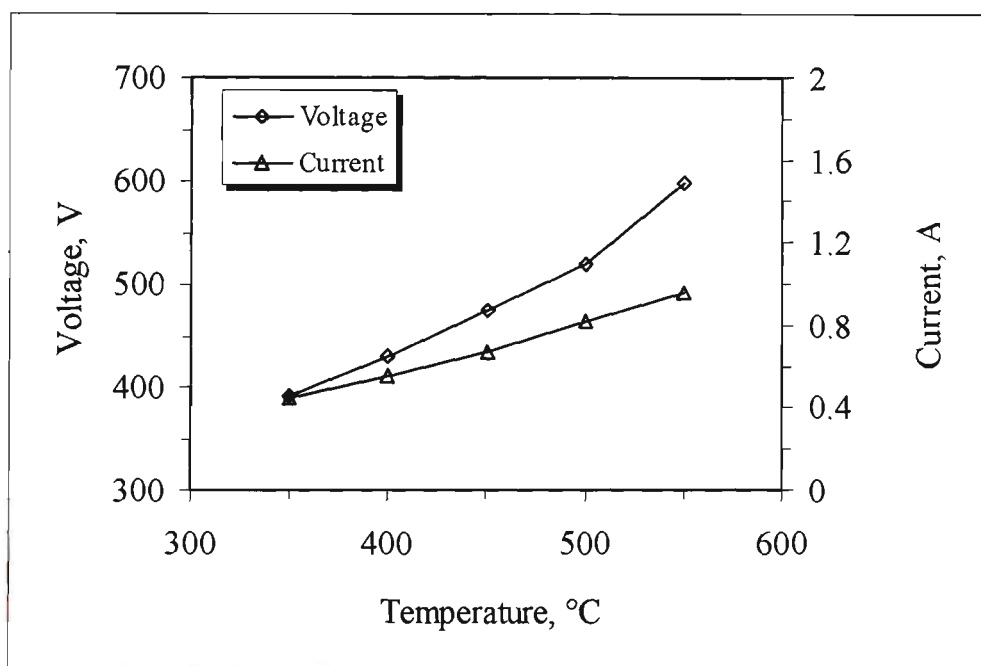


**Figure 79.** The voltage and current applied at different treatment temperatures for DC plasma nitriding.

Comparison of the two steels revealed that the surface roughness of MAXIMA™ microalloyed samples was greater than those of the En19 samples, see Figure 65. This can be explained by the pre-nitriding microstructure of these steels. The grain size and carbide distribution in the steel affect the surface roughness obtained after nitriding. The initial microstructure of MAXIMA™ appeared to be proeutectoid ferrite plus bainite, whereas the microstructure of En19 was tempered lath/plate martensite. Formation of nitrides and/or carbonitrides at the grain boundaries will induce some stresses in the grains due to their volume expansion at the grain boundaries. This in turn can displace individual grains in the surface layer leading to deformation or cracking of the compound layer (Theelning, 1975). The displacement of the grains at the surface is clearly shown in Figure 67-a. Additionally, the preferential sputtering of the large ferrite grain boundaries in MAXIMA™ in comparison to the fine tempered martensitic structure of En19 plays some role in the increased surface roughening of this steel.

## 5.3 Plasma Immersion Ion Implantation (PI<sup>3</sup>) and RF Plasma Nitriding of MAXIMA™

For both processes, the appearance of the samples treated at low temperature were totally different from those treated at higher temperature, see Figures 73-75. Treatment at the low temperature of 350°C in a 75%N<sub>2</sub>-25%H<sub>2</sub> atmosphere, resulted in surface morphologies typical of surface relief, while higher treatment temperatures developed surface morphologies typical of sputter etching. Grain boundaries, not seen in the original polished surfaces, were evident after treatment. The reflectivity of the surface progressively decreased with increasing treatment temperature. Nevertheless, at all treatment temperatures, RF plasma nitriding resulted in smoother surfaces. It should be noted that the portion of specimens masked from the plasma in both treatments, exhibited no increase in surface roughness or change in appearance, indicating that the phenomenon (surface roughening) was not due to the time at temperature.

One of the unique features of PI<sup>3</sup> and RF plasma nitriding is the absence of a continuous compound layer on the surface of the treated samples. Standard x-ray diffraction analysis of the samples was not able to identify any iron nitride peaks. Glancing angle x-ray diffraction (GAXRD) analysis, however, confirmed the formation of the γ' peaks only on the RF plasma nitrided samples treated at 350°C, see Figure 52. SEM examination of the cross section of the samples also confirmed the formation of iron nitride at 350°C, see Figure 48-a. It is worth mentioning that although the SEM of the PI<sup>3</sup> samples revealed the formation of iron nitride on the surface of the sample treated at 350°C (Figure 47-a), the amount (number) of these iron nitride plates was not enough to be detected by GAXRD, see Figure 52-a.

This effect may partly be explained by nucleation and growth theory. For the formation of a phase, clusters of that phase should be formed. Once a cluster is established and becomes stable, a nucleus is formed and gradually grows. In RF plasma nitriding, which is a thermochemically driven diffusion process, cluster formation on the surface happens more easily and in more sites than in the PI<sup>3</sup> process, in which the formation of clusters is interrupted due to ion bombardment (Mahboubi *et al*, 1995). Moreover, in PI<sup>3</sup> treatment, due to the implantation of nitrogen about 100 nm beneath the surface (Collins *et al*, 1995), the process of surface iron nitride formation is hindered. However, during the off period of the high voltage, since the sample is immersed in the RF plasma, there is some thermochemically driven diffusion of nitrogen from the surface of the sample, leading to formation of iron nitrides on preferential orientations in which the free energy for nucleation is less.

Although at low treatment temperatures, the surface roughness for both processes is mainly due to the surface relief phenomenon, sputtering also plays some role in roughening the surface of the treated samples, particularly in the PI<sup>3</sup> process. Due to the high energy ion bombardment of the sample in PI<sup>3</sup> treatment, there is some sputtering in addition to the ion implantation. In RF plasma nitriding, however, since no bias voltage is involved, other than the self-bias potential which is ~ 40 V, there is not much ion bombardment of the sample, hence less sputtering. Consequently, the surface roughness of the RF plasma nitrided sample was generally lower than that of PI<sup>3</sup> treated samples, see Figure 72.

At higher treatment temperatures (400°C and higher), no surface iron nitride is formed on the samples treated by either processes and the surface roughness value is much lower, see Figures 72, 76 and 77. This effect can be attributed to the increased treatment

temperature which increases the diffusion rate preventing the nitrogen build up necessary for iron nitride phase formation on the surface.

The surface roughening mechanism is also changed for the treatment at higher temperatures and is mainly due to the sputtering. Increasing the treatment temperature demands an increase in the frequency of pulse repetition of the high voltage in PI<sup>3</sup> treatment, leading to an increase in the sputtering yield. In RF plasma nitriding, however, since the sample is heated by a resistively heated stage and not ion bombardment, the RF frequency and power does not change. Therefore the increase in the surface roughness is believed to be due to the increase in the sample temperature, which in turn increases the vibrational motion of the sample atoms, making them more susceptible for sputtering.

The lack of compound layer on the surface of the specimens in the present experiments can be attributed to the low nitrogen activity of the treatment atmospheres. Since both processes are carried out at a very low pressure, typically  $1-2 \times 10^{-3}$  mbar, the nitrogen activity, which is directly proportional to the partial pressure of the nitrogen in the treatment atmosphere (Dressler; Sudarshan (ed.), 1989), is not high enough to produce a continuous iron nitrides or a compound layer. Moreover, for the low processing pressure employed in both treatments, the mean free path of the ions and atoms is in the order of several centimetres, hence there will be no redeposition of the sputtered material on the surface (this will be discussed in more detail in the next section).

The question of why the treatments are not carried out at higher pressures must then be addressed. In the PI<sup>3</sup> process, the low pressure is necessary to prevent the ions losing energy by collisions with neutral species in the chamber atmosphere. Increasing the

process pressure also results in localising the plasma around the RF antenna, preventing the homogeneous immersion of the sample in the RF generated plasma.

Existence of a compound layer can be regarded as an advantage or a disadvantage according to where the treated part is intended to be used. Due to its high corrosion resistance, the compound layer protects the part in a corrosive atmosphere. On the other hand, since it is brittle, it may spall in service, especially where the part undergoes high dynamic stresses. Furthermore, it has been reported that this brittle layer can lead to accelerated wear as a result of fragmentation during high load wear testing, causing detrimental wear of the contact tip which in turn gouged and abrasively wore the substrate at a high rate (Samandi, 1992).

PI<sup>3</sup> treatment resulted in the formation of a hardened case with higher hardness and thicker case at all temperatures. These differences can be attributed to the differences in the physics of the processes. In RF plasma nitriding the sample is immersed in an RF generated plasma and the excited neutrals and ions are diffused into the surface of the sample. In PI<sup>3</sup>, however, the ions are accelerated towards the surface of the sample by the application of high voltage (-45kV) pulses of 100μsec duration, and are implanted into the surface of the samples. Furthermore, in the periods while the high voltage is off, excited neutrals and ions are thermochemically driven into the surface. This combination of implantation and thermochemically driven diffusion of nitrogen is believed to be the reason for the production of cases with higher hardness and thicker case depth.

The maximum surface hardness was developed on samples treated at 400°C for both treatments. The temperature dependence of the dispersion hardening of the (chromium) nitride precipitates within the matrix may explain this effect (Edenhofer and Bewley,

1976). Precipitates of a certain size and number, which are coherent or semi-coherent with the matrix, will be the most effective in obstructing the movement of dislocations and in producing the maximum strengthening and hardness. At higher nitriding temperature such as 500 and 550°C, the nitride precipitates are larger in size and become incoherent along with a lower precipitate density and therefore are less effective in hardening.

Samples treated at 550°C showed the smallest increase in hardness but this was maintained at all loads, see Figure 61, indicating deeper diffusion of nitrogen into the material, producing a thicker case. Although the hardening effect at 550°C was less than that for lower temperatures, the results still showed a significant increase in surface hardness over that of the substrate material, taking into account the softening of the base material at 550°C.

## 5.4 GENERAL DISCUSSION:

### The Influence of the Mode of Plasma Generation on the Plasma Nitriding Behaviour of MAXIMA™

#### 5.4.1 Introduction

Over the past 35 years a number of theories have been proposed to model what occurs at the plasma-surface interface and in the bulk material during plasma nitriding. However, it is difficult to develop a unique picture of the mechanisms involved due to the complexity of the process and since the experimental results obtained under different process conditions employing different materials. Consequently, there is no universally accepted model which decisively explains the mass transfer of nitrogen to the workpiece surface. Although the layer formation mechanisms are still not well-understood, it has been often claimed that the following four surface reactions are involved: (i) sputtering, (ii) ion implantation, (iii) absorption of gas, (iv) condensation/deposition (Rie, 1990).

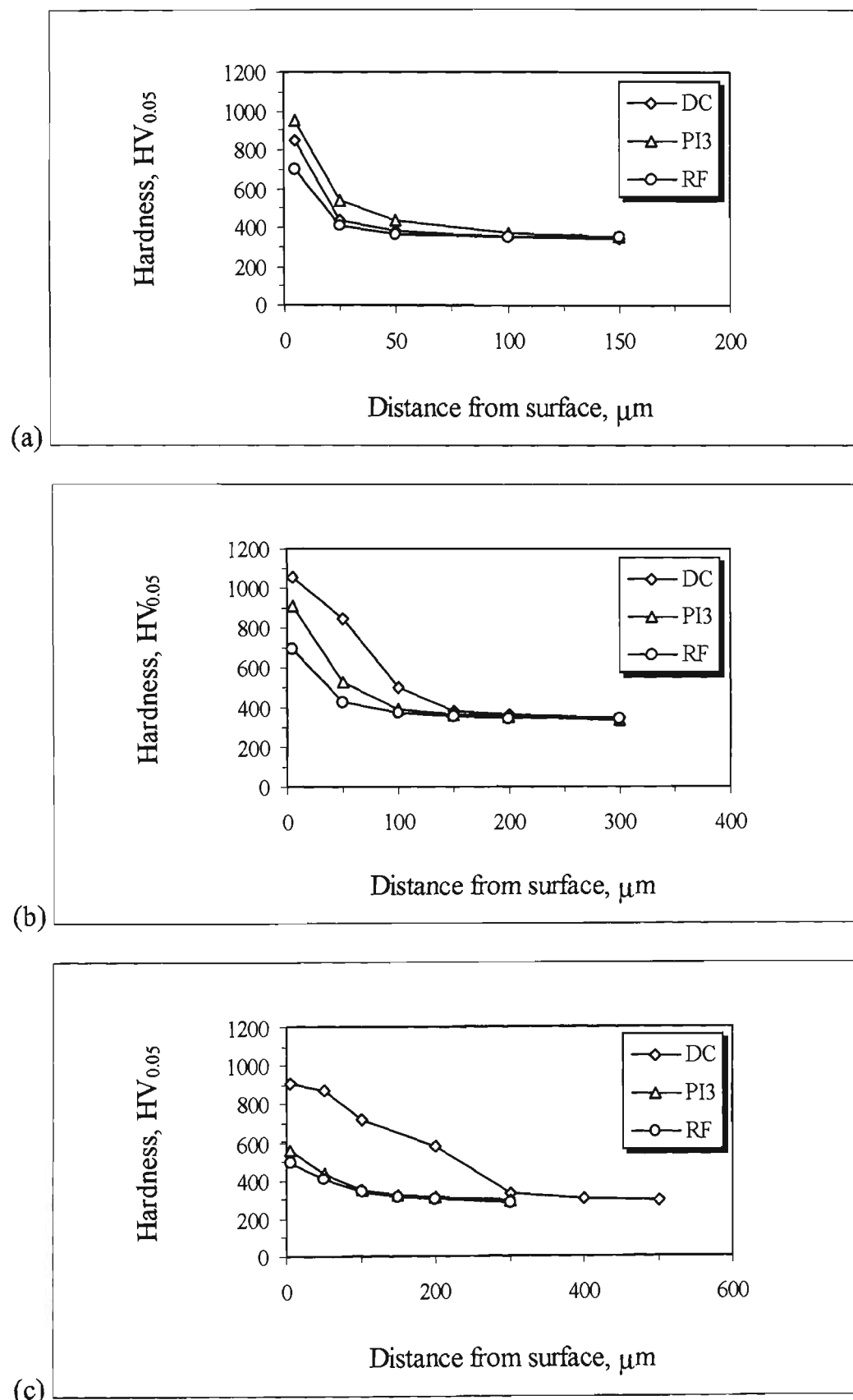
The purpose in presenting this section is to discuss and compare the effects of different modes of plasma generation on the production of nitrided surface layers. To accomplish this goal, the results obtained from the treatments of MAXIMA™ by different processes, i.e. DC plasma nitriding, RF plasma nitriding and PI<sup>3</sup> treatment, in a 75%N<sub>2</sub>-25%H<sub>2</sub> atmosphere at temperatures of 350, 450 and 550°C, have been used and re-presented in figures and graphs within the following discussion.

### 5.4.2 Discussion

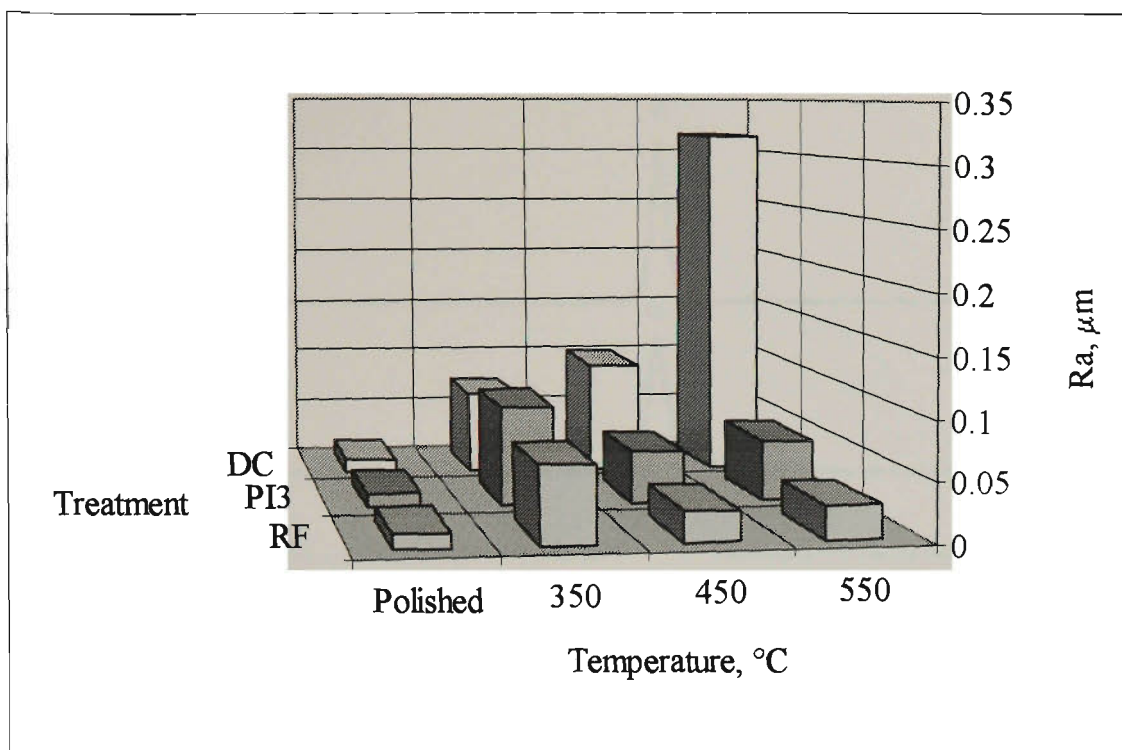
The picture emerging from the results points to a fundamentally different nitriding response of the material to the three processes. The differences are manifested in the form of higher surface hardness and roughness for DC plasma nitrided samples at 450 and 550°C. At the lowest treatment temperature (350°C) the PI<sup>3</sup> treatment produced the hardest and roughest surface layer, see Figures 80 and 81. The formation of a compound layer on the DC plasma nitrided samples (Figures 82 and 83) which was not produced by the other two processes, was the other major difference. These differences can be attributed to the different operating conditions of the processes, notably the pressure and ion energy which is related to the applied potential between the anode and the cathode (sample). Some of the differences may be partly explained using the model proposed by Kölbel (1965) and later supported by Keller (1971) and Edenhofer (1974, part 1). This model is based on sputtering by ion bombardment and re-deposition (condensation).

The incident ions need to possess an energy exceeding a threshold value for sputtering to occur, which for iron and its alloying elements is between 20 and 30 eV (Keller, 1971). Below this threshold, the ion energy is not high enough to detach the atoms from the surface. Above the threshold, the sputtering rate increases to a maximum as the ion energy increases. At very high energies, the sputtering rate decreases due to ion penetration of the surface as ion implantation becomes dominant.

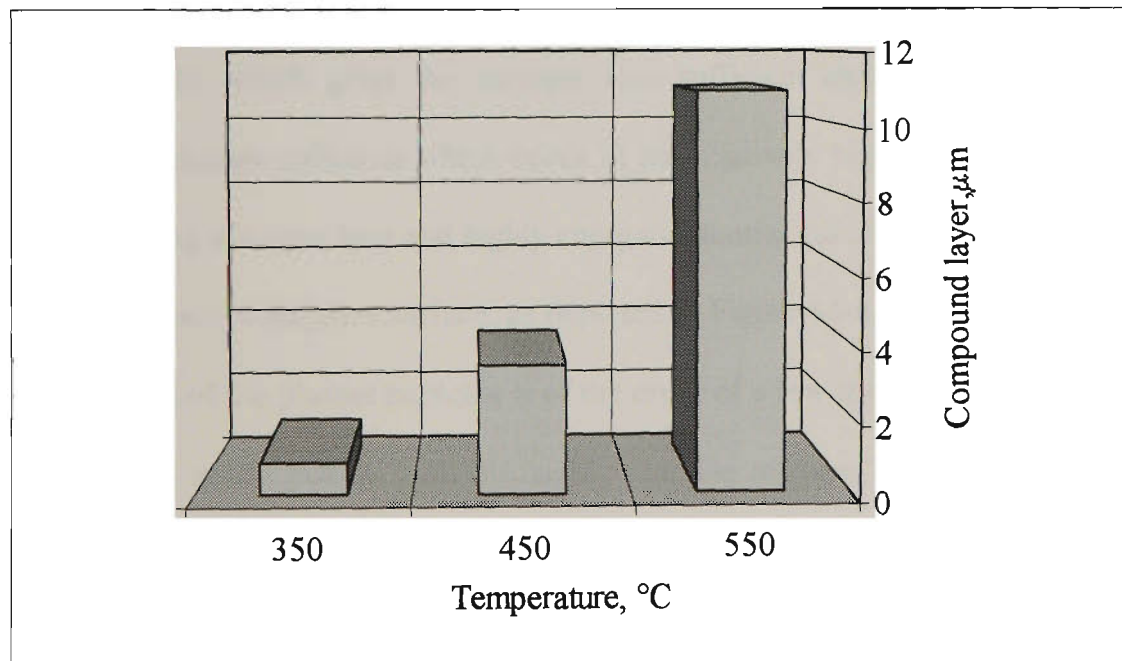
Although Edenhofer did not elaborate on the role of pressure and ion energy, it is implicit in the model that any factor which affects sputtering or collisions in the gas phase would inevitably influence the growth of the compound layer.



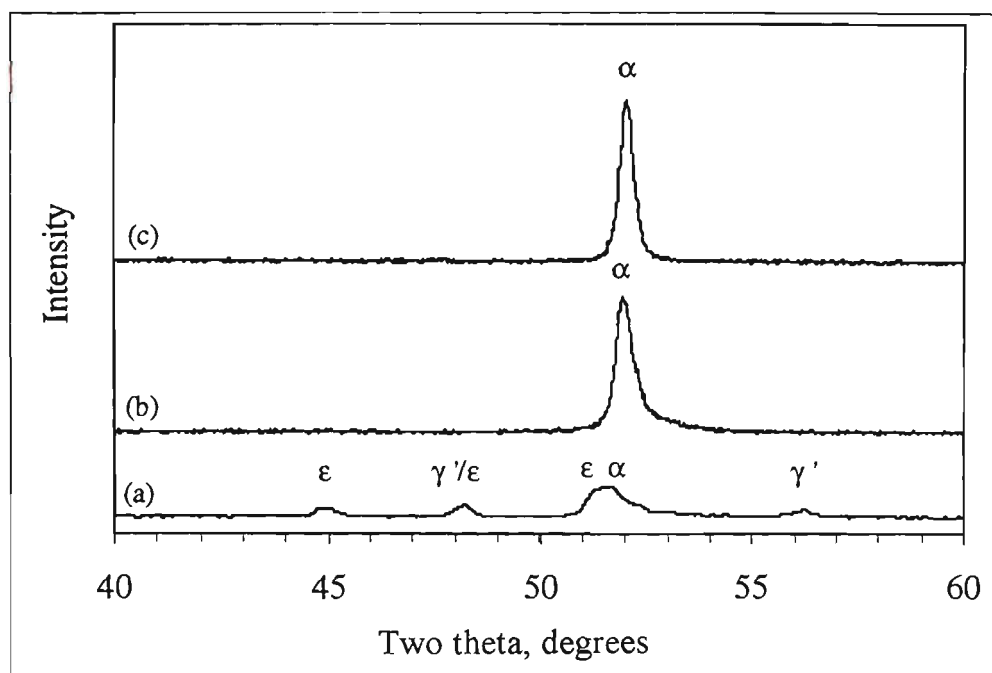
**Figure 80.** Hardness profiles of the MAXIMA™ samples treated with different processes at (a) 350, (b) 450 and (c) 550 °C for 5 hours.



**Figure 81.** Comparison of the surface roughness,  $R_a$ , values obtained from the samples treated by different processes.

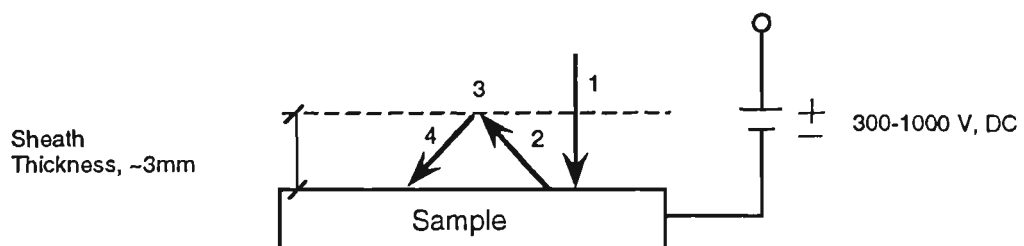


**Figure 82.** Thickness of the compound layer formed on the surface of the DC plasma nitrided samples.



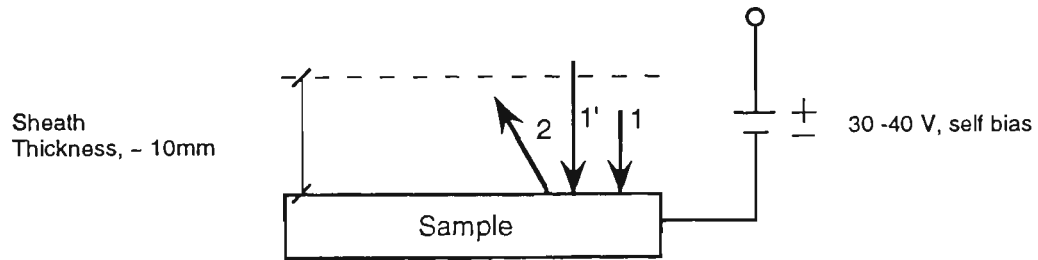
**Figure 83.** X- ray diffraction patterns of the samples nitrided at 450 °C by (a) DC plasma, (b) PI<sup>3</sup>, and (c) RF plasma.

In DC plasma nitriding, there is a few hundred volts potential difference between the cathode and anode, which gives the incident ions sufficient energies for sputtering, despite charge-exchange collisions which occur at the relatively high operating pressure (4 mbar). Incoming nitrogen ions and highly energetic neutral particles sputter elemental iron from the cathode workpiece surface, as depicted in Figure 84-a. At these pressures, the mean free path of the plasma particles is of the order of a few millimetres. Therefore, the sputtered iron atoms collide with the highly reactive nitrogen atoms in the region adjacent to the surface (the cathode fall region) and form FeN, some of which may redeposit on the workpiece surface, giving a surface morphology typical of CVD coatings, as shown in Figures 86-a and 87-a.

**DC plasma nitriding**

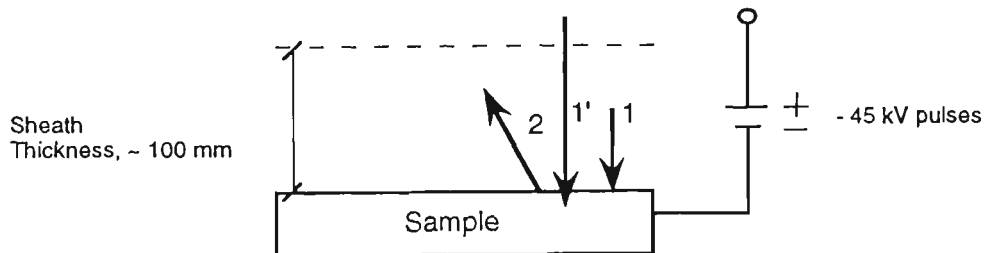
Mean free path for collision of atoms, ~ few millimeters

- 1- Bombardment of the sample by energetic ions and neutral particles
- 2- Sputtering of Fe atoms
- 3- Collision of sputtered Fe atoms with nitrogen in sheath area and formation of FeN
- 4- Re-deposition of FeN and its subsequent decomposition to lower nitrides

**RF plasma nitriding**

Mean free path for collision of atoms, ~ few centimeters

- 1- Adsorption of excited neutral particles
- 1'- Ion bombardment due to self bias
- 2- Slight sputtering due to self bias. Note that the mean free path is too large to cause any collision leading to re-deposition

**PI3**

Mean free path for collision of atoms, ~ few centimeters

- 1- Adsorption of nitrogen in high voltage - off period
- 1'- High energy ion beam implantation in high voltage - on period
- 2- Sputtering. Note that the sputtering is not as severe as in DC plasma nitriding since most of the ions are implanted beneath the surface and do not contribute in the sputtering process. Again no collision, hence, no redeposition due to large mean free path

**Figure 84.** Proposed models for nitrogen mass transfer in different plasma nitriding processes.

Increasing the treatment temperature in DC plasma nitriding involves an increase in the applied voltage and thus incident ion energy. Therefore the sputtering yield increases, leading to an increase in the rate of sputtering and redeposition processes. Hence the surface roughness increases, Figure 81. Since FeN is not a thermally stable compound, it decomposes to form iron nitrides with a lower nitrogen content such as  $\varepsilon\text{-Fe}_2\text{-}_3\text{N}$  and  $\gamma'\text{-Fe}_4\text{N}$ , releasing nitrogen atoms which are then free to diffuse into the base metal to form a layer of iron nitrides called the compound or white layer, shown in Figures 88-a, 89-a, and 90-a. This surface layer acts as a reservoir of nitrogen throughout the process from which free nitrogen diffuses into the underlying steel. When the solubility limit is reached, in the presence of alloying elements, nitrides are formed and precipitated in a very dispersed form creating the diffusion zone.

Although no compound layer was formed on the surface of the samples treated by PI<sup>3</sup> and RF plasma nitriding, the surface of the samples was hardened. This cannot be explained by the model suggested by Kölbel and Edenhofer. In RF plasma nitriding, the model proposed by Tibbets (1974, part 1) may be more appropriate.

According to this model, mass transfer of nitrogen occurs mainly by the adsorption of excited neutral atoms and not of ions on the metal surface, see Figure 84-b. Excited neutrals can be generated by sputtering and/or electron collisions in the plasma. In our RF plasma nitriding process, the sample is immersed in an RF generated plasma from which excited neutrals can be absorbed onto the sample surface and then diffuse into the sample.

The mechanism of surface hardening in the PI<sup>3</sup> process, however, is different from RF plasma nitriding and cannot be explained by Tibbets' neutral adsorption model alone.

Lakhtin (1970), Hudis (1973) and Jones *et al* (1975) have claimed that the mass transfer occurs mainly via ionised atoms and molecules. They have claimed that the ionised environment alone was not sufficient and a potential difference across the electrodes was essential to nitride the workpiece.

In the PI<sup>3</sup> process, the combination of nitrogen ion implantation and thermochemically driven absorption of excited neutrals and nitrogen atoms leads to the formation of cases with higher hardness and thicker case at low treatment temperatures. In PI<sup>3</sup>, the ions are accelerated towards the substrate by 45 kV pulses, see Figure 84-c. At this high energy, the ions are implanted beneath the surface although a small number of them, according to their incident energy and angle, induce sputtering of atoms from the surface of the sample. This results in sputter etching of the sample surface, see Figures 86-b and 87-b.

The operating condition for RF plasma nitriding is similar to PI<sup>3</sup> except that there is no high voltage involved and the only ion bombardment is due to the RF self-bias of the plasma relative to the workpiece. The self-bias has been measured to be of the order of 40 volts, just above the sputtering threshold for nitrogen on iron (Mahboubi *et al*, 1995). RF nitriding produced the least hardened and the smoothest surface layer, see Figures 80, 86-c and 87-c. The surface finish is almost unchanged except for some segments of the grain boundaries which were lightly sputtered.

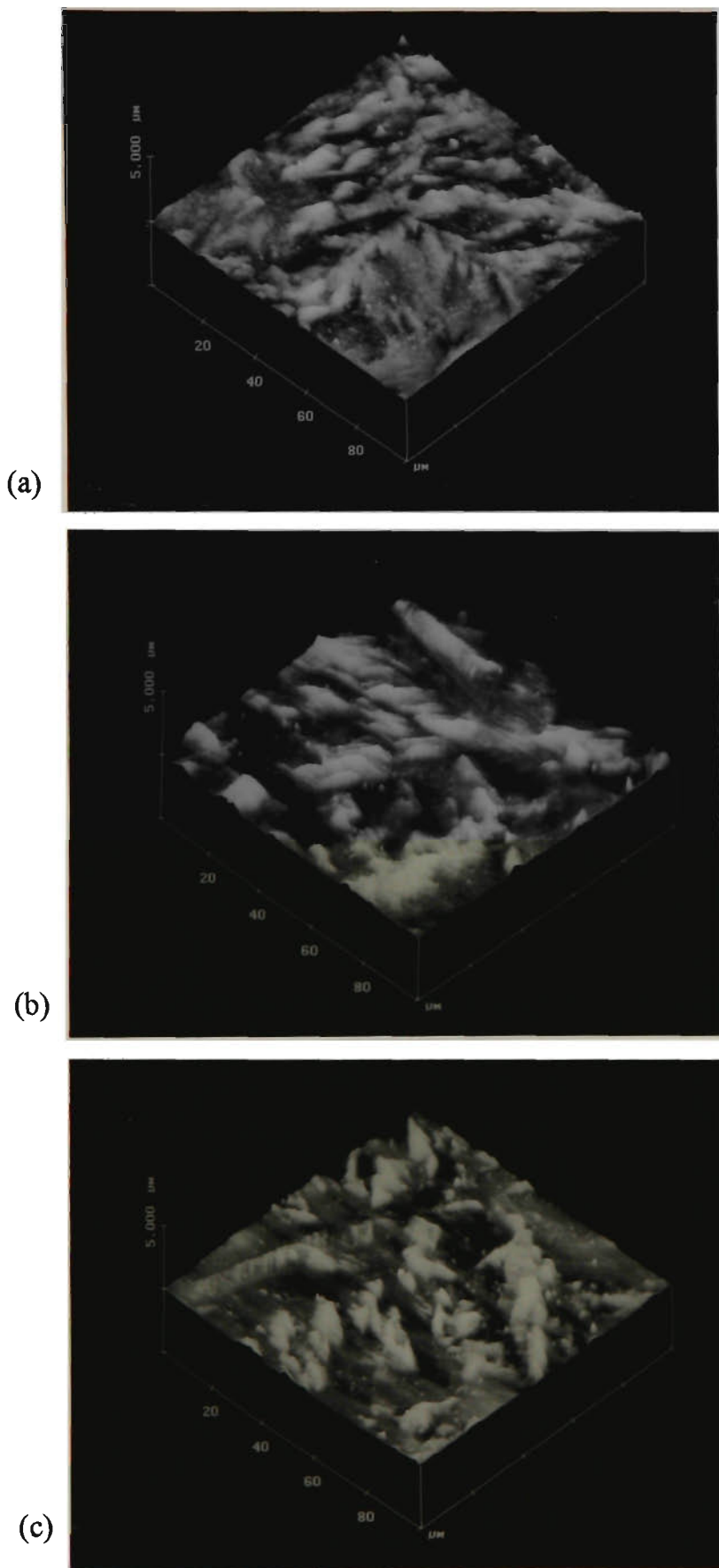


**Figure 85.** AFM images showing the surface topography of the samples treated by (a) DC plasma nitriding, (b) PI<sup>3</sup> and (c) RF plasma nitriding at 350 °C.

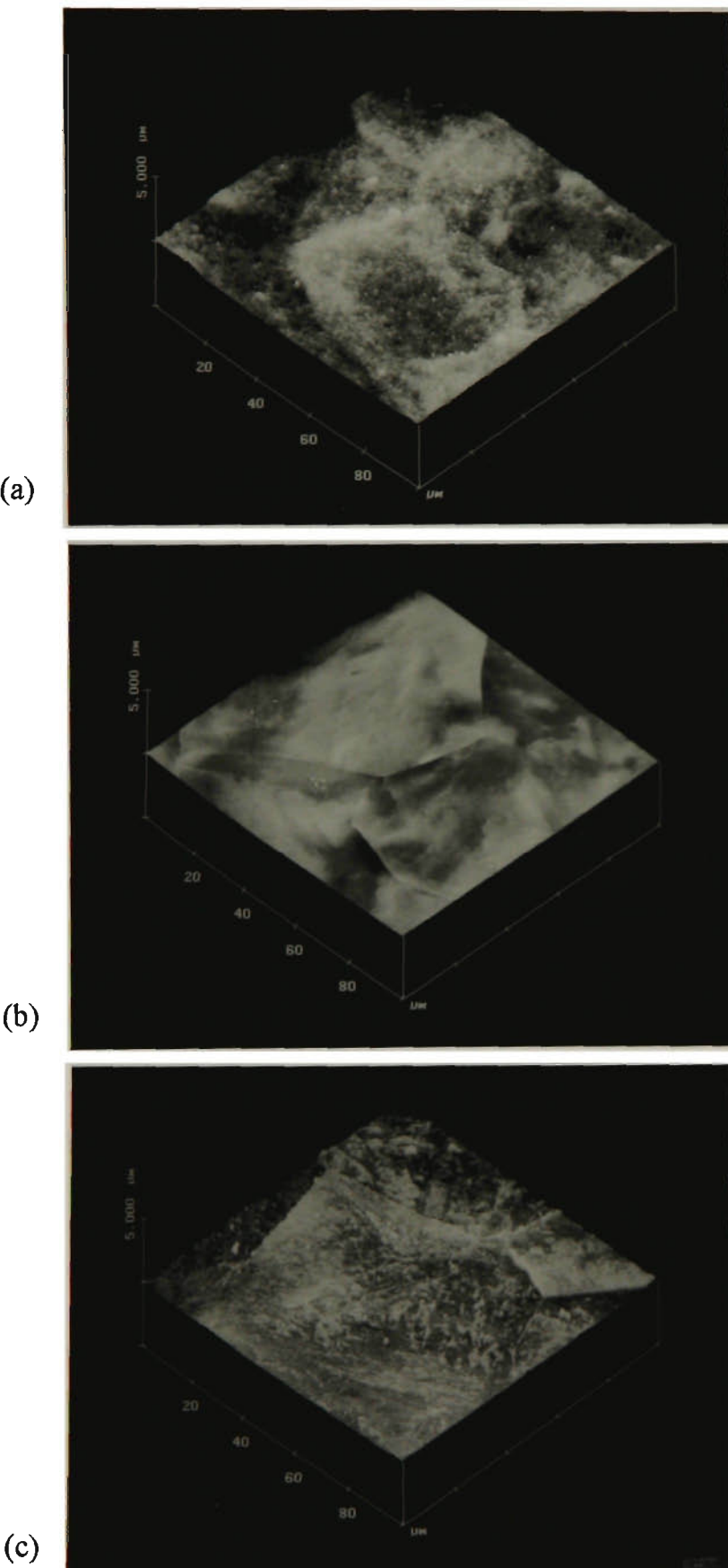


**Figure 86.** AFM images showing the surface topography of the samples treated by (a) DC plasma nitriding, (b) PI<sup>3</sup> and (c) RF plasma nitriding at 450 °C.

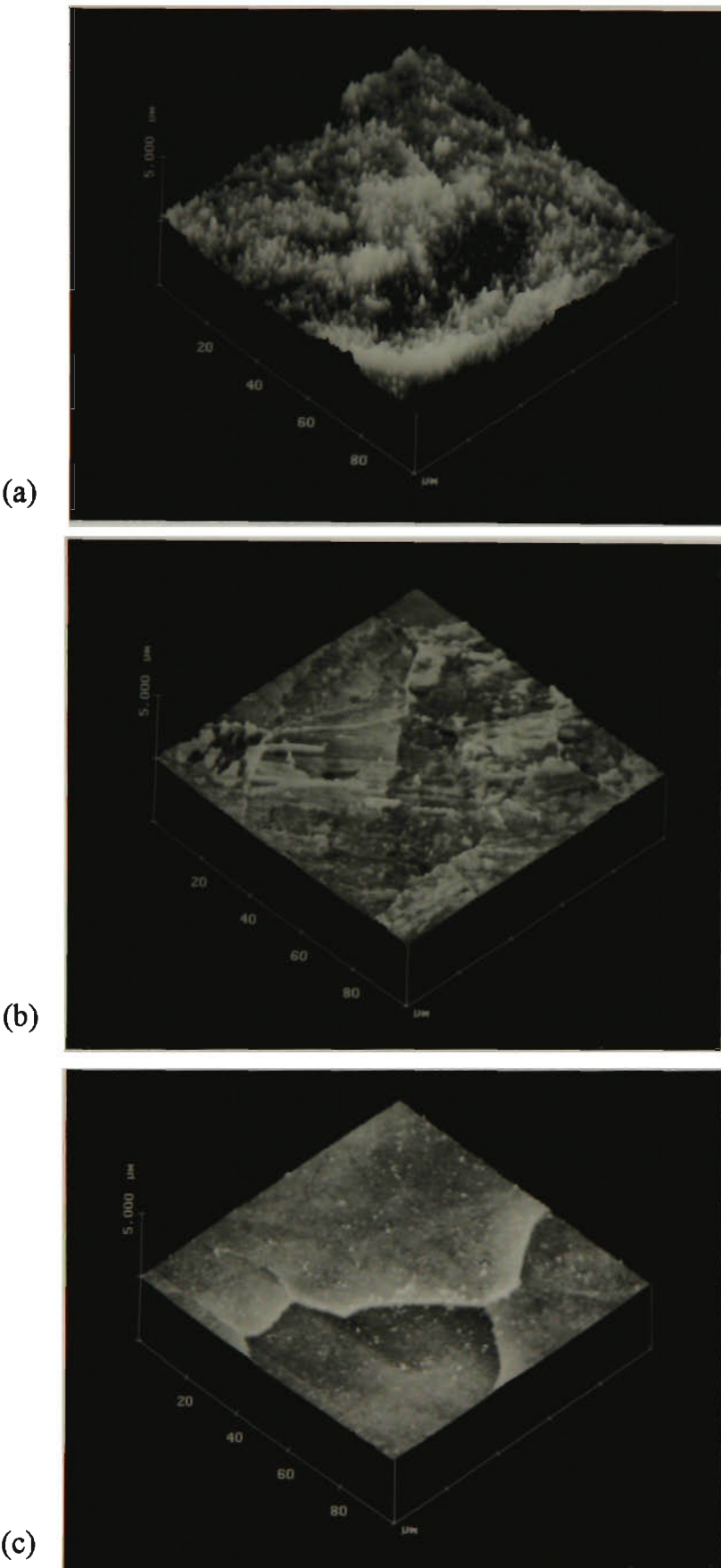


**Figure 87.** AFM images showing the surface topography of the samples treated by (a) DC plasma nitriding, (b) PI<sup>3</sup> and (c) RF plasma nitriding at 550 °C.

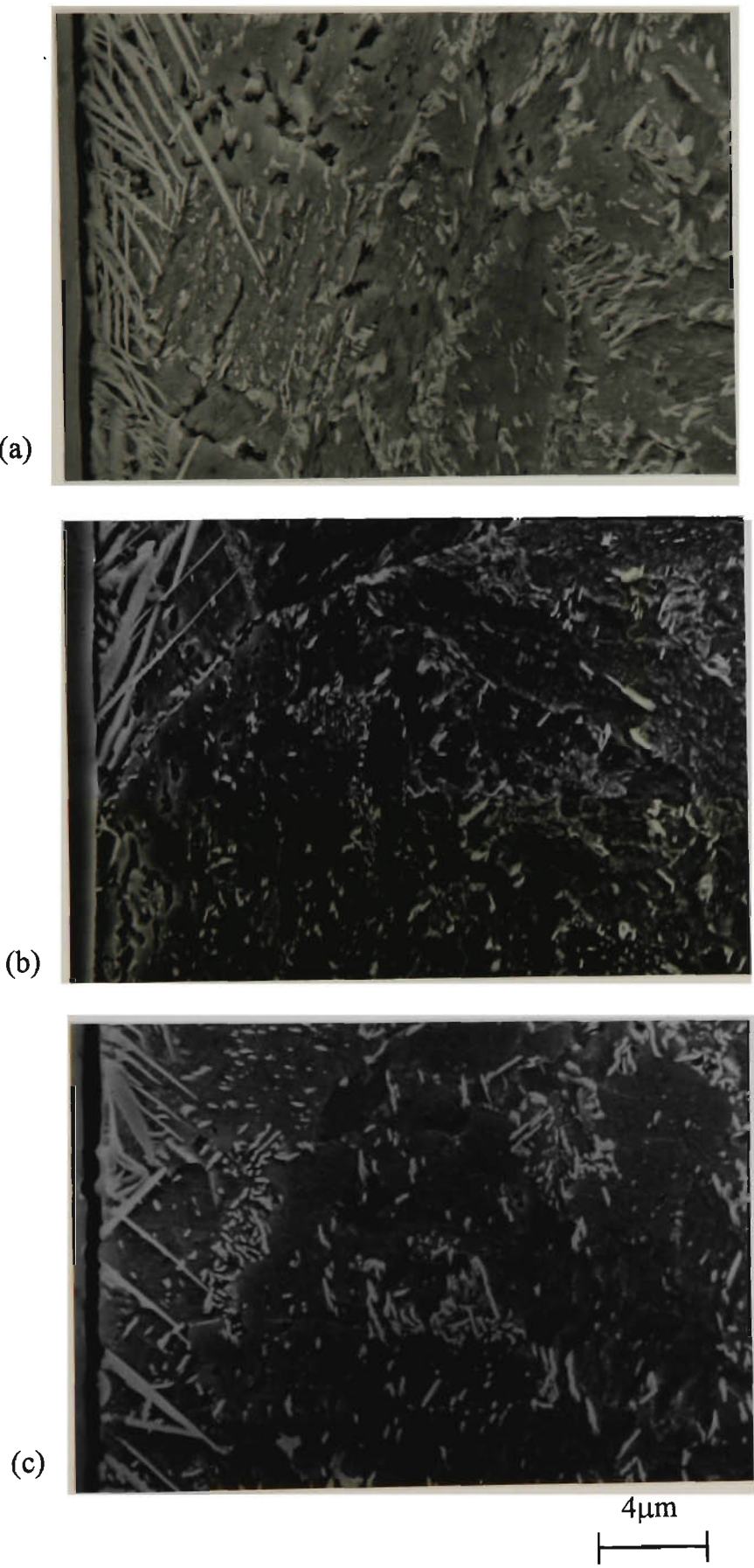


**Figure 88.** SEM micrographs of samples (a) DC plasma nitrided (b) PI<sup>3</sup>, and (c) RF plasma nitrided at 350 °C.

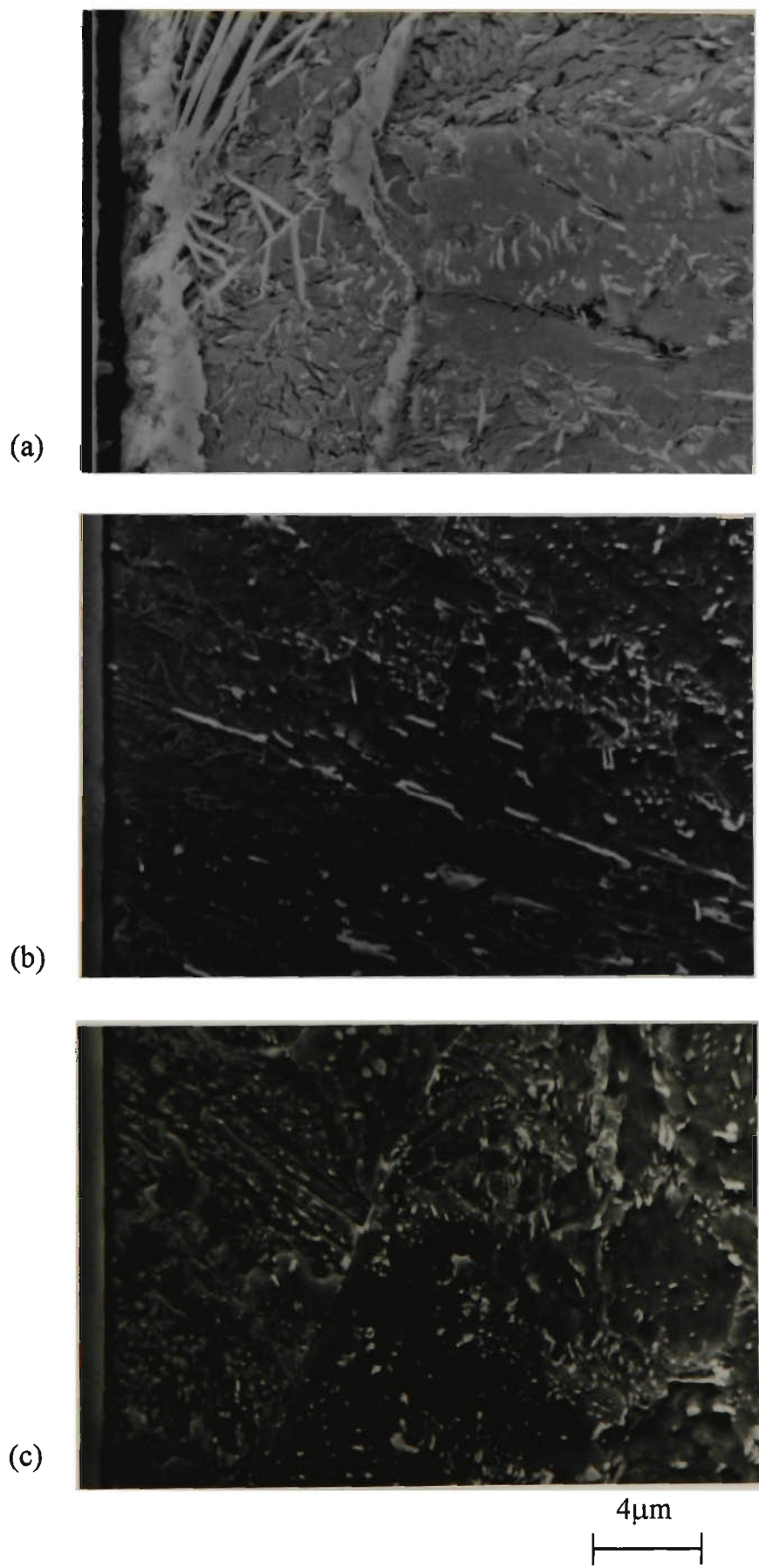


**Figure 89.** SEM micrographs of samples (a) DC plasma nitrided (b) PI<sup>3</sup>, and (c) RF plasma nitrided at 450 °C.

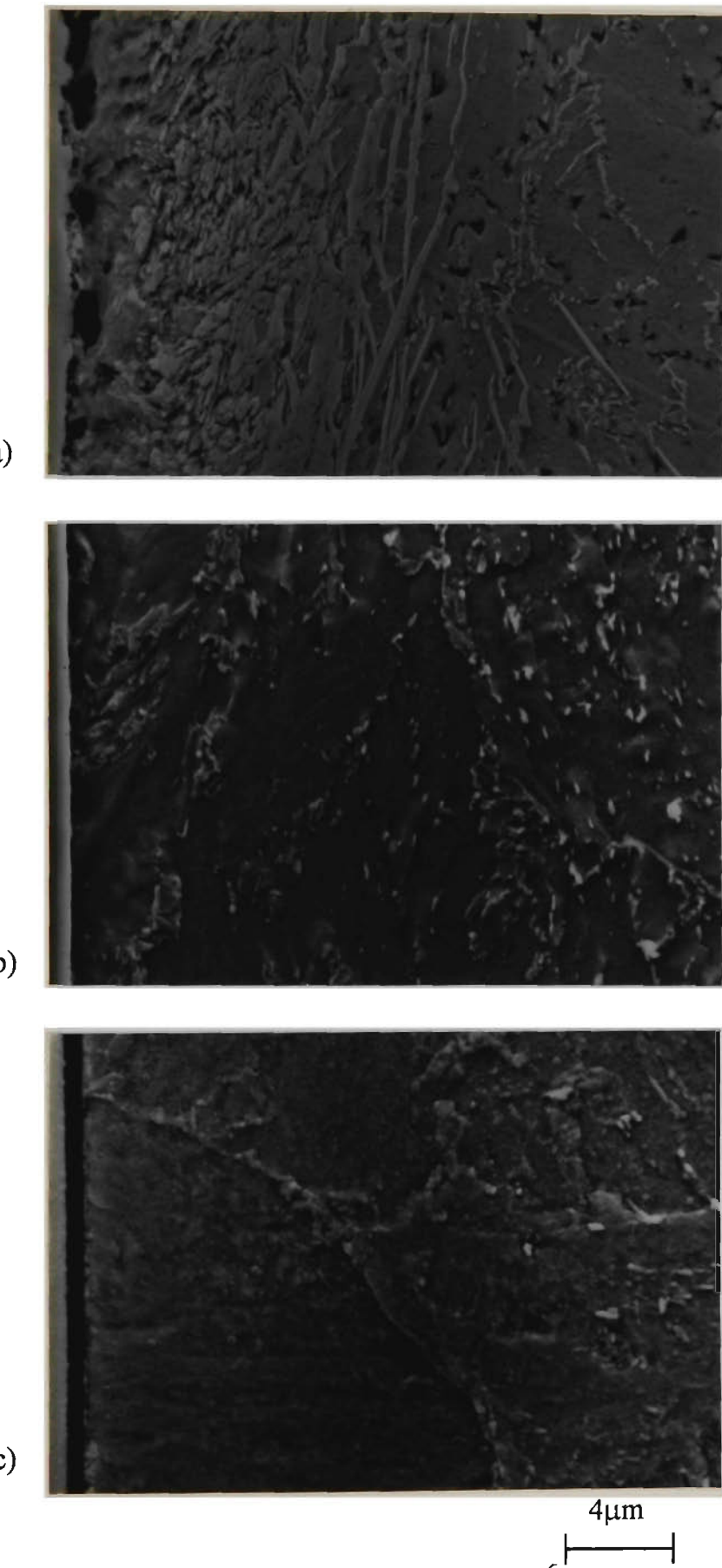


**Figure 90.** SEM micrographs of samples (a) DC plasma nitrided (b) PI<sup>3</sup>, and (c) RF plasma nitrided at 550 °C.

In RF plasma nitriding and PI<sup>3</sup>, the operating pressure is about  $10^{-3}$  mbar, three orders of magnitude lower than that of DC plasma nitriding, so the mean free path of the plasma particles is several tens of centimetres. Due to this large mean free path, the sputtered atoms do not collide with any nitrogen in the vicinity of the sample surface and contrary to DC plasma nitriding, there will not be any significant re-deposition of iron nitrides, see Figure 84-b. Thus no compound layer is formed.

The major difference in the appearance of the DC plasma nitrided samples and those treated by RF plasma nitriding and PI<sup>3</sup> processes is the formation of a dark grey ring parallel to the edge of the sample. The degree of the grey tone increases with increasing treatment temperature. The differences stem from basic differences in the operating conditions of the processes.

Ring formation on the surface of the DC plasma nitrided sample is due to the non-uniform sputtering and redeposition which occurs during the process. Removal of sample material by sputtering predominates at edges and corners while on flat faces, such as the centre of the sample, vapour deposition prevails (Wells and Strydom, 1986 and 1988). This may be explained by the large gradient in the electric field and current density around the edges and sharp corners (Lanagan, 1988). The cathodic sheath formed around the sample is of the order of a few millimetres, (~1-3 mm), depending on the chamber pressure and the applied voltage. The current density is not uniform across the sample and tends to rise towards the edge and then fall. The current density dictates the density of the reactive species and this in turn governs the sputtering rate. Hence, more sputtering occurs around sharp edges and corners of the sample, resulting in the formation of the dark grey ring parallel to the edge of the sample.

The uniform appearance of the samples treated by RF plasma nitriding and PI<sup>3</sup> processes and the lack of any ring around the edge of the treated samples, can be explained by the large cathodic sheath length involved in these processes. The large cathodic sheaths in RF plasma nitriding (~10mm) and PI<sup>3</sup> (~100mm) (Collins and Tendys, 1994) are less sensitive to the corners and edges of the sample leading to an almost uniform current density and in turn uniform sputtering rate across the sample. Moreover, unlike DC plasma nitriding in which the sample is a part of plasma generation system (cathode), in PI<sup>3</sup> and RF plasma nitriding, the sample is separated from the plasma generation and is immersed in a uniform and diffuse plasma.

At 350°C, maximum hardening was observed on the samples treated by the PI<sup>3</sup> process. This may be attributed to the high nitrogen ion implantation involved in the process. At this temperature, the low diffusion rate of nitrogen allows a high nitrogen concentration to build-up at the surface, leading to the formation of a hard case, which produces a relatively large amount of surface relief, see Figure 85-b. As the temperature increases so does the diffusion rate of nitrogen. Since the process is carried out at low pressure, hence low nitrogen activity (Dressler; Sudarshan (ed.), 1989), the increase in the diffusion rate of nitrogen cannot be matched by the nitrogen source. This results in a decrease in the surface concentration of nitrogen and a subsequent lower increase in hardness. For 450 and 550°C treatment temperatures, the DC plasma nitrided samples showed higher hardness with the difference being more pronounced for 550°C, see Figure 80. At these higher temperatures, the increase in diffusion rate of nitrogen is supported by the compound layer formed on the surface in this process which serves as a constant reservoir of nitrogen.

# **6. CHAPTER SIX:**

## **CONCLUSIONS**

---

### **6.1 Effect of Hydrogen Content on DC Plasma Nitriding of MAXIMA™**

An investigation which was carried out to determine the optimum level of hydrogen for DC plasma nitriding of hot rolled Cr-bearing microalloyed steel, MAXIMA™, yielded the following conclusions:

- DC plasma nitriding of MAXIMA™ in 100%N<sub>2</sub> resulted in the lowest hardness and shallowest case. The treatment in 75%N<sub>2</sub>-25%H<sub>2</sub> atmosphere yielded the highest hardness and thickest case. These improvements in hardness and case depth were attributed to the presence of hydrogen in the nitriding atmosphere.
- Plasma nitriding in the atmospheres of 50%N<sub>2</sub>-50%H<sub>2</sub> and 25%N<sub>2</sub>-75%H<sub>2</sub> gave fairly similar results in terms of hardness and case depth, which fell between the results obtained from treatments in the 75%N<sub>2</sub>-25%H<sub>2</sub> and 100%N<sub>2</sub> atmospheres.
- The highest surface roughness was obtained after DC plasma nitriding in the 100%N<sub>2</sub> atmosphere due to the severe sputtering of the substrate by N<sub>2</sub><sup>+</sup> ions as well as from the higher applied voltage required for the treatment.

- Treatment in the 75%N<sub>2</sub>-25%H<sub>2</sub> atmosphere resulted in the smoothest surface due to a reduction in the number of nitrogen ions in favour of hydrogen and hydrogen-nitrogen ions which led to a reduction in the sputtering.
- The thickest compound layer was formed on the sample treated in the 75%N<sub>2</sub>-25%H<sub>2</sub> atmosphere. The compound layer that formed on the surface of the sample treated in the 100%N<sub>2</sub> was the second thickest layer due to a high sputtering which removed some of the already formed layer. Increasing the hydrogen concentration resulted in a decrease of the compound layer thickness due to a significant decrease in the number of nitrogen ions (molecules, atoms).

## 6.2 Comparative Study of MAXIMA™ and En19 Steels

The nitriding response of MAXIMA™ was compared against a traditional nitriding steel En19 (AISI 4140), and the following conclusions were drawn:

- DC plasma nitriding of MAXIMA™ developed cases having a higher surface hardness, sharper case/core interface and higher surface roughness than those obtained on En19 steel. These were attributed to the higher Cr content and pre-nitriding microstructure of MAXIMA™.
- The compound layer and the diffusion layer of MAXIMA™ were thinner than those for En19 at all treatment temperatures. This was most likely due to the lower carbon and higher chromium contents of MAXIMA™.

- Although the morphologies of the compound layers produced on the surface of the two steels were different due to the difference in their pre-nitriding microstructure, similar phases ( $\gamma'$  and  $\varepsilon$ ) were formed.
- Both steels showed a maximum surface hardness at the 450°C treatment temperature owing to the temperature dependence of dispersion hardening of chromium nitride within the matrix.
- MAXIMA™ steel showed some reduction in core hardness which was more pronounced at the higher nitriding temperatures. This was probably because of the coarsening of carbides and the recovery of dislocation structure present in the as-rolled condition.
- Substitution of En19 with MAXIMA™ may be preferable in some applications where a higher surface hardness is required.

### **6.3 Plasma Immersion Ion Implantation and RF Plasma Nitriding of MAXIMA™**

The basic aim of this study was to make a comparison between PI<sup>3</sup> and RF plasma nitriding using MAXIMA™ steel. Based on the results obtained, the following conclusions can be derived:

- The PI<sup>3</sup> process produced surface layers with more favourable properties such as higher hardness and thicker case, than RF plasma nitriding. The superior properties of

PI<sup>3</sup> treated samples are believed to be due to the additional high voltage ion implantation employed in PI<sup>3</sup>. The DC self-bias in RF plasma nitriding, although capable of driving nitrogen into the steel, is insufficient on its own to develop the optimum properties and has to be boosted by high voltage pulses.

- For the conditions employed, no compound layer was formed on the surface of the treated samples by either of the two processes due to the low nitrogen activity of the atmosphere. This is attractive for applications that demand a high hardness but without compound layer at the surface.
- For both processes, the low temperature treatment (350°C) developed surfaces with the highest hardness and roughness. These were attributed to the low diffusion rate of nitrogen which led to its build up at the surface leading to the formation of a hard case and resulting in surface relief which roughens the surface.

## **6.4 The Influence of the Mode of Plasma Generation on the Nitriding Behaviour of MAXIMA™**

It would appear that all of the mechanisms suggested by different authors play some role in the plasma nitriding process. Determining which of these is dominant is not straight forward and depends upon the operating conditions of different nitriding processes. Nonetheless, the following conclusions can be drawn:

- The mass transfer in DC plasma nitriding is more likely to be due to the sputtering and redeposition model. In PI<sup>3</sup>, however, ion implantation and diffusion of the implanted nitrogen are the major means of mass transfer. Mass transfer in RF plasma nitriding is likely to be mainly due to the adsorption of neutral particles.
- No compound layer was formed on the surfaces of the samples treated by PI<sup>3</sup> and RF plasma nitriding at any treatment temperature. On the other hand, DC plasma nitriding produced a compound layer that increased in thickness with increasing temperature.
- The best case, in terms of hardness and depth, was produced by PI<sup>3</sup> at 350°C and by DC plasma nitriding at 450 and 550°C. From this, it can be concluded that the PI<sup>3</sup> process is suitable for low temperature plasma nitriding of steels which soften (temper) at higher nitriding temperatures and DC plasma nitriding is the preferred nitriding process at higher temperatures where a high hardness and a thicker case are required. At all applied temperatures, RF plasma nitriding produced hardened cases with the poorest properties.
- DC plasma nitriding produced the surfaces with the highest roughness values ( $R_a$ ) followed by PI<sup>3</sup> treatment, except for the 350°C temperature in which the PI<sup>3</sup> produced the roughest surface. The surface roughness value of the samples treated by RF plasma nitriding are the lowest of all treatment temperatures.

## **7. APPENDICES**

---

### **7.1 Appendix A:**

#### **Metallography of Nitrided Samples**

Sample preparation of plasma nitrided steels for revealing the true microstructure requires different technique than is normally required. Firstly, the high hardness differential between the case and the core causes some problems. In addition, the white layer, which is usually the primary subject of metallographic examination, is partly or completely destroyed by ordinary preparation techniques (*Metals Handbook, Desk Edition*, 1985).

##### **7.1.1 Edge Retention**

Preservation of the edges of nitrided steels is of the utmost importance. For edge preservation, any of three recommended methods can be used: (a) use of hard mounting materials or iron-filled epoxy mounting materials; (b) surrounding the specimen in the mount with bits of ceramic, small hardened steel balls, chilled iron shot, or with a pipe section, or (c) nickel plating of the specimen.

Plating of the nitrided specimens in order to protect the edges and to preserve the white layer, is essential and must be done without blasting or severe etching. Due to the lack

of good adherence of chromium plated layers to nitrided surfaces without an unacceptable amount of surface preparation, chromium plating is unsatisfactory. Copper, cadmium, and zinc plates are too soft. It has been proved that nickel plating is the best technique and is now common practice. In addition to protecting and preserving the edges during cutting, it also helps maintain sample flatness during grinding and polishing. The thickness of the plate layer is not that critical, a plate thickness of about 50 $\mu\text{m}$  is usually sufficient, but a thicker plate layer is not harmful.

### 7.1.2 Grinding and Polishing

Like other steel specimens, coarse and fine grinding is required for nitrided specimens. Coarse grinding is usually done with 80, 100, or 120 mesh abrasive and fine grinding is usually done with papers of progressively finer grit size, such as 240, 320, 400, 600, and 1200 mesh.

After grinding, specimens are polished on a napless cloth covered disk, rotating at 150 to 300 rpm, impregnated with 6-mm diamond (paste) spray, followed by 1- $\mu\text{m}$  diamond (paste) spray. The specimen is held by hand and moved in the direction opposite to the direction of wheel rotation. Alternatively, automated devices can be used for grinding and polishing. Time required for polishing varies with hardness and size of the specimen, but the average time is 2 to 4 minutes. It should be mentioned that the polishing time should be reduced to the minimum necessary to achieve the required polish but avoiding edge roundness.

### 7.1.3 Etching

To ensure that all disturbed metal is removed and that the true structure is revealed, the best practice is to etch the polished specimen, immediately repolish very lightly (just enough to remove the evidence of etching), and etch again and continue this procedure for two or more cycles. If proper care is taken during the initial grinding and polishing, this practice is not needed.

Nitrided steel specimens are occasionally etched in nital for routine examination. A 0.5% nital (0.5% nitric acid, 99.5% ethanol) preferentially attacks grain and phase boundaries. A 2.5% nital solution is used for microscopic examination and up to 5% nital for case-depth measurements at low magnification. Nital is the only reagent which leaves the compound zone white. However the  $\epsilon$ -nitride phase in alloy steels is attacked with prolonged etching (Mridha and Jack, 1982).

It is claimed that the Oberhoffer's reagent is the most useful single etchant for revealing the different zones in a nitrided steel as well as distinguishing the dissimilar phases of the compound layer (Mridha and Jack, 1982). Also, when it is preceded by etching in picrate, the presence of cementite in the compound layer is clearly revealed. Both the nitrided and carbide-enriched zones in nitrided chromium-containing steels and the cementite at prior austenite grain boundaries within the nitrided zone are delineated by this reagent.

The boundary of the nitrided zone is most clearly delineated by Marble's reagent and Oberhoffer's reagent. They also reveal the extent of the carbide-enriched region below the nitrided zone.

A list of etching reagents and etching conditions used are presented in Table 8.

**Table 8.** List of etching reagents and etching conditions (Mridha, 1982).

Reagents	Etching conditions
Nital 2.5%: 2.5ml nitric acid, 97.5ml ethyl alcohol	2-8 sec at room temp.
Oberhoffer: 1g cupric chloride, 30g ferric chloride, 0.5g stannous chloride, 50ml HCL, 500ml distilled water, 500ml ethyl alcohol	2-5 sec only for compound layer
Marble's reagent: 10g copper sulphate, 50 ml HCL, 50 ml distilled water	2-10 sec

### 7.1.4 Nickel Electroplating in Watts Bath

When nickel sulphate is dissolved in water it ionises. By establishing an electric potential between two electrodes which are immersed in the solution, positively charged nickel ions are attracted to the more negative electrode (cathode), acquiring a negative charge and are then electrically neutralised, being deposited as metal on the cathode (article). The negatively charged sulphate ions migrate to the positive electrode (anode), giving up their charge at the anode and combine with either the metal of the anode, or with the electrolyte itself (if the anode is chemically inert). If the anode is made of pure nickel, it gradually dissolves during passage of current and combines with the sulphate radical, forms more nickel sulphate and replenishes the solution. Consequently, in the nickel plating process, the nickel metal transfers from nickel anode through the solution and deposits on to the cathode. If 1 amp flows for 1 hour, approximately 12 microns will be deposited over 1 dm<sup>2</sup> (the International Nickel Company, (Mond)).

The Watt's bath is one of the standard general purpose nickel plating solutions. It consists of nickel sulphate, nickel chloride, boric acid. The composition and operating conditions of Watts bath are presented in Table 9 (Samuels, 1967).

The nickel chloride serves to prevent anode passivity and ensures that the anode dissolves at high efficiency. It also provides additional nickel ions and enhances the conductivity of the electrolyte. Increasing the chloride content lowers the ductility, hardens the deposit, and increases internal stress in the plated layer. The boric acid acts as a buffer to maintain the acidity of the solution and to prevent wide changes of PH or hydrogen ion concentration in the vicinity of the cathode. To avoid the formation of rough deposits, the anode is put in a cotton or synthetic fibre anode bag while in use (Brimi and Luck, 1965).

Fluctuations in the operating temperature can have a pronounced effect on the electrodeposited nickel and should be maintained within +/- 2°C of the recommended temperature (Di Bari, 1994). However, changes in the operating conditions such as current density, temperature, or PH (below 5.0) do not affect the physical properties of the deposit. Chemical composition fluctuations exert far greater influences. Specimens to be plated should be cleaned, degreased, and washed prior to plating. Tiny bubbles of hydrogen gas evolving at the cathode may prevent deposition of metal there and gives rise to a local pitting in the deposit. These bubbles can be dislodged by agitating the solution (The International Nickel Company, (Mond)).

**Table 9.** *The Watts bath compositions and its operational conditions (Samuels, 1967).*

Composition	Operating condition
Nickel sulphate, $\text{NiSO}_4 \cdot 6\text{H}_2\text{O}$	300 g/l of distilled water
Nickel chloride, $\text{NiCl}_2 \cdot 6\text{H}_2\text{O}$	60 g/l of distilled water
Boric acid, $\text{H}_3\text{BO}_3$	40 g/l of distilled water
PH	4
Temperature	55°C
Voltage	1-3 volts
Current density	25 mA/cm <sup>2</sup>
Agitation	Vigorous stirring (to avoid pitting)
Anode	Anode nickel (99%)

## 7.2 Appendix B:

### Glow Discharge Optical Emission Spectroscopy

Glow Discharge Optical Emission Spectroscopy (GDOES) is a rapid depth profiling technique using a Grimm-style 'hollow anode' lamp (Grimm, 1968). A schematic cross-section of a Grimm lamp is shown in Figure 91. The sample is placed against the O-ring which provides the seal between the sample and the cathode block. The cathode block can be made from copper, although a ceramic material is preferred. The anode is constructed from copper.

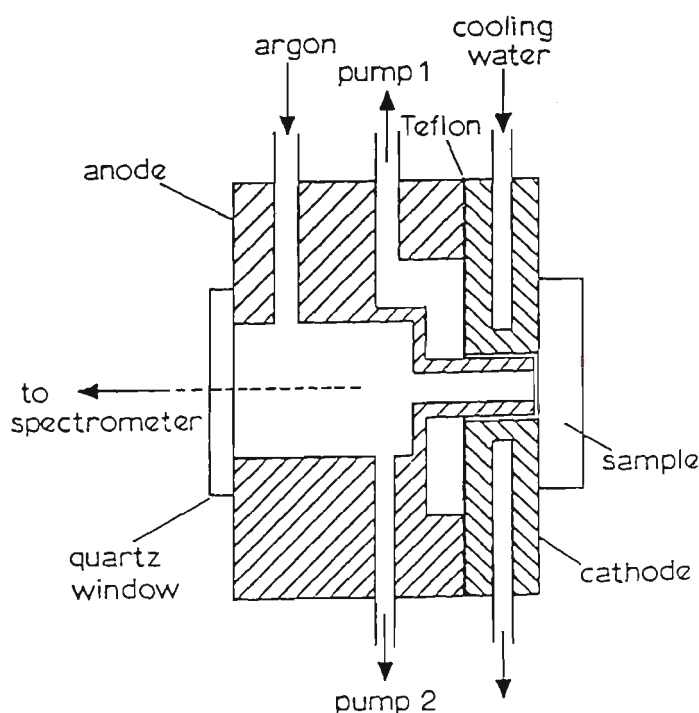


**Figure 91.** Schematic diagram of a Grimm lamp (Berner et al, 1980).

The sample is held in place by the vacuum in the lamp and a brass water-cooled block is placed beside the sample in order to keep the sample cool during the sputtering process. The block is pressed on the sample by a pneumatic mounting composed of a jack and a drill which also provides the electrical connection to the sample.

Argon gas is bled through the anode where it is deferentially pumped to a pressure of ~ 0.2 mbar and then ~ 700 V is applied between the anode and the sample. Consequently, a current of ~ 60 mA flows between the sample and the inside of the hollow anode which causes ionisation of the argon gas. Much of the ionisation occurs close to the sample surface (Boumans, 1991) resulting in rapid and relatively uniform sputtering of the sample surface which is defined by the diameter of the anode. The sputtered material travels up the inside of the hollow anode where it is highly excited electronically by the plasma. The excited atoms emit their characteristic electro magnetic spectra and the wavelength of the spectra is characteristic of the composition of the layer being sputtered. The concentration of the various elements is determined by spectral analysis of the radiation emitted by the plasma.

A MgF<sub>2</sub> window is used to pass the emissions from the lamp to a series of spectrometers without absorption of any radiation in the wavelength band concerned. With spectrophotometers covering the range 100-700 nm, detection of all elements in the Periodic table is possible. Wavelengths between 200-700 nm, which includes most metals, are detected by a polychromator while wavelengths in the range of 100-150nm, belonging to H, O, Cl and N gases and absorbed by air in the polychromator. Therefore, an evacuated nitrogen purged polychromator called FVUV Poly is used to detect these far vacuum ultra violet emissions.

Since the intensity of emissions from each element is proportional to its concentration within the matrix, semi-quantitative analysis of the spectrometer signals are possible. Highly characterised standard materials, however, are required to carry out such analysis. Since standard samples with high nitrogen contents were not available, the GDOES were used only to give a qualitative depth profile the samples.

## 7.3 Appendix C

### Surface Roughness Measurement

A surface which is nominally flat and smooth will always have some roughness texture, which may vary from fine to coarse, according to the finishing process. The term “surface texture” refers to the fine irregularities (peaks and valleys) produced on the surface by the different processes. Surface texture is an important property of an engineering component affecting its quality and function in areas such as wear, contact mechanics, lubrication, appearance, paint holding ability and the conformance of products to specified dimensions. It is a result of the interaction of the physical processes that have acted on the component in its formation and the material that the component is made from. By convention, the texture comprises two components, roughness and waviness. Roughness consists of the finer irregularities characteristic of the process itself, such as grit spacing of a grinding wheel. Waviness consists of the more widely spaced irregularities that are often produced by vibration during the machining process. Usually, however, the terms “surface texture” and “roughness” are used interchangeably, because roughness is specified and measured much more often than waviness.

There are two types of profiling techniques for surface texture, profile methods or raster area methods, depending on whether the height measurements are made simply along a line or over an area. Both types of techniques develop quantitative knowledge of the surface peaks and valleys by point-by-point measurement with a high-resolution probe. The profile may be produced by optical interferometric fringes, by a contacting stylus that traverses the surface, or by a noncontacting probe (Song and Vorburger, 1992).

The stylus method has been widely used by engineers, opticians, and tribologists and was also used in this investigation. Therefore, the stylus technique and some of the related parameters appearing in the thesis will be discussed briefly in this appendix.

In the instrument used, a diamond tipped stylus transverses the surface being profiled with a constant speed. The shape of the stylus plays an important role and can influence the appearance of the line profile it measures. Because the stylus tip has a finite sharpness, it cannot show very fine detail and tends to distort some shapes. For example, valleys in the surface are shown narrower than they actually are and peaks are shown broader. Also, because only a fairly small portion of the surface can realistically be measured, the profilometer data are not absolute values and should be used only as relative data for comparison purposes.

The instrument converts the vertical height as a function of horizontal displacement to a voltage as a function of time leading to a graphical representation of the surface by a line profile. Once the trace has been produced, filters are applied numerically to the recorded raw profile, enabling the removal of either short or long wavelength components (Maddrell, 1991).

Traditionally, the analog output of the profilometer is analysed in terms of the deviation of the profile from the centreline. Two slightly different measures have been used, the roughness average,  $R_a$ , and the root mean square value, RMS, (also called  $Rq$ ).  $R_a$  is the mean vertical deviation from the centreline through a prescribed sampling length. Thus, the  $R_a$  value of the surface is the average height of the profile above and below the mean line as illustrated in Figure 92 (Dagnall, 1980). It is the value most often used in Europe.

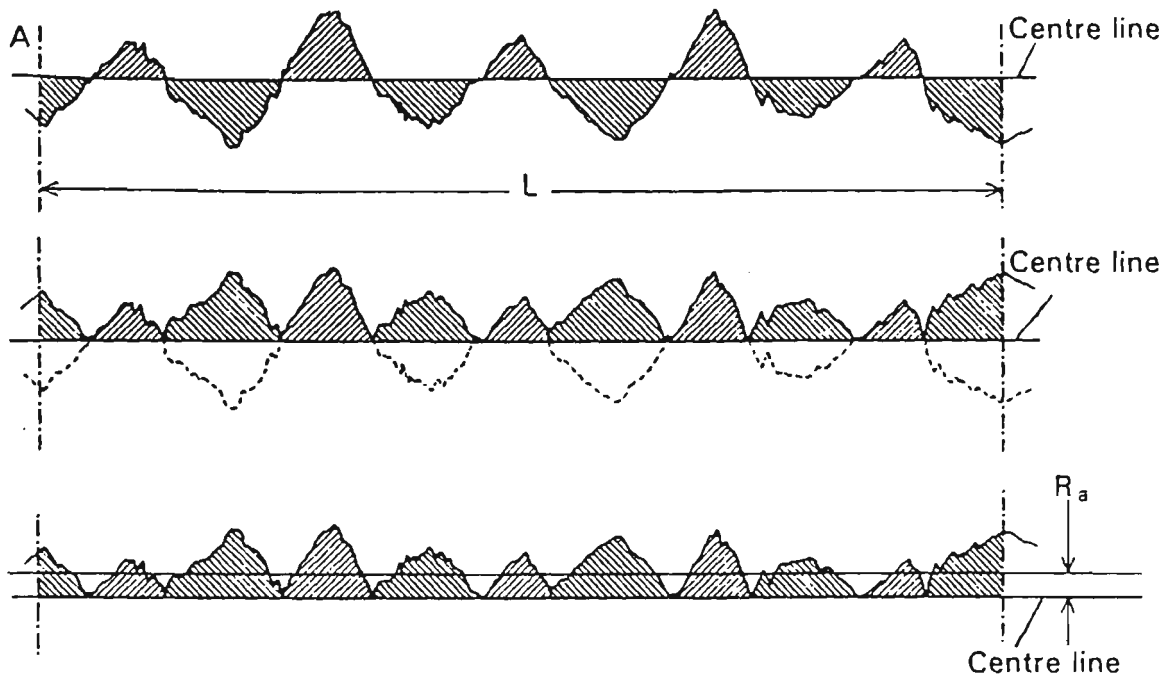


**Figure 92.** Graphical derivation of  $R_a$  (a) profile with centre line, (b) lower portions of the profile inverted and (c)  $R_a$  is the mean height of the profile.

The root mean square value, RMS, is the value most commonly used in the United States (Larsen-Basse, 1992). It is calculated as the square root of the mean of the squares of the deviations and represents the standard deviation of the height distribution.  $R_a$  and  $R_g$  are closely related and are useful estimators of the average heights and depths of surface profiles. Roughness average is used in the automotive and other metalworking industries to specify the surface of the components. The RMS roughness is commonly specified for the surfaces of optical components.

There are a great variety of surface parameters which have been developed to characterise the function of engineering surfaces for particular applications and explanation of all of them are out of the scope of this Appendix.

## 7.4 Appendix D:

### Atomic Force Microscope

Atomic Force Microscope (AFM) belongs to Scanning Probe Microscopes (SPMs), a family of instruments used to study the surface of materials. All the SPMs contain the components shown in Figure 93. The AFM uses a very sharp tip (few microns long and less than 100 Å in diameter) to probe and map the morphology of a surface (Howland *et al*, 1993). The tip is on the end of a cantilever with a low spring constant (of the order of 1 Newton/m). In contact mode, the tip-to-sample spacing is fixed by maintaining a constant and very low force on the cantilever, pushing the tip against the sample. This force is in the range of interatomic forces (Van der Waals forces) (about  $10^{-9}$  Newton, or 1/10000 of the weight of a fly (Babcock, 1994)), hence the name "atomic force" microscopy (Strausser and Heaton, 1994). The force is low enough such that the tip usually causes no damage to the surface under investigation, particularly for harder surfaces. Interaction between the tip and specimen deflect the cantilever while the specimen is moved by means of a piezoelectric scanner. The vertical motion of the tip as it slides over the sample surface is detected by the change in the position of a laser beam reflected from the back of the cantilever, see Figure 94. The measured cantilever deflections allow a computer to generate a map of the surface topography.

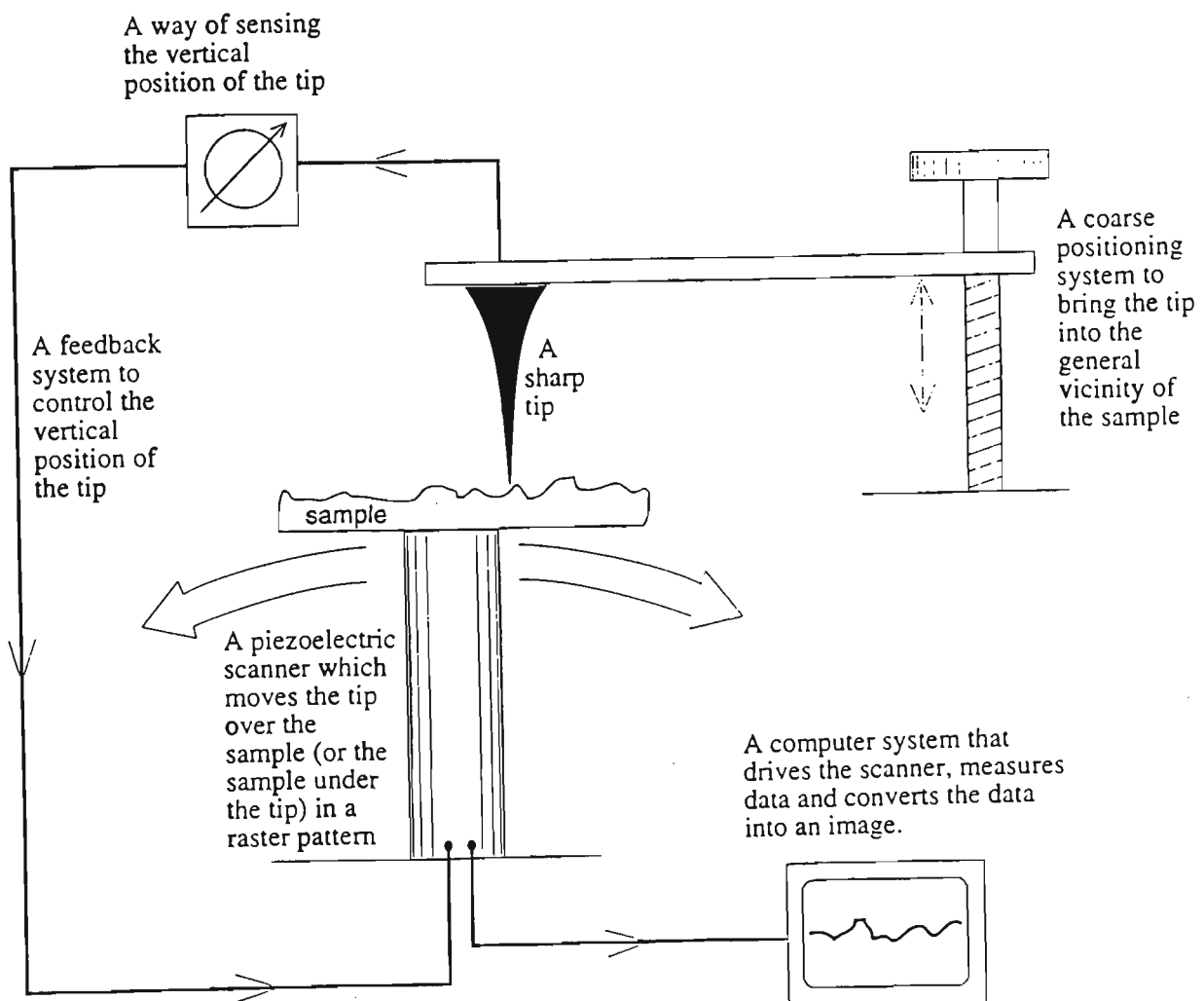


**Figure 93.** Schematic of a generalised scanning probe microscope (Howland et al. 1993).

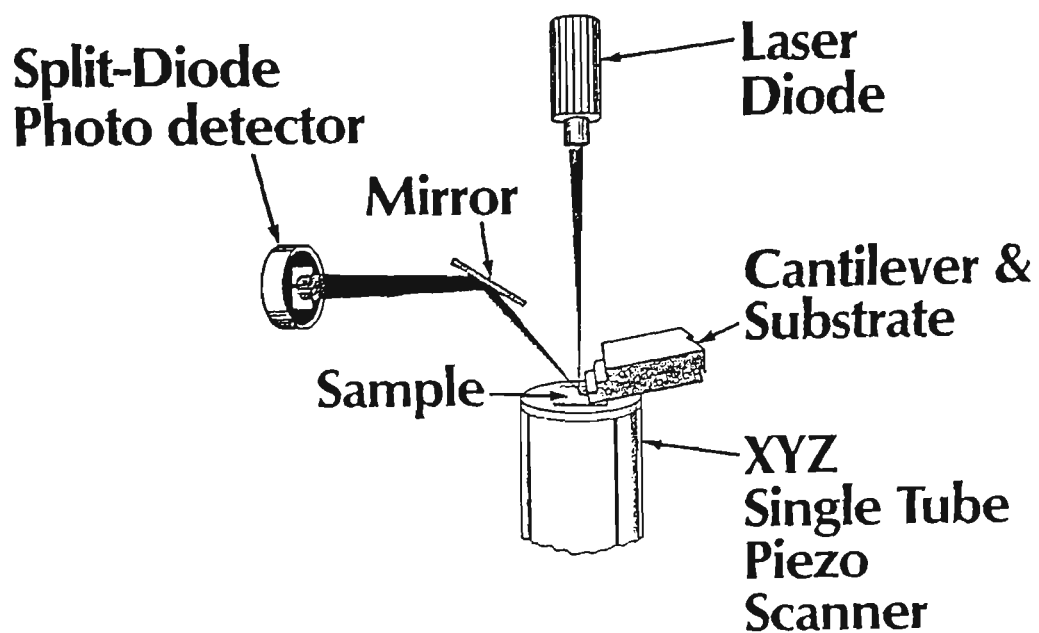


**Figure 94.** Beam deflection system for vertical motion detection. This system has the sensitivity to detect vertical motion of  $0.01\text{ nm}$  as the tip scans the sample surface (Strausser and Heaton, 1994).

## 8. REFERENCES

---

Avner S., *Introduction to physical metallurgy*, McGraw-Hill, Inc., 1974.

Bangaro N.V., Voigt R.C., and Svoboda J. M., "Development of high performance HSLA cast steel", unpublished paper.

Bell T., Birch B. J., Korotchenko V., and Evans S. P., *Heat treatment '73*, The Metals Society, London, 1975, p. 51.

Bell T., *Survey of the heat treatment of engineering components*, The Iron and Steel Institute, 1973, p.43.

Berghaus B., German Patent, DPR 668,639, 1932.

Berghaus B., German Patent, DPR 851, 560, 1939.

Berneron R., Michael H., Gatois M., *Heat treatment '79*, The Metals Society, London, 1980, pp. 45.

Bobcock K., *Photonics Spectra*, Laurin Publishing Co., Inc., May 1994.

Boumans P. W. J. M., *Spectrochim. Acta*, 46B (1991) 711.

Brimi M. A., Luck J. R., *Electrofinishing*, American Elsevier, New York, 1965.

Brockman A., Tuler F. R., *Journal of Applied Physics*, 52 (1981) 468.

Chapman B., *Glow Discharge Processes*, John Wiley & Sons, New York, 1980.

Child H. C., *Surface hardening of steel; Engineering design guides:* 37, Oxford university press, 1980, p. 18.

Cho K. S. and Lee C. O., *Journal of Engineering Materials and Technology*, 102 (1) (1980) 229.

Colijn P. F., Mittemeijer E. J., and Rozendaal H. C. F., *Z. Metallk.*, 74 (1983) 620.

Colligon J. S., *Vacuum*, 36 (7-9) (1986) 413.

Collins G. A. and Tendys J., *Plasma Sources Science and Technology*, 3 (1994) 10.

Collins G. A., Hutchings R., and Tendys J., *Materials Science and Engineering*, A139 (1991) 171.

Collins G. A., Hutchings R., and Tendys J., *Surface and Coatings Technology*, 59 (1993) 267.

Collins G. A., Hutchings R., Short K. T., and Tendys J., *Heat Treatment of Metals*, 22 (1995) 91.

Collins G. A., Hutchings R., Tendys J. and Samandi M., *Surface and Coatings Technology*, 68/69 (1994) 285.

Collins G. A., Short K. T., Tendys J. and Van Der Valk C. H., "Control and Performance of a Plasma Immersion Ion Implantation System for the Surface Treatment of Metal Components", submitted to *Surface and Coatings Technology*.

Conrad J. R., Baumann S., Fleming R. And Meeker G. P., *Journal of Applied Physics*, 65 (1989) 1707.

Conrad J. R., Radke J. L., Dodd R. A., Worzala F. J., and N. C. Tran, *Journal of Applied Physics*, 62 (11) (1987) 4591.

Dagnall H., *Exploring Surface Texture*, Rank Taylor Hobson, 1980.

Dahmen U., Ferguson P., and Westmacott K. H., *Acta Metallurgica*, 35 (1987) 1037.

Dearnaley G. and Hartley N. E. W., *Proceedings of the 4th Conference on the Scientific and Industrial Applications of Small Accelerators*, Denton, TX, 1975, IEEE, New York, 1976, p. 20.

Dearnaley G., Goode P. D., Minter F. J., Peacock A. T., Hughes W. and Proctor G. W., *Vacuum*, 36 (11/12) (1986) p. 807.

Di Bari G. A., "Nickel Plating", in *ASM Handbook*, Vol. 5, Metals Park, OH, 1994, p. 201.

Dressler S., *Surface Modification Technologies: An Engineer Guide*, in T. S. Sudarshan (ed.), Marcel Dekker, Inc., New York, 1989.

Edenhofer B. and Bewley T. J, *Heat Treatment '76*, The Metals Society, London, 1976, p. 7.

Edenhofer B., *Härterei-Tech. Mitt.* 29 (1974) 105.

Edenhofer B., *Heat Treatment '79*, The Metals Society, London, 1980, p. 52.

Edenhofer B., *Heat Treatment of Metals*, 1974. part 1, p. 23.

Edenhofer B., *Heat Treatment of Metals*, 1974. part 2, p. 59.

Egan J. J.: US Patent 1837256, 1931.

- Elder J. E. Thamburaj R., and Patnaik P. C., *Surface Engineering*, 5 (1) (1989) 55.
- East J. D. and Verrijp M. B., *Journal of Iron and Steel Institute*, 176 (1954) 24.
- Fenske G., "Ion Implantation", in *ASM Handbook*, Vol. 18, ASM, Metals Park, OH, 1992.
- Field F. H. and Franklin J. L., *Electron Impact Phenomena*, Academic Press, 1957.
- Goldschmidt H. J., *Interstitial alloys*, Butterworths, London, 1967.
- Grill A. and Itzhak D., *Thin Solid Films*, 101 (1983) 219.
- Grimm W., *Spectrochim. Acta*, 23B (1968) 433.
- Gulyaev A., *Physical Metallurgy*, Vol. 1, Mir publishers, Moscow, 1980, p.320.
- Hanada Y., Bell T., Sun Y., *Surface Engineering*, 11 (2) (1995) 149.
- Handbook of chemistry and physics*, 55th edn, section F, Dow Chemicals, 1974-1975.
- Hartley N. E. W. and Watkins R. E. J., in Dearnaley G. (ed.), *Materials Engineering Applied*, 1 (1978) 28.
- Hartley N. E. W., Dearnaley G. and Turner J. F., *Conference Proceedings on Ion Implantation*, Yorktown Hts, 1972, (Plenum Press, 1973), p. 423.
- Hill R. E. and Abbaschian R., *Physical Metallurgy Principles*, PWS-KENT, Boston, MA, 3rd edn., 1993.
- Howatson A. M., *Introduction to Gas Discharges*, Pergamon Press, London, 1965.

- Howland R. S., Okagaki J., and Mitobe L., *How to Buy a Scanning Probe Microscope, Key Features to Look for When Purchasing an SPM*, Park Scientific Instruments, 1993.
- Hudis M., *Journal of Applied Physics*, 44 (4) (1973) 1489.
- Hutchings R, *Materials Science and Engineering*, A184 (1994) 87.
- Hutchings R., Collins G. A., and Tendys J., *Surface and Coatings Technology*, 51 (1992) 489.
- Hutchings R., Kenny M. J., Miller D. R., and Yeung W. Y., *Proceedings of the 1st Australian International Conference on Surface Engineering: Practice and Prospects, Adelaide, March 1991*, Techsearch, Adelaide, 1991.
- Inal O. T. and Kazim O., in *Ion Nitriding, Proceedings of an International Conference on Ion-Nitriding*, Spalvins T. (Ed.), 15-17 Sep. 1986, Clev., Ohio, ASM Int., 1987, p. 31.
- Inal O. T. and Robino C. V., *Thin Solid Films*, 95 (1982) 313.
- Jack D.H. and Jack K. H., *Materials Science and Engineering*, 11(1973) 1.
- Jack K. H., *Acta Crystallographica*, 5 (1952) 404.
- Jack K. H., *Heat treatment '73*, The Metals Society, London, 1975, p. 39.
- Jack K. H., *High Nitrogen Steels, HNS 88*, Proceedings of the international conference organised by The Institute of Metals and the Societe Francais de Metallurgie and held at Lille in France on May 18-20, 1988, Edited by Foct J. and Hendry A., The Institute of Metals, 1989, p. 117.

Jack K. H., *Proceedings of the Royal Society, A*, 195 (1948) 34.

Japanese Industrial Standard (JIS) G0562, *Surface Engineering*, 11 (1) (1995) 57.

Jones C. K., Martin S. W., Sturges D. J., Hudis M., *Heat Treatment'73*, Metals Society, London, 1975, p. 71.

Karpenko G. V., Pokhmurovskii V. I., Dalisov V.B., Zamikhovskii V. S., *Influence of diffusion coatings on the strength of steel*, Trans Tech Publications, Switzerland, 1979.

Keller K., *Härterei-Tech. Mitt.* 26 (1971) 120.

Keller K., *PhD Thesis*, Technical University of Rhine-Westphalia, 1969.

Knerr C. H., Rose T. C., Filkowski J. H., "Gas Nitriding", in *ASM Handbook*, Vol.4, ASM, Metals Park, OH, 1991, p. 387.

Kölbl J., *Die Nitritschichtbildung bei der Climmnitrierung*; Westd. Verlag Köln ,1965, Forschungsberichte des Landes Nordrhein-Westfalen, Nr. 1555.

Kool W. H., Mittemeijer E. J., and Schalkoord D., *Mikrochimica Acta*, Suppl. 9 (1981) 349.

Kossowsky R. (ed.), "Surface Modification Engineering: Volume 1 Fundamental Aspects", CRC press, Boca Raton, Florida, 1989.

Kossowsky R. (ed.), *Surface Modification Engineering: Volume 2 Technological Aspects*, CRC press, Boca Raton, Florida, 1989.

Kovacs W. and Russelll W., In Spalvins T. (ed.), *Ion Nitriding*, ASM, Metals Park, OH, 1987, p. 9.

- Kubaschewski O., *Iron-Binary phase diagrams*, Springer-Verlag, Berlin, 1982, p. 67.
- Kuppusami P., Sundararaman D. and Raghunathan V. S., *Surface Engineering*, 9 (2) (1993) 137.
- Lakhtin Yu. M., Krymskii Yu. M.; *Protective Coating on Metals*, 2 (1970) 179.
- Lampe T., Eisenberg S., and Laudien G., *Surface Engineering*, 9 (1993) 69.
- Lanagan J., "Plasma Surface Engineering of Titanium alloys", *PhD thesis*, University of Birmingham, 1988.
- Larsen-Basse J., in *ASM Handbook*, Vol. 18, ASM, Metals Park, OH, 1992, p. 27.
- Legg K. O. and Solinck-Legg H., in Sudarshan T. S. and Bhat D. G. (ed.), *Trends in Ion Implantation and Ion-Assisted Coatings, Proceedings of the 1st International Conference on Surface Modification Technologies*, Phoenix, AZ, Jan. 1988, The Metallurgical Society of AIME, Warrendale, PA, 1988, p. 79.
- Leutenecher R., in H. K. Pulker. (ed.), *Surface Modifications by Ion Beam Techniques*, John Wiley and Sons, 1989, p.241.
- Lightfoot B. J. and Jack D. H., *Heat treatment '73*, The Metals Society, London, 1975, p. 59.
- Lisper G. G., *Vacuum*, 45 (5) (1994) 525.
- Loh N. L., "Plasma Nitriding and the Fatigue Properties of 722M27 Steel", *PhD Thesis*, Liverpool University, 1980.

Maddrell E. R., "A Review of the Techniques and Applications of Surface Roughness Measurement", BHP CPD Research and Technology Report No. 1039, Jan. 1991.

Mahboubi F., Samandi M., Dunne D. and Collins A. G., *Proceedings of the 5th Word Seminar on Heat Treatment and Surface Engineering*, 26-29 Sept. 1995, Isfahan, Iran.

Mahboubi F., Samandi M., Dunne D., "Plasma Immersion Ion Implantation and RF Plasma Nitriding of a Microalloyed Steel"; "submitted" to *Surface and Coating Technology*.

Mahboubi F., Samandi M., Dunne D., "The Heat Is On"; *Proceedings of the 1st International Conference on heat treatment*, 24 & 25 May, 1995, Melbourne, Victoria, Institute of Metals & Materials, Australia.

Mahboubi F., Samandi M., Dunne D., Bloyce A., Bell T, *Surface and Coating Technology*, 71 (1995) 135.

Marciniak A., and Karpinski T.; *Industrial Heating*, April 1980, p. 42.

Meijering J. L., *Advances in material research*, Wiley Interscience, New York, Vol. 5, 1971, p. 1.

*Metals Handbook Desk Edition*, Boyer H. E., and Gall T. L.(eds.), ASM, Metals Park, OH, 1985.

Mongis J., Peyre J. P. and Tournier C., *Heat treatment of Metals*, 3 (1984) 71.

Mridha S. and Jack D. H., *Metallography*, Elsevier Science Publishing Co., Inc., 1982, p 163.

Nasser E., *Fundamentals of Gaseous Ionisation and Plasma Electronics*, New York, Wiley, 1971.

*Nickel Plating, Technique and Application*, the International Nickel Company(Mond) Limited.

O'Brien J. M., "Plasma (Ion) Nitriding", in *ASM Handbook*, Vol.4, ASM, Metals Park, OH, 1991, p. 420.

Palmiere E. J., Burke M. G., Garcia C. I. and DeArdo A. J., in DeArdo A. J. (ed.), *Processing, Microstructure and Properties of HSLA Steels*, The Minerals, Metals and Materials Society, Warrendale, PA, 1988, p. 439.

Paules J. R., *JOM*, January 1991, p. 41.

Penning F. M., *Electrical Discharges in Gases*, Philips Technical Library, 1957.

Petitjean L., Ricard A., Casedesus P., Michel H., and Gantois M. *Conference Proceedings of the 4th International Colloquium on Plasmas and Cathodic Sputtering*, Nice, 1982, p. 183.

Petitjean L. and Ricard A., *Journal of Applied Physics*, 17 (1984) 919.

Repas P. E., *Microalloyed HSLA Steels*, ASM International, Metals Park, OH, 1988, p. 5.

Ricard A., Osegura J., Michel H., Gantois M.; *Proceedings of the 1st International Conference on Plasma Surface Engineering*, Garmisch-Partenkirchen, FRG, 1988, DGM, 1989, p.83.

Ricard A., Petitjean L., Casedesus P.; *Conference Proceedings of the 4th International Colloquium on Plasmas and Cathodic Sputtering*, Nice, 1982, p. 25.

Rickerby D.S., Hendry A. and Jack K. H., *Heat Treatment '81*, The Metals Society, London, 1983, p. 130.

Rie K. T., *Ion nitriding and Ion carburising*, *Proceedings of the 2nd International Conference on Ion nitriding/carburizing*, 18-20 Sept. 1989, Cincinnati, Ohio, USA, ASM International, c1990, p. 45.

Robino C. V. and Inal O. T., *Materials Science and Engineering*, 59 (1983) 79.

Rossnagel S. M., Cuomo J. J., Westwood W. D., *Handbook of Plasma Processing Technology*, Noyes Publications, New Jersey, 1990.

Rossnagel S. M., Cuomo J. J., in Westwood W. D. (ed.), *Handbook of Plasma Processing Technology: Fundamentals, Etching, Deposition, and Surface Interactions*, NOYES, Park Ridge, New Jersey, USA, 1990.

Rozendaal H. C. F., Colijn P. F., and Mittemeijer, *Surface Engineering*, 1 (1985) 30.

Ruhl R. C. And Cohen M., *Transaction AIME*, 245 (1969) 241.

Samandi M., Li X. and Shadden B. A., *Conference Proceedings, Microscopy: Materials & Techniques*, Mascot, New South Wales, Australia, Edited by Institute of Metals and Materials Australia Ltd., 21-22 Sept., 1993, p. 31.

Samandi M., Pauza A., Hatziandoniou G., Yasbandha H., Hutchings R., Collins G. A., and Tendys J., *Surface and Coating Technology*, 54-55 (1993) 447.

- Samandi M., Pauza B. A., Hatzianoniou G., Yasbandha H., Hutchings R., Collins G. A. and Tendys J., *Surface and Coating Technology*, 54-55 (1992) 447.
- Samandi M., Shedden B. A., Bell T., Collins G. A., Hutchings R., and Tendys, *Journal of Vacuum Science and Technology*, B, 12 (1004) 935.
- Samandi M., Shedden B. A., Smith D. I., Collins G. A., Hutchings R., and Tendys J., *Surface and Coating Technology*, 59 (1993) 261.
- Samuels L. E., *Metallographic Polishing by Mechanical Methods*, Sir Isaac Pitman & Sons Ltd., 1967.
- Shoemaker R., *Industrial Heating*, 42 (9) (1975) 22.
- Sigmund P., *Physical Review*, 184 (2) (1969) 383.
- Slycke J. and Sproge L., *Surface Engineering*, 5 (2) (1989) 125.
- Solinck-Legg H and Legg K. O., in Sudarshan T. S. (ed.), *Surface Modification Technologies, An Engineer's Guide*, Marcel Dekker, New York and Basel, 1989.
- Somers M. A. J. and Mittemeijer E. J., *Materials Science Forum*, 102-104 (1992) 223.
- Somers M. A. J., "Internal and External Nitriding and Nitrocarburising of Iron and Iron-Based Alloys", PhD thesis, Delft University of Technology, 1989.
- Song J. F., and Vorburger T. V., "Surface Texture", in *ASM Handbook*, Vol.18, ASM, Metals Park, OH, 1992, p.334.
- Spalvins T., *Ion Nitriding*, Splavins T. (ed.), ASM, 1987, p. 1.

- Strafford K. N., Datta P. K., Gray J. S., *Surface Engineering Practice, Processes, Fundamentals and Applications in Corrosion and Wear*, Ellis Horwood, 1990.
- Strausser Y. E., and Heaton M. G., *American Laboratory*, May 1994.
- Szabo A., Wilhelm H., *Härterei-Tech. Mitt.*, 39 (1984) 148.
- Tendys J., Donelly I. J., Kenny M. J., and Pollock J. T. A., *Applied Physics Letters*, 53 (1988) 2143.
- Thelning K. E., *Steel and its heat treatment*, Bofors Handbook, Butterworths, Boston, 1975.
- Thornton J. A., *Ion Nitriding*, Splavins T. (ed.), ASM, 1987, p. 19.
- Tibbets G. G., *Journal of Applied Physics*, 45 (11) (1974) 5072.
- Van Wiggen P.C., Rozendaal H. C. F. and Mittemeijer E. J., *Journal of Materials Science*, 20 (1985) 4561.
- Wear Resistant Surfaces, A Guide to Their Production, Properties and Selection*, Department of Trade and Industry (Britain), Her Majesty's Stationery Office, London, 1986.
- Wehner G. K., *Physical Review*, 102 (3) (1965) 690.
- Wells A. and Strydom L. le R., *Surface Engineering*, 2 (1986) 263.
- Wells A. and Strydom L. le R., *Surface Engineering*, 4 (1988) 55.
- Xu B., Zhang Y.; *Surface Engineering*, 1987, 3 (3) (1987) 226.